Molecular and cellular mechanisms involved in the process of atrioventricular canal morphogenesis in zebrafish

Hélène Vignes

Université de Strasbourg

UNIVERSITÉ DE STRASBOURG

École Doctorale des Sciences de la Vie et de la Santé STRASBOURG

ÉCOLE DOCTORALE DES SCIENCES DE LA VIE ET DE LA SANTE (ED 414)

Institut de Génétique et de Biologie Moléculaire et Cellulaire (IGBMC)

THÈSE présentée par :

Hélène VIGNES

soutenue le : **02 juillet 2021**

pour obtenir le grade de : **Docteur de l'université de Strasbourg**
Discipline/ Spécialité : Physique cellulaire

Mécanismes moléculaires et cellulaires impliqués dans le processus de morphogenèse du canal atrio-ventriculaire chez le poisson zèbre

THÈSE dirigée par :

Dr. VERMOT Julien	DR, Université de Strasbourg - IGBMC, FR / Imperial College London, GB
Dr. QUINTIN Sophie	CR, Université de Strasbourg - IGBMC, FR

RAPPORTEURS :

Prof. Dr. AFFOLTER Markus	PR, Université de Bâle – Biozentrum, CH
Dr. MAITRE Jean-Léon	CR, Institut Curie, FR

AUTRES MEMBRES DU JURY :

Dr. MAO Yanlan	LMCB Group leader, MRC- LMCB, GB
Dr. RIVELINE Daniel	DR, Université de Strasbourg – IGBMC, FR

"Productive stupidity means being ignorant by choice. Focusing on important questions puts us in the awkward position of being ignorant. One of the beautiful things about science is that it allows us to bumble along, getting it wrong time after time, and feel perfectly fine as long as we learn something each time. No doubt, this can be difficult for students who are accustomed to getting the answers right. No doubt, reasonable levels of confidence and emotional resilience help, but I think scientific education might do more to ease what is a very big transition: from learning what other people once discovered to making your own discoveries. The more comfortable we become with being stupid, the deeper we will wade into the unknown and the more likely we are to make big discoveries."

Essay from Martin A. Schwartz
The importance of stupidity in scientific research

(Schwartz, 2008)

ACKNOWLEDGEMENTS/ REMERCIEMENTS

First of all, I would like to thank the members of my jury, Prof. Markus Affolter, Dr. Jean-Léon Maître, Dr. Yanlan Mao and Dr. Daniel Riveline for accepting to evaluate my PhD work. I would like to thank especially Dr. Jean-Léon Maître and Dr. Anne-Cécile Reymann who were part of my mid-thesis committee for their advice and guidance during the several “mid-thesis” presentations I have done during my PhD. The discussions we had together were really stimulating and inspiring. Many thanks to Dr. Daniel Riveline for driving the Master II programme on Cell Physics in which I was lucky enough to participate and was happy to be a kind of guinea pig at its first launch. It confirmed my interest in scientific research and also stimulated my curiosity for biophysics and the study of morphogenesis. Thank you also, Dr. Daniel Riveline, for your personal investment in the choice of the laboratory in which I wanted to pursue my PhD.

Next, I would like to thank my PhD supervisor, Julien, for all these years we spent together. A PhD is a long road that is not straight at all and that has very exciting moments as well as more disappointing ones, but I can say that overall I enjoyed my time in your laboratory very much. I would like to thank you for trusting in me when I applied to your laboratory. For your support and your patience when we had to first improve my master II presentation (and this was not an easy task…) in order to obtain the fellowship from the IGBMC PhD programme. Then, I am grateful that you let me have a large degree of freedom on my project so that I could develop my own ideas. This also helped me personally to become more confident about myself. Thanks also for all the opportunities to go to conferences and meet interesting people (unfortunately only through zoom recently) and also to establish this collaboration with the Jug lab and Norden lab, in Dresden (MPI-CBG). This was a great chance for me to learn a lot of new stuff about great science and share ideas. Thanks also for all the moments you organized so that everyone was feeling good in the team (lab retreats, Christmas lunch, lab anniversary and petanque, “World Cup tournament” (even if the leader here was clearly Anne-Laure), dinner in the city center, …). This last year was a bit more complicated to manage with the Covid and the fact that you had to establish the new lab at Imperial but I would like to thank you for the possibility you offered me to continue working in Strasbourg to finish the project.

Due to the relocation of the lab, I was lucky to get the support of a co-supervisor, Sophie, who helped me during this last year. Thanks a lot Sophie for the time you invested, our monthly-discussion, and for your constant support just to check if I was feeling alright.

This project benefited greatly from our collaboration with the Jug & Norden's labs. I would like to thank all the members of these two labs for their welcome and kindness. A special thanks to Mangal, for all the analyses he performed for me and staying nice even though I sent him tons of new data! Sorry for pushing you so much especially during these last months. Thanks also to Iskra, with whom it was pleasure to discuss and perform experiments.

Then, I would like to also thank the people who are working on the IGBMC platforms, and especially the Imaging and Fish facility platforms. Thanks to Elvire and Erwan for their technical support but also all the good time we spent laughing and discussing.
Un grand merci à Sandrine, Sylvie et aussi des anciens membres de l'animalerie zebra, Norbert et Clarisse, pour tout le soin que vous avez apporté à toutes les lignées de poisson zèbre. Merci pour toutes ces matinées où vous m'avez aidé en retirant les séparations. C'était toujours un plaisir de vous croiser à l'animalerie, avec la musique de Nostalgie à fond !

Thanks also to all the teams that take part in the "Biophysics Club" (organized previously by Julien and now by Daniel), the "Developmental Concept Club" (organized by Sophie Jarriault and Juliette Godin), as well as the Department Seminars (organized by France Chivaille) for all the nice scientific discussions!

I now want to address a lot of thanks to people from the Vermot lab, which was quite big when I joined but little by little got reduced before the moving of the lab.
First, I would like to thank my two colleagues and friends, Anne-Laure and Nathalie, who made me feel great in the lab from my first day.
Thank you, Anne-Laure, for showing me everything about zebrafish, experiments and for being so patient with my clumsiness at first. Without you, I would have taken so much longer to be properly trained. Thank you for trusting me for experiments that are on your paper. But mostly, thanks to both of you, for your constant support, and our giggles, that everyone could here in the whole corridor.
I would like also to thank Elena, with whom the time I spent was too short but that I enjoyed a lot. No doubt that we will see each other again in the future. Thanks a lot to the two Portuguese of the team, Rita & Pedro, who, on top of being excellent scientists that always made lab meetings really stimulating, are amazing colleagues with whom it was always a pleasure to discuss. Thanks also to former members, Paula (for our teamwork on Francesco's project), Marina (welcome back to Strasbourg!), Hajime (for your incredible scientific knowledge, hope to see you soon in Japan!) and Laia. A big thank also to Stephane for your help in the management of the lab during all these years.
I would like to also thank Renee, who closes the IGBMC Vermot lab with me this year 2021, for all her advice, proofreading of English and her kindness… fingers crossed for your paper!

[2]It was also a pleasure to start working with the new members of the Vermot lab, Emmanuelle and Christina who joined at Imperial. It would have been great though if our benches would have been a bit closer! A special thanks to Christina for all your help on the paper and I enjoyed a lot working and discussing with you during this last year.

Thanks to Renee, Pedro, Sophie, Julien and Basile for proofreading some parts of this thesis manuscript.

Pour finir cette partie de remerciements, j'aimerais tout d'abord remercier des professeurs extraordinaires que j'ai pu croiser au long de ma scolarité et qui ont construit ma passion pour les sciences. Tout d'abord, Monsieur Bellanca-Penel et Monsieur Krieger pour leur engagement dans l'apprentissage de la physique-chimie et des mathématiques au lycée Ampère de Lyon. Ensuite, j'aimerais tout particulièrement remercier Monsieur Celle pour ses cours de biologie, sur tableau, qui m'ont tout simplement fascinée, lors de la première année de CPGE BCPST.

Merci à tous mes amis qui viennent de divers horizons (collège, lycée, chorale, prépa, ESBS, poterie…) et qui m'ont soutenu durant toutes ces années de thèse.

Un immense merci à ma famille.

A mes parents, qui ont toujours cru en moi et qui ont toujours respecté mes choix. Merci pour ce soutien sans faille et cette envie constante que vous avez de voir votre « petit oiseau » s'épanouir.

A Bruno et à Alice, merci pour avoir toujours été un grand-frère et une grande-sœur bienveillants. Je me réjouis de pouvoir fêter cette fin de thèse avec vous !
Merci également de me rendre la plus heureuse des tatas, avec Charline, Edgar et Lucien (et …). Ces trois-là ont été une réelle source de bonheur pendant cette thèse !

A Basile, sans qui ces années auraient été beaucoup moins belles. Merci infiniment pour tous ces moments où tu as su me remonter le moral, pour nos échanges scientifiques mais surtout pour partager mon quotidien.

RESUME DU PROJET DE THESE

INTRODUCTION

La morphogenèse est un processus complexe alliant à la fois l'expression génétique et la mécanique. Pendant le développement embryonnaire, les forces mécaniques sont essentielles car elles permettent le remodelage et la morphogenèse des tissus, des organes et des organismes en entier. Les forces mécaniques générées au cours du développement peuvent provoquer des changements au sein du tissu comme par exemple le nombre de cellules, leur forme ainsi que leur position. De plus, les cellules sont également capables de sentir les contraintes physiques venant de leur environnement extérieur (flux, pression hydraulique, matrice extracellulaire) et de les traduire en réactions biochimiques entrainant l'expression de gènes spécifiques au sein de la cellule. Ce processus est connu sous le nom de mécanotransduction.

Un exemple particulièrement pertinent pour étudier l'importance des forces biophysique au cours du développement embryonnaire est la morphogenèse du cœur. En effet, il est connu que la formation du cœur dépend des signaux mécaniques générés par le battement du cœur ainsi que par le flux sanguin. Cependant, la façon dont ces forces modulent le comportement des cellules cardiaques reste mal comprise. Au sein de du laboratoire dans lequel j'ai réalisé ma thèse, nous utilisons le poisson zèbre (*Danio Rerio*) comme organisme modèle vertébré, principalement en raison de sa fertilisation *ex-utero* et du fait que les embryons sont transparents lors des premiers stades embryonnaires. En effet, ces caractéristiques rendent l'étude de la dynamique de la formation du cœur par imagerie *in vivo* plus facile que dans d'autres

systèmes d’étude comme la souris ou le poulet. De plus, la petite taille des embryons leur permet de survivre quelques jours en l ’absence de tout battement cardiaque car le dioxygène peut facilement diffuser à travers tous les tissus de l’organisme. Grâce à cette propriété, il est possible d’étudier de graves défauts cardiovasculaires.

Le cœur embryonnaire du poisson zèbre se transforme au cours du développement, passant d'une structure tubulaire linéaire à une structure composée de deux chambres, un ventricule et un atrium. Il est composé de 3 couches tissulaires : la couche externe constituée de cellules mésothéliales, l'épicarde, une couche composée de cellules du muscle cardiaque, appelé le myocarde, et en effet une couche constituée de cellules non contractiles tapissant l'intérieur du cœur, appelé l'endocarde. Les cellules de l'endocarde sont en contact direct avec le flux sanguin et subissent des forces biophysiques tout à fait uniques. Ces cellules sont connues pour être très importantes en tant que capteurs et transducteurs de forces mécaniques (Heckel et al., Curr Biol, 2015).

Dans ce projet, nous nous sommes concentrés sur les cellules endocardiques et nous souhaitons comprendre le lien entre les forces mécaniques et l'établissement de la forme pendant la morphogenèse de l'AVC (Canal Atrio- Ventriculaire), la région où les valves se formeront entre le ventricule et l'atrium. Au début de la morphogenèse de la AVC, il est connu qu'il y a, localement, une augmentation de la densité cellulaire, les cellules se retrouvent plus proches les unes des autres et forment un cluster (Steed et al., Nature Communications, 2016 & Pestel et al., Development, 2016). Ce cluster de cellule est la tout première étape dans la formation des valves et ensuite des processus complexes de morphogenèse vont amener à la formation de valves matures. De plus, des expériences de photoconversion ont montré qu'il existe un

mouvement de convergence du tissu endocardiale vers l'AVC entre 36 heures post-fertilisation (hpf) et 48 hpf (Boselli et al, Development, 2017). Cependant, ce mouvement n'est pas observé chez le mutant silent heart, qui présente une mutation du gène *tnnt2*, essentiel pour l'assemblage des sarcomères et la contractilité cardiaque des cellules du myocarde. Ces mutants sont donc caractérisés par l'absence de contraction cardiaque et n'ont donc pas de flux sanguin. Par conséquent, nous avons commencé ce projet avec l'hypothèse qu'au début de la morphogenèse de l'AVC, il y a un mouvement de convergence des cellules endocardiales, associé à une augmentation locale de la densité cellulaire et que cet évènement morphogénétique dépend des forces mécaniques. Cependant les mécanismes moléculaires et cellulaires qui conduisent à ce mouvement tissulaire sont encore inconnus. Dans ce projet de thèse, nous avons voulu étudier la force motrice qui guide ce processus et le rôle des forces mécaniques.

Nous avons formulé plusieurs hypothèses sur ce qui pourrait être la force motrice du processus. Nous pensons qu'il puisse s'agir soit d'une force où les cellules seraient poussées vers la région de l'AVC (cela pourrait s'expliquer par les comportements cellulaires suivants : une prolifération cellulaire asymétrique et/ou une migration cellulaire active en direction de l'AVC). A l'inverse, il pourrait aussi s'agir d'une force où les cellules seraient tirées (force de traction) par les cellules dans la région de l'AVC (qui pourrait être due à une diminution locale du volume cellulaire au niveau de l'AVC). Dans la suite de ce résumé, je vais donc vous exposer les résultats que nous avons pu obtenir au cours de ce travail de thèse.

Les objectifs spécifiques de ce projet étaient :

Objectif 1. Caractériser les comportements cellulaires associés au mouvement de convergence.

Objectif 2. Caractériser l'impact des forces mécaniques sur le processus.

Objectif 3. Caractériser la force motrice du mouvement et comment elle est régulée.

RESULTATS

Tout d'abord, nous avons évalué la polarité cellulaire dans l'endocarde, en examinant la position relative entre l'appareil de Golgi et le noyau. Nous avons pu observer qu'à 28hpf, la majorité des cellules de l'endocarde (environ 70%) sont polarisées vers la sortie du cœur (dans la même direction que le flux sanguin). Cependant, les cellules présentes au sein de l'atrium gardent cette polarité au cours des divers stades embryonnaires (de 28hpf à 48hpf) alors que les cellules qui composent le ventricule changent graduellement de polarité à polarité à partir de 30hpf et la majorité se retrouve polarisée vers l'entrée du cœur à 48hpf. Ces résultats indiquent que la convergence du tissu endocardiale commence déjà très tôt, puisque l'orientation des cellules commence déjà à changer à partir de 30hpf.

Pour caractériser plus en détail le comportement des cellules, nous avons ensuite effectué une analyse 3D des changements de taille des cellules au cours de la morphogenèse de l'AVC. Nous avons constaté que la morphogenèse de l'AVC est associée à une diminution importante du volume cellulaire spécifiquement dans la région de l'AVC pour créer une zone de convergence entre l'atrium et le ventricule.

Afin d'examiner les changements de volume des cellules, nous avons développé un outil de segmentation des noyaux basé sur le deep learning, grâce à notre collaboration avec l'équipe de Florian Jug au MPI-CBG, à Dresde. Grâce à cet outil, nous avons d'abord pu montrer que nous avons une corrélation entre le volume et le noyau de la cellule au sein du tissu endocardiale. Nous avons ensuite utilisé cet outil pour étudier processus dans des conditions avec des gènes mutés. Nous avons d'abord montré que dans le mutant silent heart, lorsqu'il n'y a pas de contraction du cœur et qu'il n'en résulte pas de flux sanguin, la diminution du volume cellulaire ne se produit pas au niveau de l'AVC. Cependant, en raison du phénotype assez drastique de ce mutant, nous avons cherché à étudier une situation intermédiaire en injection le morpholino *tnnt2a* à une concentration très faible, résultant en un cœur qui battait encore un peu mais avec une amplitude réduite par rapport à un wild-type (WT). Dans ce cas nous avons quand même observé une diminution du volume cellulaire mais plus faible par rapport aux témoins et aussi une diminution du nombre de cellules qui composent l'AVC. Ces résultats montrent et renforcent l'importance du rôle des forces mécaniques pour amener à une morphogenèse correcte de l'AVC. De plus, grâce à un traitement pharmaceutique qui nous a permis d'abolir complètement la division cellulaire (en bloquant les cellules en phase S), nous avons montré que le changement de volume cellulaire est indépendant de la prolifération cellulaire. En effet, la diminution du volume cellulaire avait toujours lieu dans les embryons traités. De plus, les cœurs avaient en tout moins de cellules dans le cœur mais le cœur avait gardé la même taille globale en ayant des cellules plus grosses dans chaque compartiment du cœur (phénomène de mise à l'échelle). Mécaniquement, nous avons montré que les canaux sensibles aux forces mécaniques TRPP2/TRPV4 et également l'acide hyaluronique (présent dans la matrice extracellulaire entre le myocarde et l'endocarde) sont des

modulateurs essentiels des changements de volume cellulaire au cours de ce processus. Nous avons également identifié deux aquaporines qui sont exprimées spécifiquement au niveau de l'AVC à ces stades de développement et qui pourraient jouer un rôle dans la régulation du volume cellulaire. En conclusion, notre étude révèle que les changements de volume cellulaire sont essentiels dans les premiers stades de la morphogenèse cardiovasculaire.

Liste d’articles :

• DUCHEMIN Anne-laure, VIGNES Helene, VERMOT Julien, 2019. Mechanically activated Piezo channels modulate outflow tract valve development through the Yap1 and Klf2-Notch signaling axis. eLife. 2019;8:e44706. DOI :10.7554/eLife.44706

• DUCHEMIN Anne-laure, VIGNES Helene, VERMOT Julien, CHOW Renée, 2019. Mechanotransduction in cardiovascular morphogenesis and tissue engineering. Current opinion in genetics & development. août 2019. Vol. 57, pp. 106-116. DOI 10.1016/j.gde.2019.08.002. (CO-FIRST)

• VIGNES Hélène, VAGENA-PANTOULA Christina, NORDEN Caren, PRAKASH Mangal, JUG Florian, VERMOT Julien. Extracellular mechanical forces drive endocardial cell volume decrease during cardiac valve morphogenesis (bioRxiv 2021.07.27.453460; DOI https://doi.org/10.1101/2021.07.27.453460)

Liste des communications orales et posters :

Présentations orales :

• 8th World Congress of Biomechanics (Jul 08-12.2018) _ Dublin, Irlande. Biophysical mechanisms involved in regulating cell behaviors during zebrafish heart morphogenesis. VIGNES Hélène, VERMOT Julien

• Cardiovascular Development Meeting (Oct, 22-24.2018) _ Marseille, France. Deciphering the mechanisms involved in the process of atrioventricular canal convergence during zebrafish heart morphogenesis. VIGNES Hélène, BOSELLI Francesco, STEED Emily, VERMOT Julien

Posters :

• Mechanical Forces in Development (Jul 03-06.2019) _EMBL, Heidelberg, Germany. Cellular and molecular mechanisms of atrioventricular canal tissue convergence during zebrafish heart morphogenesis. VIGNES Hélène, PRAKASH Mangal, JUG Florian, VERMOT Julien

• Tri-regional Development and Stem cell Biology Meeting (Oct.15-16.2020) _ IGBMC, Strasbourg, France. Cellular and molecular mechanisms of atrioventricular canal tissue convergence during zebrafish heart morphogenesis. VIGNES Hélène, PRAKASH Mangal, JUG Florian, VERMOT Julien IGBMC, Strasbourg, France

Thesis outline

INTRODUCTION 1

1 Embryo morphogenesis:
an interplay between biochemical signaling and mechanical processes 2

1.1 Pioneer theoretical ideas and experiments about morphogenesis 3

1.2 The discovery of genes involved in patterning 6

1.3 The essential role of mechanical forces in morphogenesis 7

1.3.1 Intrinsic and extrinsic forces 7
A. Intrinsic force generation 8
B. External forces 10

1.3.2 Force transmission and robustness 14

1.3.3 Mechanotransduction 15

1.4 Collective cell behaviors drive tissue morphogenesis 16

1.4.1 Cell shape changes 17

1.4.2 Cell volume changes 18
A. Osmotic pressure 18
B. Examples of tissue remodeling 21
C. The importance of cell proliferation for cell size 22

1.4.3 Cell proliferation 25

1.4.4 Polarized collective cell migration 26

1.4.5 Cell intercalation 27

1.4.6 Cell apoptosis 29

2 The cardiovascular system: function, anatomy, embryonic development, and mechanogenetic interplay 31

2.1 Overview of the cardiovascular system 32

2.1.1 Physiological function 32

2.1.2 Histo-anatomical features 33
A. Heart chambers and valves 33
B. Tissues composing the heart 35
C. Congenital diseases associated with cardiovascular defects 35

2.2 Embryonic development of the vertebrate cardiovascular system 37

2.2.1 Zebrafish, a powerful vertebrate model to study cardiovascular defects 37

2.2.2 Heart development in zebrafish 39
A. From cardiac progenitors to the primitive heart tube 39
B. From the heart tube to the chambered heart 40
C. Cardiac valve development 41
D. Trabeculation 42

2.3 Cardiovascular development is dependent upon mechanical forces 43

2.3.1 Response of endothelial cells to mechanical forces 44

2.3.2 The importance of cardiac-generated forces in the developing heart 46
A. Zebrafish mutants with deficiencies in cardiac force generation 46
B. Shear stress seems to be the main force to which cells respond 47
C. Oscillatory blood flow is essential for AVC cell identity 48
D. Cardiac forces influence endocardial cell proliferation 50

2.4 Atrio-ventricular canal development 52

2.4.1 Mechanostransduction in the valve-forming regions 52
A. PIEZO channels 52
B. TRP channels: TRPP2 and TRPV4 53

2.4.2 Cardiac jelly composition changes during AVC development 55

2.4.3 Tissue remodeling during early heart morphogenesis 59

OBJECTIVES OF THE THESIS 61

RESULTS - PART I 67

Extracellular mechanical forces drive endocardial cell volume decrease during cardiac valve morphogenesis

RESULTS - PART II 109

Generation of CRISPR mutants for Aqp8a.1 and Aqp1a.1 / Inhibition of ion channels

GENERAL DISCUSSION AND PERSPECTIVES 131

RESULTATS (EN FRANCAIS) 144

ANNEX 1 162

Duchemin, A.L., Vignes, H., and Vermot, J. (2019). Mechanically activated Piezo channels modulate outflow tract valve development through the yap1 and KLF2-notch signaling axis. Elife 8.

ANNEX 2 190

Duchemin, A.L., Vignes, H., Vermot, J., and Chow, R. (2019). Mechanotransduction in cardiovascular morphogenesis and tissue engineering. Curr. Opin. Genet. Dev. 57, 106–116.

REFERENCES 202

INTRODUCTION

The early stages of the primitive heart tube development are characterized by a cellular clustering event, at 48 hours-post fertilization (hpf), within the endocardial monolayer localized at the Atrio-Ventricular Canal (AVC), where the valves will later form (Pestel et al., 2016; Emily Steed, Faggianelli, et al., 2016). Prior to this event, the endocardial tissue converges towards the AVC region (from 36hpf to 48hpf) (Boselli et al., 2017). During my thesis work, I studied the **cellular behaviors** associated with endocardial tissue convergence. Interestingly, I found that the increase in cellular density at the AVC is not only the result of cell deformation (by cell elongation along the apico-basal axis) but rather due to a significant **cell volume decrease** at the AVC region. Following, I thought to uncover how the **mechanical forces generated by the cell microenvironment at the AVC** (blood flow, heart contraction, ECM composition) could regulate the size of these cells. I identified the mechanosensitive **TRP channels (Trpp2 and Trpv4)** and **hyaluronic acid (HA)** as key players regulating cell volume decrease. Interestingly, I also found two aquaporin channels (Aqp8a.1 and Aqp1a.1) to be exclusively expressed within cells that change volume, and I tried to decipher their roles in the regulation of the cell volume.

To introduce the project, I will first give a general overview of the different processes involved in morphogenesis (Part 1). Next, I will introduce more specifically cardiac morphogenesis with an emphasis on the findings made in the zebrafish, *Danio Rerio,* the model organism used in this work (Part 2). Finally, I will outline the thesis project, describing the questions that I chose to address and the main hypotheses.

1 Embryo morphogenesis:

an interplay between biochemical signaling and mechanical processes

How does the remarkable diversity and fidelity of biological forms arise? This is certainly one of the most fascinating questions in biology. These incredible arrays of forms emerge by a process called **morphogenesis**. Embryo morphogenesis corresponds to the complex set of processes that lead to appropriate shape formation during development. The morphogenesis of an organism is a highly precise process and understanding how this reproducibility is achieved is one of the key questions in the field of developmental biology.

The establishment of a specific shape for each species has always been an intriguing question since the ancient Greek period to nowadays. Already the philosopher Aristotle (384–322 BC), in his “Four causes”, was interested in understanding the internal force necessary to acquire a functional organized shape, from materials. Later, in 1744, Abraham Trembley, who was a naturalist, discovered that Hydra fragments can regenerate a complete Hydra organism, raising even more questions about what is the **nature of the information leading to shape emergence**. However, although great enthusiasm was present to understand this process better, scientists could not provide theoretical and empirical answers before the early XXth century.

1.1 Pioneer theoretical ideas and experiments about morphogenesis

In the XXth century, many influential theoretical ideas, as well as experiments in the field of developmental biology, arose.

In 1917, the mathematician D'Arcy Thompson provided the theoretical foundations of morphogenesis in his book "On growth and form" (Thompson, 1942)(Thompson, 1917*). By giving some concrete examples, he exposed the **importance of physics** to drive cell and tissue shape changes. In fact, he found numerous correlations between biological forms and geometries seen in inert matter. He proposed that physical principles such as **force balance and energy minimization are applicable to living matter**. However, its innovative ideas were kind of overshadowed by the major advances in molecular biology. For instance, the discovery of the chromosome theory of inheritance (Boveri, and Sutton, 1902* and Morgan, 1910*), the fact that genes are controlled temporally and spatially with the understanding of the DNA structure (Watson & Crick, 1953), the analysis of the lactose operon (Jacob and Monod, 1953*) as well as the genetic code (Nirenberg and Matthaei, 1961*; Nirenberg and Leder, 1964*). With the understanding of the **chemical basis of heredity**, scientists aimed at providing a **chemical nature of morphogenesis**. As DNA becomes the carrier of the genetic information, it could potentially explain the reproducibility observed in biological forms.

Boveri showed in 1904 that abnormal chromosomal segregation in urchin eggs that were double-fertilized led to developmental defects. From this, he concluded that the **chromosomes carry morphogenetic information**. In 1924, Spemann and Mangold discovered that transplanting a group of dorsal cells into the ventral pole, at gastrulation stages, led to a secondary body axis. The discovery of what is called the "**Spemann organizer"** revealed that **morphogenesis was driven by signals that are produced by a group of cells that instructs other cells** (induction phenomenon). These observations lead to the idea that morphogenesis is determined by the formation of spatial patterns following a specific body plan leading to cell differentiation

but how the plan could be established and what were the mechanisms at play remained unclear.

In 1952, Alan Turing presented a theoretical model called the "**reaction-diffusion model**" explaining how spatial patterns can form autonomously, by breaking the symmetry (Alan Mathison Turing, 1952). His model is based on a chemical nature of morphogenesis. In the seminal paper, he studied a system made of two molecules, called **morphogens** ("form producers") that spread out from a source, interact with each other, and have different diffusion rates [Figure 1.A]. He demonstrated mathematically that this system gives six potential steady states and one of the solutions yields the generation of a spatially periodic wave pattern, called **Turing pattern**. In 1972, Geier and Meinhardt showed that the formation of a Turing pattern is only possible if the two molecules correspond to a self-catalyzing activator and an inhibitor with the inhibitor diffusing faster than the activator, resulting in a highly reproducible pattern (Gierer & Meinhardt, 1972; Meinhardt, 2012).

Then, Lewis Wolpert (who passed away this year 2021) came back to the idea of the "Spemann organizer" and based on experiments with hydra, he came up with the concept of **positional information** (Wolpert, 1969). Central to this concept is the idea that there is a cell parameter, its positional value that is related to the position of the cell within the developing tissue. Based on this information, cells sense and interpret spatial gradients of morphogens that are secreted from a group of cells (source) across the tissue and this leads to cell differentiation during tissue development [Figure 1.B].

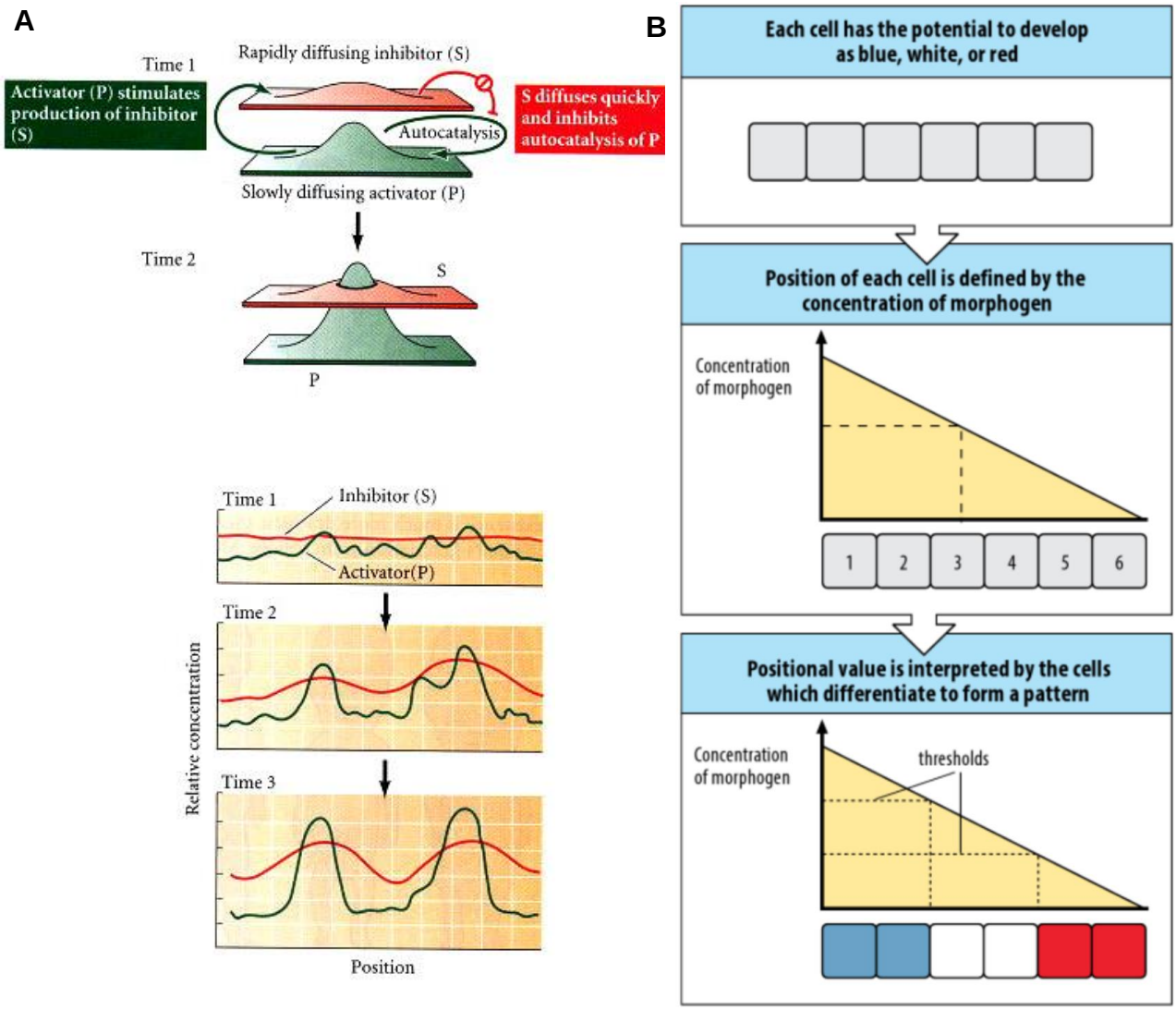

<u>Figure 1. The two theoretical models providing explanations on how tissues can be patterned by chemical cues.</u> (**A**) **The Turing's "reaction-diffusion" model**. *It consists of a system of two interacting morphogens consisting of a rapidly diffusing inhibitor (called S) and an auto-catalyzed slowly diffusing activator (called P). P also stimulates the production of S. Interactions between the 2 morphogens lead to a sharp peak of the activator P and a smaller peak of the inhibitor S. This system leads to self-organizations as the fluctuations of both S and P are random at the beginning but get amplified in order to lead to spontaneous periodic pattern formation.* [from (Gilbert, 2000)] **(B) The Wolpert's model of positional information, the French flag**. *Each cell within the developing tissue acquires positional information based on the sensing of different concentrations of morphogens across the tissue leading to differentiation based on concentration thresholds of morphogens.* [from (Lewis Wolpert et al., 2015)]

1.2 The discovery of genes involved in patterning

Later, numerous studies demonstrated experimentally the evidence that **tissues are patterned by morphogen gradients**.

The first morphogen to be identified was the transcription factor **Bicoid** (Bcd), during early development of *Drosophila Melanogaster* embryos (Driever & Nüsslein-Volhard, 1988). In fact, embryos carrying a mutation in the gene bicoid lack the anterior structures (head and thorax), which are replaced by posterior structures (Frohnhöfer & Nüsslein-Volhard, 1986). Moreover, *bcd* mRNA is produced during oogenesis and is localized at the anterior pole of the embryo (Berleth et al., 1988; Frigerio et al., 1986). After translation, Bcd protein diffuses and controls, in a concentration-dependent manner, the expression of Hunchback and other gap genes, which have been shown previously to be essential for proper embryo segmentation (activating afterwards pair-rule genes and polarity genes) (Driever & Nüsslein-Volhard, 1988; Nüsslein-volhard & Wieschaus, 1980). The mode of action of this morphogen follows the concept of positional information (Wolpert's theory). Therefore, the existence of positional information within the embryo is defined by the cascade activity of different genes leading then to the correct establishment of antero-posterior coordinates for each cell.

After this first experimental evidence, several other morphogens were identified in numerous contexts of tissue morphogenesis. For instance, **Decapentaplegic** (Dpp) acts as a morphogen during *Drosophila* appendage (wing) development (Lecuit et al., 1996). **Wingless** (Wnt family) establishes the dorso-ventral axis of the *Drosophila* wing (Carl J. Neumann and Stephen M. Cohen, 1997) while **Activin** (TGF-beta superfamily) acts as a morphogen during Xenopus mesoderm induction (McDowell et al., 1997).

Moreover, increasing experimental data supports the formation of Turing patterns (self-organization) during development. For instance, **Nodal/Lefty** (from the TGF family) were shown to be a short-range activator/long-range inhibitor system driving left-right asymmetry during zebrafish embryogenesis (Müller et al., 2012) and **Wnt/Dkk** also acts as an activator/inhibitor system during hair follicle differentiation and spacing (Sick et al., 2006).

These studies laid the groundwork for **addressing morphogenesis via genetic and molecular approaches.** The findings in developmental biology at that time, mainly consisted in determining which gene does what, where and when. The information that leads to cell differentiation, and thus to the appropriate cell identity, was revealed to have a chemical nature, controlled by a **precise temporal and spatial progression of gene activities**.

However, even though these discoveries about the critical role of signaling molecules in morphogenesis were essential and fascinating for the fields of morphogenesis and developmental biology, they are not sufficient to explain how the shape of a tissue/organism is established. **What is leading to effective shape changes?** The morphogen concept cannot explain the physical deformation of the cell and, at a larger scale, the whole tissue.

1.3 The essential role of mechanical forces in morphogenesis

1.3.1 Intrinsic and extrinsic forces

Despite its genetic aspect, it is clear that morphogenesis is a physical process in which the three-dimensional (3D) structure of the tissue has to change. For d'Arcy Thompson, the specific form of an object is a "diagram of forces" ("On growth and form", 1917) (Thompson, 1942) and nowadays the fact that mechanical forces generate and establish shape changes is regaining more and more attention (Lecuit & Mahadevan, 2017). Recent technical advances that enable to measure and monitor the forces, in the order of pN to nN, both *in vitro* and *in vivo (*Atomic Force Microscopy (AFM), micropipette aspiration, optical and magnetic tweezers, molecular force sensors…) (Balaban et al., 2001; Sugimura et al., 2016) as well as mathematical modeling and interdisciplinary approaches, have laid to a change in our understanding of morphogenesis. To shape a tissue, there must be **mechanical forces at work that**

can be intrinsic, originating from the cellular structures and/or extrinsic coming from the cell microenvironment that act on the biological system and are essential for its remodeling.

A. Intrinsic force generation

1. Cell contractility

Intrinsic forces correspond to the forces that employ energy consumption (ATP hydrolysis) and are **actively generated** by the cells themselves. This property leads to autonomous cell behavior within a tissue and has been well studied ((Heisenberg & Bellaïche, 2013; Munjal & Lecuit, 2014). Intrinsic forces are mainly driven by the particular organization and contractile cortical forces of the cytoskeletal network within the cell [Figure 2.A].

This cytoskeleton-dependent cell contractility relies mostly upon the activity of molecular motors such as myosins (often non-muscle Myosin II), pulling on the actin filaments (F-actin). This leads to changes in the actin network and to an increase of the **cortical cell tension**. Local regulation of the force generated can be achieved through the assembly and the architecture of the F-actin network as well as by regulating the activity of the non-muscle Myosin II (Lecuit et al., 2011).

Importantly, morphogen gradients and gene activities, described earlier in this chapter, have been reported to widely control the transcription of downstream effectors such as cytoskeleton regulators, emphasizing the interplay between genetics and cell contractility.

Cell contractility is required for proper tissue morphogenesis in several developmental contexts. For instance, it has been shown that forces established by pulsatile cell-autonomous contractility are responsible for the compaction of the mouse embryonic cells prior to the formation of the blastocyst (Jean Leon Maître et al., 2015). In addition, the reorganization of the cytoskeletal network by actin polymerization leads to the formation of membrane protrusions (lamellipodia, filopodia) that are essential in the context of cell migration (Borisy & Svitkina, 2000). Moreover, other components of

the cytoskeleton, microtubules, and intermediate filaments are also essential for the control of cell mechanics and are largely implicated in tissue morphogenesis (Sanghvi-Shah & Weber, 2017; Singh et al., 2018).

2. Hydrostatic pressure

The inward contractile force generated by the actomyosin cytoskeleton is counterbalanced at the single-cell level, by the **internal hydrostatic pressure** (or, in plant cells, the cell wall stiffness is counterbalanced by the **turgor pressure**) [Figure 2.A] (Salbreux et al., 2012; Zonia & Munnik, 2007). Hydrostatic pressure corresponds to the pressure that a confined fluid exerts on its own boundaries. In cells, it is therefore oriented toward the cell membrane, in the opposite direction than the contractile force described earlier.

This intracellular pressure can vary in magnitude either through the establishment of an osmotic gradient (different osmolyte concentrations across the cell membrane and opening of ions transporters) leading to a directional flow of water across the plasma membrane, and therefore changing the water content inside the cell. This will be explored further in later parts of this thesis (see Part 1 section 1.4.2. A). The interplays between all these forces (membrane tension, active contractility, water, and ion flows) can thus alter the shape and morphology of individual cells and therefore participate in the maintenance of the cell shape.

Nevertheless, in multicellular organisms, in addition to intrinsic forces, cells also experience constant physical interactions with their environment. This causes external force application that, in turn, modulates the generation of intrinsic forces. Such interactions can occur with neighboring cells or tissues, the surrounding extracellular matrix (ECM) or with other interfaces specific to each cellular context, for example the blood flow in the case of endothelial cells.

B. External forces

1. Adhesion forces

In their 3D environment, cells are in direct contact with a substrate (ECM) and with other neighboring cells in order to form a continuous tissue and maintain tissue integrity.

Adhesion corresponds mechanically to the establishment of bonds between molecules. **Cell-substrate adhesion** is, in most cases, mediated via integrin molecules and protein complexes called focal adhesions (Gumbiner, 1996). **Cell-cell adhesion** is primarily governed by molecules from the cadherin superfamily (Gumbiner, 1996). Adhesion molecules that make the physical contacts between the cells and their surrounding environment are often directly linked to the cell cytoskeleton, or through other intermediate molecules such as catenins in the context of cadherins (Gumbiner, 1996) [Figure 2.B].

2. The interplay between adhesion and cortical tension

The role of adhesion in morphogenesis is studied for a long time now, starting with the differential adhesion hypothesis (DAH) by Steinberg in 1963 (Steinberg, 1963). This hypothesis relies on the fact that differences in adhesion strength can lead to cell sorting. Steinberg proposes a thermodynamic model of adhesion based on the quantitative differences in the density of adhesion molecules. He demonstrated experimentally that the concentration of the adhesion molecules correlates with the adhesion strength (Steinberg & Takeichi, 1994). However, the forces between cell adhesion molecules alone were later proved to be too weak to explain cell-cell adhesion (Shi et al., 2008). Indeed, by measuring the separation force between two cells, it was revealed that the adhesion force is dependent upon the dynamic coupling of adhesion molecules and the actin cytoskeleton (Chu et al., 2004; Jean Léon Maître et al., 2012). Therefore, the surface tension is a function of both adhesion and cortical tension and the contribution of these two factors is not dissociable. The cortical tension

tends to decrease the cell-cell contact size whereas adhesion acts as a resisting force to active remodeling and will tend to increase the contact between cells. **Adhesion and cortical tension therefore act together, to regulate cell shape and at a larger scale eventually regulate tissue remodeling.**

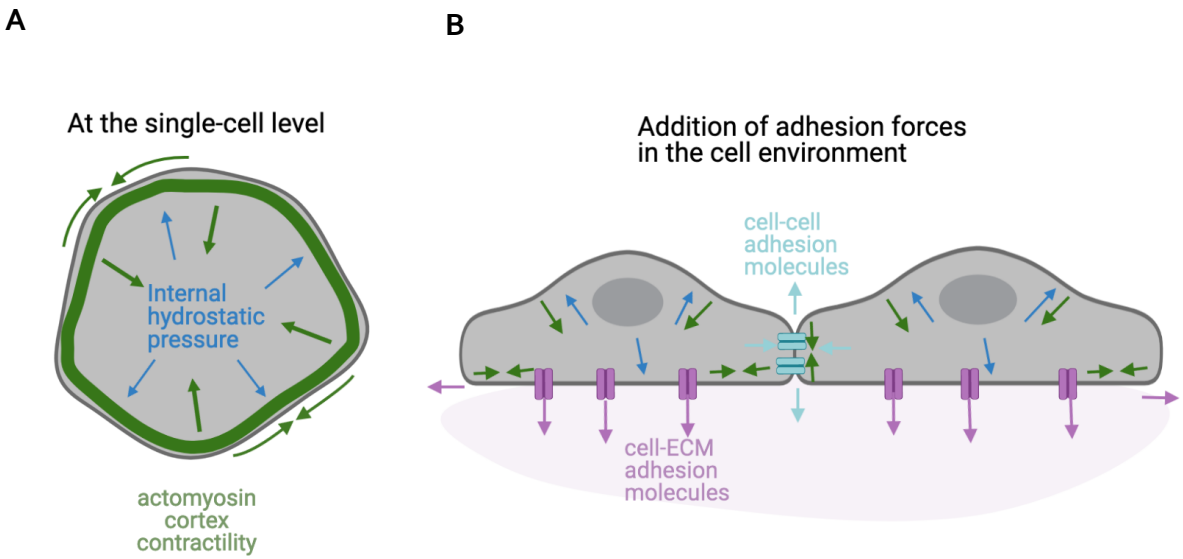

Figure 2: **Mechanical forces at the cellular scale.** (**A**). *At the single-cell level, cortex contractility based on the actomyosin network produces an inward force counterbalanced by the internal hydrostatic pressure of the cell.* (**B**) *On top of the forces presented in A, cells entering in contact with the extracellular matrix as well as the interactions with the neighboring cells will lead to adhesion forces. (Image made with Biorender.com).* [Inspired from the review (Mao & Baum, 2015)]

3. Interactions with the extracellular matrix

Cells anchored to their *in vivo* substrate, the ECM, **pull and apply contractile forces on the ECM and respond according to its resistance**. In fact, cells remodel their cytoskeleton organization and adhesion sites in response to the mechanical properties of the substrate. Thanks to the link between adhesion molecules and the cytoskeleton, cells are able to sense and respond to the mechanical properties of the substrate (Discher et al., 2005).

The ECM is a network composed of different molecules (proteins and sugars) secreted by the cells themselves and constitutes a physical support for the cells. **Depending on the amount and nature of the molecules, the biophysical properties of the ECM are different**. It can contain several types of components but the most frequent ones are: elastic fibers, collagen, glycosaminoglycans (GAGs) such as Hyaluronic Acid (HA), Heparan Sulfate (HS) or Chondroitin Sulfate (CS) (Humphrey et al., 2014) [Figure 3]. Elastic fibers are important mechanically as they confer extensibility and elastic behavior to the tissue, by enabling a recoil to the original shape after mechanical load. Collagens are abundant within the body and confer stiffness and strength to the ECM. GAGs are long polysaccharide chains of high molecular weights that are negatively charged. Inside the ECM, GAGs are linked to core proteins in order to form proteoglycans (PGs). GAGs produce an osmotic pressure and attract water *in vivo* (Comper & Laurent, 1978) thus promoting ECM hydration, which can also contribute to the mechanical load applied onto cells.

The ECM should not be seen as a stable scaffold for the cells. In fact, it is built up during development and the production, degradation, and turnover of all its components play crucial roles during tissue remodeling (Humphrey et al., 2014). ECM degradation can be achieved by specific proteins such as matrix metalloproteinases (MMP), adamalysins and hyaluronidases. These highly dynamic changes can alter the forces exerted onto the cells in contact with the ECM.

Recently, live imaging of *de novo* ECM formation, in Drosophila embryos, revealed that turnover of the basal ECM is extremely rapid (between 7-10 hours). Moreover, in mutants deficient for the metalloproteinase MMP1 the turnover rate was reduced, and this had an effect on tissue morphogenesis (Matsubayashi et al., 2020). Indicating that ECM remodeling is fundamental for the process of morphogenesis.

Furthermore, the ECM contains growth factors and/or signaling molecules that can attach to the plasma membrane by the means of specific receptors and activate different cellular responses. This topic will be developed in the context of the heart morphogenesis where signaling molecules travel between the tissue layers (myocardium, endocardium) and instruct cells (see the Part 2 of the introduction, section 2.3.2. D & 2.4.2). Therefore, the ECM network also plays a role in the signaling between cells composing different tissues.

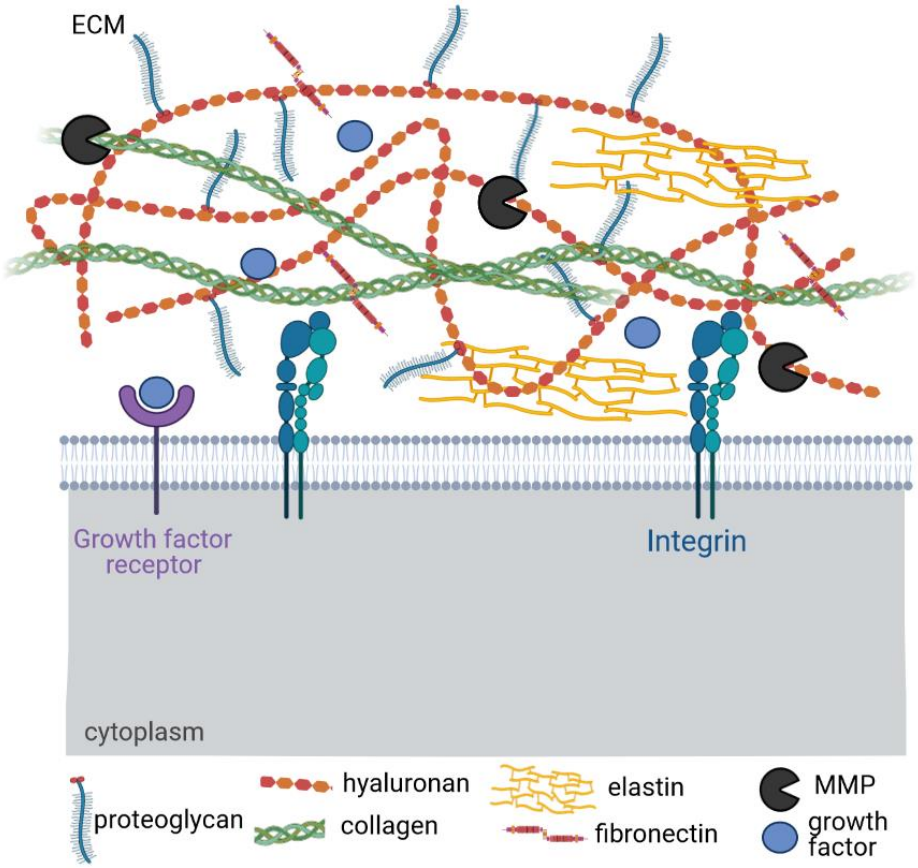

Figure 3: The extracellular matrix (ECM): a complex and highly dynamic network of fibers (collagen, elastin, fibronectin) and GAGs that are linked to core proteins in order to form proteoglycan (PGs). *MMP= matrix metalloproteinase, which can degrade some components of the ECM when needed. The mechanical load coming from the different components of the ECM can be sensed via integrins at the plasma and transduced into the cell. (Image made with Biorender.com).*

4. Additional *in vivo* physical constraints

Moreover, cells can experience additional physical stimuli that will also impact their behaviors. External forces can arise from the presence of fluid flows that apply **shear stress** on the cells. This has a strong implication for shaping tissues throughout development and, in particular during cardiovascular system morphogenesis (Boselli et al., 2015; Freund et al., 2012). Forces generated by increased fluid pressure during lumen expansion also have an impact on tissue morphogenesis (Navis & Bagnat,

2015). Tissues can also experience **stretching** and **compression forces** due to growth or other constraints applied by adjacent tissues (Villedieu et al., 2020)

5. Tissue properties

On top of the force balance encountered in every tissue, the cell and tissue material properties, so-called rheology, also have to be taken considered (Petridou & Heisenberg, 2019). Tissues can behave and deform differently when exposed to intrinsic or extrinsic forces depending on if they have more a solid- or fluid-like behavior. If tissues behave more like solids, they will tend to suffer an elastic deformation, where the initial shape is recovered after force removal. However, if tissues are more fluid-like, they will deform irreversibly.

1.3.2 Force transmission and robustness

The transmission of the intracellular forces to other cells is critical in order to properly sculpt tissues. Effective long-range force propagation happens through adhesion complexes that hold the cells together and maintain them mechanically coupled. The junctions link neighboring cells and their internal actin cytoskeleton. Moreover, other structures, such as **supracellular actin cables** that are encountered in several developing tissues allow efficient force transmission (Röper, 2013). Thanks to these cables, transcellular tension is generated at the tissue-scale, and is fundamental in several morphogenetic events such as epiboly in zebrafish (Behrndt et al., 2012) or even *Drosophila* dorsal closure (Solon et al., 2009).

Recent studies demonstrated that, during the formation of the cephalic furrow (Eritano et al., 2020) and the folding of the *Drosophila* leg (E. Martin et al., 2020) long-range anisotropic mechanical forces generated across the tissue via the planar polarization of the Myosin II play a key role in ensuring **robustness** during morphogenesis in a mechanically noisy environment.

Moreover, after the establishment of the proper shape of a tissue or an organ during development, it is extremely important to maintain this shape even though fluctuating mechanical forces are incessantly applied to the cells composing the tissue. Myosin II polarization is essential for this, by playing a role in **force buffering** (Duda et al., 2019). Indeed, by stretching the wing disc, the authors observed the formation of polarized Myosin II cables that induce tissue stiffening and prevent further changes in shape, thereby buffering force fluctuations.

In the previous sections, we have discussed how intrinsic mechanical force generation, external forces, as well as properties of the environment drive the changes in shape and position of cells, tissue, and organs. However, an additional level of complexity arises when considering that cells also have the ability to sense, interpret and respond to mechanical forces by converting mechanical forces into electrochemical signal via a process called **mechanotransduction**.

1.3.3 Mechanotransduction

Mechanotransduction refers to the process by which a cell can sense external physical stimuli and transduce them into an electrochemical information inside the cells. This can lead to specific gene expression that can influence cell specification and/or morphogenesis.

It is clear from many observations *in vitro* and *in vivo* that cells are able to sense mechanical stimuli and that is important to dictate their identity. For instance, cells subjected to different stiffness of the ECM are specified into different cell lineages: stem cells in contact with soft matrices will commit into neurons whereas the ones in contact with rigid matrices will commit into muscle (Engler et al., 2006).

During mechanotransduction, the forces can be sensed by different molecular components of the cell. Cells can sense variations in magnitude, frequency, and duration of the forces. Major efforts have been put in order to discover the cellular molecules and structures that sense and transduce mechanical stimuli (Petridou et al.,

2017). The majority correspond to components of the cell-cell and cell-ECM adhesion molecules, transmembrane mechanosensitive channels such as stretch-activated channels, cilia and elements of the cytoskeletal network as it is anchored/linked to the adhesion complexes. Cellular mechanotransduction processes will be discussed in more detailed in the context of heart morphogenesis (the topic of this thesis), in section 2.4.1 of the Part 2.

1.4 Collective cell behaviors drive tissue morphogenesis

The cell represents the functional unit composing every tissue. Therefore, to characterize the shape changes of a tissue requires studying what happens at the cellular level. After discussing the interplay between chemical and mechanical processes that underlie tissue patterning and morphogenesis, I will now describe, in this section, the different coordinated cell behaviors that can drive tissue shape changes. This section will provide an overview of specific examples of common stereotyped cell behaviors observed in different morphogenetic contexts and different model organisms: cell shape and volume changes, cell division, collective cell migration, cell intercalation, cell death and cell delamination. It is worth mentioning that the different behaviors are not necessarily exclusive and that usually several act in a concerted fashion in order to properly shape the tissue. The examples are mainly taken from studies performed on epithelia because epithelia usually consist of a monolayer of cells that can be studied in 2-dimensions (2D), making it useful to analyze and quantify cellular features.

The coordination of these different behaviors leads to complex movements at the tissue scale that include for instance folding, invagination, tube formation, and tissue extension or shrinkage. However, this collective dynamic is not just arising from many individual cells that will at some point in development do something different than their neighbors, but it is the result of a coordination of all the cells by reciprocal

interactions and by maintaining the tissue integrity. It is thus not surprising that mechanotransduction at adhesion complexes, discussed in the last section, is pivotal for the tissue cohesiveness and coordinated cell behaviors. The study of cell behavior allows to get a precise understanding of global tissue remodeling. The recent development of multidisciplinary approaches as well as major advances in microscopy, the possibility to perform live-imaging, lineage tracing and the development of performant image analysis tools in combination with simulation/modelling have been key to push this field forward. Moreover, major advances in genetics, with new gene editing technologies, to create mutants, transgenics or even knockdown were essential in the discovery of genes involved in cell behavior changes.

1.4.1 Cell shape changes

Cell shape changes can drive important tissue movements during morphogenesis. The cell shape is determined by the multiple forces acting on the cell surface that have been described earlier in this introduction (the balance between internal and the external forces applied onto the cell as well as the cell rheological properties) and also the geometrical constraints of its environment. Cell shape regulation is governed by genetic pathways as well as mechanics and needs to be tightly controlled during development.

Apical and basal constriction

Cell shape changes have been mostly reported in the context of active force generation by the acto-myosin cytoskeleton that can then lead to a shrinkage of either the apical cell surface area (the most studied mechanism) or the basal cell surface area.

This accumulation of a contractile actomyosin cortex at the apical/basal side of the cell can lead to a reduction of the apical/basal cell surface and the cells will therefore adopt a **wedge shape** (Sawyer et al., 2010). At the tissue level, this change will have some repercussions on neighboring cells and can induce significant tissue

movements, through the cell junctions. In fact, the well-studied mechanism of apical constriction drives the process of invagination during gastrulation (conserved among vertebrates, *Xenopus* and invertebrates *Drosophila*) (Quintin et al., 2008). It has also been involved in the context of tube formation during vertebrate neurulation (A. C. Martin & Goldstein, 2014). Among others, it has also been reported to play a key role in the airway epithelium where it drives the initial budding during monopodial branching in the chick (Kim et al., 2013). Basal constriction has been less frequently reported compared to apical constriction during morphogenesis but is also involved in some contexts such as the zebrafish midbrain-hindbrain boundary morphogenesis (Gutzman et al., 2018) or the optic cup morphogenesis (Sidhaye & Norden, 2017).

However, other cell shape changes mechanisms will be detailed in the subsections about cell division, cell migration, cell intercalation, and cell death. Cell shape changes are considered to be a cell deformation without changes in the intracellular volume. We will see in the next section the implication of cell volume changes which has been less studied and therefore less linked to tissue-scale changes.

1.4.2 Cell volume changes

A. Osmotic pressure

Cell volume is a **highly regulated parameter** within differentiated cells that participate in their physiological homeostasis (Hoffmann et al., 2009). Cells are made of **70% of water** and **30% of dry mass**, which includes ions, proteins, nucleic acids and metabolites. Extracellular compartments are also made of water, proteins and ions. Ions are present in large concentrations within cells depending on the nature of the ion (e.g (K^+)=100mM, (Na^+)=10mM, (Cl^-)=100mM in a mammalian cell (heart or red blood cell)) (Nelson, 2003) and protein concentrations are usually about 20 to 30 times less abundant than ions (Lecuit, n.d.). Specialized transmembrane channels enable the transport of ions down their concentration gradients and also according to the

electrical differences in charge between the intracellular and the extracellular compartments ((-) charges will go towards (+) charges and inversely). For proteins, the lipid bilayer is impermeable to them and they will therefore accumulate in the compartment where they are produced or transported, creating a concentration gradient. A change in the quantity of dry mass within the cell due to increased protein translation can also lead to a modification in the importation of water molecules in order to readjust the osmotic pressure.

Those differences in terms of ion/protein concentration between the intracellular and the extracellular compartments will create **osmotic pressure**. In fact, as other components, H_20 molecules will also move via diffusion from regions of low concentration of ions/proteins to regions of large concentration of ions/proteins. The osmotic pressure can be defined as the pressure needed to be applied in order to avoid a water influx or efflux and depends only on different osmolyte concentrations across the semi-permeable plasma membrane.

The amount of flow of water, that will dictate cell volume, is determined by two forces, the **hydrostatic pressure, p** and the **osmotic pressure, π,** such as:

$$J_{water} = k\,(\Delta p - \Delta \pi)$$

where J_{water} represents the flow of water, and k, the filtration coefficient.

At steady state, there will be no flow of water, ie. $J_{water}=0$, when $\Delta p=\Delta \pi$.

The steady state cell volume is maintained through the activity of different transmembrane channels at the plasma membrane. Among them, active pumps are key in establishing a constant membrane potential across the cell membrane (Hoffmann et al., 2009) [Figure 4]. One major actor is the Na^+K^+ ATPase that moves 3 Na^+ out of the cell and 2 K^+ inside the cell at the cost of hydrolyzing one ATP molecule. Together with other active pumps that move ions against their concentration gradients, they maintain a constant ion concentration disequilibrium between the interior and the exterior of the cells. For instance, a large concentration of Na^+ outside of the cell and

a large concentration of K^+ inside of the cell are crucial for cell volume maintenance (Mongin & Orlov, 2009) (Lecuit, n.d.).

However, when the cell experiences major perturbations in intracellular or extracellular ion/protein concentrations, water influx or efflux will lead to cell volume increase (i.e swelling) or cell volume decrease (i.e shrinkage).The rate of water movements can be significantly enhanced via the presence of passive transmembrane aquaporins (AQPs) that increase the membrane permeability to water, as it has been characterized in astrocytes (Mola et al., 2016). It has also been quantified *in vitro* in HeLa S3 cells that the expression level of AQP4 protein anchored at the plasma membrane increases the permeability to water from 0.83 um/s to 2.7 um/s, measured by using Coherent Anti-Stokes Raman Scattering (CARS) microscopy (Ibata et al., 2011). Moreover, more and more studies focus on understanding the osmosensing mechanisms within the cell (Hoffmann et al., 2009). For instance, the well-established stretch-sensitive channel TRPV4 (Arniges et al., 2004; Hoffmann et al., 2009b; Liedtke et al., 2000; Strotmann et al., 2000) has been reported to play a role as an osmosensitive channel.

As cell size changes can significantly affect the physiological properties of the cell, mechanisms of Regulatory Volume Decrease (RVD) (controlled through VRAC channels among other ion channels) or Regulatory Volume Increase (RVI) (controlled through the NHEI channel among other ion channels) will in most cases rapidly mediate the recovery of the initial cell size (Jentsch, 2016).

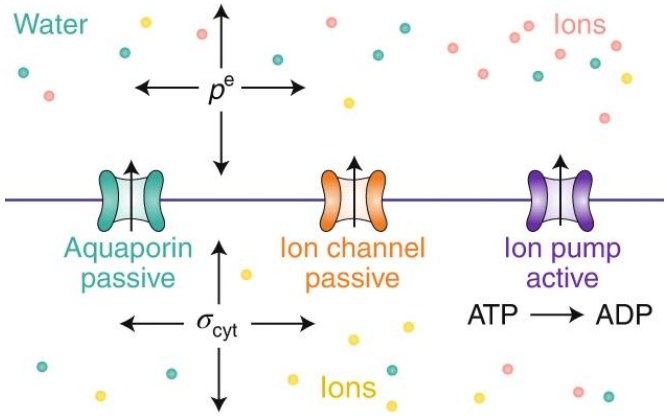

Figure 4: Main players during osmotic imbalance across the plasma membrane. *Aquaporin channels are passive transmembrane channels that can enhance the permeability of the membrane and therefore increase the rate at which water influx or efflux can take place. Passive ion channels can move ions across the plasma membrane according to their concentration gradients. Active ion pumps use the hydrolysis of ATP in order to move ions against their concentration gradients.* [Image taken from (Cadart et al., 2019)]

B. Examples of tissue remodeling

Recent papers shed light on the importance of cell volume changes as a **driver of tissue remodeling**. In the *Drosophila* embryo the amnioserosa (AS) cell volume decrease leads to the generation of contractile forces that pull on the whole epiderm to drive dorsal closure (Saias et al., 2015). Mechanistically, cell volume decrease is based on caspase activation and ion fluxes through the K^+ ion channels (demonstrated by specific inhibition of K+ channels by TEA, a K^+ channels inhibitor) (Saias et al., 2015). Cell volume changes are also involved in the epithelial morphogenesis of the Kuppfer's vesicle (KV) (the transient left-right organizer in the *Zebrafish* embryo) (Dasgupta, Merkel, et al., 2018). Here, asymmetric cell volume changes (anterior cells become larger while the posterior cells become smaller) are also mediated by ion fluxes. Indeed, by incubating zebrafish embryos with either a chloride channel inhibitor or Ouabain to inhibit the Na+K+ATPase pump, authors could abolish these cell volume changes. Another recent study demonstrated that enterocyte cell swelling drives lumen shrinkage in intestinal organoids (Yang et al., 2020). The authors identified the SGLT-1 (sodium/glucose transporter channel) involved in the establishment of the osmotic

gradient and aquaporins as key players for the H_2O influx from the lumen (by inhibiting their activity using CuSO4 (Copper) (Yang et al., 2020).

The fact that only a few studies tackle cell volume changes *in vivo* in 3D environments can mostly be explained by the difficulty in precisely quantify the cell volume. *In vitro* studies (on adherent and suspended cells) developed methods in order to accurately quantify the cell volume through Fluorescence Exclusion microscopy (FXm) (C. Cadart et al., 2017; Zlotek-Zlotkiewicz et al., 2015). Furthermore, in the same study, quantitative phase microscopy was used to determine if the shrinkage/swelling of the volume is a consequence of a loss/gain of dry mass or a loss/gain of water (Zlotek-Zlotkiewicz et al., 2015). Unfortunately, those techniques still need to be optimized or other techniques need to be developed in order to precisely quantify cell volume changes in living organisms. Altogether, cell volume regulation recently became an intensively investigated question, but little is known about the contribution of cell volume changes in organogenesis as well as how it is regulated by environmental cues.

Altogether, these publications emphasize the role of cell size changes in tissue remodeling. It would be interesting to decipher more and more the role that external mechanical forces applied on cells play in these processes.

C. The importance of cell proliferation for cell size

Independently of the osmotic pressure, cell size regulation is also influenced by cell proliferation. Indeed, cell proliferation is tightly linked to cell growth, since a controlled balance between both processes is required to maintain cell size homeostasis. Depending on the cells/organisms and the situations considered, the complex relation between cell division and cell growth has been explained by different theoretical models: the ‘sizer’, the ‘adder’ and the ‘timer’ models [Figure 5.A] (Jones et al., 2019).

The sizer refers to the theory that the cell will not start to divide before having reached a threshold size, thus this could lead to robust cell size control [Figure 4.A].

The idea behind the ‘adder’ model is that the same amount of mass will be added in between each cell division [Figure 5.A]. The last one, the ‘timer’, is based on the idea that cells could start dividing after a certain amount of time, regardless of their growth state [Figure 5.A]. All those mechanisms enable cell size homeostasis by coordinating cell division and cell growth.

However, in several developmental contexts, cell proliferation and cell growth could somehow be dissociable from each other. For example, extracellular signals such as mitogens or growth factors, can independently promote either cell division or cell growth, respectively. Moreover, this decoupling between growth and proliferation is also observed in developmental contexts. In the first-cell stage (egg cell), cells divide without growing. On the contrary, post-mitotic neurons grow without dividing (Lloyd, 2013). In *Drosophila*, inhibiting cell proliferation (by targeting Cdk1, Cdc25 or E2F) in a portion of the wing disc leads to the absence of defect in final size compared to the part of the wing disc that was not affected. Indeed, the abolishment of cell proliferation was compensated by an increased cell growth thus leading to larger cells. (Katrin Weigmann, 1997; Neufeld et al., 1998; Su & O’Farrell, 1998) [Figure 5.B]. On the other hand, in the same developmental context, increasing the cell proliferation leads to a normal final tissue size that is composed of smaller cells, demonstrating that the tissue compensates by decreasing cell growth (Neufeld et al., 1998; Su & O’Farrell, 1998) [Figure 5.B]. This uncoupling between cell proliferation and cell growth enables to maintenance of the overall tissue size homeostasis. Therefore, the **development of appropriate tissue size can be independent of cell proliferation but involves changes in cell size.**

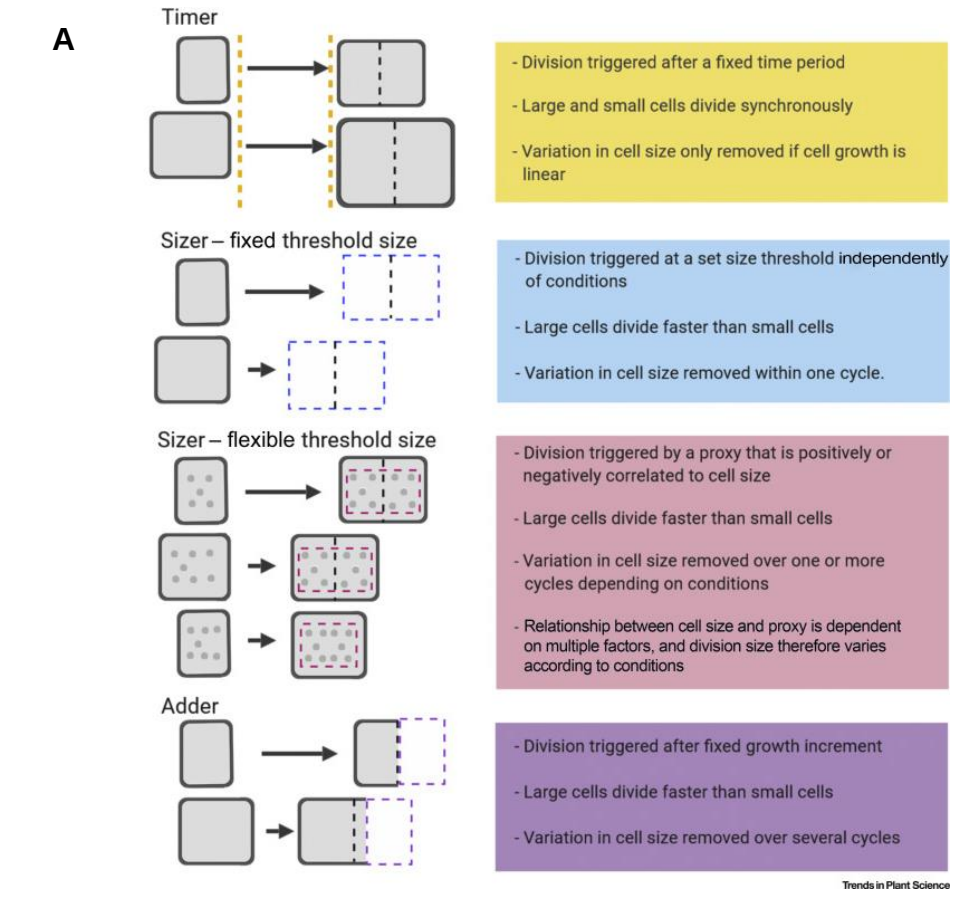

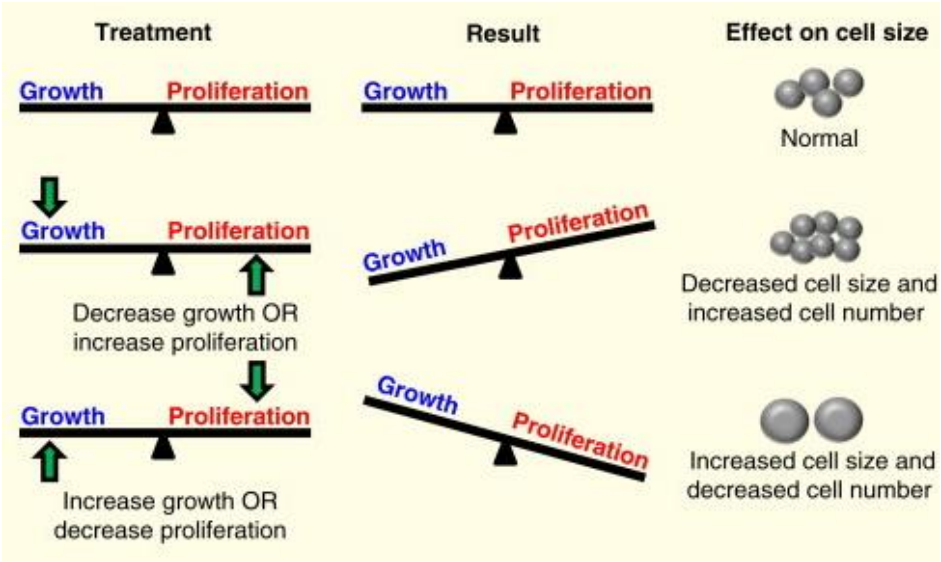

Figure 5: The importance of cell division and cell growth in the regulation of cell volume. (**A**) *The different models to explain cell size control: Timer, Sizer, Sizer-flexible threshold size and adder* [from (Jones et al., 2019)] (**B**) *Cell size homeostasis when cell growth and cell proliferation are well balanced (top panel) Disturbing the balance between cell growth and cell proliferation results in final cell size changes (middle and lower panel).* [from (Wright & Schneider, 2014)]

Cell division also plays additional roles during morphogenesis and in particular during anisotropic tissue growth, as discussed in the following section.

1.4.3 Cell proliferation

Tissue shape emergence implies the regulation of local tissue growth. Tissue growth can be explained by cell shape changes that can be anisotropically distributed between several regions or by **oriented cell proliferation**. Alternatively, **different rates of proliferation** across the whole tissue can also drive the establishment of differential zones of growth within the developing tissue.

Oriented cell proliferation has been involved in a large number of morphogenetic contexts: in the gastrulation of the zebrafish, where oriented cell division along the animal-ventral axis, in synergy with the Hippo pathway, drives the axis elongation (Gong et al., 2004). In the *Drosophila* wing disc, the cell divisions are aligned with the tissue-scale main axis of mechanical stress in order to achieve a polarized tissue growth (also associated with Hippo signaling) (LeGoff et al., 2013). In the *Drosophila wing* imaginal disc, the cells localized in the center of the wing pouch divide along the proximal-distal (P-D) axis, whereas the cells localized in the periphery do not follow the same behavior as the central cells but divide perpendicularly to the P-D which is dependent upon **differential proliferation rates** (Mao et al., 2013).

In addition to those anisotropy in cell divisions within a tissue, dividing cells also change shape by rounding up, a process called "**mitotic rounding**". This cellular feature has been shown to be key in accelerating the invagination of the *Drosophila* tracheal placode (Kondo & Hayashi, 2013). Moreover, mitotic rounding generates a loss of cell-contacts within the central blastoderm cells in zebrafish, driving a **tissue fluidization** which is necessary for the spreading over the yolk sac ('doming' process) (Petridou et al., 2019).

Cell division is therefore key in orienting tissue growth but additional behaviors such as migration and intercalation, exposed in sections 1.4.4 and 1.4.5, respectively, can also lead to the net displacement of the cells.

1.4.4 Polarized collective cell migration

At the single-cell level, cell migration is characterized by cell shape changes associated with the protrusion of **lamellipodia** driven by the polymerization of F-actin, or alternatively by **blebbing**, due to the internal hydrostatic pressure generated by the cortex (Paluch & Raz, 2013).

Within a tissue, the coordinated migration of groups of cells that drive cell movement is referred to as **collective cell migration**. During collective migration, the cells move as a block rather than individually. This coordinated motion will lead to tissue remodeling during different contexts of embryonic morphogenesis, as well as tissue repair (e.g. wound repair) or cancer invasion (Friedl & Gilmour, 2009). Cells have to remain physically and functionally connected by adherens junctions in order to achieve coordinated tissue movement (Carmona-Fontaine et al., 2008). The direction of collective cell migration is set by chemotaxis, such as chemokine or growth factors gradients, or by mechanotaxis, such as the substrate stiffness gradients (Barriga et al., 2018). Recently, topology of the external environment has been revealed as another cue to direct cell migration (Bajanca et al., 2019; Caballero et al., 2015; Lo Vecchio et al., 2020).

In the context of collective cell migration, cells acquire two distinct identities: the leader cells, which are positioned at the front edge or at the tip and drive migration, and the follower cells right behind. The leader cells exhibit a highly dynamic actomyosin cytoskeleton and show protrusive activity mediated by actin and myosin, dependent on the activity of RhoGTPases such as Rac or Cdc42 (Zegers & Friedl, 2014).

To illustrate collective cell migration during embryo development, I chose to develop the example of primary branching morphogenesis during tracheal

development in *Drosophila Melanogaster.* Tracheogenesis is interesting as it occurs without cell division so the movement cannot be driven by cell proliferation (Samakovlis et al., 1996). It is described that tissue movement is driven by collective migration following a chemoattractant. Branchless (Bnl), a fibroblast growth factor (FGF)-like ligand, is expressed in non-tracheal cells adjacent to the location where cells will migrate to form branches and act as a chemoattractant (Sutherland et al., 1996). Tracheal cells form highly dynamic protrusions called filopodia induced by the activation of the Bnl/FGF signaling cascade (Ribeiro et al., 2002). The tip cells (leading cells) sense Bnl/FGF and migrate towards the source, and tube-forming stalk cells (follower cells) follow those tip cells to form a tube during tracheal branching morphogenesis.

The elongation of the tube then, is then by stalk-cell intercalation (Caussinus et al., 2008), this cellular behavior is further discussed in the next section.

1.4.5 Cell intercalation

Cell intercalation refers to the exchange of cell neighbors within the tissue. This is possible through the remodeling of the cellular junctions leading to the loss of contacts with the neighbouring cells in one direction and the creation of new contacts in the perpendicular direction. This topological transition is called: **T1 transition** [Figure 6] and is based on the polarized activity of Myosin II (Bertet et al., 2004).

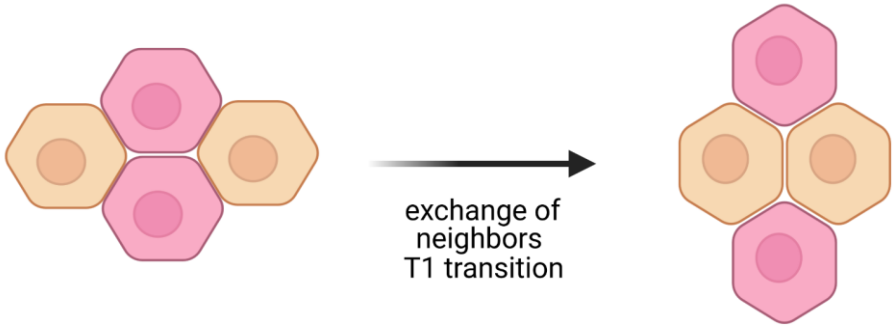

Figure 6: T1 transition: topological changes within the developing tissue. *The pink cells are not neighbors anymore through the T1 transition whereas the orange cells become neighbors. (Image made with Biorender.com)*

This behavior drives the process of **convergence-extension**, in the well-studied example of *Drosophila* germ-band extension (Bertet et al., 2004). In fact, cell intercalations can dictate the directionality of tissue shape changes if they are polarized and irreversible. Thus, leading to tissue shrinkage in one direction and tissue elongation in the orthogonal direction. Moreover, during **tubulogenesis** (the change from a flat epithelium towards a tube) of the salivary gland in *Drosophila,* radially-oriented cell intercalations drive the invagination in association with apical constriction (Sanchez-Corrales et al., 2018). In addition, left-right asymmetrically polarized Myosin II leads to cell intercalation driving **directional cell movement** during the clockwise rotation of the *Drosophila* genitalia development (Sato et al., 2015).

Interestingly, topological changes that can be induced either by cell intercalation or by cell division can play a role in **dissipating the mechanical stress** present within the developing tissue. An example can be found during spreading of the enveloping cell layer , in Zebrafish epiboly, where cell division is key in order to release mechanical stress (Campinho et al., 2013).

1.4.6 Cell apoptosis

Apoptosis is a biological process by which a cell will undergo programmed cell death. The apoptotic cell will exhibit a cell shape change through an apical constriction leading to a “rosette” configuration (topological change) of the neighboring cells and will then be extruded from the tissue [Figure 7.A-B]. Recently, apoptotic forces were revealed to be the drivers of tissue movements during morphogenesis. In *Drosophila* dorsal closure, apoptotic cells within the AS pull on the surrounding neighbors resulting in closure [Figure 7.A]. In fact, by either reducing apopotosis, via the anti-apoptotic caspase-supressor *p35,* or by enhancing apoptosis with pro-apoprotic *grim*, specifically within the AS cells, either slows down or speeds up the rate of the cell-sheet movement (Toyama et al., 2008). Another example was recently reported in *Drosophila* embryos but in the context of epithelium folding of the leg morphogenesis (Monier et al., 2015) [Figure 7.B]. Apoptotic cells exert pulling forces on their neighbors, which propagate through the whole tissue and increase the tissue tension, triggering folding. Interestingly, ectopically inducing apoptosis led to ectopic fold formation, reinforcing the key role of apoptosis-driven forces in tissue shaping (Monier et al., 2015).

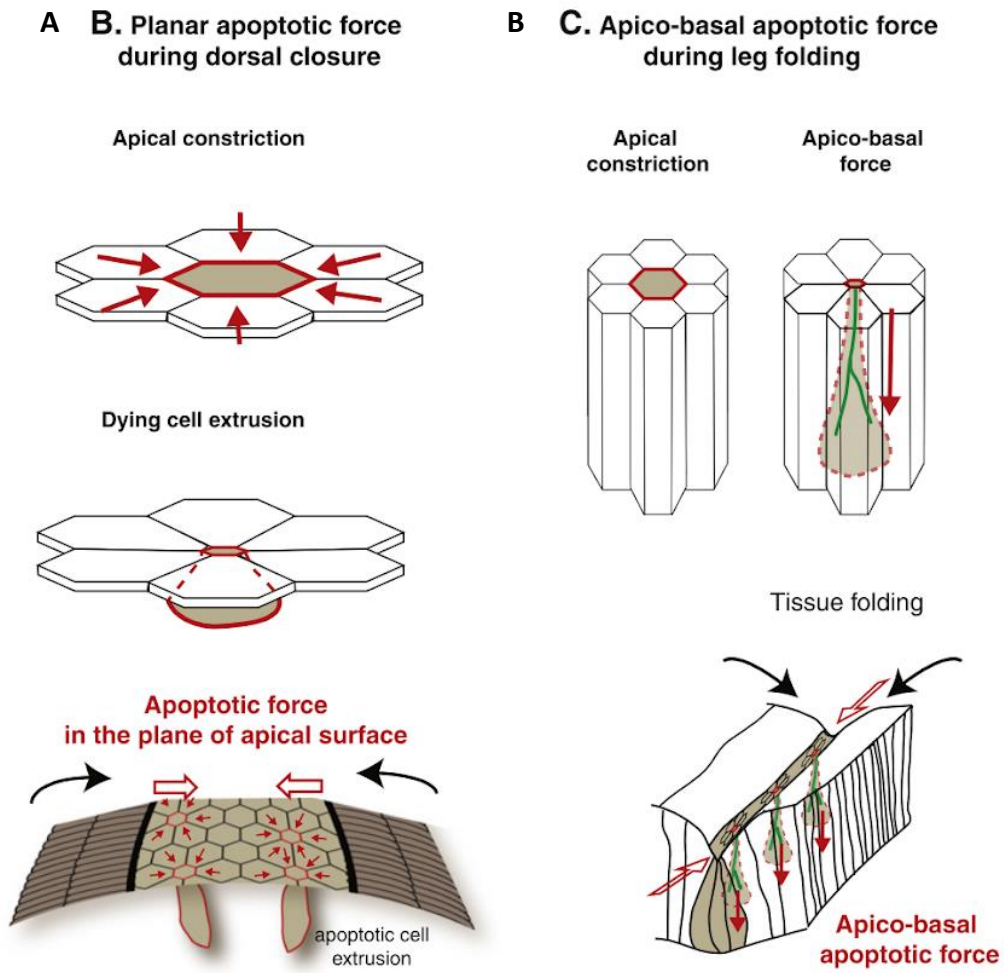

<u>Figure 7: The importance of apoptotic forces in tissue movement.</u> ***(A)*** *Apoptotic forces generated by cells within the amnioserosa lead to dorsal closure in Drosophila embryos.* ***(B)*** *During Drosophila leg morphogenesis, transient apoptotic forces pull on their neighbors, increasing the tissue tension and driving tissue folding.* [from (Ambrosini et al., 2017)]

Altogether, we have seen in Part I that morphogenesis is a spatio-temporally controlled process that include patterning and gene expression as well as intrinsic forces generation and sensing of extrinsic forces. The interconnection and feedback between biochemical signaling and mechanical processes lead to collective cellular behaviors driving effective tissue shape changes.

2 The cardiovascular system:

function, anatomy, embryonic development, and mechanogenetic interplay

In the first part of this introduction, I discussed the interplay between genetics and mechanical forces that drives shape emergence. Multicellular organisms develop by two morphological processes: **gastrulation** and then **organogenesis**, where the three germ layers (endoderm, ectoderm, and mesoderm) of the embryo give rise to the different organs of the body. Organogenesis is a complex phenomenon as it requires the action of multiple morphogenetic and patterning processes and proper cell differentiation, the latter of which allow cells to perform specified functions, such as contraction in the case of muscle cells or be electrically excitable in the case of neuronal cells. The organ needs to morph into a given morphology and is made of several types of tissues that will together enable its physiological function and therefore also sustain the organism's homeostasis.

The heart is one of the first functional organs during embryonic development. In humans, it starts beating around 22-23 days in the foetus, and shortly after, blood flow is initiated throughout the whole body. However, at this early stage of development, its morphogenesis is not finished and will continue while the heart is beating. **Therefore, tissues composing the developing heart and vessels are permanently exposed to external forces (caused by heart contraction and blood flow) and these forces have been shown to be necessary for proper shape establishment and remodeling** (discussed in 2.3.2). Studying cardiovascular morphogenesis thus offers an ideal model to better understand the interplay between mechanical forces and gene expression driving morphogenesis during embryonic development. First, I will describe the cardiovascular system, its function, its anatomy, and congenital diseases associated with defects during cardiovascular morphogenesis (Section 2.1). After, I will review the main steps underlying cardiovascular development (Section 2.2). Then, we

will see the importance of myocardial-generated mechanical forces in proper shape establishment (Section 2.3) before focusing on the morphogenesis of the Atrio-Ventricular Canal, which corresponds to one of the sites of valve formation (Section 2.4).

2.1 Overview of the cardiovascular system

2.1.1 Physiological function

In vertebrate organisms, the cardiovascular system is a **closed circulatory system** that transports oxygen (by the means of red blood cells) and nutrients to the different organs and also removes waste from tissues. Cardiac function is required from the early stages of development, thus explaining why the heart is one of the first organs to acquire its function. Blood motion is also necessary to transport agents of the immune response (white blood cells) and platelets that are necessary for blood clotting (Rogers, 2010). The blood compartment represents an approximately fixed volume which does not leave the network of vessels (arteries, veins, capillaries) and this generates high hydrostatic pressure that is efficient for metabolic supply and gas exchange. Mammal and birds' hearts have four chambers and a double circulatory system, with the flow of blood in the **systemic circuit and the pulmonary circuit** [Figure 8]. In the systemic circuit, oxygenated blood is ejected by the heart through the aorta [Figure 8.A] and then goes through the different organs and the oxygen-depleted blood goes back to the heart via the vein network. In the pulmonary circulation, oxygen-depleted blood exits the heart through the pulmonary artery [Figure 8.A], is reoxygenated by the lungs, and this re-oxygenated blood goes back to the heart via the pulmonary vein. However, fishes (e.g zebrafish) just have a **2-chambered heart and a single circulatory system** where blood leaves the heart, is oxygenated by the gills, goes to the different organs, and comes back to the heart in an oxygen-depleted form [Figure 8.B]. Invertebrate organisms (mollusks, arthropods), on the contrary, present an open circulatory system that generates low hydrostatic pressure. For

instance, *Drosophila Melanogaster* has a pump (tube-like heart) that delivers hemolymph (interstitial fluid) throughout the body (Rotstein & Paululat, 2016). This less efficient system is sufficient for insects as it just supplies organs with nutrients, and gas exchanges are made through a specialized system, the trachea.

2.1.2 Histo-anatomical features

A. Heart chambers and valves

Both the different types of chambers (atrium, ventricle) and the different types of vessels (arteries, veins) have distinct anatomical features, which are adapted for the efficient circulation of blood throughout the body.

The heart within the body is surrounded by the pericardial cavity, which protects the organ. The heart is made of two types of chambers, which are called **ventricles** and **atria**. The atrium corresponds to the collecting chamber whereas the ventricle will pump the blood into the vascular system. The cardiac cycle comprises two distinct phases: **diastole,** when the cardiac muscle relaxes to let blood flow inside the ventricle, and **systole,** when the ventricular chamber contracts to propel the blood into the circulation. The mammalian heart includes two distinct halves for its double circulation system: two right chambers (a right atrium and a right ventricle) located before the lungs and two left chambers (a left atrium and a left ventricle) placed after the lungs. The multiple chambers of the heart are separated by a set of valves.

The valves are essential structures that **maintain an efficient unidirectionality of the blood flow by avoiding blood retrograde flow during the cardiac cycle.** Mammals therefore present four different valves (Tricuspid and Pulmonary valves on the right side of the heart, and Mitral and Aortic valves on the left side of the heart) [Figure 8.A]. Zebrafish, the vertebrate organism model that has been used in this thesis, has only two chambers (one Atrium and one Ventricle) and has three sets of bicuspid valves separating the atrium and the ventricle, the **Atrio-Ventricular canal (AVC) valves** that correspond to the Mitral valves of mammals and the **Outflow tract**

(OFT) valves at the exit of the heart that corresponds to the pulmonary and aortic valves [Figure 8.B] (Beis et al., 2005; Duchemin et al., 2019).

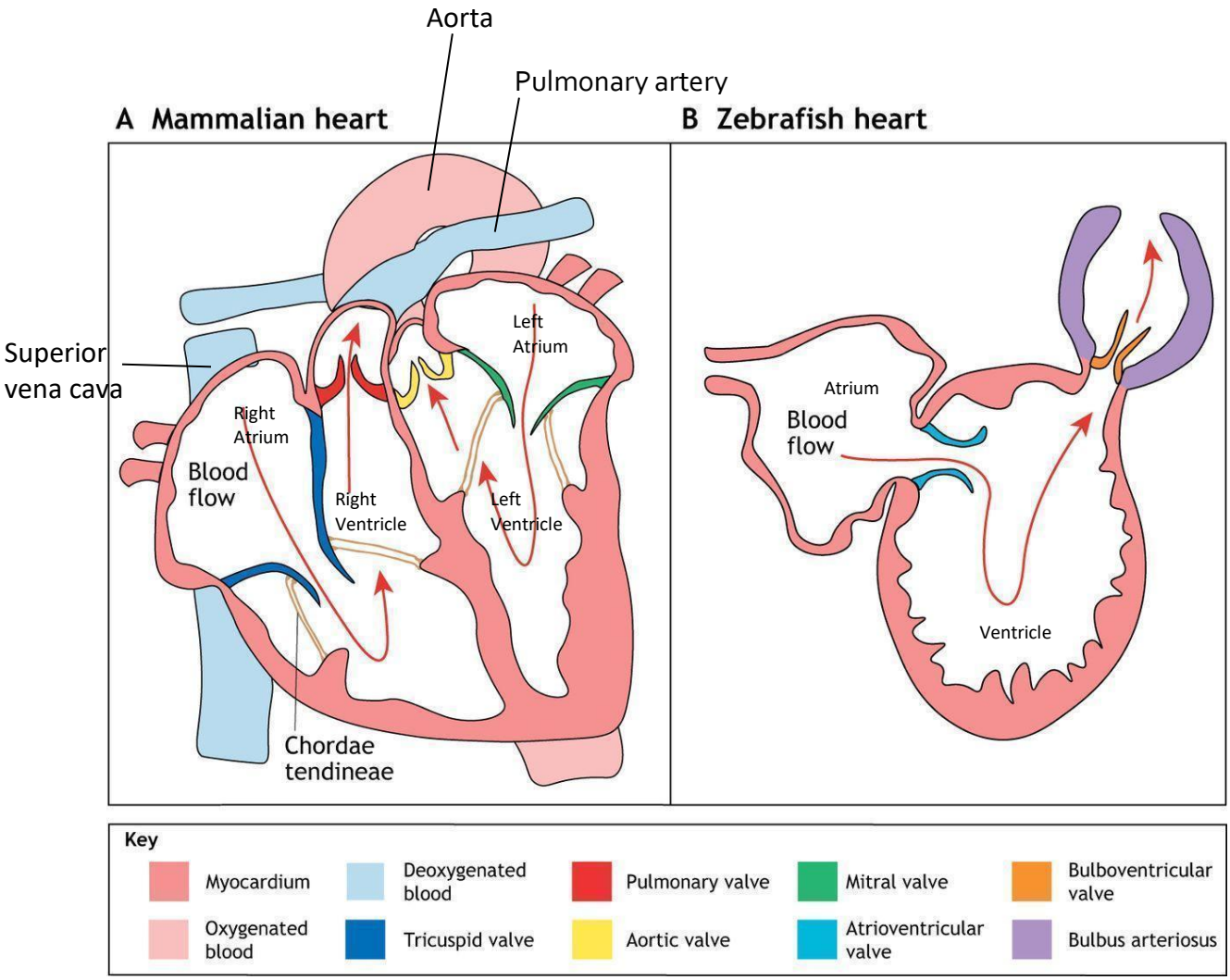

Figure 8. Anatomy of the heart: differences between mammalian heart and the zebrafish heart. (**A**) *The mammalian heart consists of two separated halves made on both sides of an atrium and a ventricle (4 chambers in total), separated by different valves.* (**B**) *The Zebrafish heart is simpler due to its single circulatory system and thus includes only one atrium and one ventricle, separated by valves. The red arrows represent the blood flow direction.* [adapted from (O'Donnell & Yutz, 2020)]

B. Tissues composing the heart

At the tissue-level, the heart is composed of three main tissues that are myogenic (myocardium) and non-myogenic (epicardium and endocardium). The outer layer is the **epicardium**, which is made of mesothelial cells. The epicardium plays several important roles during development, most notably for myocardial growth and coronary vessel patterning, and is also involved in cardiac repair (Quijada et al., 2020). The **myocardium** is the middle tissue layer and is made of contractile cells called cardiomyocytes that are responsible for the contraction of the heart. Some myocardial cells are specialized and form the **conduction system,** allowing the propagation of the electrical wave through the myocardium (Kennedy et al., 2016). The last layer, the inner layer of the heart, corresponds to the **endocardium**. This layer is made of specialized cardiac endothelial cells that experience quite unique mechanical forces that are applied on them due to their direct contact with the blood flow as well as the contraction of the heart (Haack & Abdelilah-Seyfried, 2016). An elastic extracellular matrix, called the **cardiac jelly**, lies between the myocardium and the endocardium and is deprived of cells. During heart development, the differentiation of these three different tissues is spatially and temporally controlled.

C. Congenital diseases associated with cardiovascular defects

The complex morphogenetic process of cardiac development, resulting from cell fate specification, interaction between different tissues as well as mechanosensing/ mechanotransduction, implies that any defects during its development could lead to malformations and could alter its function.

Congenital cardiomyopathies have an incidence of 5 out of 1000 births (FRM numbers). Amongst the different cardiac diseases, valvulopathies are frequent and are due to defects of the valve structures impairing their function. Most cases of valvulopathies either result in stenosis, where blood flow cannot pass through the valve region due to obstruction, or in regurgitation, where the valves incompletely close at each cardiac cycle leading to a retrograde blood flow between the chambers. Most of the time, the deficient heart valves need to be surgically replaced in order to maintain

the proper function of the heart. These defects are found mainly to affect the aortic and mitral valves (bicuspid aortic valve (BAV), calcified aortic valve disease (CAVD), myxomatous mitral valve disease (MMVD)) (Bäck et al., 2013; Hinton & Yutzey, 2011). They can originate during embryonic development (based on genetic mutations or abnormal hemodynamic forces linked to abnormal valve structure) or can be the result of the abnormal reactivation of developmental signals during adulthood (LaHaye et al., 2014).

BAV is due to the abnormal development of the aortic valve that comprises 2 leaflets instead of 3, leading to an impaired structure of the valve.

CAVD occurs when the aortic valves get thicker and calcified. This defect happens progressively and can eventually lead to the obstruction of the aortic valve (stenosis), so blood flow cannot travel from the left ventricle to the aorta. Interestingly, the well-organized structure of the valve ECM was found to be disrupted and presented higher levels of collagens and proteoglycans in explanted diseased valves from pediatric patients (Hinton et al., 2006). This over-production of ECM can be explained by the increased mechanical stress applied to the valve.

MMVD, which happens at the mitral valve, leads to thicker valves inducing regurgitation. In MMVD, it has also been reported that the structure of the ECM is impaired (increased level of proteoglycans, and disruption of collagen and elastin fibers) (Aupperle & Disatian, 2012).

The study of these defects in numerous animal models has shown that inhibition of Notch signaling (for BAV and CAVD), GATA5/ GATA6 (for BAV), cilia (for BAV and MMVD), and filamin A (for MMVD) are associated with developmental defects (LaHaye et al., 2014). Therefore, more and more studies associate genetic mutations with the development of phenotypes that resemble human diseases.

However, numerous congenital heart diseases have not been associated with genetic origins or environmental causes (Levine et al., 2015). Additional non-genetic factors might play a key role in the development of cardiac defects during embryogenesis. Therefore, it is important to understand better how those defects occur during development in order to develop new therapeutic treatments or to get new insights for the regenerative medicine. Recently, the zebrafish model organism became key to study severe cardiovascular defects as well as the importance of mechanical forces and blood flow during embryonic development of the vertebrate

cardiovascular system. Its main advantages for the study of cardiovascular morphogenesis will be discussed in the next section.

2.2 Embryonic development of the vertebrate cardiovascular system

2.2.1 Zebrafish, a powerful vertebrate model to study cardiovascular defects

Studying the specific genetic programs as well as the contribution of blood flow and heart contraction in mammalian models (mice, rat, chicken) is really challenging due to early lethality during embryonic development caused by severe cardiovascular defects (Brown et al., 2016). This is one of the reasons why the vertebrate model *Danio Rerio,* a teleost fish belonging to the *Cyprinidae* family, became from the 1990s a widely used vertebrate model organism for the study of cardiovascular development. In fact, among its numerous advantages, thanks to the small embryonic size at early stages of development, oxygen supply throughout the whole body is achieved just through simple diffusion. This enables studies of severe cardiac defects as they are able to **survive for a few days even in the absence of heart contraction and resulting blood flow** (D. Y. R. Stainier et al., 1996). Moreover, the **extra-uterine fertilization** enables the manipulation and injection of compounds into fertilized eggs at the first-cell stage. Also, due to the optical embryo transparency (improved by the addition of 1-phenyl 2-thiourea (PTU) at 8 hpf in the fish water), it is possible to **easily image the internal organs at cellular resolution** [Figure 9]. Zebrafish development is relatively quick compared to other vertebrate model systems (D. Y. R. Stainier, 2002). Moreover, it represents an interesting model for genetic studies. Indeed, its genome has been fully sequenced and well-annotated, and around 70% of the human genes have an ortholog into the zebrafish genome (Howe et al., 2013). However, due to a whole-genome duplication event that happened during evolution at the teleost

radiation, the zebrafish genome often contains several paralogs of the same gene (Howe et al., 2013).

To address gene function during development, Morpholino antisense oligonucleotide (MO)- based approach has been widely used and is now becoming controversial as phenotypes that were often found in the morphants were not found in the corresponding mutants, raising the question of the specificity of the MO approach (Kok et al., 2015; D. Y. R. Stainier et al., 2017). This is why, within the Zebrafish community, researchers are relying more and more on gene knock-down methods based on genetic editing through the CRISPR-Cas9 or TALEN technologies.

Several large-scale forward and reverse genetic screens have been successfully conducted in the zebrafish based mainly on Ethylnitrosurea (ENU)-mediated mutagenesis (resulting in the generation of random mutations inside the genome) (Alexander et al., 1998; Chen et al., 1996; W. Driever et al., 1996; Haffter et al., 1996). These screens led to the identification of a multitude of genes involved in cardiac formation and result in phenotypes close to cardiac defects seen in humans (D. Y. R. Stainier et al., 1996).

Overall, the zebrafish is a powerful model to study the development of the cardiovascular system. Since I used the zebrafish as the model organism for my thesis, for the following sections of Introduction Part 2, I will mostly focus on the key steps of early heart development in the zebrafish.

Figure 9. Bright-field image of a zebrafish embryo at 48hpf

2.2.2 Heart development in zebrafish

A. From cardiac progenitors to the primitive heart tube

As presented above, the zebrafish has a simpler heart (composed of only two chambers) compared to mammals but the key steps of heart development are known to be conserved (Staudt & Stainier, 2012).

The primitive heart tube originates from two bilateral pools of cardiac progenitor cells that are specified within the **Anterior Lateral Plate Mesoderm (APLM**) (originating from the subdivision of the mesoderm after gastrulation) [Figure 10]. It is known that cardiac progenitors (myocardial and endocardial) can already be found from the blastula stage (Keegan et al., 2004), but it is still controversial as to whether they originate from two distinct pre-specified progenitors or if it is multipotent progenitors that then get differentiated into myocardial and endocardial progenitors (Haack & Abdelilah-Seyfried, 2016).

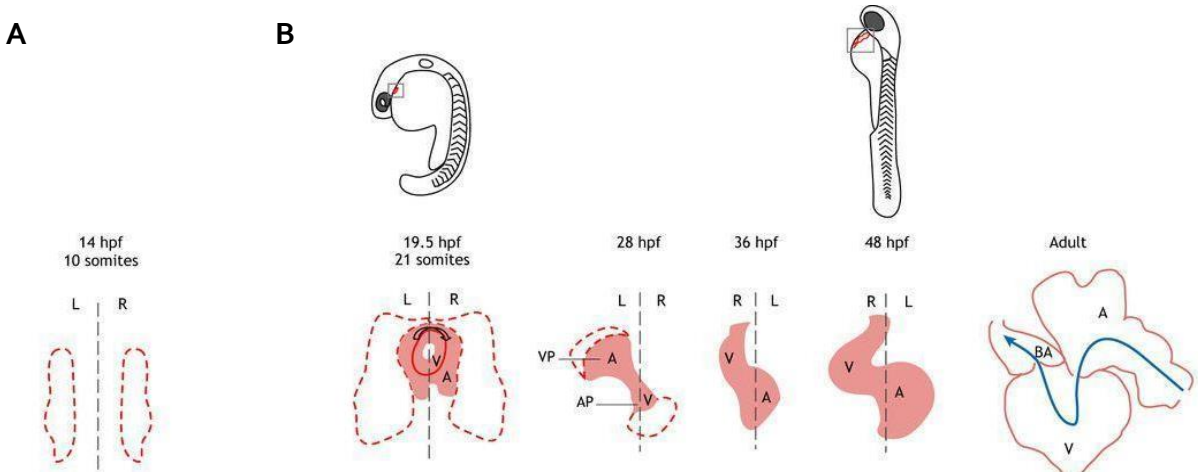

Figure 10: Different steps of early cardiac development. *(A) Cardiac progenitors are located in two bilateral pools inside the Anterior Lateral Plate Mesoderm (ALPM). (B) The fusion of the progenitors leads to first a disc, a transient cone, and then the primitive heart. At 28hpf, an accretion of cells from the SHF occurs. Then, the heart starts its asymmetry breaking by adopting a C-shape at 36hpf and an S-shape at 48hpf once the cardiac looping process is finished. Red dotted lines represent the heart fields.* [from (Desgrange et al., 2018)]

The cardiac progenitors then fuse at the midline of the embryo and form a **disc** (at 21 somites, around 19hpf) [Figure 10]. From the disc-stage, cardiac progenitors go through an intermediate step to form a **cone** shape before forming the primitive heart tube (D. Y. Stainier et al., 1993). The progenitors forming this primitive heart tube are called the **First Heart Field (FHF)**. The tube then extends towards the left of the midline. This process is called **cardiac jogging** (Chen et al., 1997) and happens around 23hpf**.** After jogging, the primitive heart tube will be repositioned towards the midline (Chin et al., 2000). The primitive heart tube will then start beating between 22-24hpf as a suction pump (Forouhar et al., 2006). However, it is incompletely lumenized at this stage and only starts beating regularly at **around 2.6Hz from 28hpf** (Boselli et al., 2015). In the primitive heart tube, the depolarization wave of the cardiomyocytes happens at the same speed through the whole heart (Chi et al., 2008).

B. From the heart tube to the chambered heart

This straight tube then undergoes a rightward looping, **cardiac looping**, in order to have the two chambers that are well-positioned in respect to one another (starts from 36hpf and is finished at 48hpf) [Figure 10]. In zebrafish, the looped heart is characterized by a flat **S-shape** whereas it has a helical shape in mammals. The heart at that stage is exclusively composed of a monolayer of myocardial cells and a monolayer of endocardial cells that are separated by the cardiac jelly. The epicardial layer will cover the heart at later developmental stages, originating from the precursor population, the pro-epicardium (PE), which is forming a cluster at the dorsal pericardial wall at 48hpf. PE cells will then be released in the pericardial cavity, get advected into the pericardial flow, and finally attach to the myocardium in order to form the epicardium (Peralta et al., 2013).

Concomitant to the looping of the heart, a constriction will occur between the two chambers, at the AVC, forming an endocardial ring. The chambers will also expand in size, by a process called **cardiac ballooning**. This step implies changes in cell shapes in both the myocardium and the endocardium tissue layers (Auman et al., 2007; Dietrich et al., 2014). In addition, other cells from the **Secondary Heart Field (SHF)**, that correspond to late-differentiating mesodermal progenitor cells (also

originating from the APLM in zebrafish), are added to the forming heart (Mosimann et al., 2015). In mature mammal hearts, the FHF mainly gives rise to the left ventricle whereas the SHF gives rise to the right and left atria and the right ventricle (Meilhac & Buckingham, 2018). In zebrafish, the myocardium is not highly proliferative, so its elongation mainly happens through the addition of SHF cells at both poles (de Pater et al., 2009; Y. Zhou et al., 2011). However, for the endocardium, tissue growth has been revealed to be mainly due to cell proliferation instead of the accretion of additional external cells in the zebrafish embryo (Dietrich et al., 2014).

Interestingly, electrical wave propagation through the heart now adopts a new pattern. Indeed, by using a transgenic zebrafish line with a myocardial-specific promoter (*cmlc2*) and a calcium indicator (*CaMP*) (*Tg(cmlc2:CaMP)*, it has been shown that the propagation of the calcium wave still happens at the same speed through the atrial chamber but is delayed at the AVC from 36hpf to 48hpf (Chi et al., 2008). This delay in the propagation wave at the AVC is essential for the sequential beating of the chambers (atrium, ventricle). Therefore, both electrical and anatomical changes lead to the development of an **oscillatory flow profile** in the region of the AVC that has been shown to be essential for the establishment of AVC cell identity (presented in 2.3.2.C).

C. Cardiac valve development

Once the cardiac looping is completed (at 48hpf), the process of valve formation will start at the AVC. This process involves complex cellular morphogenetic events. The first cellular event at the onset of valve development corresponds to a **local cell clustering** at the AVC [Figure 11.A]. This is also characterized by a cell shape change where the AVC cells become **cuboidal** whereas the cells in the chambers remain flat and elongated (squamous) (Pestel et al., 2016; Steed et al., 2016). This event is then followed by the change of behavior of a few cells (between 1 and 3 cells (Guanawan et al., 2020) that will exhibit cell protrusions before physically moving inside the cardiac jelly [Figure 11.B-C] (Steed et al., 2016). This process involves, in mammals, a process called endothelial-to-mesenchymal transition (Bolender & Markwald, 1979). Once inside the cardiac jelly, the cell will proliferate [Figure 11.D]. Through a complex

remodeling, this multi-layered structure will lead to cushions and then mature **valve leaflets** that can efficiently close at each cardiac cycle. AVC valves will become functional by 120hpf and OFT valves by 144hpf (Duchemin et al., 2019).

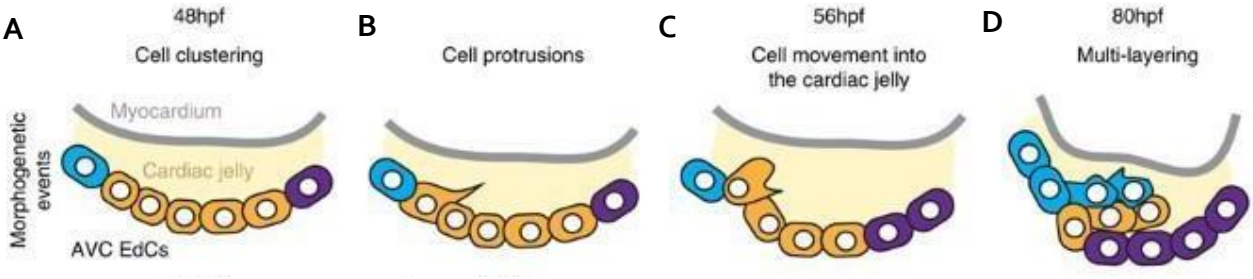

Figure 11: Schematic of the different steps involved in valve formation. *(A) Local cell clustering at the AVC at 48hpf. (B) Cell protrusions sent towards the cardiac jelly at around 50hpf. (C) Collective cell migration inside the AVC. (D) Cells proliferate inside the cardiac jelly to form a multi-layered structure at the origin of the mature valve leaflet.*

D. Trabeculation

At around 72hpf, the structure of the myocardium also starts to change from a monolayer towards a complex three-dimensional structure within the outer layer of the ventricular chamber (J. Liu et al., 2010). The myocardium is formed by a thin layer of compact cardiomyocytes and also ridges, called **trabeculae**, which protrude into the lumen of the ventricle, increasing the surface of the myocardium (see Annex 2, Figure 3.c-d). Trabeculae have been shown to play a role in providing oxygen and nutrients to the cardiomyocytes before the establishment of coronary vessels (Sedmera & McQuinn, 2008) and also able to increase cardiac performance (Meyer et al., 2020).

Having reviewed the major stages of cardiac development, I will now focus on the critical role that mechanical forces play in proper cardiovascular morphogenesis.

2.3 Cardiovascular development is dependent upon mechanical forces

Heart morphogenesis happens concomitantly to the generation of forces by the myocardium. The forces associated with heart function are of diverse natures and include wall shear stress generated by the blood flow (a frictional force) (Freund et al., 2012), hydrostatic pressure, as well as cyclic strain due to stretch. The endocardium in particular experiences numerous different forces due to its direct contact with blood flow, as can be observed in Figure 12. Moreover, on top of being of different natures, forces are also different in terms of amplitude, frequency, and direction and all those parameters may affect the cellular response to the applied force.

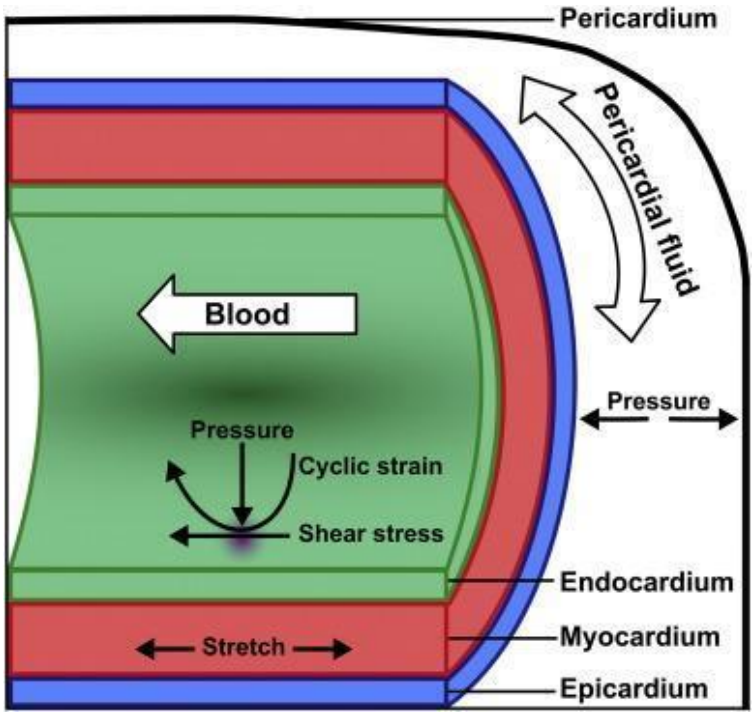

Figure 12: The nature of the different forces during heart morphogenesis. *Wall shear stress is applied on the endocardial cells that are in direct contact with the blood flow. A perpendicular hydrostatic pressure is also applied directly on the endocardial cells. Cyclic strain and stretch result from the contraction of the myocardial layer. The heart is also within the pericardial cavity, which is filled with a fluid that also exerts pressure on the whole heart.* [from (Andrés-Delgado & Mercader, 2016)]

In this section, I will discuss only the contribution of mechanical forces in the context of the early stages of blood vessel development (where the influence of blood flow on endothelial cell behavior has been extensively studied) as well as heart formation (chamber ballooning, valve formation). Other contributions during pharyngeal arch artery remodeling and trabeculation can be found in the review I co-wrote in Annex 2.

2.3.1 Response of endothelial cells to mechanical forces

The majority of our knowledge concerning the impact of flow forces on cell behaviors come from the study of endothelial cells, both *in vitro* (Human umbilical vein endothelial cells (HUVECs), human pulmonary artery endothelial cells (HUPAECs) …) and *in vivo*, with numerous studies having been conducted in zebrafish embryos.

Endothelial cells line the interior of the vessels and are exposed to shear stress, which was revealed to influence their behaviors and drive proper vessel formation/remodeling. In fact, it has been known for a long time that *in vitro* endothelial cells exposed to shear stress undergo **cell shape changes by elongating and aligning with the direction of the flow** (Levesque & Nerem, 1985). This change in behavior is accompanied by a reorganization of the F-actin and a partial disassembly and reassembly of the adherens junction proteins (e.g VE-cadherin, the predominant cadherin in endothelial cells, as well as alpha- and beta-catenins) (Noria et al., 1999, 2004). Moreover, the shear stress direction sets the orientation of endothelial cell division, which is the same as the shear stress direction, therefore promoting vessel lengthening (Zeng et al., 2007).

In vivo, within the immature vascular plexus, blood flow coordinates and drives **endothelial cell polarity changes**, shown both in mouse and zebrafish (Franco et al., 2015). In the regions with high shear stress, cells were observed migrating against the direction of the blood flow (assessed by the relative Golgi-nucleus axis). This **flow-driven polarized migration** was shown to be essential in the context of vessel

regression (vessel remodeling step during angiogenesis), by inducing cells to leave the segments with low flow to migrate in and stabilize the more irrigated neighboring segment with higher flow (Franco et al., 2015). In the developing vessels of the zebrafish, Kwon et al. also observed this polarity change against the blood flow (Kwon et al., 2016). Moreover, by altering the blood circulation, they observed that:

- In embryos injected with the *tnnt2a* morpholino (that inhibits cardiomyocyte contractility), the polarization pattern was lost.
- In embryos where the heart was stopped transiently with the use of 2,3-butanedione monoxime (BDM), the endothelial cell polarization was impaired, but this was reversible.

These observations demonstrate the important role of blood flow in influencing cell behavior. In this context, Kwon et al identified a G-Protein Coupled Receptor, the Apelin Receptor (aplnr), as being key in the mechanosensation of the shear stress, driving the polarity changes, as the percentage of polarized cells was decreased in *aplnrb* mutants (Kwon et al., 2016).

In another developmental context within the vessels, blood flow has been shown to be essential for the process of endothelial-to-hematopoietic transition. Within the ventral wall of the dorsal aorta, some endothelial cells extrude and lead to hematopoietic stem cells (Kissa & Herbomel, 2010). Recently, it has been shown that decreasing blood flow or inhibiting blood flow (through inhibition of the heart contractility) increased the rate of cell extrusion from the dorsal aorta of the zebrafish (Campinho et al., 2020). Similarly, decreasing mechanosensation of the endothelial cells through the inhibition of the stretch-sensitive channel, *transient receptor potential polycystin 2 (Trpp2),* also led to increased cell extrusion (Campinho et al., 2020). Therefore, blood flow forces in this context helps to maintain endothelial cells within the vessels by limiting their extrusion.

2.3.2 The importance of cardiac-generated forces in the developing heart

A. Zebrafish mutants with deficiencies in cardiac force generation

The forces experienced by the endocardial cells within the heart are stronger compared to the ones experiences by the endothelial cells within the vessels (Freund et al., 2012). Moreover, they were also found to be key for cardiac morphogenesis (Emily Steed, Boselli, et al., 2016). Several zebrafish mutants revealed the fundamental role of heart-generated mechanical forces during heart morphogenesis. The mutant called ***silent heart (sih)*** carries a mutation for the gene *tnnt2* encoding for a cardiac troponin T that plays a key role in cardiomyocyte sarcomere assembly (Sehnert et al., 2002). These embryos present cardiac edema, do not have a contractile heart, and therefore also no resulting blood flow but are still able to undergo cardiac looping (Sehnert et al., 2002). However, in this mutant, heart valve development is impaired and the AVC region fails to form, visualized by an absence of an endocardial ring formation (Bartman et al., 2004). In this same study, based on genetic screens, the authors identified another mutant for a cardiac sarcomeric actin, called *cardiofunk (cfk)*, that presents cardiac dilation and lacks blood flow at 36hpf. This mutant was also not able to form an endocardial ring at the AVC at 48hpf (Bartman et al., 2004). Those studies highlight the importance of cardiac-generated forces in the heart for its own development.

In the developmental context of cardiac ballooning, when the two chambers expand in size, forces derived from heartbeat were revealed to be important for cell shape changes (Auman et al., 2007). This process is characterized by cell shape elongation of the cardiomyocytes in the region of the curvature. Auman et al combined experiments within two chamber-specific mutants, based on the differential expression of the myosin heavy chain (*myh*) in the ventricle (*myh7*) and in the atrium (*myh6*). From this, the authors observed that in the *wea* mutant, carrying a mutation in the atrial *myh6 (or amhc)*, the atrial chamber was deprived of contraction resulting in low blood flow

within the ventricle (Berdougo et al., 2003). This led to defects in the overall ventricle size and intro less elongated ventricular cardiomyocytes (Auman et al., 2007; Berdougo et al., 2003). On the opposite, in the *haf* mutant, carrying a mutation in the ventricular *myh7 (or vmhc),* the contraction was completely blocked specifically within the ventricle (Auman et al., 2007). This mutation led to a phenotype where ventricular cardiomyocytes were larger compared to the cardiomyocyte size of wild-type embryos. From those two observations, the authors shed light on the importance of a balance between blood flow and cardiac contractility required for proper cell shape changes during chamber ballooning.

All the studies presented so far highlight the difficulty to decipher the contribution of one particular source of force (blood flow or heart contraction) experienced by the cells. In fact, affecting the contractility of the cardiomyocytes also affect the flow pattern onto the cardiac cells.

B. Shear stress seems to be the main force to which cells respond

In order to decouple cardiac contractility and blood flow, Hove et al., experimentally injected large beads at the entrance or at the exit of the heart [Figure 13] (Hove et al., 2003). They found that the physical blockage of blood flow without affecting heart contraction led to cardiac defects (absence of cardiac looping and impaired valve development). Thus, this suggests that it is mainly the shear stress applied on the endocardial cells which are important for valve development. In another study, the authors identified an allele of the gene *southpaw* (*spaw*) in which the looping of the heart was randomized with hearts being still straight, rightwards or leftwards looped (Kalogirou et al., 2014). They observed that in the mutants for which the heart did not loop, the flow pattern at the AVC was altered leading to defects in valve morphogenesis, even though the cardiac contractility was not altered (Kalogirou et al., 2014). Therefore, this study also concludes about the importance of the intracardiac flow as being the main driver of proper cardiac valve morphogenesis (Kalogirou et al., 2014).

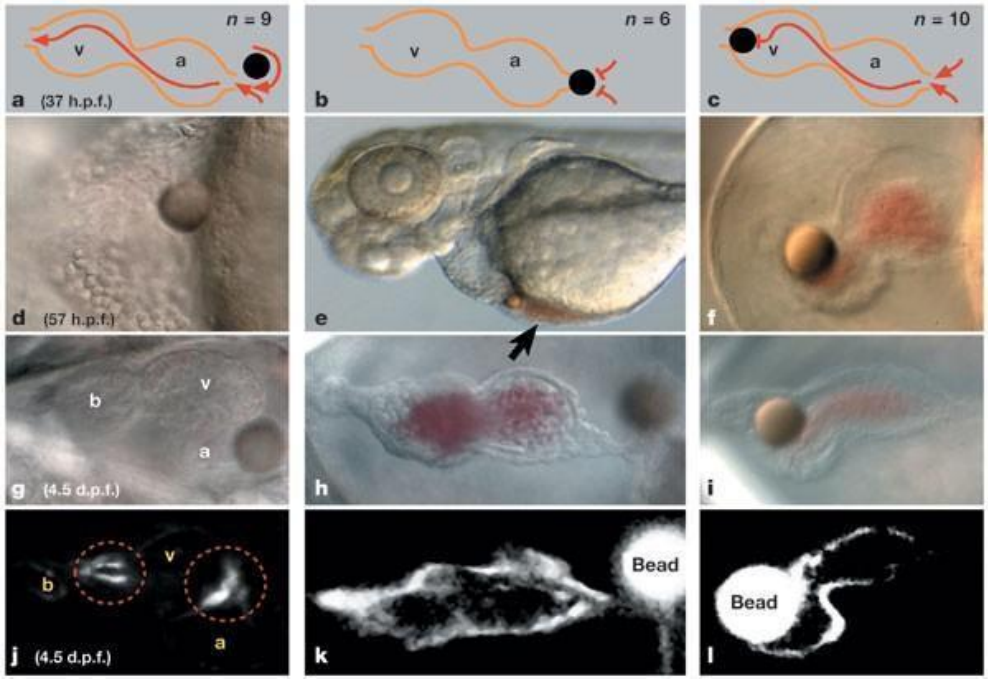

Figure 13: Altering blood flow via the injection of large beads (50µm) within the developing heart leads to cardiac morphogenetic defects. (a,b,c) *The bead was injected at 37hpf and was either situated at the inflow resulting in blocking blood flow (b) or still letting blood to flow within the heart (a) or was situated at the outflow and in that case blocking the water efflux (c). (d-f) Bright-field images of the injected embryos at 37hpf. Heart development was normal at 4.5dpf when the bead was present at the inflow, but blood flow was still present within the heart (g) and the valve developed properly (j). However, both when the bead was localized in the inflow and blocked blood flow influx or in the outflow and blocked blood flow efflux, the heart did not loop properly (h,i) and heart valve development was impaired (k,l)* [from (Hove et al., 2003)].

C. Oscillatory blood flow is essential for AVC cell identity

More specifically, it has been described that it is mostly the **retrograde nature** of blood flow that is important in order to specify the cell identity of the AVC cells (Vermot et al., 2009). AVC endocardial cells at 48hpf express characteristic markers such as the transcription factor Krüppel-life factor 2a (**Klf2a**) (Vermot et al., 2009), the zebrafish Notch homolog (**Notch1b**). AVC endocardial cells are also different from the cells localized in the two chambers based on the specific expression of leucocyte cell

adhesion molecule ***Alcam*** (also known as Dm-grasp) (Beis et al., 2005) [Figure 19]. The myocardial cells localized at the AVC specifically express bone morphogenetic protein 4 (**Bmp4**) [Figure 14] [Figure 19].

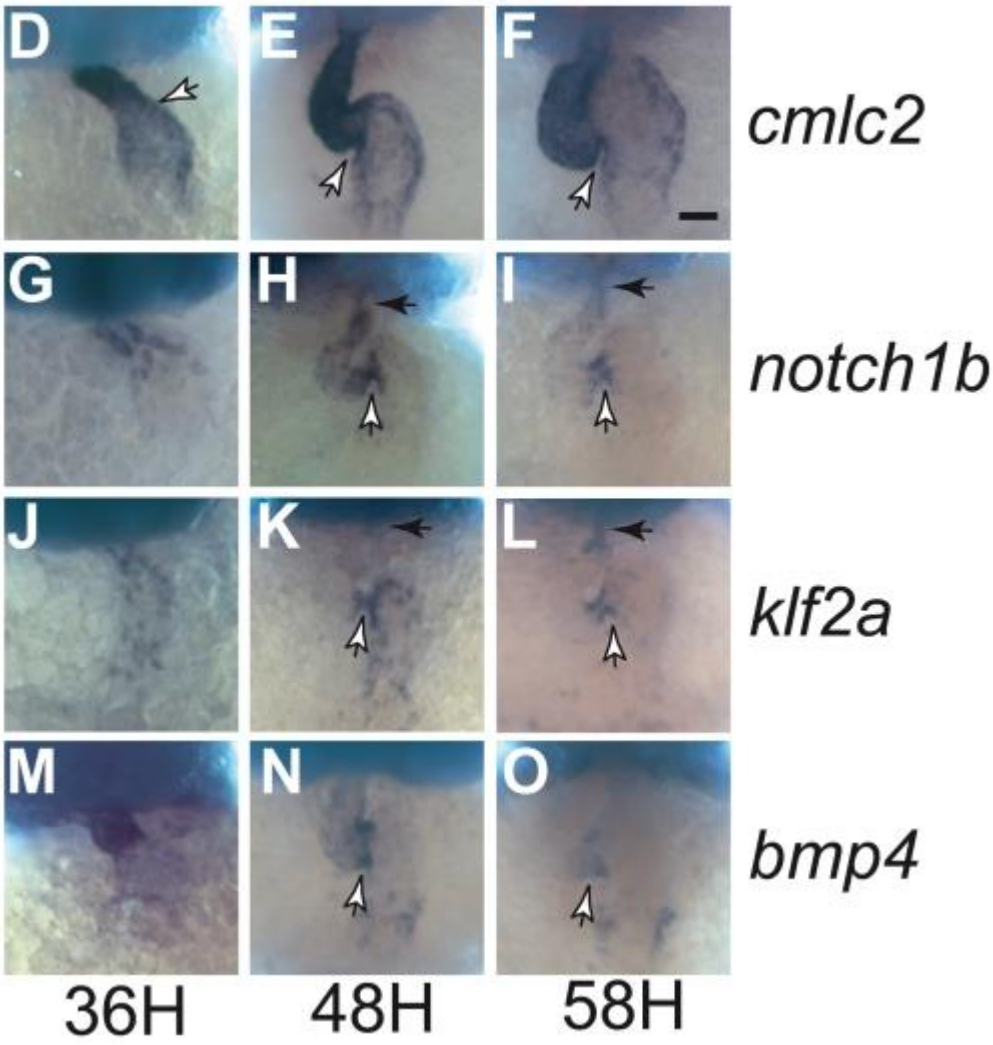

Figure 14: In situ hybridization showing the spatial mRNA expression patterns of the cmlc2, notch1b, klf2a, and bmp4 from 36hpf to 58hpf. *The white arrows indicate the AVC, and the black arrows indicate the OFT.* [from (Vermot et al., 2009)].

The flow in the developing zebrafish heart being at low Reynolds number (viscous forces dominate onto inertia forces), people aimed at trying to alter the blood viscosity to determine its impact on heart development. The *gata1* and *gata2* genes are involved in early hematopoiesis in zebrafish and their inhibition results in less or

the absence of red blood cells within the heart, leading to a decreased blood viscosity (Vermot et al., 2009). It was found that targeting the ***gata2*** gene with a morpholino leads to a decrease of blood viscosity and a highly reduced retrograde flow at the AVC. Moreover, decreasing the heart rate with **lidocaine** (sodium channel blocker) also led to a decreased retrograde blood flow in the AVC region. These different treatments induced a strong reduction in *klf2a* expression within the AVC during valve development and subsequent **defects in AVC valve morphogenesis**. Therefore, this study unravels that the **retrograde nature of the flow** at the AVC leads to the expression of the transcription of *klf2a* and its identified downstream target, *notch1b* that are both essential for cardiac valve morphogenesis (Samsa et al., 2015; Vermot et al., 2009).

More recently, modeling and red blood cell tracking, helped to show that the amplitude of the fundamental frequency (τ_1) of the wall shear stress is higher in the AVC region (Heckel et al., 2015). This parameter described the oscillatory flow experienced by the endocardial cells (Heckel et al., 2015).

D. Cardiac forces influence endocardial cell proliferation

Inhibiting both blood flow and cardiac contractility with the ***silent heart*** **mutant also alters the proliferation rate of the endocardium**, between 30hpf and 54hpf (confirmed by BrdU experiment) (Dietrich et al., 2014). Control embryos have on average around 80 cells in the ventricle and 70 cells in the atrium whereas the *silent heart* mutant has only approximately 40 cells and 25 cells in the ventricle and the atrium, respectively (Dietrich et al., 2014) [Figure 15]. By targeting gata2, authors reduced retrograde blood flow and observed that this is accompanied by a decrease in the ventricular cell number. Moreover, morphant embryos for gata2 or both gata1/ gata2 (leading to a reduction of blood viscosity and shear stress) (Vermot et al., 2009) were observed to have a decreased atrial cell number [Figure 15]. Importantly, those changes were revealed to not be due to increased apoptosis within the tissue (shown via immunolabeling with the Caspase 3 antibody). Therefore, **blood flow is key in regulating endocardial cell proliferation**. Moreover, the chemical communication between the two layers (myocardium, endocardium) was found to be important for the

endocardial cell proliferation, as inhibiting the BMP signaling from the myocardium, which expresses the ligand, to the endocardium, that possesses BMP receptors, decreases the endocardial cell proliferation (Dietrich et al., 2014). Therefore, the **communication between the different tissues composing the heart can also modulate the cell behavior, and specifically in that context cell proliferation**.

Recently, it has also been shown that increasing the size of the myocardial atrium results in an increase in the cell proliferation of the endocardium, reinforcing the importance of the communication between the two tissues (Bornhorst et al., 2019). In this study, the authors showed that the expansion of the myocardial atrial chamber generates higher junctional forces within the endocardium leading to VE-cadherin (Cdh5) force sensing/transmission that triggers the translocation of Yap1 within the endocardial nuclei subsequently enhancing cell proliferation.

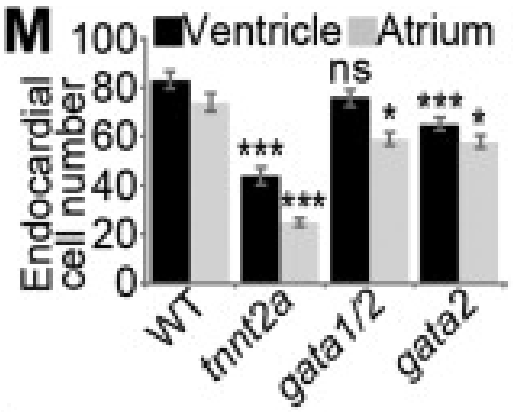

Figure 15. Endocardial cell number at 54hpf within the two chambers in wild-type and conditions where the flow forces are altered. *Mean with SEM; n ≥ 5 hearts per condition; ***p < 0.001, *p < 0.05, ns, not significant* [data from (Dietrich et al., 2014)]

Altogether, in this section 3, we have seen that the shear stress in the AVC region is a key external mechanical stimulus for proper heart morphogenesis.

But how is shear-stress in the valve-forming regions sensed and transduced during valve development? How does mechanotransduction work? I will now focus

only on the processes happening in the valve-forming region, and on AVC morphogenesis in particular in order to provide context for my work.

2.4 Atrio-ventricular canal development

2.4.1 Mechanostransduction in the valve-forming regions

A lot of endothelial cellular components have been described to be mechanosensitive and to play a role in mechanosensation and the modulation of endothelial cells' behavioral changes. The great majority of them are presented within the review I co-wrote in Annex 2. Here, I will focus on the stretch-sensitive channels Piezo and also members from the TRP family (TRPP2 and TRPV4), that have been described at the stretch-sensitive channels involved in the morphogenesis of the valve-forming areas (OFT, AVC).

A. PIEZO channels

The mechanically activated cation channels Piezo, Piezo1, are expressed in embryonic endothelial cells. In this context, Piezo1 is involved in the development of the vascular structure of the mouse (Li et al., 2014; Ranade et al., 2014). Moreover, Piezo1 mouse mutants have defects in lymphatic valve morphogenesis (Nonomura et al., 2018). Piezo1 was also shown to be mechanically activated by shear stress in HUVECs (Li et al., 2014).

When I joined the Vermot laboratory, I worked on the research project of a former post-doctorate, Anne-Laure Duchemin, (see paper in Annex 1) (Duchemin et al., 2019). This project consisted in deciphering the mechanotransduction pathway involved in OFT valve morphogenesis, which is less investigated than AVC valve morphogenesis. First, we observed that *Piezo1*, based on a reporter line, is expressed mainly within the smooth muscle cell progenitors that surround the OFT valve

endothelium as well as within the endothelium at 72hpf. We found that the *Piezo1, Piezo2* mutants have defects in OFT valve formation (displaying a high percentage of thick or delayed valves). Moreover, Piezo1 was revealed to be essential for repressing *klf2a* expression within the OFT endothelium, whereas it was shown be necessary for the expression of *Yap1*, *Elastinb,* and *Fibronectin1* expression within the smooth muscle cells in order to lead to proper OFT valve folding. Interestingly, on top of the essential role of Piezo channels, TRP channels were also important for the OFT valve formation, as has already been reported for the AVC valves.

B. TRP channels: TRPP2 and TRPV4

The transient receptor potential (TRP) superfamily comprises cation permeable channels that are divided into seven subfamilies, based on structural homologies: the **c**anonical (TRP**C**), the **m**elastatin TRP (TRP**M**), the **v**anilloid TRP (TRP**V**), the **p**olycystic TRP (TRP**P**), the **m**uco**l**ipin TRP (TRP**ML**), the ankyrin TRP (TRP**A**) and the no mechanoreceptor potential C TRP (TRP**N**). All the TRP members have a common structure made of **six transmembrane segments** (TM1-6) and they all have a **pore region** between TM5 and TM6 which is responsible for the channel selectivity for cations (Nilius & Owsianik, 2011). Both the N-terminus and the C-terminus are localized within the cell cytoplasm and their length and binding regions, motifs vary greatly between the different subfamilies of the TRP channels (Nilius & Owsianik, 2011). The majority of the members of this family have been characterized to **be gated by different heat/cold, osmosis, mechanical cues** (Mendoza et al., 2010; Thodeti et al., 2009), **and chemical (exogenous and endogenous ligands) stimuli** (Voets et al., 2005). Interestingly, TRPP2 (also called PKD2 or CUP) and TRPV4 have been identified to play a key role in the mechanotransduction of the oscillatory flow at 48hpf within the AVC region (Heckel et al., 2015). In fact, in both *trpp2* -/- and *trpv4* -/- embryos, Heckel and colleagues described that the signal from the zebrafish *klf2a* reporter line was decreased, *klf2a* being a key marker of the AVC cell identity [Figure 16- A.D]. Their activation based on the oscillatory flow sensing at the AVC drives Ca2+

entry, the expression of the transcription factor Klf2a and subsequent proper valve formation [Figure 16- E] (Heckel et al., 2015).

In the context of the OFT valves, we found that TRP channels were also essential for valve modeling and Trpp2 led to klf2a activation in the posterior region of the valve endothelium (paper in annex 1) (Duchemin et al., 2019).

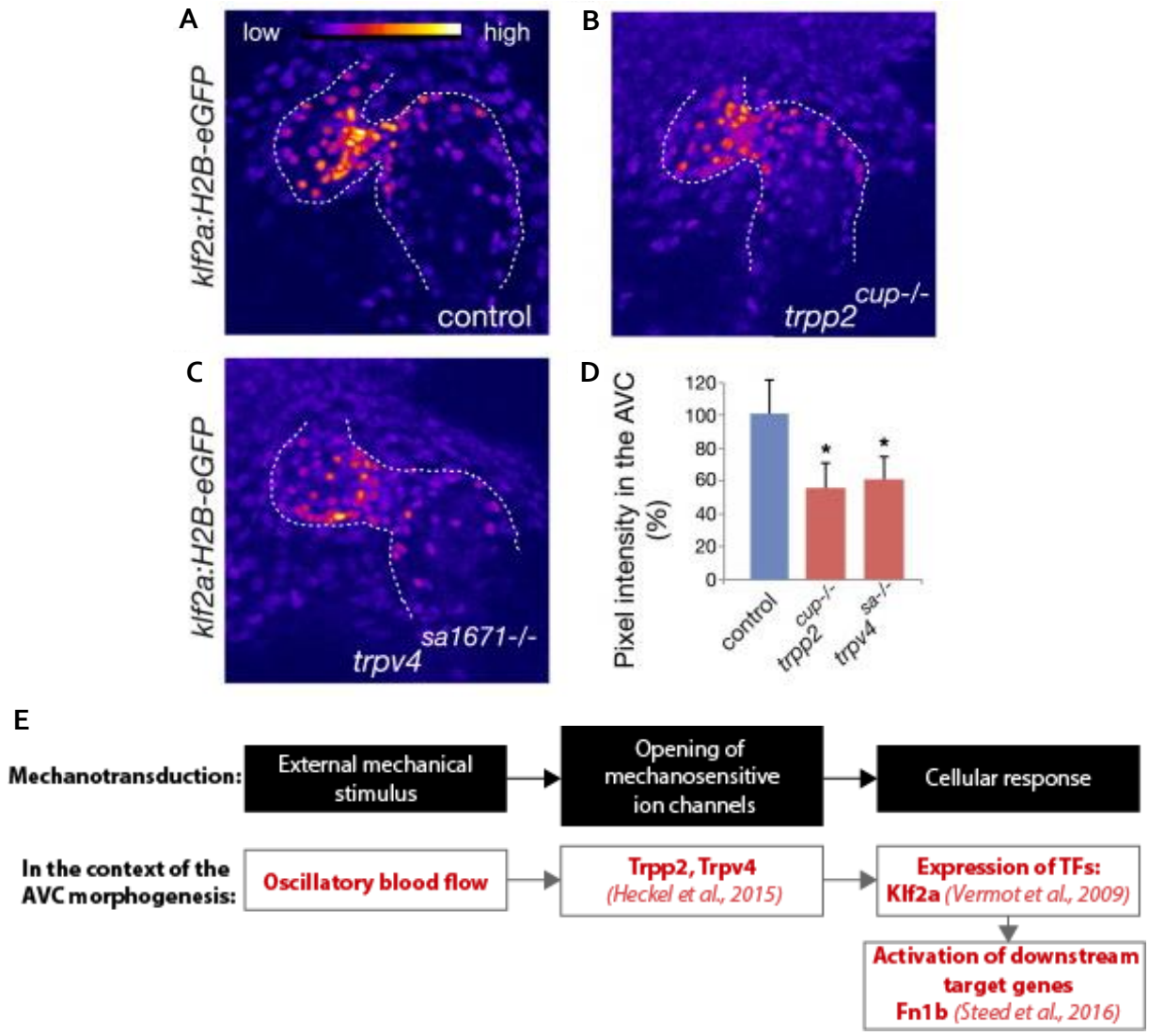

Figure 16. Expression of transcription factor klf2a (assessed by the klf2a reporter (klf2a:H2B-eGFP)). (**A**) *Klf2a is strongly expressed within the AVC cells of a control embryo at 48hpf. Both in trpp2-/-* (**B**) *and in trpv4 -/-* (**C**), *the expression of klf2a is reduced at the AVC, at 48hpf.* (**D**) *Quantification of the expression level based on the pixel intensity at the AVC.* [from *(Heckel et al., 2015)*]. (**E**) *Scheme of the mechanotransduction pathway at the AVC.*

Kfl2a expression, through TRP channels mechanotransduction, was then found to target the expression of Fibronectin1b (Fn1b), which is present in the cardiac jelly at 48hpf (Steed et al., 2016) [Figure 16.E, Figure 18].

However, Fn1b is not the only component to be present in the cardiac jelly, as an important remodeling of the ECM takes place during AVC morphogenesis.

2.4.2 Cardiac jelly composition changes during AVC development

On top of being blood flow or cardiac contractility dependent, proper valve morphogenesis is also dependent upon the components present inside the cardiac jelly (the ECM lining between the myocardium and the endocardium). Concomitant to the establishment of oscillatory blood flow at the AVC, interactions between the myocardial and the endocardial layers will produce different components of the cardiac jelly. Amongst them, the GAGs are largely present during AVC morphogenesis [Figure 18].

One of the building blocks of all the GAGs (hyaluronic acid (HA), heparan sulfate, chondroitin sulfate) is produced by the UDP-glucose 6-dehydrogenase (UGDH), which transforms UDP-glucose (UDP-G) into UDP-glucuronic acid (**UDP-GlcUA**) [Figure 17]. In the case of HA production, the sequential assembly of UDP-GlcUA with N-acetylglucosamine (UDP-GlcNAc) is made by hyaluronan synthases (HAS) that are anchored to the plasma membrane (**Figure 17**). In addition, HAS proteins also export HA into the extracellular space (cardiac jelly). HA molecules have a high molecular mass ranging from $\sim 2 \times 10^5$ to $\sim 10 \times 10^6$ daltons (Da) (T. D. Camenisch & McDonald, 2000).

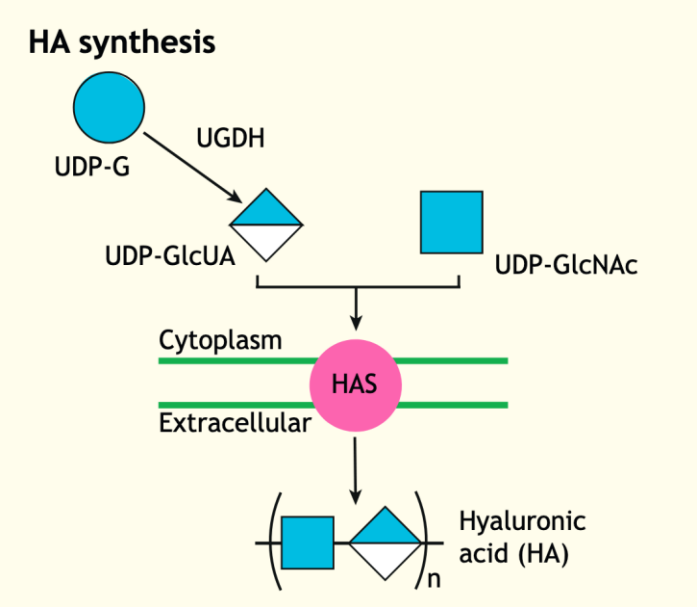

Figure 17: Hyaluronic acid (HA) production involves 2 steps. *Firstly, the UDP-glucuronic acid (UDP-GlcUA) is produced by the UDP-glucose 6-dehydrogenase (UGDH). Secondly, the assembly and the exportation towards the cardiac jelly of the repetitive motif (UDP-GlcUA with UDP-GlcNAC) forming the HA molecule, catalyzed by the hyaluronan synthases (HAS). (HAS2 in the context of the AVC development.* [from (Derrick & Noël, 2021)]

Interestingly, the *jekyll* zebrafish mutant, which carries a mutation in the *ugdh* gene (important for all GAG synthesis), leads to defects in the early steps of valve morphogenesis at the AVC (Walsh & Stainier, 2001). The ***jekyll* mutants did not exhibit the cell clustering event** at the AVC at 48hpf and show reduced and mislocalized expression of early AVC differentiation markers, such as Bmp4 and Brl46 (a versican homolog) within the myocardium, and Notch1b within the endocardium (Walsh & Stainier, 2001).

Within the primitive heart tube, **Has2** is responsible for the production of HA and its exportation within the cardiac jelly (Todd D. Camenisch et al., 2000; Walsh & Stainier, 2001) [Figure 18.B]. *Has2* is specifically expressed within the AVC and the OFT endocardial cells (Todd D. Camenisch et al., 2000; Tong et al., 2014).

The localized expression of *has2* is **regulated by genes expressed within the myocardium**, such as the T-box factor **Tbx2** (*tbx2b* in zebrafish) or **Tbx5,** which is

also restricted to the AVC and OFT regions ((Shirai et al., 2009), shown in mouse) (Tong et al., 2014) [Figure 18]. Tbx2 is under the control of BMP signaling (BMP2/4) (Shirai et al., 2009). Tbx5 has been shown to be regulated by the direct binding of potassium channel tetramerization domain containing 10 (KCTD10), which restricts its transcription and therefore HA expansion (Tong et al., 2014).

Has2 mouse mutants were revealed to have strong defects in heart development, where cell migration and EMT at the AVC did not take place (Todd D. Camenisch et al., 2000). Moreover, in zebrafish, excessive HA deposition due to elevated levels of has2 expression leads to an enlarged expression of AVC cell identity markers with, for instance, elevated numbers of Dm-grasp (Alcama) positive cells within the heart (Lagendijk et al., 2011). Therefore, the **local presence of HA inside the cardiac jelly is essential for proper valve morphogenesis at the AVC**.

The fact that has2 expression is localized at the AVC, therefore restricting cell identity, has been shown to be regulated by the transmembrane protein Tmem2 (also known as cemip2) which is expressed in both the myocardium and the endocardium (Smith et al., 2011). In fact, zebrafish tmem2 mutants were characterized by increased deposition of HA within the cardiac jelly as well as the expansion within the heart of genetic markers normally restricted to the AVC (bmp4, tbx2b, has2, alcama, notch1b, versican) [Figure 18] (Smith et al., 2011; Totong et al., 2011). Recently, the extracellular portion of Tmem2 has been revealed to play a role as a **hyaluronidase** in this context, degrading HA inside the cardiac jelly of the two chambers, thereby restricting Wnt signaling within the myocardial cells of the AVC and enabling the proper establishment of AVC cell identity (Hernandez et al., 2019).

Additional components are found locally at the AVC at around 36hpf, the core protein **Versican** (produced by myocardial cells) [Figure 18], and the GAG **Chondroitin sulfate**. Both mouse and medaka's mutants for Versican (Mittal et al., 2019; Mjaatvedt et al., 1998) and inhibition of Chondroitin Sulfate (via DX (cis/trans-decahydro-2-napthol-b-D-xyloside) treatment of MO) (Peal et al., 2009) lead to defects in the AVC development.

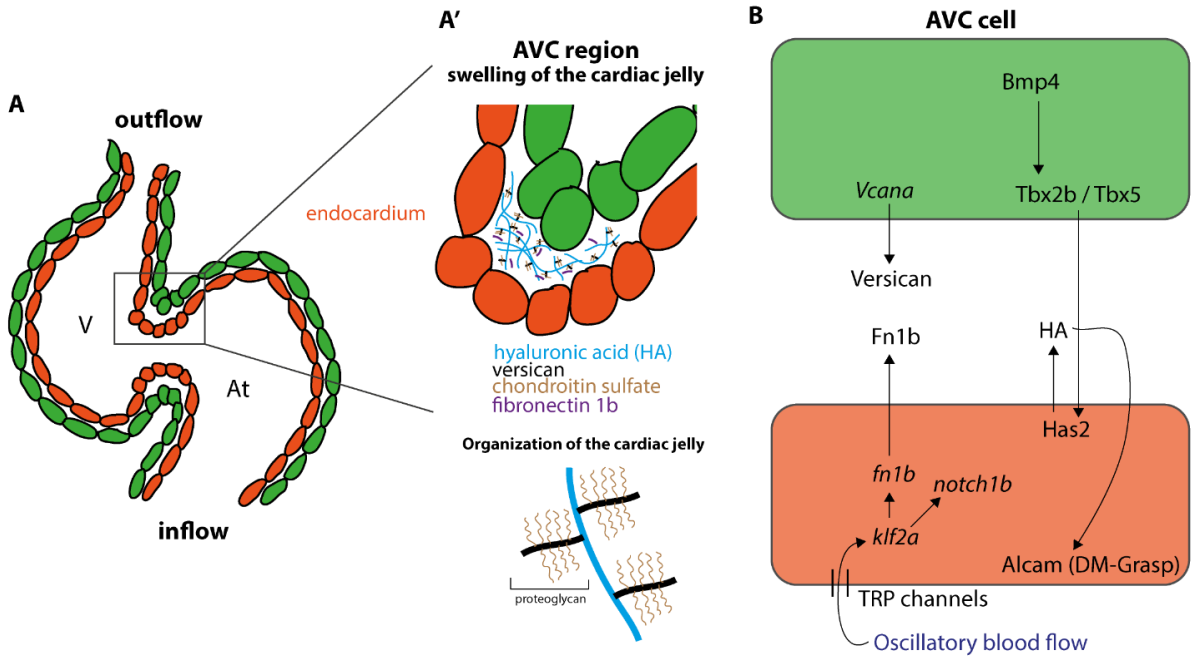

Figure 18. Matrix composition genetic interactions during AVC morphogenesis. *(**A**) Structure of the heart. At=Atrium, V=Ventricle. (**A'**) Zoom in the AVC region with the swelling of the cardiac jelly composed of different components: HA, versican, chondroitin sulfate, and fibronectin 1b. (**B**) Main genes involved in the production of the ECM at that developmental stage in the AVC cells.* [inspired from (Derrick & Noël, 2021; Segert et al., 2018)]

Importantly, it is known for a long time that the GAGs have the physicochemical property to **attract salt and large amounts of water**. This property led to the observation that the **cardiac jelly locally swells at the AVC** prior to valve formation at 48hpf, forming a **hydrated ECM** [Figure.18.A'] (Tong et al., 2014; Waldenström et al., 1991).

Therefore, we saw in this subsection that the composition and organization of the cardiac jelly are key during early AVC morphogenesis. However, the impact of the biophysical properties of its constituents on the cell behavior changes of the AVC cells is not known. More precisely, it will be interesting to decipher the impact of the osmotic pressure generated by the GAG molecules on cardiac cell behaviors.

2.4.3 Tissue remodeling during early heart morphogenesis

Even if the main steps of AVC valve morphogenesis are known, the cell behaviors underlying the emergence of the AVC region are currently not well understood. A previous paper from the Vermot lab has investigated what happens **at the tissue-scale** during the AVC formation (Boselli et al., 2017). To do so, they photoconverted the endocardial cells present in the ventricle and the atrium at 36hpf, prior to the AVC emergence (characterized by a cell cluster formation, also called endocardial ring) [Figure 19.A]. However, they did not photoconvert the region corresponding to the AVC. After photoconversion, they let the photoconverted-embryo develop normally, and they imaged the same heart again at 48hpf. They observed that the non-converted region, the AVC, shrunk between 36hpf and 48hpf. This observation led to the conclusion that a tissue convergence towards the AVC region happens between 36hpf and 48hpf. Importantly, this tissue movement is dependent upon mechanical forces as it does not occur in the *sih* mutant [Figure 19]. However, the presence of red blood cells is not essential for this process as embryos injected with the *gata1* morpholino did not have defects in tissue convergence.

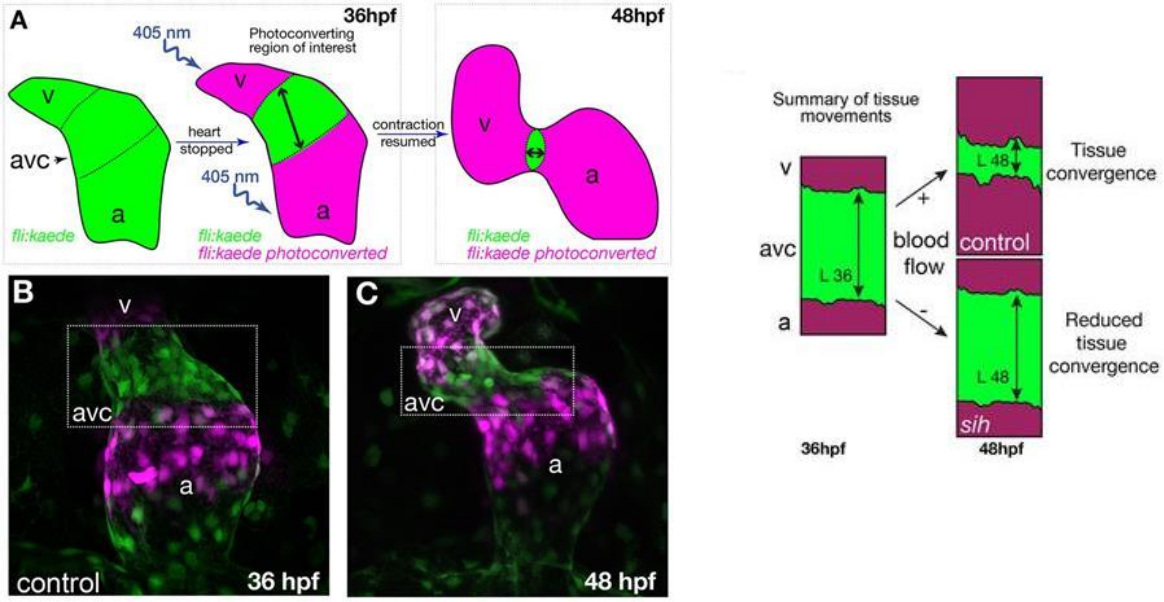

Figure 19. A photoconversion experiment reveals an endocardial tissue convergence towards the AVC region from 36 to 48hpf. (**A**) *Schematic of the*

photoconversion experiment based on the zebrafish line Tg(fli:kaede), fli being a promotor specific for the endothelium and Kaede a photoconvertible protein that normally emits in the green spectrum but upon irradiation with UV light (405nm) changes conformation and emits in the red spectrum. v= ventricle and a= atrium. (**B-C**) *Confocal images showing a photoconverted heart at 36hpf and the result after 12 hours of growth, at 48hpf.* (**D**) *Schematic representing the tissue convergence movement in control embryos (based on the shrinkage of the AVC region from 36 to 48hpf) and the absence of tissue movement in the sih mutant.* [from (Boselli et al., 2017)]

This experiment sheds light on the important tissue remodeling prior to the AVC development. However, the cellular behaviors behind this tissue movement remain unknown.

In conclusion of this Part 2, we saw that cardiogenesis is a complex morphogenetic process. Defects during embryonic development can lead to congenital heart diseases, which are a major medical issue. Thanks to the zebrafish model organism, which enables to study the molecular and cellular origins of cardiovascular defects, it has become clear that blood flow, and in particular oscillatory wall shear stress encountered in the AVC region is essential for proper valvulogenesis. The sensing and the mechanotransduction of this mechanical cues have been revealed to imply the stretch-sensitive TRP channels (TRPP2 and TRPV4) leading to gene activation such as the transcriptional factor Klf2a. In addition, the cardiac jelly undergoes a complex remodeling and starts to be enriched in mainly GAG molecules (such as hyaluronic acid) that attract water leading to a swelling of the ECM during AVC development. At the cellular level, the beginning of AVC morphogenesis is characterized by an increase in cell density, with cells are becoming closer to each other, locally at the AVC at 48hpf. Prior to this event, we saw in the last section that the whole endocardial tissue undergoes a convergence towards the AVC region from 36 to 48hpf.

Based on this literature background, I will now discuss the objectives and main aims of my thesis project.

OBJECTIVES OF THE THESIS

Molecular and cellular mechanisms involved in the zebrafish Atrio-Ventricular Canal (AVC) morphogenesis

In the introduction of this thesis, the key morphogenetic events at early AVC development were outlined. We have seen that AVC formation is characterized by convergent movement of the endocardial tissue towards the AVC region from 36hpf to 48hpf. At 48hpf, the cells present within the AVC region become closer to each other, forming a cluster, and exhibit a cuboidal shape [Figure 20].

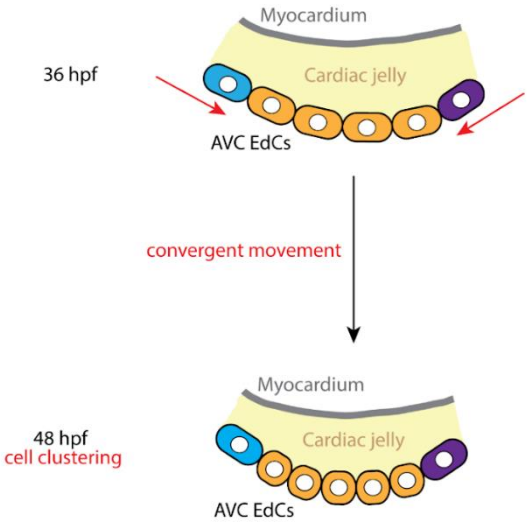

Figure 20. <u>Early AVC morphogenesis: Tissue convergence towards the valve-forming area followed by an increase of the cell density into that region.</u> [inspired by (Steed et al., 2016)]

Based on these two main observations, my thesis project sought to decipher the **driving force behind this movement of the endocardial tissue as well as to understand the role of mechanical forces in this process**.

To achieve this, my project had 3 main aims:

1. Characterize the changes associated with tissue convergence at the cellular level

The point of this first aim is to determine the behaviors of endocardial cells that occur during tissue remodeling (as discussed in the Part 1/1.4 of the introduction). My efforts focused on examining in-plane tissue cell polarity changes, cell volume changes, as well as the proliferation of the endocardial cells in the process, following these parameters from 28hpf (primitive heart tube) until 48hpf (looped heart and establishment of the AVC cell clustering)

2. Characterize the impact of mechanical forces and the composition of the cardiac jelly in the process

This part consisted of modifying either the forces generated by the myocardium (contraction of the heart and resulting blood flow) or the mechanotransduction within the endocardium to study their roles in this morphogenetic process.

In addition to these forces, the components of the cardiac jelly are also key in the proper development of the AVC. Therefore, we also aimed to decipher the impact of hyaluronic acid on the endocardial cell behaviors investigated in Aim 1.

3. Characterize the driving force of the tissue movement and how it could be regulated

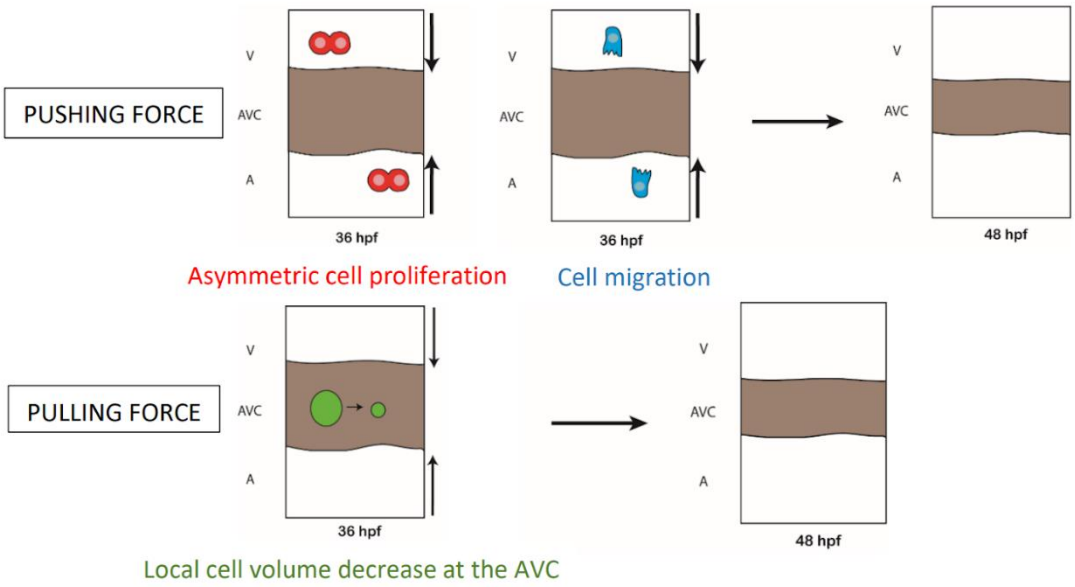

Figure 21. The hypotheses behind the driving force of the convergence movement

For the identification of the driving force of the process, we started with some hypotheses that could explain the tissue convergence towards the AVC and the cell clustering event. I will go through these different points:

On the one hand, the movement of endocardial cells towards the AVC could be explained by a **pushing force** towards that region [Figure 21, top panel]. This might be induced by the increased proliferation of cells within the two chambers that will push the cells towards the AVC. A different alternative would be that the cells inside the AVC region exhibit higher cell proliferation rates but do not grow as much as the cells within the two chambers. Finally, a pushing force could also be due to the active migration of the endocardial cells towards the AVC region.

On the other hand, the atrial and ventricular endocardial cells might be pulled towards the AVC [Figure 21, bottom panel]. This **pulling force** might originate from a local cell volume decrease at the AVC.

RESULTS – PART I

RESULTS - PART I

Extracellular mechanical forces drive endocardial cell volume decrease during cardiac valve morphogenesis

Hélène Vignes[1], Christina Vagena-Pantoula[2], Mangal Prakash[3,4], Caren Norden[3,5], Florian Jug[3,4,6], Julien Vermot[1,2]

[1] *Institut de Génétique et de Biologie Moléculaire et Cellulaire (IGBMC), Centre National de la Recherche Scientifique UMR7104, Institut National de la Santé et de la Recherche Médicale U1258 and Université de Strasbourg, Illkirch, France*

[2] *Department of Bioengineering, Imperial College London, London, United Kingdom*

[3] *Max Planck Institute of Molecular Cell Biology and Genetics, Dresden, Germany*

[4] *Center for Systems Biology Dresden, Dresden, Germany,*

[5] *Instituto Gulbenkian de Ciência, Oeiras, Portugal*

[6] *Fondazione Human Technopole, Milan, Italy*

Keywords

zebrafish ; endocardium ; ECM ; mechanobiology

ABSTRACT

Organ morphogenesis involves dynamic changes of tissue properties at the cellular scale. In addition, cells need to adapt to their mechanical environment through mechanosensitive pathways. How mechanical cues influence cell behaviors during morphogenesis, however, remains poorly understood. Here we studied the influence of mechanical forces during the formation of the atrioventricular canal (AVC) where cardiac valves develop. We show that in zebrafish the AVC forms within a zone of tissue convergence between the atrium and the ventricle which is associated with increased activation of the actomyosin meshwork and endocardial cell orientation changes. We demonstrate that tissue convergence occurs with a major reduction of endocardial cell volume triggered by mechanical forces and the mechanosensitive channels TRPP2/TRPV4. In addition, we show that the extracellular matrix component hyaluronic acid controls cell volume changes. Together, our data suggest that cell volume change is a key cellular feature activated by mechanical forces during cardiovascular morphogenesis. This work further unravels how mechanical forces and extracellular matrix can influence tissue remodeling in developing organs.

INTRODUCTION

Most organs need to acquire a defined shape for optimal function. Organogenesis is controlled both spatially and temporally as a result of the interplay between genetic and mechanical factors (Mammoto & Ingber, 2010; Sivakumar & Kurpios, 2018). Mechanical cues can originate from diverse contexts: the cell environment for example the surrounding extracellular matrix (ECM), neighboring cells, or neighboring tissues (Charras & Sahai, 2014; Hannezo & Heisenberg, 2019; Martino et al., 2018; Petridou et al., 2017; Villedieu et al., 2020). Further, mechanical forces can originate from the tissue itself (Boselli et al., 2015; Xiong et al., 2020). Cells constitute the functional unit of every tissue and can sense and react to those different forces driving coordinated cell behaviors (cell shape changes, cell intercalation, cell apoptosis, etc) that are essential for tissue remodeling (Heisenberg & Bellaïche, 2013; Lecuit et al., 2011). Yet how mechanical forces affect cell behaviors and tissue shape at the cellular scale remains unknown.

Amongst the different cellular mechanisms that control morphogenetic processes (Heisenberg & Bellaïche, 2013; Lecuit et al., 2011; Mao & Baum, 2015), cell volume changes have recently emerged as an essential modulator of tissue shape. In *Drosophila Melanogaster*, cell volume decrease drives the tissue movement during dorsal closure, (Saias et al., 2015). Moreover, cell volume changes are also key in regulating the lumen volume of intestinal organoids (Yang et al., 2020) and the Küpffer vesicle morphogenesis in zebrafish (Dasgupta et al., 2018). *In vitro,* external mechanical cues can trigger cell volume changes (Guo et al., 2017; Wang et al., 2020; Xie et al., 2018). Cell volume is controlled by osmotic regulation, cell cytoskeletal contractility as well as cell growth and division (Cadart et al., 2019). However, how cell volume changes can lead to tissue remodeling in broader tissular contexts, such as the cardiovascular system, remains unclear.

The heart acquires its function early during embryonic development in order to pump blood throughout the body. Defects in heart formation and especially heart valve anomalies can lead to congenital heart diseases with major medical implications (Lincoln & Yutzey, 2011). The fluid shear stress and stretching forces generated by heartbeat have been reported to be essential for proper valve morphogenesis (Auman et al., 2007; Bartman et al., 2004; Hove et al., 2003; Kalogirou et al., 2014; Vermot et

al., 2009). The inner tissue layer of the heart corresponds to the endocardium, constituted of specialized endothelial cells called endocardial cells (EdCs). Like endothelial cells, EdCs are potent mechanosensors and mechanotransducers of mechanical forces (Campinho et al., 2020). The membrane-bound stretch-sensitive channels Piezo1, TRPP2, and TRPV4 are important for mechanical force sensing during cardiac valve development (Duchemin et al., 2019; Faucherre et al., 2020; Heckel et al., 2015). Moreover, EdCs interact also with their ECM (i.e. cardiac jelly), produced by both myocardial and endocardial cells, and which plays key roles during cardiac morphogenesis (Steed et al., 2016; Derrick et al., 2019; Derrick & Noël, 2021; Grassini et al., 2018).

One of the main components of the cardiac jelly is hyaluronic acid (HA), which is a negatively charged glycosaminoglycan (GAG). HA has the property to generate osmotic pressure and therefore attracts water, resulting in a local swelling of the cardiac jelly at the AVC (Camenisch et al., 2000; Cowman et al., 2015; Lockhart et al., 2011; Schroeder et al., 2003; Tong et al., 2014). However, the roles of the forces generated by the heartbeat as well as the impact of biophysical properties of the ECM on the modulation of EdC shape during primitive heart tube formation are currently not well understood.

In zebrafish, the formation of a local cell cluster within the single-layered endocardial sheet at the AVC marks the onset of cardiac valve formation (Pestel et al., 2016; Steed et al., 2016). At the tissue level, this event is preceded by a symmetry-breaking event promoted by a tissue convergence towards the AVC (Boselli et al., 2017). Here, we used this morphogenetic model to investigate the early cellular features involved in endocardial tissue convergence, starting from 28hpf, when the zebrafish heart has a tubular structure, until 48hpf when the heart has looped and the two chambers (atrium, ventricle) are formed. We found that tissue convergence is associated with a global EdC orientation change directed towards the AVC and a cell clustering event that is associated with a local cell volume decrease of the AVC cells. Interestingly, neither the cell cluster formation nor the cell volume changes were linked to cell proliferation. At the molecular level, we found that the cell volume decrease depends on the mechanosensitive TRP channels (both TRPP2 and TRPV4) and the ECM component hyaluronic acid. We propose a model where mechanotransduction and the osmotic pressure generated by HA accumulating within the cardiac jelly

dictates local cell volume changes in the endocardium. This may be a general feature by which mechanical forces shape the cardiovascular system, such as the heart or blood and lymphatic vessels in the vascular system.

RESULTS

EdC polarisation during AVC development

Using zebrafish for high precision live imaging, we analyzed the morphogenetic patterns of the endocardium at cellular resolution. Axial cell polarity is a well-established readout of the orientation and the coordination of cell movements within endothelial tissues (Franco et al., 2015; Kwon et al., 2016; Pouthas et al., 2008). Taking advantage of this fact, we investigated the dynamics of endocardial cell orientation during AVC development *in vivo* to characterize the general morphogenetic features underlying AVC formation. We used a zebrafish transgenic line that labels the Golgi apparatus and the nucleus specifically in endothelial cells *Tg(fli1:nEGFP); Tg(fli1a:B4GALT1-mCherry)* (Kwon et al., 2016), thereby providing a readout of the global tissue patterning at the cellular scale. Nucleus-to-Golgi axis orientation was analyzed every two hours from 28hpf to 36hpf and at 48hpf in order to track EdC orientation changes (Figure 1.A, Figure S1.A, Video S1). We classified the cells into three categories: 1) nucleus-to-Golgi axis towards the outflow, 2) nucleus-to-Golgi axis towards the inflow and 3) no clear nucleus-to-Golgi axis orientation (Figure 1.B; Figure S1.B). For statistical analysis, we quantified nucleus-to-Golgi axis changes in the ventricle (Figure 1.C) and in the atrium over time (Figure 1.C'). Before heartbeat (22hpf), 48.6±5.7% of the cells showed a nucleus-to-Golgi axis towards the outflow (n=130 cells, N=3 embryos) (Figure S1.C). After blood flow initiation, we found that the majority of the cells (66.5±2.0%, n=271 cells, N=5 embryos for the atrium and 70.2±4.6%, n=198 cells, N=5 embryos for the ventricle) showed a nucleus-to-Golgi axis towards the outflow at 28 hpf in both chambers (Figure 1 C-C'). While nucleus-to-Golgi axis patterns remained unchanged from 28hpf to 48hpf within the atrium (Figure 1.C'), ventricular cells gradually reversed their nucleus-to-Golgi between 28 and 48hpf (48.2±2.0%, n=578 cells, N=7 embryos) to point towards the AVC (Figure 1.C). These results indicate that tissue convergence is accompanied by a global orientation of the nucleus-to-Golgi axis towards the AVC, starting from 30hpf underlining the collective movements of the endocardial cells required to initiate the formation of cardiac valves (Figure 1.F).

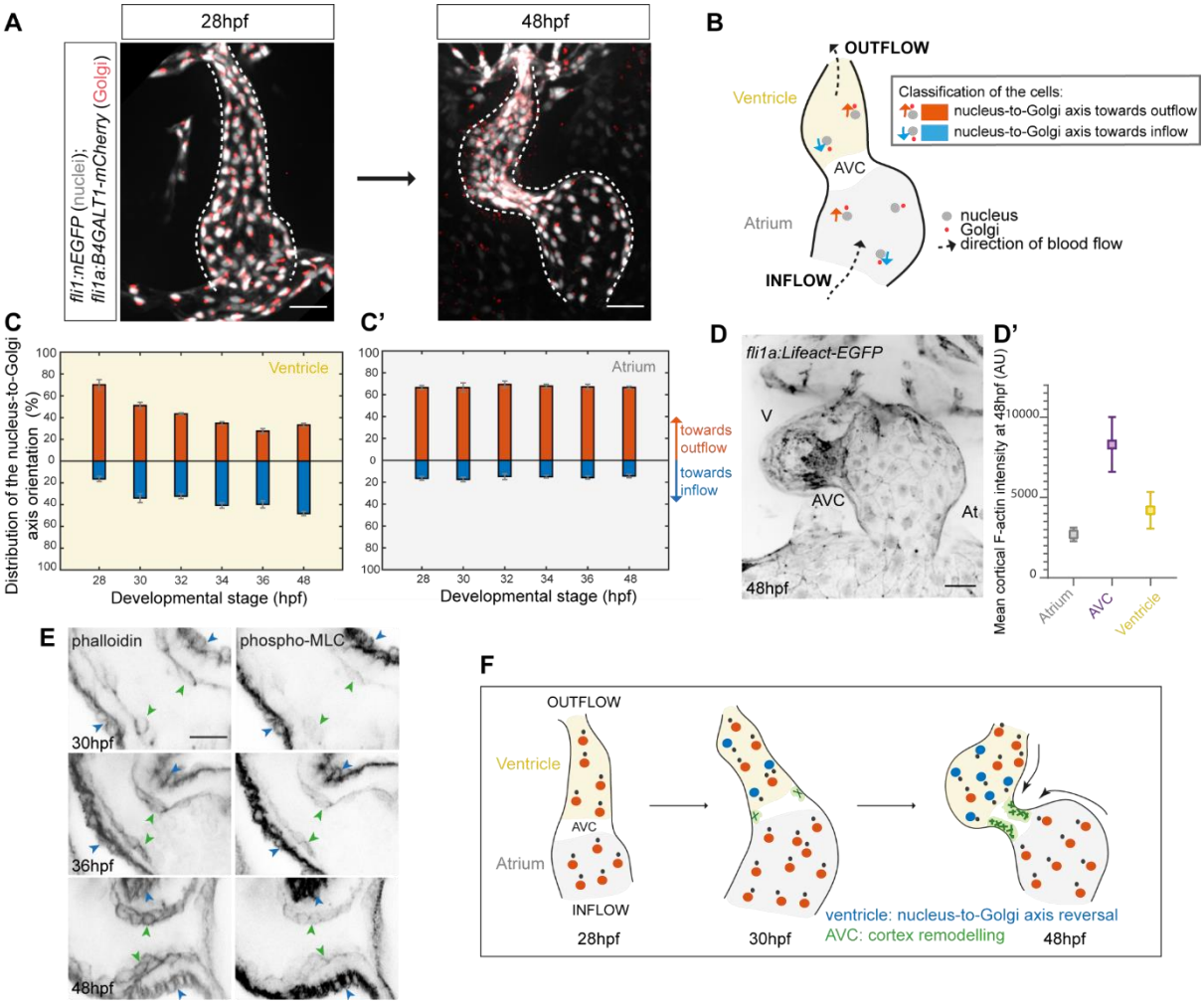

Figure 1. Ventricular EdC nucleus-to-Golgi axis reversal and F-actin remodeling at the AVC happens concomitantly from 30hpf to 48hpf (**A**) Maximal projection of 28hpf to 48hpf hearts from *fli1a: B4GALT1-mCherry; fli1: nEGFP* embryos to track changes in EdC nucleus-to-Golgi axis orientation. White dotted lines outline the endocardium. Scale bars, 30µm. (**B**) Schematic explanation of the way cell orientation was classified within the endocardium. (**C-C'**) Quantification of the percentage of cells with the nucleus-to-Golgi axis oriented towards the outflow and towards the inflow from 28hpf to 48hpf (N=5 embryos, 28hpf ; N=5 embryos, 30hpf ; N=4 embryos, 32hpf ; N=4 embryos, 34hpf ; N=5 embryos, 36hpf ; N=7 embryos, 48 hpf ; Error bars show the s.e.m) in the ventricle (**C**) and in the atrium (**C'**). (**D**) Maximal projection of *fli1a: LifeAct-EGFP* heart showing an increase in F-actin fluorescence intensity at the AVC. V=ventricle, At= atrium. Scale bar, 30µm. (**D'**) Quantification of the F-actin fluorescent intensity based on the data in (D). A.U= arbitrary units. Error bars represent the s.d. (**E**) Single z-plane immunofluorescence with phalloidin and phospho-myosin light chain (MLC) antibody in the AVC showing the presence of a strong F-actin and phospho-MLC signal in the myocardium (blue arrows) and an increasing signal through time in the AVC (green arrows) from 30hpf, 36hpf, to 48hpf. Scale bars, 20µm (**F**) Schematic representation of the general cellular morphogenetic features underlying AVC development.

EdC volume during AVC development

Considering the global change in EdC orientation at the onset of AVC morphogenesis, we reasoned that the cells located in the area of convergence had to specifically change shape within the AVC. We therefore hypothesized that a local cell size change at the AVC could contribute to the process of AVC morphogenesis. To address this, we analyzed EdC volume changes during AVC morphogenesis. We first quantified the cell area and the cell height (apicobasal direction) separately in order to compare the cell size between all three regions (atrium, AVC, ventricle) in order to calculate the mean cell volume. To measure the area of the apical cell surface, we used a transgenic zebrafish line (*TgBAC(ve-cad:ve-cad-TS)*) labeling vascular endothelial (VE)-cadherin (Lagendijk et al., 2017) (Figure 2.A). We estimated the cell size by multiplying the apical cell surface area by the cell thickness (Figure 2.B). Based on these calculations, the size of AVC cells is 412.2±21.6 μm^3 (n= 41 cells), while that of cells located in the atrium and the ventricle are 1348±67.9 μm^3 (n= 48 cells) and 933.1±47.8 μm^3 (n= 34 cells), respectively (Figure 2.C). We concluded that cell size varies depending on the different regions of the heart with cells being smaller in the AVC.

To overcome the difficulties associated with 3D manual segmentation, we developed a robust and quantitative deep-learning-based routine to obtain a reliable assessment of the cell volume from nuclei segmentation. Indeed, it has been reported that nuclear volume directly scales with the cell volume in different contexts (Cantwell & Nurse, 2019; Greiner et al., 2015; Huber & Gerace, 2007). We thus focused on extracting the nuclei volume which is easier to segment than the cell borders when in 3D. Quantitative data was obtained by using a trained classifier by deep learning. To confirm the validity of the approach, we showed that nucleus volume correlates with cell volume in our system (Figure 2.D). To demonstrate this correlation more clearly, we analyzed individual cells for both their cell surface and their nucleus volume and found a strong correlation between those two parameters (Figure 2.E).

We next assessed the temporal variation of cell volume during the progression of tissue convergence. At 28hpf, cells in the AVC were not different in size compared to cells located inside the ventricle (426.7±32.8 μm^3 at 28hpf in the AVC), whereas they started to be smaller from 36hpf until 48hpf (390.6±12.9 μm^3 at 36hpf, and of 284.9±6.1 μm^3 at 48hpf) (Figure 2F). We confirmed these results by quantifying the mean

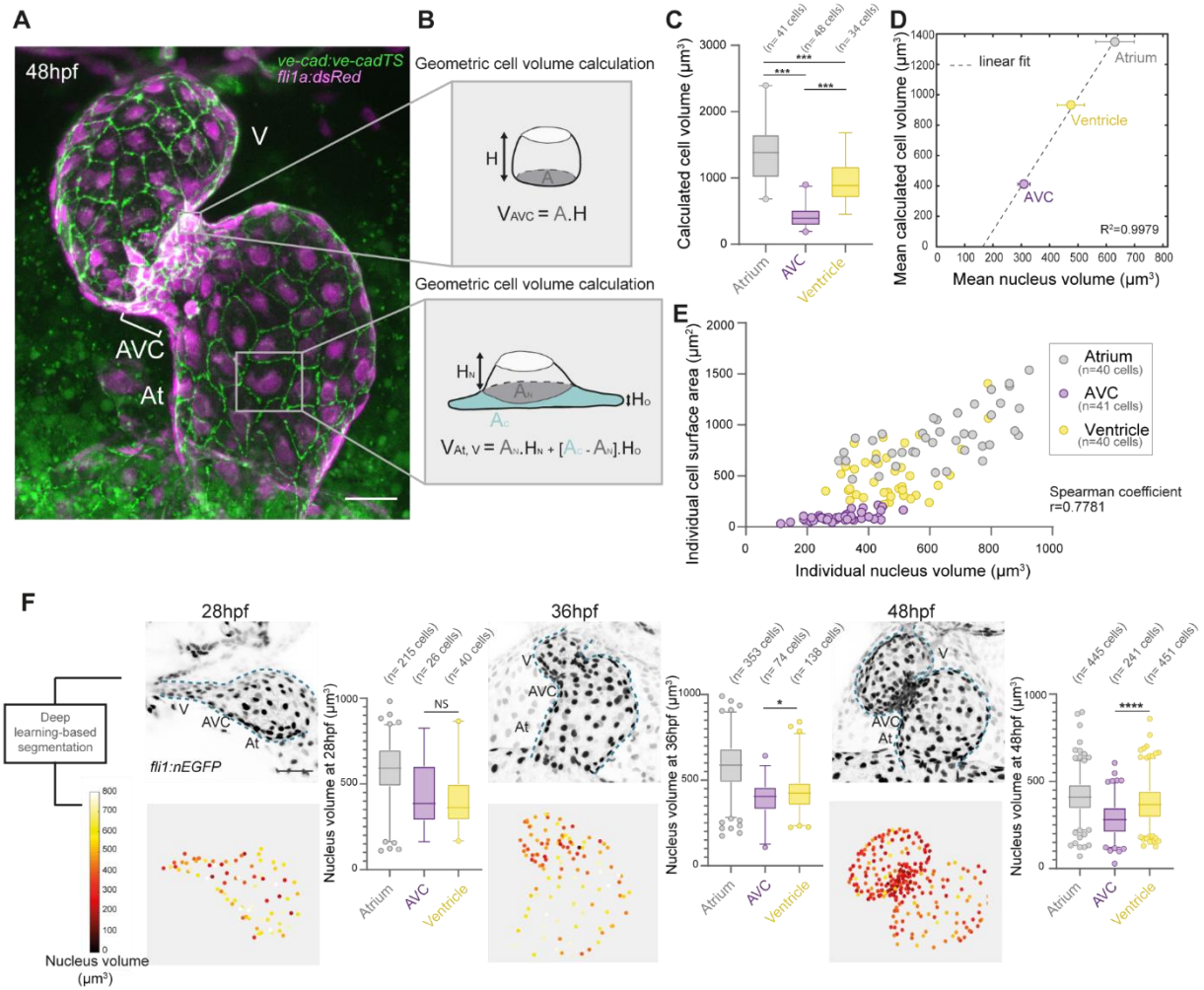

Figure 2. 3D analysis of EdC size reveals a significant decrease in cell volume at the AVC (**A**) Maximal projection of a stopped heart from a *ve-cad:ve-cadTS ; fli1a :dsRed* embryo. V=ventricle, At=atrium. Scale bar, 30 µm. (**B**) Schematics depicting methods used to calculate the cell volume in EdCs of the AVC (top panel) and in EdCs of the ventricle and the atrium (bottom panel). A= area, A_N= area of the nucleus, A_C= area of the cytoplasm, H= height of the cell, H_N= Height at cell region containing the nucleus, H_O= Height in other regions of the cell (**C**) Quantification of the cell volume shows differences between EdCs located in the atrium (n=41 cells), AVC (n=48 cells), and ventricle (n=34 cells) with AVC EdCs having the lowest cell volume. Mann-Whitney test. (**D**) Nucleus volume scales with cell volume. Correlation (R^2=0.9979) between the mean cell volume (calculated in (C)) and the mean nucleus volume quantified via segmenting nuclei using deep learning. Error bars represent the s.e.m for both axes (**E**) Individual cell surface area is positively correlated with individual nucleus volume (Spearman coefficient= 0.7781). Each dot represents a cell analyzed for both its surface area and nucleus volume (**F**) Quantification of the nucleus volume at 28, 36 and 48hpf reveals a significant decrease in cell volume of the AVC EdCs over development time. Top panels represent maximal projections of *fli1:nEGFP* stopped hearts, with blue dotted lines outlining the endocardium, and lower panels represent heat-maps of nucleus volume for the same embryonic heart. Unpaired two-tailed t-test. (N=5 embryos, 28hpf; N=5 embryos, 36hpf; N=5 embryos, 48hpf).

distance between each nucleus and its three nearest neighbors (Figure S2.A). Moreover, we found that cell volume change is correlated with enrichment in actin filaments (F-actin) and phospho-myosin light chain (p-MLC) specifically in the cells that will form the AVC, suggesting that cells display active contractility in the AVC (Figure 1.D-E, Video S2). This observation indicates that the mechanical properties and behaviors of the cells in the AVC could be different from the endocardial cells located in the heart chambers. Overall, these results show that AVC EdCs undergo a substantial decrease in cell volume along with actin cortex remodeling. This argues that EdC contractility and cell volume decrease are involved in endocardial tissue remodeling.

Cell volume decrease is independent of cell proliferation in the AVC

Differential cell proliferation rates or differential progression through the cell cycle between the three regions of the primitive heart tube (atrium, AVC, ventricle) could result in EdC cluster formation. We thus assessed if cell proliferation is associated with heart chamber-specific cell volume changes. To do so, we abolished cell division by using a combination of 30mM Hydroxyurea and 150µM Aphidicolin, two drugs that induce cell cycle arrest in the S phase (Figure 3.A). Embryos were treated from 30hpf until 48hpf without major phenotypic defects (Figure S1A-A'). Anti-phospho-Histone 3 immunolabeling confirmed that cell proliferation inhibition was effective in the presence of the drugs (Figure S3.B-B'). During the treatment, the number of EdCs doubled while cell numbers remained similar between 30hpf and 48hpf when proliferation was inhibited (Figure 3.A). The endocardial tissue and shape of the overall heart were qualitatively unchanged: the heart looped, and the overall volume of the heart was not significantly different between control and treated embryos (Figure 3.B, Figure S3.C-C'). When nuclei volume was quantified, we could not detect a difference in the cell size ratio between the three regions of the heart (atrium, AVC, ventricle) in controls and treated embryos (ratio of 1.48, 1.48, and 1.53 respectively in the atrium, AVC, and ventricle), suggesting a global scaling effect linking cell number and cell size (Figure 3.C). Similarly, we could not detect any difference in the mean nucleus-nucleus distance (ratio of 1.26, 1.27, and 1.15 respectively in the atrium, AVC, and ventricle) between controls and treated embryos (Figure S3.D). Importantly, cells were significantly smaller in the AVC of the treated embryos in the absence of proliferation comparable to cells located in the ventricle (Figure 3.C). These results show that cell

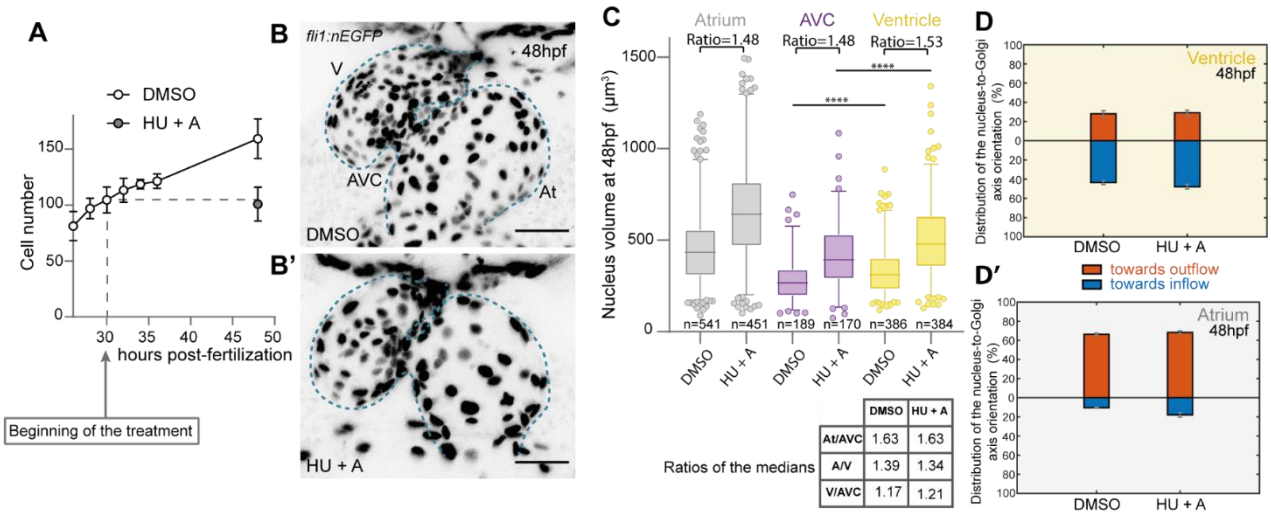

Figure 3. AVC cell volume reduction occurs independently of cell proliferation

(**A**) Total EdC number quantification in control embryos (treated with 0.5% DMSO), and embryos treated from 30hpf with a mix of two S-phase inhibitors, 30mM Hydroxyurea (HU) and 150 µM Aphidicolin (A). (for controls: N=5 embryos, 26hpf ; N=5 embryos, 28hpf ; N=5 embryos, 30hpf ; N=4 embryos, 34hpf ; N=5 embryos, 36hpf and N=7 embryos, 48hpf and N=10 HU+A embryos). Error bars represent the s.d (**B-B'**) Maximal projection of *fli1:nEGFP* embryos showing a control (DMSO) (**B**) and a treated embryo (HU+A) (**B'**) at 48 hpf. Blue dotted lines outline the endocardium. Scale bar, 50 µm. (**C**) Quantification of nucleus volume in atrium, AVC, and ventricle in controls (DMSO) and treated embryos (HU+A). The ratios of the medians are conserved between each region for both conditions. (N=7 embryos, DMSO and N=10 embryos, HU+A). Unpaired two-tailed t-test (**D-D'**) Quantification of the percentage of cells with the nucleus-to-Golgi axis towards the outflow and towards the inflow at 48hpf in controls (DMSO) and in treated embryos (HU+A) (N=3 embryos, DMSO and N=4 embryos, HU+A), for the ventricle (**D**) and for the atrium (**D'**). Error bars indicate the s.e.m.

volume decrease at the AVC is independent of EdC proliferation. Moreover, the nucleus-to-Golgi axis pattern at 48hpf was similar in treated and control embryos in both the ventricle (Figure 3.D) and the atrium (Figure 3.D'). This additionally suggests that tissue convergence occurs independently of cell proliferation.

Mechanical forces are important regulators of cell volume decrease

As mechanical forces have been shown to be involved in endocardial tissue remodeling (Steed et al., 2016, Heckel et al., 2015, Dietrich et al., 2014), we next studied the impact of altering cardiac contraction and blood flow on EdC size. To do so, we first analyzed cell volume changes based on nuclei labelling in silent heart mutants (*sih*$^{-/-}$), which carry a mutation in the gene *troponin T2a* (*tnnt2a)* and are therefore devoid of heart contraction and resulting blood flow (Sehnert et al., 2002) (Figure 4.A-A'). Cell volume did not show significant differences between the three regions of the heart (atrium, AVC, ventricle) and cells located in the AVC did not show a smaller volume compared to control embryos (nucleus volume of 481.7±25.5 µm^3 in *sih*$^{-/-}$, n=68 cells, N=12 embryos, nucleus volume of 273.2±7.6 µm^3 in *sih*$^{+/+}$ *sih*$^{+/-}$, n=197 cells, N=8 embryos) (Figure 4.B). Less cells were present within the AVC compared to controls (Figure 4.D) and the nucleus-nucleus distance was significantly increased at the AVC in *sih*$^{-/-}$ embryos (Figure S4.B). Interestingly, F-actin remodeling was absent in the AVC cells of the *sih*$^{-/-}$ embryos compared to controls (Figure S4.A). Furthermore, at 48hpf cells located in the atrium showed random nucleus-to-Golgi axes distribution (Figure 4.F') (towards the outflow: 35.3±2.9%; towards the inflow: 36.0±3.3% for n= 208 cells, N=6 embryos) different to what was observed in controls (towards the outflow: 68.7±1.4%, n=195 cells, N=3 embryos) (Figure 4.F').Ventricular nucleus-to-Golgi axis reversal did not occur in *sih*$^{-/-}$ embryos and instead cells tended to show a nucleus-to-Golgi axis towards the outflow (towards the outflow: 46.0±2.6%, towards the inflow:27.3±4.4%, n=314 cells, N=6 embryos) compared to controls (towards the inflow: 53.5±2.5%, n=217 cells, N=3 embryos) (Figure 4.F).These data are consistent with the observation that tissue convergence does not occur in absence of mechanical forces generated by the heartbeat (Boselli et al., 2017). To confirm these results, we partly inhibited heart activity by injecting a low concentration of the *tnnt2a* morpholino (Video S3) (Figure A''). As expected, the flow velocity was lower (176.7±30.0 µm/s, N=12 embryos), compared to controls (1222.6±128.0 µm/s, N= 3 embryos) (Figure 4.E). Interestingly, cell volume decrease at the AVC was affected

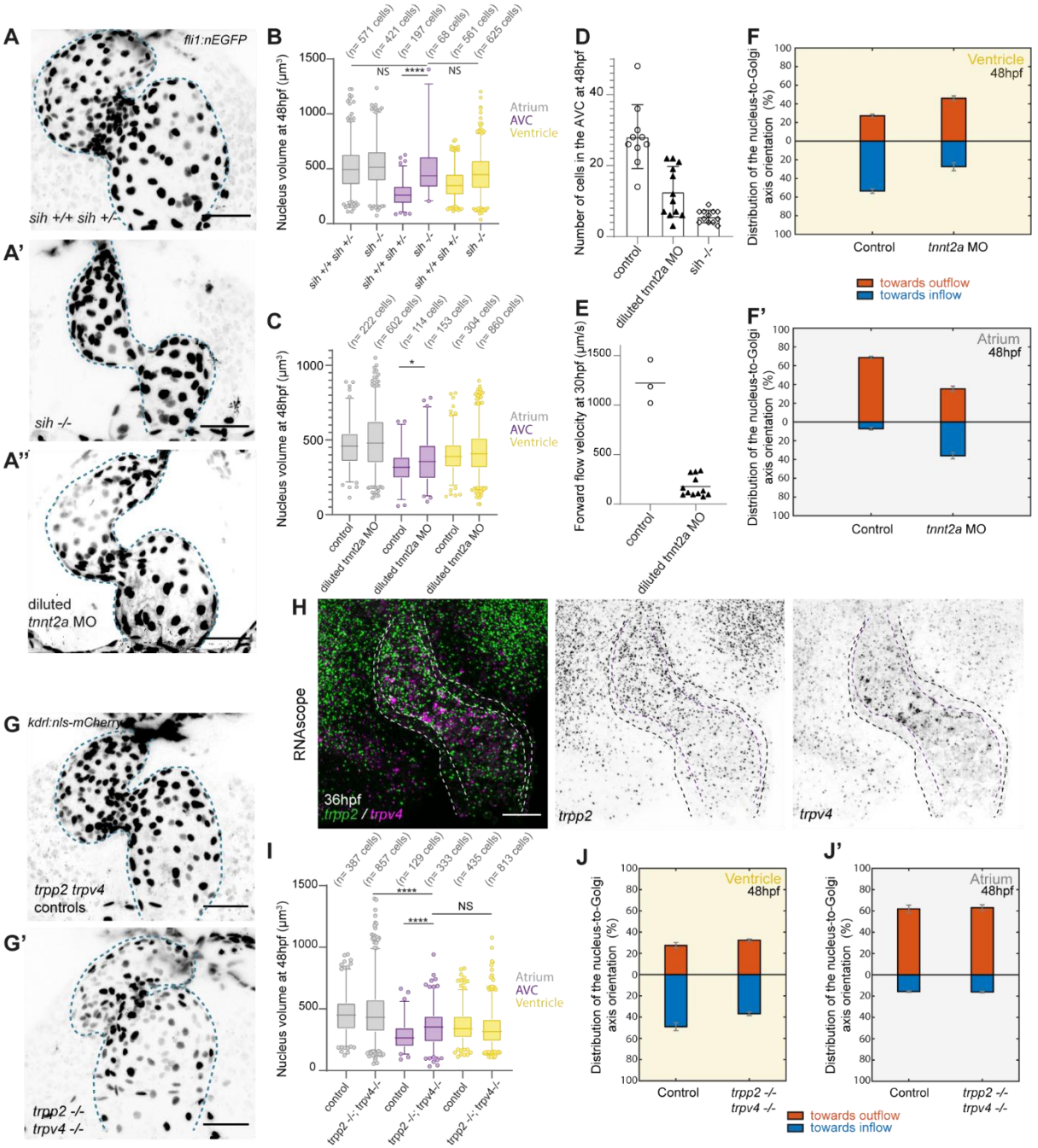

Figure 4. Mechanical forces and TRP channels mediate AVC endocardial cell volume decrease during early AVC morphogenesis (**A-A''**) Maximal projection of *kdrl :nls-mCherry* heart at 48 hpf for *sih*$^{+/+}$ *sih*$^{+/-}$ (**A**), *sih*$^{-/-}$ (**A'**) and diluted *tnnt2a* morpholino (**A''**). Scale bars, 50 µm. Blue dotted lines outline the endocardium (**B**) Quantification of the nucleus volume in atrium, AVC, and ventricle in both *sih*$^{+/+}$ *sih*$^{+/-}$ and *sih*$^{-/-}$. (N= 8 *sih*$^{+/+}$ *sih*$^{+/-}$ embryos, N=12 *sih*$^{-/-}$ embryos). Unpaired two-tailed t-test. (**C**) Quantification of the nucleus volume in the atrium, AVC, and ventricle in controls (sham) and diluted *tnnt2a* morpholino (MO)-injected embryos. (N= 3 controls (sham), N=12 embryos injected with diluted *tnnt2a* morpholino (MO)-injected embryos). Unpaired two-tailed t-test. (**D**) Number of EdC cells present in the AVC region based

on the data presented in (A) for controls, diluted *tnnt2a* MO-injected embryos, and *sih*$^{-/-}$. (**E**) Quantification of the forward flow (in the direction of the outflow) velocity at 30hpf based on manual tracking of fluorescent nano-droplets injected in the blood circulation, as explained in Figure (5.B). (**F-F'**) Quantification of the percentage of cells with the nucleus-to-Golgi axis towards the outflow and towards the inflow in the ventricle (**F**) and the atrium (**F'**) at 48hpf in controls (sham) and *tnnt2a* morphants (at high concentration). (N=3 embryos, sham and N=6 embryos, *tnnt2a* MO) Error bars indicate the s.e.m.(**G-G'**) Maximal projection of the stopped heart of *kdrl:nls-mCherry* embryos at 48hpf for *trpp2*,*trpv4* controls (**G**) (including trpp2$^{+/+}$,trpv4$^{+/+}$; *trpp2*$^{+/-}$*,trpv4*$^{+/+}$ and *trpp2*$^{+/+}$*,trpv4*$^{+/-}$) and their siblings *trpp2*$^{-/-}$*, trpv4*$^{-/-}$ (**G'**). Scale bars, 50 μm. Blue dotted lines outline the endocardium. (**H**) Maximum projection of confocal micrograph for *trpp2* and *trpv4* probes at 36hpf. The outer black dotted line represents the myocardial layer and the inner violet dotted line represents the endocardial layer (**I**) Quantification of nucleus volume in the atrium, AVC, and ventricle in *trpp2*,*trpv4* control embryos (including trpp2$^{+/+}$,trpv4$^{+/+}$; *trpp2*$^{+/-}$*,trpv4*$^{+/+}$ and *trpp2*$^{+/+}$*,trpv4*$^{+/-}$) and their *trpp2*$^{-/-}$*,trpv4*$^{-/-}$ siblings. (N= 15 embryos for *trpp2*$^{-/-}$*trpv4*$^{-/-}$ and N=6 control embryos). Unpaired two-tailed t-test. (**J-J'**) Quantification of the percentage of cells with the nucleus-to-Golgi axis towards the outflow and towards the inflow at 48hpf in controls and *trpp2-/- trpv4 -/-* in the ventricle (**J**) and in the atrium (**J'**). The antibody GM130 was used to label the golgi. (N= 3 embryos, controls and N= 4 embryos, *trpp2-/- trpv4 -/-*). Error bars represent the s.e.m.

(nucleus volume of 360.9±11.7 µm^3, n=153 cells, N= 12 embryos in *tnnt2a* morphants, nucleus volume of 324.9±10.5 µm^3, n=114 cells, N=3 embryos) (Figure 4.C) suggesting that even subtle hemodynamic decrease alters cell volume. Overall, these results indicate that mechanical forces are important regulators of cell volume decrease.

The stretch sensitive channels TRPP2 and TRPV4 are key modulators of cell volume decrease

The stretch-sensitive channels Transient Receptor Potential Polycystin 2 (TRPP2) and Transient Receptor Potential Vanilloid 4 (TRPV4) are important regulators of heart valve development (Heckel et al., 2015). Interestingly, TRPV4 is also a well-known contributor to cell volume regulation in astrocytes where it acts as an osmosensitive channel (Benfenati et al., 2011). We thus hypothesized that TRP channels could modulate cell volume during AVC morphogenesis. We investigated mutants for *trpv4* and *trpp2* channels. *trpp2* mRNA is ubiquitously distributed in the embryo but is enriched within the endocardial layer of the heart whereas *trpv4* is mostly expressed in the endocardium and specifically enriched in the AVC region (Figure 4.H). By looking at both *trpv4* $^{-/-}$ and *trpp2* $^{-/-}$ single mutant embryos, we found that EdC nucleus volume at the AVC was unchanged compared to controls (Figure S4.D). Since genetic compensation is a widespread feature in zebrafish (El-Brolosy & Stainier, 2017) we analysed double *trpv4* $^{-/-}$*;trpp2* $^{-/-}$ mutants (Figure 4.G-G'). Cell volume decrease was not observed in the AVC of *trpv4* $^{-/-}$*;trpp2* $^{-/-}$ compared to controls (nucleus volume of 351.9±7.9 µm^3, n=333 cells, N=15 embryos in *trpv4* $^{-/-}$*;trpp2* $^{-/-}$, nucleus volume of 282.4±9.8 µm^3, n=129 cells, N=6 in *trpv4* $^{+/+}$*;trpp2* $^{+/+}$) (Figure 4.I), and nucleus-nucleus distance was significantly increased in AVC EdCs of the double mutants (Figure S4.E). Importantly, heart rate was not significantly different between mutants, suggesting that heart function and flow forces are normal (Figure S4.F). These data show that the Trpp2 and Trpv4 mechanosensitive channels are important regulators of cell volume decrease. Moreover, the percentage of ventricular EdCs with nucleus-to-Golgi axis towards the inflow 36.9±1.7 % (n= 309 cells, N=4 embryos) is reduced compared to controls (49.0±3.8 % (n= 223 cells, N=3 embryos) (Figure 4.J) and the distribution of the nucleus-to-Golgi axes was unchanged in the atrium (Figure 4.J'). This suggests that the tissue convergence is affected in the absence of the TRP channels.

In the context of osmotically-driven cell volume increase (i.e. cell swelling) TRPV4 interacts with aquaporin channels to modulate cell volume (Benfenati et al., 2011; Conner et al., 2012; Iuso & Križaj, 2016). Aquaporins are passive transmembrane channels that can enhance membrane permeability (Ibata et al., 2011; Mola et al., 2016). We studied the spatio-temporal expression patterns of aquaporins and focused on two aquaporin channels present in the developing cardiovascular system: *aqp8a.1* and *aqp1a.1 (*Figure S2.B-S2.D*)*. Both *aqp8a.1* and *aqp1a.1* mRNA are expressed within the heart (Figure S2.B), with expression starting from 30hpf specifically in AVC cells (9/32 embryos (*aqp8a.1*), 4/20 embryos (*aqp1a.1*)). At this stage, *aqp1a.1* is also expressed in the red blood cells, as previously reported (16/20 embryos) (Chen et al., 2010) (Figure S2.B). At 36hpf, *aqp8a.1* and *aqp1a.1* mRNAs are expressed in both AVC and OFT cells (24/27 embryos (*aqp8a.1*), 19/19 embryos (*aqp1a.1*). At 48 hpf, *aqp8a.1* is undetectable (36/36) whereas *aqp1a.1* mRNA expression is highly specific in the AVC and OFT regions (31/31). Using fluorescent probes, we confirm that these channels are expressed specifically in the AVC and OFT regions and further show that their expression is restricted to the endocardium (Figure S2.C). Interestingly, both the expression of *aqp8a.1* and *aqp1a.1* were absent in the *sih* $^{-/-}$ embryos, suggesting that their expression is dependent on mechanical forces (Figure S4.C). These data indicate that cells specifically located in the AVC are equipped with water channels whose expression depends on heart function.

Hyaluronic acid modulates AVC endocardial cell volume changes

One of the most abundant components of the cardiac jelly is the glycosaminoglycan (GAG) hyaluronic acid (HA). GAG accumulation is known to apply osmotic pressure and to attract water (Cowman et al., 2015; Lockhart et al., 2011). *In vitro*, GAG leads to cell shrinkage of HEK cells (Joerges et al., 2012). HA is assembled by *hyaluronan synthase* genes and is then secreted into the ECM. In particular, *has2* is specifically expressed by EdCs of the AVC (Patra et al., 2011; Tong et al., 2014). As expected, *has2* expression in the heart starts at 30hpf and is restricted to the AVC from 30hpf to 48hpf (Figure S5.A). We used HA-binding protein (HA-BP) to study the protein localization (Figure 5.A). HA was found to be present exclusively within the cardiac jelly (Figure 5.A, Figure S5.B) and appears uniformly distributed throughout the cardiac jelly of the heart. We next assessed its potential role in cell volume regulation at the

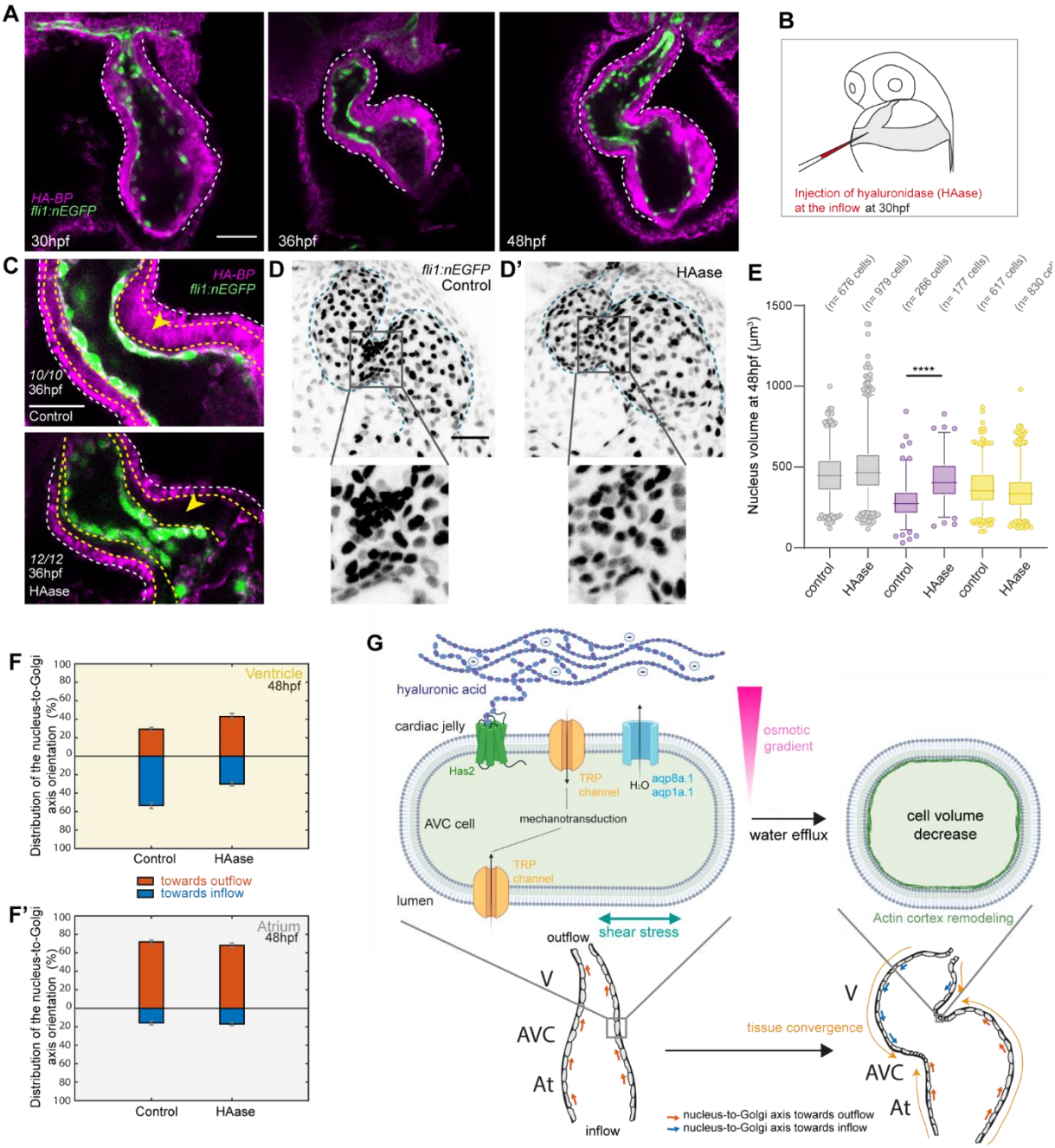

<u>Figure 5. Hyaluronic acid located in the cardiac jelly modulates AVC endocardial cell volume changes.</u> (**A**) Pictures of one z-plane showing the localization of HA-BP (magenta) by immunofluorescence on fixed and deyolked (to visualize the whole heart) *fli1:nEGFP* embryos (nuclei in green) at 30hpf (N=10 embryos), 36hpf (N=8 embryos), and 48hpf (N=12 embryos). Scale bar, 50 µm. White dotted lines outline the heart. (**B**) Schematic explaining the injection process of the hyaluronidase (HAase) inside the blood circulation, near the inflow region of the heart at 30hpf. (**C**) Pictures of one z-plane in the AVC region showing the presence of HA-BP inside the cardiac jelly (yellow arrow) for control (injected with PBS-injected) embryos (N=10/10) and the absence of HA-BP inside the cardiac jelly (yellow arrow) for HAase-injected embryos (N=12/12) at

36hpf. Scale bar, 30 µm. White dotted lines outline the heart. The yellow dotted lines mark the contours of the cardiac jelly. (**D-D'**) On the top panel: Maximal projections of stopped hearts at 48hpf of *fli:nEGFP* embryos for control (PBS-injected) embryos (**D**) and HAase-injected embryos (**D'**). On the bottom panel: zoom in the AVC region. Scale bar, 50 µm. Blue dotted lines outline the endocardium. (**E**) Quantification of the nucleus volume in the atrium, AVC, and ventricle in both controls (PBS-injected) embryos and HAase-injected embryos based on the raw data presented in (D). (N=8 controls, N=12 HAase-injected embryos). Two-tailed unpaired t-test. (**F-F'**) Quantification of the percentage of cells polarized towards the outflow and cells polarized towards the inflow in the ventricle (**F**) and the atrium (**F'**) at 48hpf in controls (PBS-injected) and HAase-injected embryos (N=5 embryos, controls, and N=7 embryos, HAase-injected) Error bars indicate the s.e.m. (**G**) Schematic illustrating the proposed mechanism for cell volume decrease at the AVC. Created partially with BioRender.com.

AVC by injecting hyaluronidase (HAase), which breaks down HA chains (Figure 5.B). HAase-injected embryos presented pericardial edema after 18 hours of treatment (Figure S5.C) but did not have heart rate defects at 48hpf (Figure S5.E). In this condition, HA was not detected inside the cardiac jelly of HAase-injected embryos, confirming that HA degradation was effective (Figure 5.C). Interestingly, F-actin remodeling in EdCs and cell volume decrease did not occur in the treated embryos (Figure S5.D) (N=7/7 HAase-injected embryos, N=7/7 controls). Cell volume decrease was not observed in the AVC of HAase-injected embryos compared to controls (nucleus volume of 422±10.0 μm^3, n=177 cells, N=12 embryos in HAase-injected embryos, nucleus volume of 290.6±7.0 μm^3, n= 266 cells, N=8 in controls) (Figure 5.E). Similarly, the AVC nuclei-nuclei distance was increased in HAase-injected embryos (Figure S5.F). Furthermore, the number of ventricular cells with nucleus-to-Golgi axis towards the inflow 30.1±2.2 % (n=523 cells, N=7 embryos) is reduced compared to controls 53.4±3.3% (n=425 cells, N=5 embryos) (Figure 5.F) and the distribution of the nucleus-to-Golgi axes was unchanged in the atrium (Figure 5.F'). This result indicates that tissue convergence is reduced in the absence of HA inside the cardiac jelly. We conclude that both mechanosensitivity and HA are essential modulators of the cell volume decrease in the AVC (Figure 5.G).

DISCUSSION

Using *in vivo* imaging, we show that endocardial cell volume decrease is key for tissue convergence and AVC formation, setting the stage for subsequent valve formation (Pestel et al., 2016; Steed et al., 2016). We observed that cell volume decrease is concomitant with ventricular nucleus-to-Golgi axis reversal as well as F-actin remodeling in the AVC. Additionally, we show that cell volume change is independent of cell proliferation and is regulated by mechanical forces caused by heart function, TRP channels and HA located in the cardiac jelly. Together, our results show that cell volume decrease is an important cellular feature involved in cardiovascular morphogenesis in response to mechanotransduction activated by TRP channels. We propose that cell volume change may be a general cellular feature activated by mechanical forces to control tissus shape.

TRP channels are key players in the mechanotransduction pathway leading to heart valve formation (Duchemin et al., 2019; Heckel et al., 2015). The current model suggests that those channels sense oscillatory blood flow at the AVC, which is subsequently transduced into electrochemical information, leading to the expression of mechanosensitive genes (Steed, Boselli, et al., 2016, Heckel et al., 2015). Our results suggest that additional cues, on top of oscillatory blood flow, might affect the activity of the TRP channels through the generation of an osmotic pressure generated in the cardiac jelly. The components of the cardiac jelly are important for proper AVC formation (Derrick & Noël, 2021; Grassini et al., 2018; Hernandez et al., 2019). For example, modulating the expression of the *ugdh* gene encoding for the GAG building blocks or the alteration of HA deposition in the cardiac jelly leads to defects in AVC development (Segert et al., 2018; Walsh & Stainier, 2001). Here, we show that HA regulates the size of the EdCs in the AVC, revealed by the absence of a cell volume decrease in the hyaluronidase-treated embryos. Interestingly, it is known that GAG can establish an osmotic pressure (Cowman et al., 2015) and TRPV4 channels are potent osmosensitive channels (Hoffmann et al., 2009) that physically interact with aquaporin to modulate cell volume in response to osmotic stresses (Benfenati et al., 2011). Interestingly, the cells that lose volume were also found to be equipped with aquaporin channels (aqp8a.1, aqp1a.1). Considering that Aquaporin enhances water

permeability (Ibata et al., 2011; Mola et al., 2016), the TRPV4-Aquaporin complex might increase the rate of water efflux following the establishment of an osmotic gradient. Moreover, the intracellular entry of calcium ions following the opening of the TRP channels might lead to the translocation of the aquaporin channels to the plasma membrane (Conner et al., 2012). With this, we propose a model where HA accumulation creates an osmotic pressure between the EdCs and the cardiac jelly to promote the cell volume decrease observed in the AVC (Figure 5.G). In this model, TRP channels would be involved both in the osmosensing as well as the shear stress sensing.

What is the driving force behind tissue convergence? At the tissue level, we observed a change of the nucleus-to-Golgi axis that is concomitant to cell volume changes and depending both on blood flow, and the presence of TRP channels and HA. As a consequence, the local cell volume decrease of EdCs in the AVC could pull on the surrounding cells and drive tissue convergence as well as the cell clustering. In addition, we cannot rule out that tissue convergence is in part due to an active migration of EdCs towards the AVC. Indeed, the presence of HA inside the ECM has been reported to be essential in the context of cell migration in several studies (Derrick & Noël, 2021) and ECM is key to regulate the turnover of angiogenic signals (De Angelis et al., 2017). Two main scenarios can therefore explain our results: active migration towards the AVC is taking place and then followed by an adaptive cell volume shrinkage and/or the cell volume shrinkage at the AVC pulls on the surrounding cells and leads to tissue convergence. Considering the small amplitude of the tissue movements, we favour the second scenario where cell volume decrease is sufficient to drive tissue movement as described in other species (Saias et al., 2015).

In summary, we observed that the loss of the mechanosensitive/osmosensitive TRP channels in the presence of normal blood flow affects the ability of AVC EdCs to decrease their cell volume and subsequent heart valve morphogenesis. These results indicate that EdCs process local mechanical signals to regulate their size through ion channels. The coordinated interactions between extracellular and intracellular processes involved in cell volume regulation are key to explain the mechanisms leading to tissue remodeling. Overall, a better understanding of these mechanisms will have implications for treating numerous pathological conditions including cardiovascular diseases such as congenital valvulopathies.

METHODS

Zebrafish husbandry, transgenic lines, morpholinos

Animal experiments were approved by the Animal Experimentation Committee of the Institutional Review Board of the IGBMC and followed ethical and animal welfare guidelines. 0.003% 1-phenyl- 2-thiourea (PTU) (Sigma Aldrich, P7629) was added to 0.3X Danieau's buffer at 8 hours post-fertilization in order to prevent pigment formation. Embryos were raised at 28.5 °C. The different zebrafish lines used in this study were: AB as wild-type line, *Tg(fli1a:B4GALT1galT-mCherry)*^{bns9} (Kwon et al., 2016), Tg*(fli1:nEGFP)*^{y7} (Roman et al., 2002), *Tg*(*ve-cad:ve-cadTS*) (Lagendijk et al., 2017), *Tg(fli1a:DsRed)* (Vatine et al., 2013); *Tg(fli1a:lifeact-EGFP)* (Phng et al., 2013), *Tg(kdrl:nls-mCherry)* (Nicenboim et al., 2015), *silent heart (sih)*^{tc300b} (Sehnert et al., 2002), *cup*^{tc321} (Schottenfeld et al., 2007), *trpv4*^{sa1671} (ZIRC). The genotyping primers were for *trpv4* the forward (5'-GCCTTTCAGCATGTTGTCCA-3') and the reverse (5'-GGTTCCTGCTGGTCTACGTG-3') primers with a Tm of 64.2°C for annealing and for *trpp2* the forward (5'- CCATTAGCCTGCACATTCAATC-3') and the reverse (5'-ATCGCACTGCTCATCTGAAG-3') primers with a Tm of 62.9°C for annealing. The *trpp2* homozygous mutant was selected phenotypically based on their curved tail phenotype. The morpholino (MO) used in this study targets *tnnt2a* (5'-CATGTTTGCTCTGATCTGACACGCA-3') (GeneTools) (Sehnert et al., 2002). 5.8 ng of the *tnnt2a* MO was injected into the yolk at the one-cell stage for complete heartbeat arrest and 0.14 ng was injected to reduce heartbeat amplitude (referred to as diluted *tnnt2a* MO in text).

Confocal imaging

For live imaging, dechorionated zebrafish embryos were anesthetized using 0.2mg.mL^{-1} of tricaine (Sigma Aldrich, A5040; stock at 8mg/mL adjusted to pH7-7.5) (to stop fish motion) or 50mM drug 2,3-butanedione monoxime (BDM) (Sigma Aldrich, B0753) for 10 minutes (to stop the heart) and then mounted in 1.2% UltraPure low melting-point agarose (Sigma Aldrich, 16520) that has the same concentration of tricaine or BDM as the media.

Confocal imaging was performed either on an up-right Leica SP8-Multiphoton confocal microscope (to image the stopped heart or fixed embryos) or on an inverted Leica spinning disk (to image the beating heart). The mounting was different on the two microscopes - a custom-designed mold was used for imaging on the up-right Leica SP8-MP confocal microscope (Chow et al., 2018) and a glass-bottom Petri dish (MateTek, P35G-0-14-C) for imaging on the inverted spinning disk microscope.

Image analysis

Classification of cell polarity

Individual cell polarity was analysed by manually labelling individual nuclei and Golgi apparatus using the “spots” tool in the Imaris software (3D viewer). We then classified by eye the cell polarity of each cell based on the position of its Golgi apparatus relative to its cell nucleus: polarized towards the outflow, polarized towards the inflow, or no clear polarization.

F-actin intensity measurements

10 cells were analyzed for each region of the heart (atrium, AVC, ventricle) in *fli:LifeAct-eGFP* embryos. For each cell, 10 lines were drawn perpendicular to the plasma membrane with ImageJ and the maximal intensity was measured.

Cell volume estimation measurements

Measurement points were put with the Imaris software all around the cell membrane based on the VE-cadherin signal, *Tg*(*ve-cad:ve-cadTS*). The coordinates of these measurement points were inputted into Matlab, and the individual cell surface area was calculated using Delaunay triangulation-based surface reconstruction. Using the *Tg(fli1a:DsRed)* line to visualize the cytoplasm of endothelial cells, cell height measurements were made in Imaris software (3D viewer). Since AVC endocardial cells are cuboidal, an estimation of their cell volume was computed simply by multiplying the height of the cell with the cell surface area (Figure 2.B). For EdCs in the ventricle and atrium, the height of the cell was much higher at the part of the cell containing the cell nucleus (H_N) than at other parts of the cell (H_O). Thus, their cell volume was estimated by multiplying H_N with the nucleus area, multiplying H_O with the area of the cell not containing the nucleus, and adding the two products together (Figure 2.B).

Nuclei segmentation

Nucleus segmentation of 3D images was obtained with a Deep Learning based segmentation pipeline called StarDist3D (Weigert et al., 2020). The training of StarDist3D needs ground truth instance segmentation annotations which are cumbersome to obtain, if done fully manually. Hence, this manual annotation effort was partially circumvented by adopting an iterative approach for ground-truth annotation. Firstly, only one 3D image was fully manually annotated using the open-source Labkit plugin in Fiji (Schindelin et al., 2012). A StarDist3D network was then trained using the single annotated 3D stack. This trained network was then used to predict nucleus segmentations in a separate 3D image. These predictions were then manually curated such that all segmentation errors were removed. The curated image, together with the first, manually annotated image, were then used to train yet another StarDist3D network, and this iterative training, prediction, curation loop can be continued.

In this work, this process was iterated 4 times, leading to a final StarDist3D network trained on a total of 5 full 3D images. While manual annotation of the first ground truth image took roughly 4 hours, the curation times for the subsequent 4

iterations reduced to ~2 hours, ~1 hour, ~30 minutes and ~10 minutes, respectively. Network training was performed using patches of size 48x96x96 and a batch size of 2 for 400 epochs and 100 steps per epoch, using the default parameters of the public implementation of StarDist3D (https://github.com/stardist/stardist).

The final network was used to obtain instance segmentations for all datasets used in this work. After segmentation, a custom python script was used to compute volume and 3D position of each segmented cell nucleus. By matching the 3D coordinates of nuclei positions back to the original image, nuclei were manually sorted into three groups (atrium, AVC, and ventricle) based on the region of the heart they are located in.

To obtain the mean distance between each cell and its three nearest neighbours, the 3D coordinates of the segmented nuclei were inputted into a custom Matlab script. For each nucleus, the Matlab script calculates the distance between the nucleus and all the other nuclei within the heart. Then, those values are sorted according to size, and the mean value for the three shortest distances was calculated.

Immunofluorescence

Zebrafish embryos were dechorionated and fixed for 2-3 hours at room temperature (RT) at the desired developmental stage in either 4% paraformaldehyde (PFA) in 1X phosphate-buffered saline solution (PBS) or in 4g of PFA diluted in 100mL of Fish Fix Buffer (1L: 1X PBS, 120µL 1M $CaCl_2$, 40g sucrose) for easy removal of the yolk with forceps. At early developmental stages, the removal of the yolk was beneficial for imaging the whole endocardial tissue, in particular the part of the endocardium near the outflow tract. Therefore, the yolk was removed for cell polarity, HA-BP immunofluorescence, and RNAscope experiments.

After fixation, embryos were washed in PBS implemented with 0.1% Tween20 (PBST), three times for 5 minutes. For GM130, anti-phosphorylated histone H3 antibody, and phalloidin stainings, embryos were permeabilized in 1X PBS containing 0.1% Triton X-100 (PBST) (Sigma-Aldrich, T8787) (GM130 antibody) or 0.5% Triton X-100 (phospho-H3 antibody), overnight at 4°C. Embryos were then incubated in blocking solution (PBS with 0.1% Triton X-100, 2% BSA (H2B, 1005-70), 5% NGS (Coger, VS-1000) (GM130) (Sepich & Solnica-Krezel, 2016) or (PBS with 0.5% Triton X-100, 2 mg/mL BSA, 2% NGS) overnight at 4°C. Primary antibodies were then added at the following dilutions: Mouse-anti-GM130, 1:100, BD Bioscicence-610822), (Rabbit-anti-PH3, 1:100, Millipore-06-570 in fresh blocking buffer for 2 days. Then, embryos were washed over 4 hours (with solution changes every 30 minutes) in PBST. Secondary antibodies were added: Goat-anti-Mouse (Alexa Fluor 647, Invitrogen, A32728) or Goat-anti-Rabbit (Alexa Fluor 594, Invitrogen, A11037), and counterstained with Phalloidin when necessary (Alexa Fluor 568, 1:50, Invitrogen, A12380).

For Hyaluronic Acid-Binding Protein (HA-BP, Sigma-Aldrich, 385911) immunofluorescence, the experimental procedure described in (Munjal et al., 2020) was performed on deyolked embryos.

Pharmacological treatments

Hydroxyurea and Aphidicolin

Larvae were incubated from 30hpf to 48hpf with a mix of two S-phase inhibitors: 30 mM Hydroxyurea (HU) (Sigma-Aldrich, H8627; diluted in water) and 150 µM Aphidicolin (A) (Sigma-Aldrich, 89458; diluted in DMSO).

Hyaluronidase pharmacological treatment

Zebrafish embryos were dechorionated, anesthetized with 0.2mg.mL^{-1} of tricaine, and mounted on a glass-bottom Petri dish (MateTek, P35G-0-14-C) with 1.2% UltraPure low melting-point agarose (Sigma Aldrich, 16520). The injection solution was prepared as follows: 1X PBS with 0.5% Phenol Red (Sigma Aldrich, P0290) for controls and Hyaluronidase from *Streptomyces Hyalurolyticus* (Sigma- Aldrich, H1136, diluted in 1X PBS) with 0.5% Phenol Red for treated embryos. The solutions were injected into the embryos via the cardinal vein at 30 hpf near the inflow region of the heart using glass capillaries and a NanoInjectII injector (Drummond Scientific, Broomall, PA, USA). Embryos were then carefully removed from agarose using forceps before returning them to 0.3X Danieau, 0.003% PTU and placed in a 28.5°C incubator.

Flow analysis

Embryos were injected as described in the section above, except here the injection mix was made by diluting a solution containing 95nm 561nm fluorescent nano-droplets with 3.3% Dil-TPB suspension (Kilin et al., 2014) 1:1000 in PBS. Embryos were removed carefully from the low melting point agarose and mounted again in order to be imaged under the spinning disk microscope with a Leica 40X (NA 1.1) water immersion objective. The analysis of the flow was then realized with the Manual Tracking plugin available under FiJi.

In situ hybridization

Whole-mount in situ hybridization (ISH) was performed as in Thisse and Thisse (2008). Aqp8a.1 and aqp1a.1 probes were generated for this study. The *aqp8a.1* probe was generated with a fully sequence cDNA clone (IRBOp991A0150D – Source Bioscience) with the primers:- forward primer containing the T7 promoter (5'-TAATACGACTCACTATAGCTGAAGCTCCGGGCAG-3') - reverse primer containing

the Sp6 promoter (5’ ATTTAGGTGACACTATAGCCTCTTCAGTTCCTTCTTCCATC-3’).

The aqp1a.1 probe was generated from whole extracted cDNA at 30hpf and amplified with the primers (5’-GTCATGAACGAGCTGAAGAGC-3’) and (5’-GGGTCACTTTGAGGACATCTC-3’), incorporated into the pCR-BluntII-TOPO vector (Invitrogen, 45-0245) (containing both the SP6 and T7 promoters), linearized with NotI. Both were then subsequently transcribed with the SP6 enzyme (mMessage mMachine SP6 transcription kit (Ambion)) in order to obtain the antisense RNA probe that was then purified with the RNeasy kit (Qiagen – 74104).

The has2 probe was generated from the plasmid PBSK-dg42II containing cDNA of the zebrafish has2 (provided by the Bakkers lab, The Netherlands), linearized with XbaI and subsequently transcribed using the T7 polymerase.

Imaging of ISH was then realized using a Leica M165 macroscope with a TrueChrome Metrics (Tucsen) with a Leica 1.0X objective (10450028).

RNAscope

RNAscope experiments were performed using the RNAscope Fluorescent Multiplex kit (Advanced Cell Diagnostics, 323110) and by following the manufacturer’s guidelines.

Statistical analysis

For the statistical analysis of the data, Student’s paired t-test with a two-tailed distribution or Mann-Whitney test with a two-tailed distribution were performed using the Prism software. For *p* values: < 0.05 *; < 0.01 **, < 0.001 ***, < 0.0001 ****

In each figure, the statistical test performed on the data, the number of analyzed cells (n) and/or the number of embryos (N), as well as the meaning of error bars is stated. Box plots were generated with the Prism software where horizontal lines show the median. The whiskers extend to the 2.5th and 97.5th percentiles. Data points outside whiskers are shown as individual circles.

ACKNOWLEDGMENTS

We thank R. Chow as well as D. Riveline, S. Quintin and the participants of the “Biophysics club” at the IGBMC for the fruitful discussions and help with the manuscript. We also thank the members of the Norden lab for their feedback on the project. We are grateful to all the staff members of the imaging platform at IGBMC, especially E. Grandgirard and also the members of the IGBMC fish facility (S. Pajot, S. Geschier and C. Moebs). This project has received funding from the European Research Council (ERC) under the European Union’s Horizon 2020 research and innovation programme: GA N°682939, Agence Nationale de la Recherche: ANR-15-CE13-0015-01, ANR-10-IDEX-0002–02, ANR-12-ISV2-0001-01 and ANR-10-LABX-0030-INRT and the European Molecular Biology Organization Young Investigator Program. HV was supported by the IGBMC International PhD program: ANR-10-LABX-0030-INRT.

AUTHOR CONTRIBUTIONS

Conceptualization, H.V. and J.V.; Visualization, H.V; Methodology, H.V., M.P., C.N., and F.J.; Resources, J.V.; Data Curation, H.V., C.V-P. M.P; Formal Analysis, H.V. and J.V.; Validation, H.V., C.V-P and J.V.; Writing– Original Draft, H.V and J.V.; Funding Acquisition J.V.; Supervision, J.V.; Project Administration, J.V.

COMPETING INTERESTS

The authors declare no competing or financial interes

SUPPLEMENTARY DATA

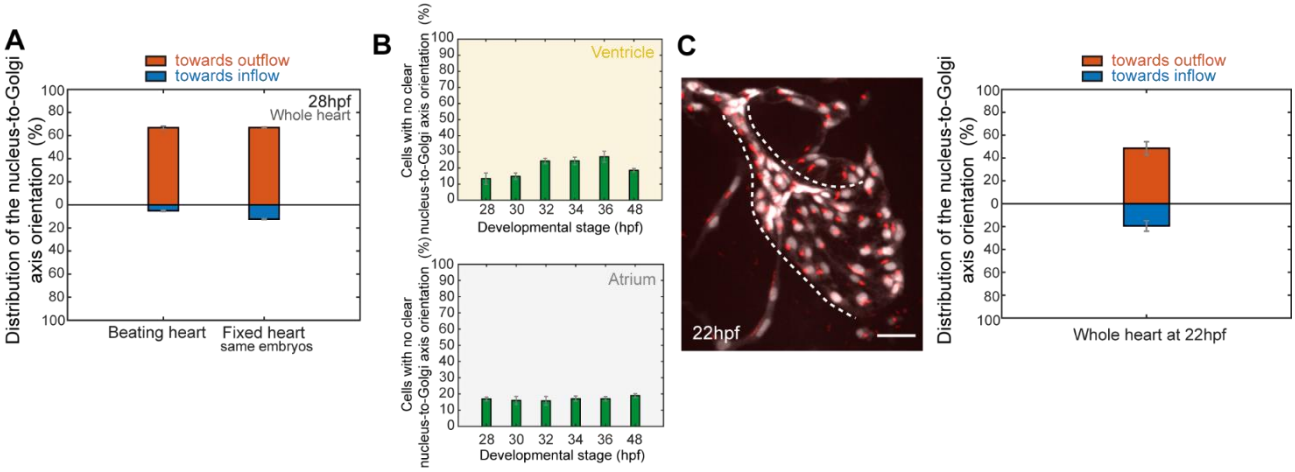

Figure S1. (**A**) Quantification of the percentage of EdCs nucleus-to-Golgi axis towards the outflow and towards the inflow at 28hpf in hearts that are beating and in the same hearts after fixation, showing that fixation does not affect the cell orientation pattern within the endocardium (N=3/3 embryos). (**B**) Quantification of the percentage of cells with no clear orientation of the nucleus-to-Golgi axis from 28hpf to 48hpf, in both ventricle and atrium. (N=5 embryos, 28hpf ; N=5 embryos, 30hpf ; N=4 embryos, 32hpf ; N=4 embryos, 34hpf ; N=5 embryos, 36hpf ; N=7 embryos, 48 hpf). Error bars show the s.e.m (**C**) Maximal projection of a fixed and deyolked heart at 22hpf (Scale bar, 30 µm.) and analysis of the EdC nucleus-to-Golgi axis distributions within the whole heart tube (N= 3 embryos).

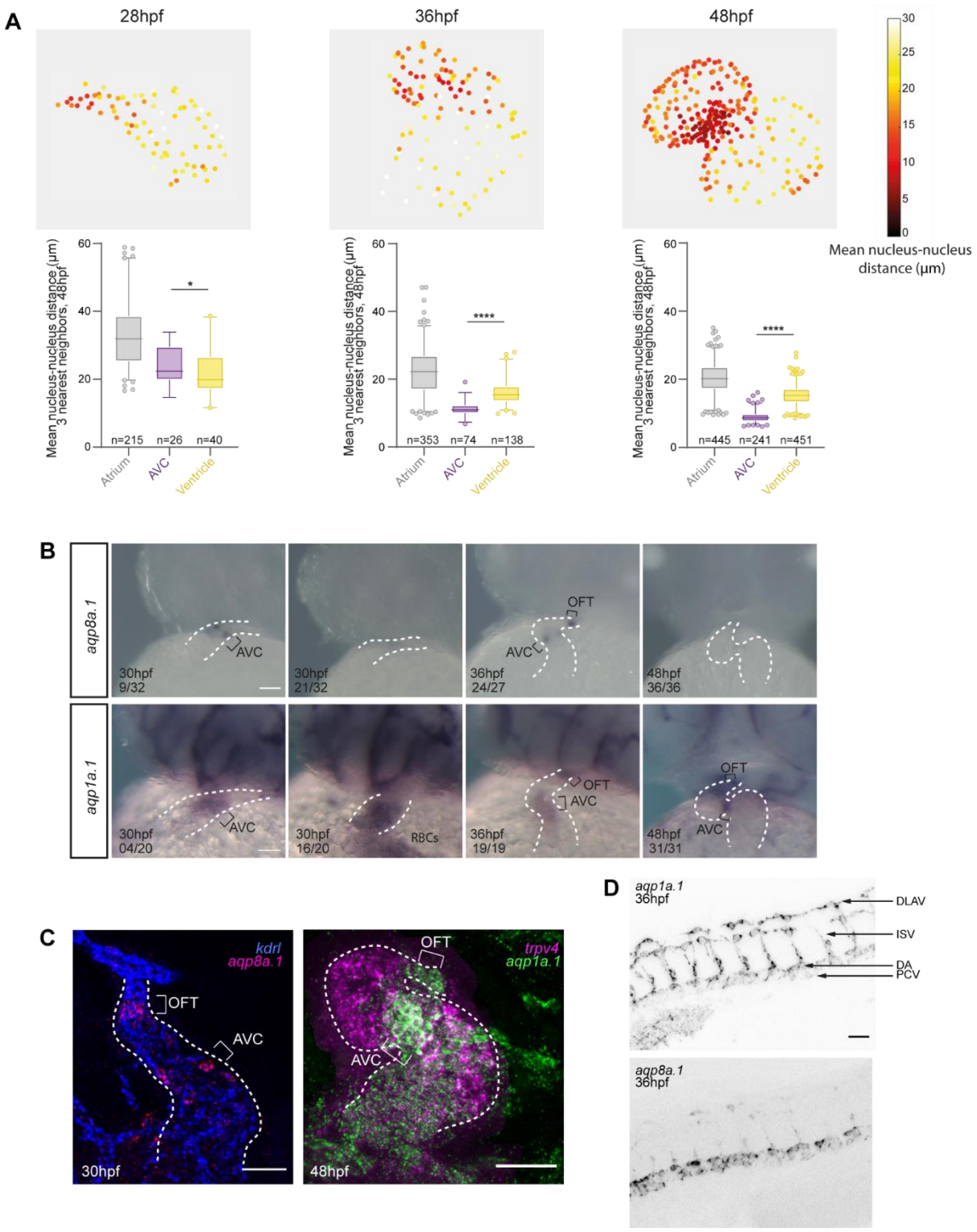

Figure S2.(**A**) Heat-maps of the distance between a nucleus and its three nearest neighbours (top panel) and quantifications of those distances by heart region (Atrium, AVC, ventricle) at 28hpf, 36hpf, and 48hpf. (N=5 embryos, 28hpf; N=5 embryos, 36hpf; N=5 embryos, 48hpf). (**B**) *In situ* hybridization with *aqp8a.1*and *aqp1a.1* probes in AB embryos at 30hpf, 36hpf, and 48hpf. White dotted lines outline the heart. Scale bars, 50 µm. (**C**) *aqp8a.1* and *aqp1a.1* mRNA expression profile in the endocardium. On the

left: maximal projection of a multiplex RNAscope with the *kdrl* and *aqp8a.1* probes at 30hpf (N=7/7 embryos). On the right: maximal projection of a multiplex RNAscope using *trpv4* and *aqp1a.1* probes at 48hpf (N=5/5 embryos). Scale bars, 50 μm. (**D**) *aqp8a.1* and *aqp1a.1* mRNA expression in the endothelium of the cardiovascular system. DLAV= dorsal longitudinal anastomotic vessels, ISV= Intersegmental vessels, DA= dorsal aorta, PCV= posterior cardinal vein. Scale bars, 50 μm.

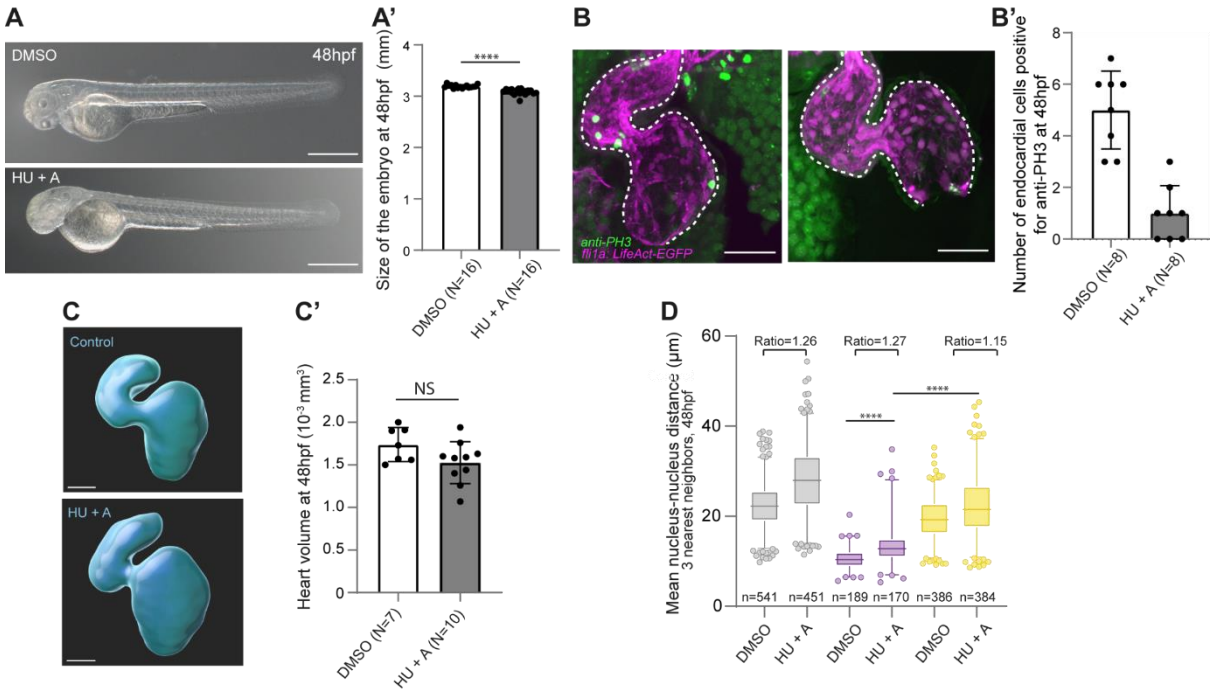

Figure S3. (**A**) Bright-field images of the embryo phenotype at 48hpf for controls (embryos treated with 0.5% DMSO from 30hpf to 48hpf) and treated embryos (embryos treated with 30mM Hydroxyurea (HU) and 150 µM Aphidicolin (A) from 30hpf to 48hpf). Scale bars, 0.5mm (**A'**) Measurements of total embryo size based on bright-field images at 48hpf (N=16 embryos, DMSO and N=16 embryos, HU+A). Mann-Whitney test. Error bars represent the s.d. (**B**) Immunofluorescence with anti-phosphorylated histone H3 in controls (DMSO) and treated (HU+A) in *fli1a:LifeAct-eGFP* embryos. Scale bars, 50 µm. White dotted lines outline the endocardium (**B'**) Analysis based on the immunofluorescence data in (B) showing the number of EdCs in the heart with anti-PH3 antibody signal at 48hpf (N=8 embryos, DMSO and N=8 embryos, HU+A). Bar plot with the mean and error bars representing the s.d. (**C**) Imaris 3D viewer representation of the whole heart volume at 48hpf. Scale bars, 50 µm. (**C'**) Quantification of the heart volume based on the Imaris data in (C) (N=7 embryos, DMSO and N=10 embryos, HU+A). Bar plot with the mean and the error bars represent the s.d. Two-tailed Mann-Whitney test. (**D**) Quantitative analysis of the mean distance between one nucleus and its three nearest neighbours at 48hpf for controls (DMSO) and treated (HU+A) *fli1:nEGFP* embryos.

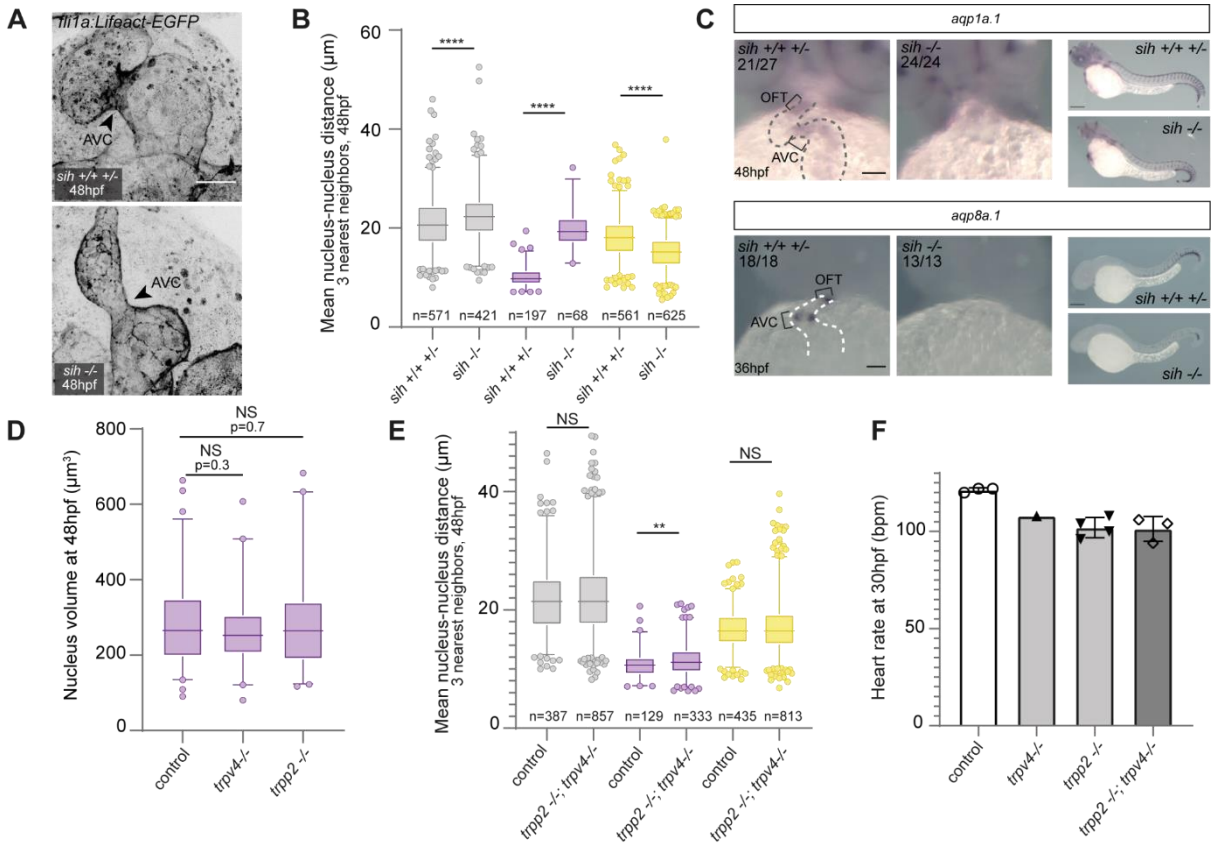

Figure S4. (**A**) Maximal projections of stopped hearts for *sih*$^{+/+}$ *sih*$^{+/-}$*; fli1a:LifeAct-EGFP* showing enrichment of F-actin signal at the AVC (arrowheads) and for their siblings *sih*$^{-/-}$*; fli1a :LifeAct-EGFP* showing the absence of F-actin signal at the AVC (arrowheads). (**B**) Quantitative analysis of the mean distance between one nucleus and its three nearest neighbours at 48hpf for *sih*$^{+/+}$ *sih*$^{+/-}$ and *sih*$^{-/-}$ *kdrl:nls-mCherry* embryos, based on the raw data presented in Figure 4.A (N= 8 *sih*$^{+/+}$ *sih*$^{+/-}$ embryos, N=12 *sih*$^{-/-}$ embryos). Unpaired two-tailed t-test. (**C**) In situ hybridizations with the aqp8a.1 and aqp1a.1 probes in *sih*$^{+/+}$*, sih*$^{+/-}$ and *sih*$^{-/-}$*.* Scale bars, 50 µm for the heart zoom and 200 µm for the entire embryo. Gray or white dotted lines outline the heart. (**D**) Quantification of the nucleus volume in the AVC in both *trpp2*,*trpv4* controls (including *trpp2*$^{+/+}$*,trpv4*$^{+/+}$; *trpp2*$^{+/-}$*,trpv4*$^{+/+}$ and *trpp2*$^{+/+}$*,trpv4*$^{+/-}$) and their *trpp2*$^{-/-}$ (*trpp2*$^{-/-}$*,trpv4*$^{+/+}$) and *trpv4*$^{-/-}$ *(*including *trpp2*$^{+/+}$*,trpv4*$^{-/-}$ and *trpp2*$^{+/-}$*,trpv4*$^{-/-}$) siblings. (N=6 embryos for the controls, N=4 embryos for *trpv4*$^{-/-}$, N=5 embryos for *trpp2*$^{-/-}$). Unpaired two-tailed t-test. (**E**) Quantitative analysis of the mean distance between one nucleus and its three nearest neighbours at 48hpf for *trpp2*, *trpv4* controls (including trpp2$^{+/+}$,trpv4$^{+/+}$; *trpp2*$^{+/-}$*,trpv4*$^{+/+}$ and *trpp2*$^{+/+}$*,trpv4*$^{+/-}$) and their siblings *trpp2*$^{-/-}$*,trpv4*$^{-/-}$ embryos. (N= 15 embryos for *trpp2*$^{-/-}$ *trpv4*$^{-/-}$ and N=6 control embryos). Error bars represent the s.e.m (**F**) Quantification of the heart rate (in bpm: beats per minute) at 30hpf at room temperature in controls (including trpp2$^{+/+}$,trpv4$^{+/+}$; *trpp2*$^{+/-}$*,trpv4*$^{+/+}$ and *trpp2*$^{+/+}$*,trpv4*$^{+/-}$), *trpp2* single mutant, *trpv4* single mutant and *trpv4 trpp2* double mutants. Bar plots represent the mean and the error bars represent the s.d.

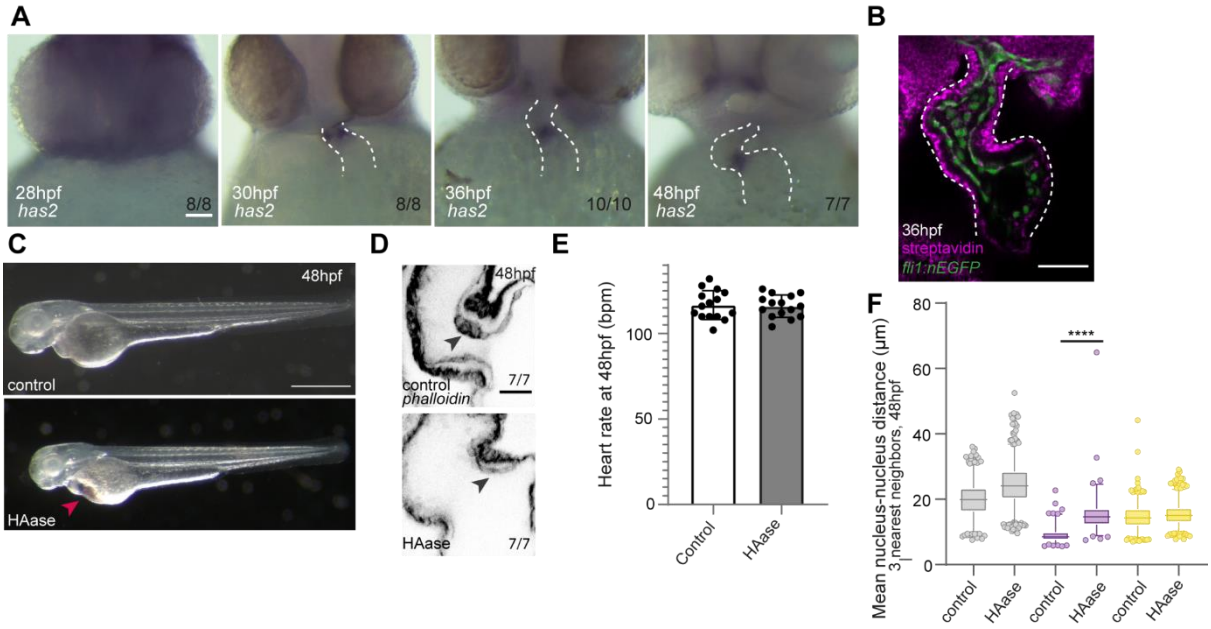

Figure S5. (**A**) *In situ* hybridization images with *has2* probe in AB embryos at 28hpf, 30hpf, 36hpf, and 48hpf. Scale bar, 50 µm. White dotted lines outline the heart. (**B**) Control immunofluorescence where Streptavidin was added in the absence of HA-BP resulting in a strong background signal in myocardial cells and a weaker background signal in endocardial cells. (N=6/6 embryos). Scale bar,50 µm. White dotted lines outline the endocardium. (**C**) Phenotype of the embryo at 48hpf. The embryos injected with HAase at 30hpf present edema (red arrow). Scale bar, 0.5mm (**D**) Phalloidin stainings in controls (N=7 embryos) and HAase-injected embryos (N=7 embryos). Black arrows point towards the endocardial cells of the AVC. (**E**) Quantification of the heart rate (in beats per minute) at 48hpf (N=15 controls, N=15 HAase-injected embryos) based on counting the number of beats per minute at room temperature. Bar plot with the mean and the error bars represent the s.d. (**F**) Quantitative analysis of the mean distance between one nucleus and its three nearest neighbours at 48hpf for controls (PBS-injected) embryos and HAase-injected embryos. Two-tailed unpaired t-test.

REFERENCES

Auman, H. J., Coleman, H., Riley, H. E., Olale, F., Tsai, H.-J., & Yelon, D. (2007). Functional Modulation of Cardiac Form through Regionally Confined Cell Shape Changes. *PLoS Biology*, *5*(3), e53. https://doi.org/10.1371/journal.pbio.0050053

Bartman, T., Walsh, E. C., Wen, K., Mckane, M., Ren, J., Alexander, J., Rubenstein, P. A., & Stainier, D. Y. R. (2004). Early Myocardial Function Affects Endocardial Cushion Development in Zebrafish. *PLoS Biology*, *2*(5), e129. https://doi.org/10.1371/journal.pbio.0020129

Benfenati, V., Caprini, M., Dovizio, M., Mylonakou, M. N., Ferroni, S., Ottersen, O. P., & Amiry-Moghaddam, M. (2011). An aquaporin-4/transient receptor potential vanilloid 4 (AQP4/TRPV4) complex is essential for cell-volume control in astrocytes. *Proceedings of the National Academy of Sciences of the United States of America*, *108*(6), 2563–2568. https://doi.org/10.1073/pnas.1012867108

Boselli, F., Freund, J. B., & Vermot, J. (2015). Blood flow mechanics in cardiovascular development. *Cellular and Molecular Life Sciences* (Vol. 72, Issue 13, pp. 2545–2559). Birkhauser Verlag AG. https://doi.org/10.1007/s00018-015-1885-3

Boselli, F., Steed, E., Freund, J. B., & Vermot, J. (2017). Anisotropic shear stress patterns predict the orientation of convergent tissue movements in the embryonic heart. *Development*, *144*(23), 4322–4327. https://doi.org/10.1242/dev.152124

Cadart, C., Venkova, L., Recho, P., Lagomarsino, M. C., & Piel, M. (2019). The physics of cell-size regulation across timescales. *Nature Physics* (Vol. 15, Issue 10, pp. 993–1004). https://doi.org/10.1038/s41567-019-0629-y

Camenisch, T. D., Spicer, A. P., Brehm-Gibson, T., Biesterfeldt, J., Augustine, M. Lou, Calabro, A., Kubalak, S., Klewer, S. E., & McDonald, J. A. (2000). Disruption of hyaluronan synthase-2 abrogates normal cardiac morphogenesis and hyaluronan-mediated transformation of epithelium to mesenchyme. *Journal of Clinical Investigation*, *106*(3), 349–360. https://doi.org/10.1172/JCI10272

Campinho, P., Vilfan, A., & Vermot, J. (2020). Blood Flow Forces in Shaping the Vascular System: A Focus on Endothelial Cell Behavior. *Frontiers in Physiology* (Vol. 11). https://doi.org/10.3389/fphys.2020.00552

Cantwell, H., & Nurse, P. (2019). Unravelling nuclear size control. *Current Genetics* (Vol. 65, Issue 6, pp. 1281–1285). https://doi.org/10.1007/s00294-019-00999-3

Charras, G., & Sahai, E. (2014). Physical influences of the extracellular environment on cell migration. *Nature Reviews Molecular Cell Biology*, *15*(12), 813–824. https://doi.org/10.1038/nrm3897

Chen, L.-M., Zhao, J., Musa-Aziz, R., Pelletier, M. F., Drummond, I. A., & Boron, W. F. (2010). Cloning

and characterization of a zebrafish homologue of human AQP1: a bifunctional water and gas channel. *American Journal of Physiology. Regulatory, Integrative and Comparative Physiology*, *299*(5), R1163-74. https://doi.org/10.1152/ajpregu.00319.2010

Conner, M. T., Conner, A. C., Bland, C. E., Taylor, L. H. J., Brown, J. E. P., Parri, H. R., & Bill, R. M. (2012). Rapid aquaporin translocation regulates cellular water flow: mechanism of hypotonicity-induced subcellular localization of aquaporin 1 water channel. *The Journal of Biological Chemistry*, *287*(14), 11516–11525. https://doi.org/10.1074/jbc.M111.329219

Cowman, M. K., Lee, H. G., Schwertfeger, K. L., McCarthy, J. B., & Turley, E. A. (2015). The content and size of hyaluronan in biological fluids and tissues. *Frontiers in Immunology* (Vol. 6, Issue JUN). https://doi.org/10.3389/fimmu.2015.00261

Dasgupta, A., Merkel, M., Clark, M. J., Jacob, A. E., Dawson, J. E., Manning, M. L., & Amack, J. D. (2018). Cell volume changes contribute to epithelial morphogenesis in zebrafish Kupffer's vesicle. *ELife*, *7*. https://doi.org/10.7554/eLife.30963

De Angelis, J. E., Lagendijk, A. K., Chen, H., Tromp, A., Bower, N. I., Tunny, K. A., Brooks, A. J., Bakkers, J., Francois, M., Yap, A. S., Simons, C., Wicking, C., Hogan, B. M., & Smith, K. A. (2017). Tmem2 Regulates Embryonic Vegf Signaling by Controlling Hyaluronic Acid Turnover. *Developmental Cell*, *40*(2), 123–136. https://doi.org/10.1016/j.devcel.2016.12.017

Derrick, C. J., & Noël, E. S. (2021). The ECM as a driver of heart development and repair. *Development* (Vol. 148, Issue 5). https://doi.org/10.1242/dev.191320

Derrick, C. J., Sánchez-Posada, J., Hussein, F., Tessadori, F., Pollitt, E. J. G., Savage, A. M., Wilkinson, R. N., Chico, T. J., van Eeden, F. J., Bakkers, J., & Noël, E. S. (2021). Asymmetric Hapln1a drives regionalized cardiac ECM expansion and promotes heart morphogenesis in zebrafish development. *Cardiovascular Research*. https://doi.org/10.1093/cvr/cvab004

Dietrich, A. C., Lombardo, V. A., & Abdelilah-Seyfried, S. (2014). Blood Flow and Bmp Signaling Control Endocardial Chamber Morphogenesis. *Developmental Cell*, *30*(4), 367–377. https://doi.org/10.1016/j.devcel.2014.06.020

Duchemin, A. L., Vignes, H., & Vermot, J. (2019). Mechanically activated Piezo channels modulate outflow tract valve development through the yap1 and KLF2-notch signaling axis. *ELife*, *8*. https://doi.org/10.7554/eLife.44706

El-Brolosy, M. A., & Stainier, D. Y. R. (2017). Genetic compensation: A phenomenon in search of mechanisms. *PLoS Genetics* (Vol. 13, Issue 7). Public Library of Science. https://doi.org/10.1371/journal.pgen.1006780

Faucherre, A., Moha ou Maati, H., Nasr, N., Pinard, A., Theron, A., Odelin, G., Desvignes, J. P., Salgado, D., Collod-Béroud, G., Avierinos, J. F., Lebon, G., Zaffran, S., & Jopling, C. (2020). Piezo1 is required for outflow tract and aortic valve development. *Journal of Molecular and Cellular Cardiology*, *143*, 51–62. https://doi.org/10.1016/j.yjmcc.2020.03.013

Franco, C. A., Jones, M. L., Bernabeu, M. O., Geudens, I., Mathivet, T., Rosa, A., Lopes, F. M., Lima, A. P., Ragab, A., Collins, R. T., Phng, L.-K., Coveney, P. V., & Gerhardt, H. (2015). Dynamic Endothelial Cell Rearrangements Drive Developmental Vessel Regression. *PLOS Biology*, *13*(4), e1002125. https://doi.org/10.1371/journal.pbio.1002125

Grassini, D. R., Lagendijk, A. K., De Angelis, J. E., Da Silva, J., Jeanes, A., Zettler, N., Bower, N. I., Hogan, B. M., & Smith, K. A. (2018). Nppa and nppb act redundantly during zebrafish cardiac development to confine AVC marker expression and reduce cardiac jelly volume. *Development*, *145*(12). https://doi.org/10.1242/dev.160739

Greiner, A. M., Klein, F., Gudzenko, T., Richter, B., Striebel, T., Wundari, B. G., Autenrieth, T. J., Wegener, M., Franz, C. M., & Bastmeyer, M. (2015). Cell type-specific adaptation of cellular and nuclear volume in micro-engineered 3D environments. *Biomaterials*, *69*, 121–132. https://doi.org/10.1016/j.biomaterials.2015.08.016

Guo, M., Pegoraro, A. F., Mao, A., Zhou, E. H., Arany, P. R., Han, Y., Burnette, D. T., Jensen, M. H., Kasza, K. E., Moore, J. R., Mackintosh, F. C., Fredberg, J. J., Mooney, D. J., Lippincott-Schwartz, J., & Weitz, D. A. (2017). Cell volume change through water efflux impacts cell stiffness and stem cell fate. *Proceedings of the National Academy of Sciences of the United States of America*, *114*(41), E8618–E8627. https://doi.org/10.1073/pnas.1705179114

Hannezo, E., & Heisenberg, C.-P. (2019). Leading Edge Review Mechanochemical Feedback Loops in Development and Disease. *Cell*. https://doi.org/10.1016/j.cell.2019.05.052

Heckel, E., Boselli, F., Roth, S., Krudewig, A., Belting, H. G., Charvin, G., & Vermot, J. (2015). Oscillatory flow modulates mechanosensitive klf2a expression through trpv4 and trpp2 during heart valve development. *Current Biology*, *25*(10), 1354–1361. https://doi.org/10.1016/j.cub.2015.03.038

Heisenberg, C. P., & Bellaïche, Y. (2013). Forces in tissue morphogenesis and patterning. *Cell* (Vol. 153, Issue 5, p. 948). https://doi.org/10.1016/j.cell.2013.05.008

Hernandez, L., Ryckebüsch, L., Wang, C., Ling, R., & Yelon, D. (2019). Tmem2 restricts atrioventricular canal differentiation by regulating degradation of hyaluronic acid. *Developmental Dynamics*, *248*(12), 1195–1210. https://doi.org/10.1002/dvdy.106

Hoffmann, E. K., Lambert, I. H., & Pedersen, S. F. (2009). Physiology of Cell Volume Regulation in Vertebrates. *Physiological Reviews*, *89*(1), 193–277. https://doi.org/10.1152/physrev.00037.2007

Hove, J. R., Köster, R. W., Forouhar, A. S., Acevedo-Bolton, G., Fraser, S. E., & Gharib, M. (2003). Intracardiac fluid forces are an essential epigenetic factor for embryonic cardiogenesis. *Nature*, *421*(6919), 172–177. https://doi.org/10.1038/nature01282

Huber, M. D., & Gerace, L. (2007). The size-wise nucleus: Nuclear volume control in eukaryotes. *Journal of Cell Biology* (Vol. 179, Issue 4, pp. 583–584). https://doi.org/10.1083/jcb.200710156

Ibata, K., Takimoto, S., Morisaku, T., Miyawaki, A., & Yasui, M. (2011). Analysis of aquaporin-mediated

diffusional water permeability by coherent anti-Stokes Raman scattering microscopy. *Biophysical Journal*, *101*(9), 2277–2283. https://doi.org/10.1016/j.bpj.2011.08.045

Iuso, A., & Križaj, D. (2016). TRPV4-AQP4 interactions 'turbocharge' astroglial sensitivity to small osmotic gradients. *Channels* (Vol. 10, Issue 3, pp. 172–174). https://doi.org/10.1080/19336950.2016.1140956

Joerges, J., Schulz, T., Wegner, J., Schumacher, U., & Prehm, P. (2012). Regulation of cell volume by glycosaminoglycans. *Journal of Cellular Biochemistry*, *113*(1), 340–348. https://doi.org/10.1002/jcb.23360

Kalogirou, S., Malissovas, N., Moro, E., Argenton, F., Stainier, D. Y. R., & Beis, D. (2014). Intracardiac flow dynamics regulate atrioventricular valve morphogenesis. *Cardiovascular Research*, *104*(1), 49–60. https://doi.org/10.1093/cvr/cvu186

Kilin, V. N., Anton, H., Anton, N., Steed, E., Vermot, J., Vandamme, T. F., Mely, Y., & Klymchenko, A. S. (2014). Counterion-enhanced cyanine dye loading into lipid nano-droplets for single-particle tracking in zebrafish. *Biomaterials*, *35*(18), 4950–4957. https://doi.org/10.1016/j.biomaterials.2014.02.053

Kwon, H. B., Wang, S., Helker, C. S. M., Rasouli, S. J., Maischein, H. M., Offermanns, S., Herzog, W., & Stainier, D. Y. R. (2016). In vivo modulation of endothelial polarization by Apelin receptor signalling. *Nature Communications*, *7*. https://doi.org/10.1038/ncomms11805

Lagendijk, A. K., Gomez, G. A., Baek, S., Hesselson, D., Hughes, W. E., Paterson, S., Conway, D. E., Belting, H. G., Affolter, M., Smith, K. A., Schwartz, M. A., Yap, A. S., & Hogan, B. M. (2017). Live imaging molecular changes in junctional tension upon VE-cadherin in zebrafish. *Nature Communications*, *8*(1), 1–12. https://doi.org/10.1038/s41467-017-01325-6

Lecuit, T., Lenne, P.-F., & Munro, E. (2011). Force Generation, Transmission, and Integration during Cell and Tissue Morphogenesis. *Annual Review of Cell and Developmental Biology*, *27*(1), 157–184. https://doi.org/10.1146/annurev-cellbio-100109-104027

Lincoln, J., & Yutzey, K. E. (2011). Molecular and developmental mechanisms of congenital heart valve disease. *Birth Defects Research Part A: Clinical and Molecular Teratology*, *91*(6), 526–534. https://doi.org/10.1002/bdra.20799

Lockhart, M., Wirrig, E., Phelps, A., & Wessels, A. (2011). Extracellular matrix and heart development. *Birth Defects Research Part A: Clinical and Molecular Teratology*, *91*(6), 535–550. https://doi.org/10.1002/bdra.20810

Mammoto, T., & Ingber, D. E. (2010). Mechanical control of tissue and organ development. *Development* (Vol. 137, Issue 9, pp. 1407–1420). https://doi.org/10.1242/dev.024166

Mao, Y., & Baum, B. (2015). Tug of war-The influence of opposing physical forces on epithelial cell morphology. *Developmental Biology* (Vol. 401, Issue 1, pp. 92–102).

https://doi.org/10.1016/j.ydbio.2014.12.030

Martino, F., Perestrelo, A. R., Vinarský, V., Pagliari, S., & Forte, G. (2018). Cellular mechanotransduction: From tension to function. *Frontiers in Physiology* (Vol. 9, Issue JUL). https://doi.org/10.3389/fphys.2018.00824

Mola, M. G., Sparaneo, A., Gargano, C. D., Spray, D. C., Svelto, M., Frigeri, A., Scemes, E., & Nicchia, G. P. (2016). The speed of swelling kinetics modulates cell volume regulation and calcium signaling in astrocytes: A different point of view on the role of aquaporins. *GLIA*, *64*(1), 139–154. https://doi.org/10.1002/glia.22921

Munjal, A., Hannezo, E., Mitchison, T. J., & Megason, S. G. (2020). Extracellular hyaluronate pressure shaped by cellular tethers drives tissue morphogenesis. *BioRxiv* (p. 2020.09.28.316042). https://doi.org/10.1101/2020.09.28.316042

Nicenboim, J., Malkinson, G., Lupo, T., Asaf, L., Sela, Y., Mayseless, O., Gibbs-Bar, L., Senderovich, N., Hashimshony, T., Shin, M., Jerafi-Vider, A., Avraham-Davidi, I., Krupalnik, V., Hofi, R., Almog, G., Astin, J. W., Golani, O., Ben-Dor, S., Crosier, P. S., … Yaniv, K. (2015). Lymphatic vessels arise from specialized angioblasts within a venous niche. *Nature*, *522*(7554), 56–61. https://doi.org/10.1038/nature14425

Patra, C., Diehl, F., Ferrazzi, F., van Amerongen, M. J., Novoyatleva, T., Schaefer, L., Mühlfeld, C., Jungblut, B., & Engel, F. B. (2011). Nephronectin regulates atrioventricular canal differentiation via Bmp4-Has2 signaling in zebrafish. *Development*, *138*(20), 4499–4509. https://doi.org/10.1242/dev.067454

Pestel, J., Ramadass, R., Gauvrit, S., Helker, C., Herzog, W., & Stainier, D. Y. R. (2016). Real-time 3D visualization of cellular rearrangements during cardiac valve formation. *Development*, *143*(12), 2217–2227. https://doi.org/10.1242/dev.133272

Petridou, N. I., Spiró, Z., & Heisenberg, C. P. (2017). Multiscale force sensing in development. *Nature Cell Biology* (Vol. 19, Issue 6, pp. 581–588). https://doi.org/10.1038/ncb3524

Phng, L. K., Stanchi, F., & Gerhardt, H. (2013). Filopodia are dispensable for endothelial tip cell guidance. *Development*, *140*(19), 4031–4040. https://doi.org/10.1242/dev.097352

Pouthas, F., Girard, P., Lecaudey, V., Ly, T. B. N., Gilmour, D., Boulin, C., Pepperkok, R., & Reynaud, E. G. (2008). In migrating cells, the Golgi complex and the position of the centrosome depend on geometrical constraints of the substratum. *Journal of Cell Science*, *121*(14), 2406–2414. https://doi.org/10.1242/jcs.026849

Roman, B. L., Pham, V. N., Lawson, N. D., Kulik, M., Childs, S., Lekven, A. C., Garrity, D. M., Moon, R. T., Fishman, M. C., Lechleider, R. J., & Weinstein, B. M. (2002). Disruption of acvrl1 increases endothelial cell number in zebrafish cranial vessels. *Development* (Vol. 129). http://dev.biologists.org/

Saias, L., Swoger, J., D'Angelo, A., Hayes, P., Colombelli, J., Sharpe, J., Salbreux, G., & Solon, J. (2015). Decrease in Cell Volume Generates Contractile Forces Driving Dorsal Closure. *Developmental Cell*, *33*(5), 611–621. https://doi.org/10.1016/j.devcel.2015.03.016

Schottenfeld, J., Sullivan-Brown, J., & Burdine, R. D. (2007). Zebrafish curly up encodes a Pkd2 ortholog that restricts left-side-specific expression of southpaw. *Development*, *134*(8), 1605–1615. https://doi.org/10.1242/dev.02827

Schroeder, J. A., Jackson, L. F., Lee, D. C., & Camenisch, T. D. (2003). Form and function of developing heart valves: Coordination by extracellular matrix and growth factor signaling. *Journal of Molecular Medicine* (Vol. 81, Issue 7, pp. 392–403). https://doi.org/10.1007/s00109-003-0456-5

Segert, J., Schneider, I., Berger, I. M., Rottbauer, W., & Just, S. (2018). Mediator complex subunit Med12 regulates cardiac jelly development and AV valve formation in zebrafish. *Progress in Biophysics and Molecular Biology*, *138*, 20–31. https://doi.org/10.1016/j.pbiomolbio.2018.07.010

Sehnert, A. J., Huq, A., Weinstein, B. M., Walker, C., Fishman, M., & Stainier, D. Y. R. (2002). Cardiac troponin T is essential in sarcomere assembly and cardiac contractility. *Nature Genetics*, *31*(1), 106–110. https://doi.org/10.1038/ng875

Sepich, D. S., & Solnica-Krezel, L. (2016). Intracellular Golgi Complex organization reveals tissue specific polarity during zebrafish embryogenesis. *Developmental Dynamics*, *245*(6), 678–691. https://doi.org/10.1002/dvdy.24409

Sivakumar, A., & Kurpios, N. A. (2018). Transcriptional regulation of cell shape during organ morphogenesis. *Journal of Cell Biology* (Vol. 217, Issue 9, pp. 2987–3005). https://doi.org/10.1083/jcb.201612115

Steed, E, Faggianelli, N., Roth, S., Ramspacher, C., Concordet, J. P., & Vermot, J. (2016). Klf2a Couples Mechanotransduction and Zebrafish Valve Morphogenesis Through Fibronectin Synthesis. *Nature Communications*, *7*(May), 11646. https://doi.org/10.1038/ncomms11646

Steed, Emily, Boselli, F., & Vermot, J. (2016). Hemodynamics driven cardiac valve morphogenesis. *Biochimica et Biophysica Acta - Molecular Cell Research*, *1863*(7), 1760–1766. https://doi.org/10.1016/j.bbamcr.2015.11.014

Steed, Emily, Faggianelli, N., Roth, S., Ramspacher, C., Concordet, J. P., & Vermot, J. (2016). Klf2a couples mechanotransduction and zebrafish valve morphogenesis through fibronectin synthesis. *Nature Communications*, *7*(1), 1–14. https://doi.org/10.1038/ncomms11646

Tong, X., Zu, Y., Li, Z., Li, W., Ying, L., Yang, J., Wang, X., He, S., Liu, D., Zhu, Z., Chen, J., Lin, S., & Zhang, B. (2014). Kctd10 regulates heart morphogenesis by repressing the transcriptional activity of Tbx5a in zebrafish. *Nature Communications*, *5*. https://doi.org/10.1038/ncomms4153

Vatine, G. D., Zada, D., Lerer-Goldshtein, T., Tovin, A., Malkinson, G., Yaniv, K., & Appelbaum, L. (2013). Zebrafish as a model for monocarboxyl transporter 8-deficiency. *Journal of Biological*

Chemistry, *288*(1), 169–180. https://doi.org/10.1074/jbc.M112.413831

Vermot, J., Forouhar, A. S., Liebling, M., Wu, D., Plummer, D., & Fraser, S. E. (2009). Reversing Blood Flows Act through klf2a to Ensure Normal Valvulogenesis in the Developing Heart. *PLoS Biology*, *7*(11), 12–14. https://doi.org/10.1371/journal.pbio.1000246

Villedieu, A., Bosveld, F., & Bellaïche, Y. (2020). Mechanical induction and competence in epithelial morphogenesis. *Current Opinion in Genetics and Development* (Vol. 63, pp. 36–44). https://doi.org/10.1016/j.gde.2020.03.003

Walsh, E. C., & Stainier, D. Y. R. (2001). UDP-glucose dehydrogenase required for cardiac valve formation in zebrafish. *Science*, *293*(5535), 1670–1673. https://doi.org/10.1126/science.293.5535.1670

Wang, M., Yang, Y., Han, L., Xu, F., & Li, F. (2020). Cell mechanical microenvironment for cell volume regulation. *Journal of Cellular Physiology*, *235*(5), 4070–4081. https://doi.org/10.1002/jcp.29341

Weigert, M., Schmidt, U., Haase, R., Sugawara, K., & Myers, G. (2020). Star-convex Polyhedra for 3D Object Detection and Segmentation in Microscopy. https://github.com/

Xie, K., Yang, Y., & Jiang, H. (2018). Controlling Cellular Volume via Mechanical and Physical Properties of Substrate. *Biophysical Journal*, *114*(3), 675–687. https://doi.org/10.1016/j.bpj.2017.11.3785

Xiong, F., Ma, W., Bénazéraf, B., Mahadevan, L., & Pourquié, O. (2020). Mechanical Coupling Coordinates the Co-elongation of Axial and Paraxial Tissues in Avian Embryos. *Developmental Cell*, *55*(3), 354-366.e5. https://doi.org/10.1016/j.devcel.2020.08.007

Yang, Q., Xue, S.-L., Chan, C. J., Rempfler, M., Vischi, D., Gutierrez, F. M., Hiiragi, T., Hannezo, E., & Liberali, P. (2020). Cell fate coordinates mechano-osmotic forces in intestinal crypt morphogenesis. *BioRxiv*, 2020.05.13.094359. https://doi.org/10.1101/2020.05.13.094359

RESULTS – PART II

RESULTS - PART II

In this Part, I will expose the different results that I obtained that were not included into the manuscript. I will focus on the analysis of the function of the aquaporin channels and on the impact of inhibiting ion transports on the cell size regulation.

I. Investigating the function of the aquaporin channels in cell size regulation

A. CRISPR mutants

To analyze the functions of the aquaporins (*aqp8a.1* and *aqp1a.1*) previously identified as expressed within the cells that lose volume (Manuscript, Figure supplementary 2), I generated **mutants** based on the CRISPR (Clustered regularly Interspaced Short Palindromic Repeats)/Cas9 type II technology. This work consisted in a major task during my thesis. I will rapidly present, based on the Figure 1, this gene-editing technology originally described by Emmanuelle Charpentier and Jennifer.A Doudna, who received the Chemistry Nobel Prize for this discovery in 2020 (Jinek et al., 2012).

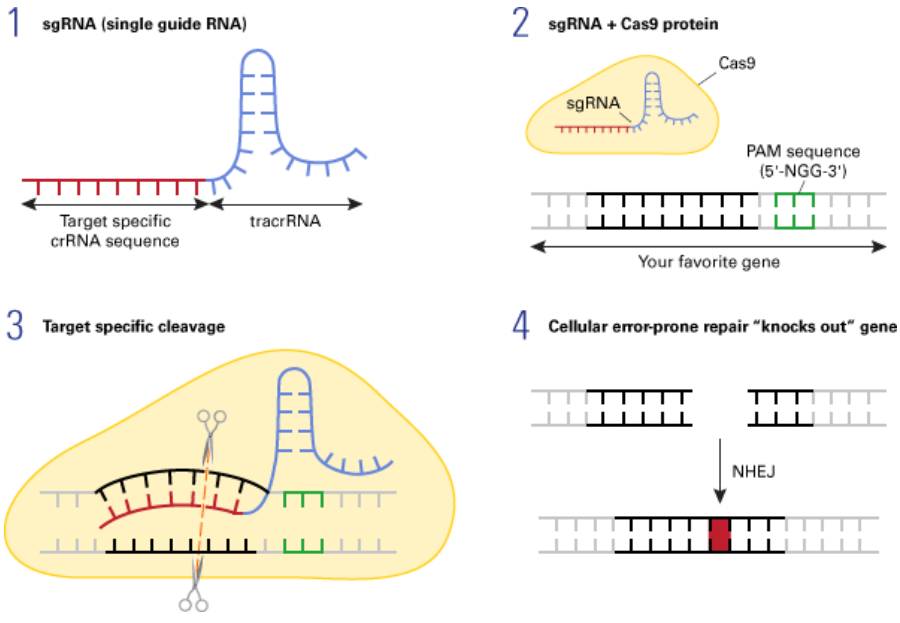

Figure 1: The CRISPR-Cas9 methodology. (**1**) The single guide RNA (sgRNA) consists of a 20 base pairs sequence which targets a specific region of the gene of interest (crRNA: CRISPR RNA) associated with a constant part for each sgRNA (tracrRNA: trans-activating crRNA). (**2**) This RNA-structure and a specific "NGG" sequence on the genome called PAM (Proto-spacer Adjacent Motif) sequence will guide the Cas9 nuclease to cut the targeted gene region. (**3**) The sgRNA/Cas9 complex induces a double strand-break in DNA a few bp upstream the PAM. (**4**) This double-strand break will then be repaired by Non-Homologous-End-Joining (NHEJ), which can introduce random insertions or deletions, leading to a potential gene knock-out (Image from Takara.com)

The *aqp8a.1* gene consists of 6.95kb and includes 5 exons (1029 base pairs (bp)) that encode for a total of 260 amino acids (aa) (Figure 3.A). For the *aqp8a.1* gene, I aimed at removing almost the entire gene from the chromosome 12 by designing two different single guide RNAs (sgRNAs) with one sgRNA targeting the (-) stand before the ATG (**sgRNA1 - aqp8a.1**) and one targeting the intron on the (+) strand between exon 4 and exon 5 (**sgRNA2 - aqp8a.1**) (Figure 3.A).

The *aqp1a.1* gene consists of 11.91kb and include 4 exons (1435bp) that encode for a total of 260 aa. For the aqp1a.1, just one single guide RNA was designed to cut within the exon 1 of the aqp1a.1 gene on the strand (+) (**sgRNA – aqp1a.1**) located on the chromosome 2.

Those gRNAs were constructed, and then injected into one-cell stage embryos (for details on the protocol see the Material & Methods section).

The successful cleavage by the CRISPR associated nuclease 9 (Cas9), indicated by the presence of insertions/ deletions (INDELs) at the targeted region, was assessed with the T7 endonuclease assay (Material & Methods) in the F0 generation. For both strategies (1 sgRNA for the aqp1a.1 and a pair of 2 sgRNAs for the aqp8a.1), the experiment worked extremely well giving us embryos carrying INDELs after a single injection session (of approximately 50 eggs).

Embryos for which an INDEL was detected were then grown to adulthood before being crossed with wild-type fish (AB) to obtain the F1 generation, which was then sequenced to determine the specific mutation.

Analysis of the CRISP/Cas9-generated mutants in aqp8 & aqp1

- **Aqp1a.1:** deletion of 3bp and insertion of 5bp leading to a premature stop codon

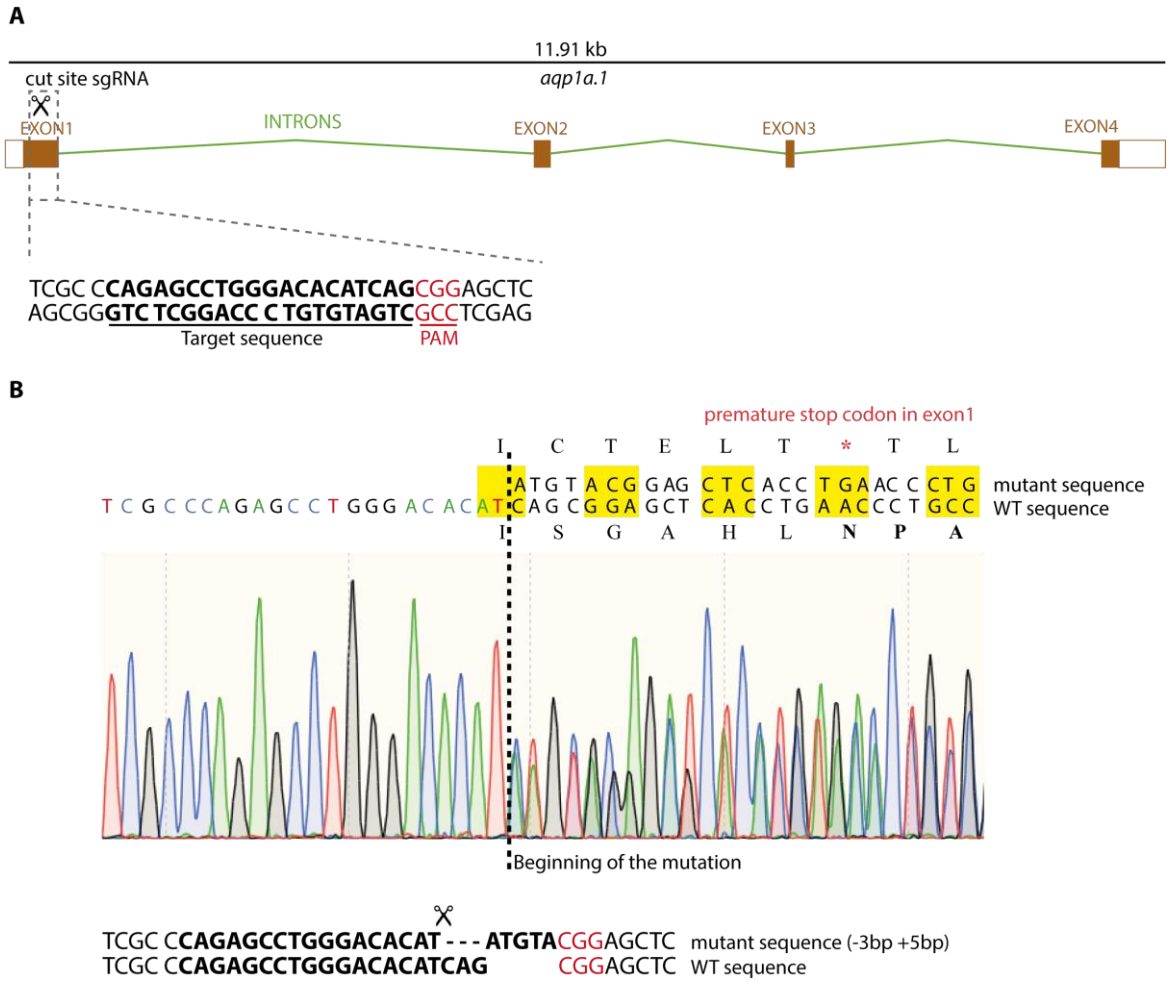

Figure 2: Aqp1a.1 CRISPR mutant (**A**) Presentation of the strategy followed for the *aqp1a.1* CRISPR mutant: the sgRNA targets a site within the exon1. (**B**) Results from the sequencing of a heterozygous embryo carrying the CRISPR-induced INDEL (a deletion of 3bp and an insertion of 5bp, in the F1 generation. This INDEL generates a frameshift within the coding sequence leading to a premature stop codon and the absence of the N-P-A motif which is essential for the specificity of the aquaporin channel towards water.

The mutation induced in the *aqp1a.1* gene by the cleavage of the Cas9 corresponds to a deletion of 3 bp (CAG) and an insertion of 5 bp (ATGTA) (Figure 2. B). This leads to a frameshift in the coding sequence that introduces a premature stop codon (TGA) within the coding sequence of the exon 1 (Figure 2.B). Therefore, we

could expect that this would lead to a loss-of-function of the protein, allowing us to study its function.

- **Aqp8a.1:** big deletion of 5891bp from the 5'-UTR sequence before the exon 1 until the intron between exon 4 and exon 5, without insertions

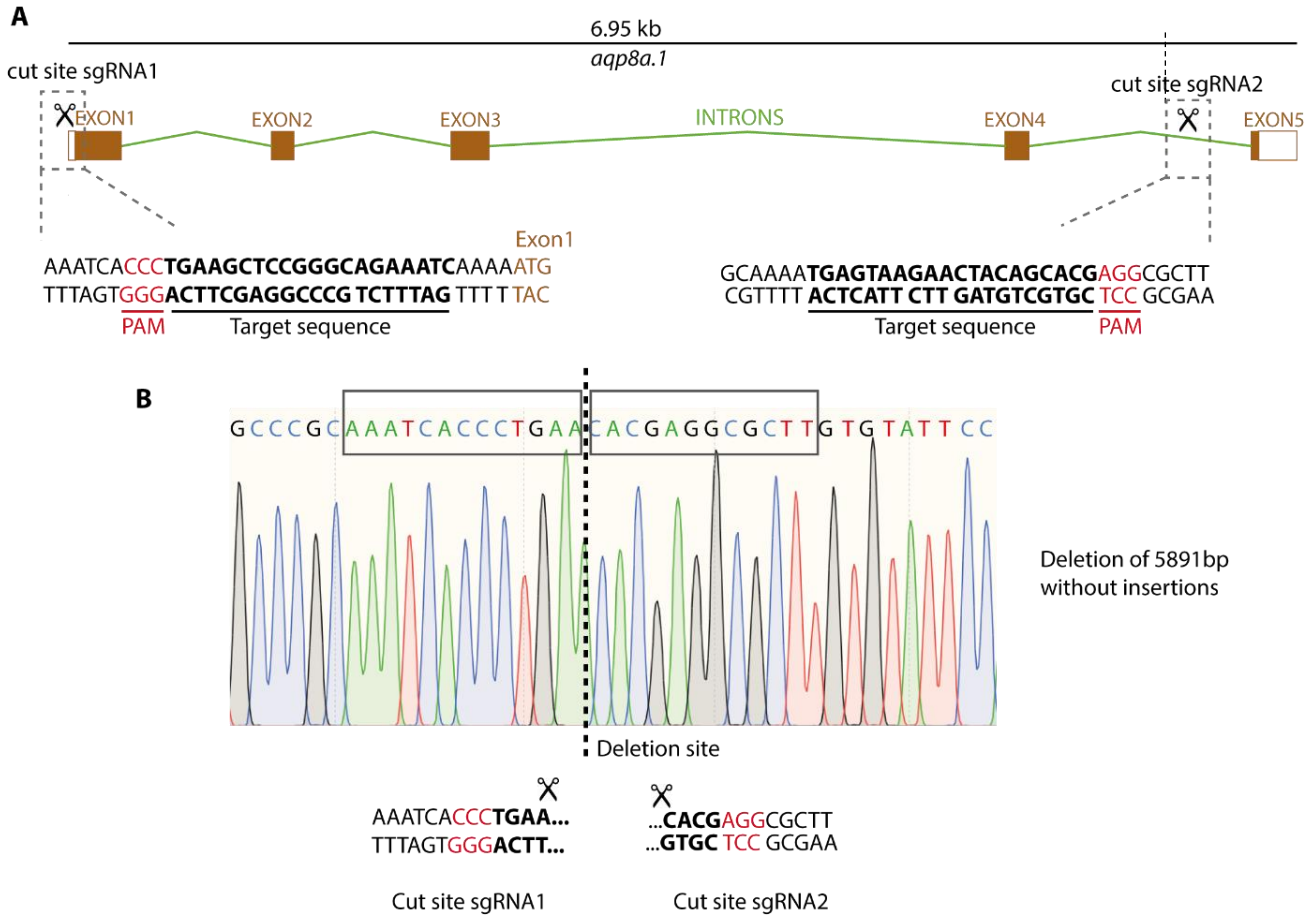

Figure 3: Aqp8a.1 CRISPR mutant (**A**) Presentation of the strategy followed for the *aqp8a.1* CRISPR mutant: a pair of sgRNAs were designed with the sgRNA1 targeting the 5' UTR region right before the ATG of the exon 1 and the sgRNA2 targeting the intron region between the exons 4 and 5 (**B**) Results from the sequencing of an embryo carrying the CRISPR-induced deletion of the region delimited by the 2 sgRNA cut sites (5891bp deletion). This deletion occurred without new bp insertions during NHEJ repair.

The cleavage at both sides of the *aqp8a.1* gene induced a deletion of 5891bp corresponding to the entire region between the two sgRNAs targeted sites.

The generated mutants were subsequently mated with a genetic background fluorescently labeled for nuclei and F-actin *Tg(fli1a:LifeAct-eGFP; kdrl:nls-mCherry),* to analyze the nuclei volume in the F2 or F3 generation.

For the *aqp1a.1*, three different tanks were established based on the genotype of the fish: *aqp1a.1* +/+, *aqp1a.1* +/- and *aqp1a.1* -/- (F3 generation). First, I investigated the phenotype of the *aqp1a.1* +/+ and of the *aqp1a.1* -/-. Interestingly, the mutant embryos presented a strong phenotype, with an apparent decrease of the density of nuclei in the AVC region, as well as looping defects (Figure 4.A-A'). Moreover, cell volume decrease at the AVC was absent in the *aqp1a.1* -/- embryos compared to the *aqp1a.1* +/+ embryos (Figure 4.B) (mutants nucleus volume of 373.0±13.1 μm^3 compared to 248.9±10.1 μm^3 in controls, from 3 independent experiments). Therefore, this phenotype argues for a role of the aqp1a.1 gene in water efflux at the AVC, leading to subsequent cell volume shrinkage. To confirm this result, we then decided to cross sibling fish from the *aqp1a.1*+/- tank, to image the nuclei at 48hpf in additional mutants. Surprisingly, when doing so, no phenotype was found in the embryos that were found to be *aqp1a.1* -/- compared to controls (Figure 4.C-C'). However, we noticed that the controls were also quite abnormal, with defects in cell clustering at the AVC compared to the sibling *aqp1a.1* +/+ tank (compare Figure 4.A and Figure 4.C).

From these results, it is therefore impossible/ambiguous to conclude on the involvement of Aqp1a.1 in the AVC cell volume decrease. Further experiments need to be performed to validate or not the phenotype observed in the tank composed exclusively of *aqp1a.1* mutant.

In the *aqp8a.1* CRISPR mutant, in spite of the large deletion, no defects of the AVC development were observed (data not shown). However, to test if there might be a compensation in the between those two genes, the double heterozygous line was generated. By crossing those *aqp8a.1* +/- *aqp8a.1*+/- fish together, the phenotype of the double mutants could be investigated (Figure 5. A-A'). Even if this experiment was repeated 4 times, only 6 double mutants (*aqp8a.1* -/- *aqp1a.1* -/-) and 6 controls (*aqp8a.1* +/+, *aqp1a.1* +/+) were obtained, indeed there is only one chance out of sixteen to get one of these two genotypes.

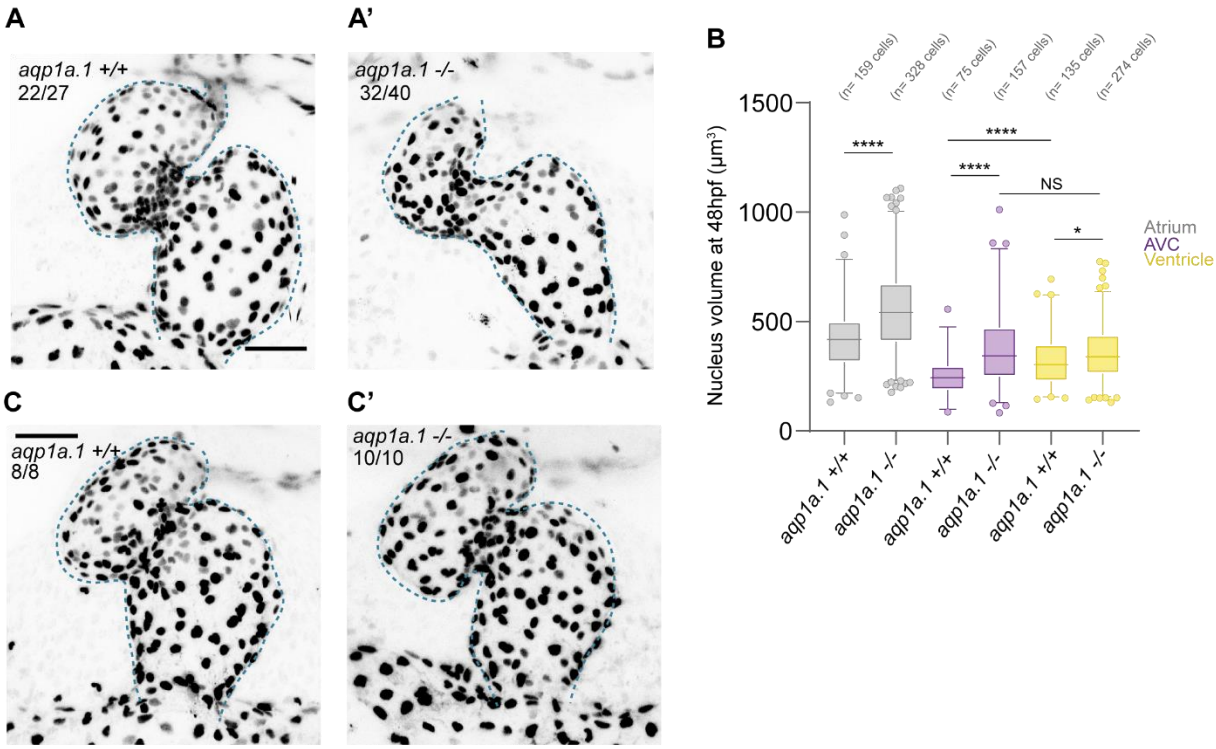

<u>Figure 4: Phenotype of the *aqp1a.1* CRISPR mutants.</u> (**A-A'; C-C'**) Maximal projection of *kdrl:nls-mCherry* embryos showing a control, *aqp1a.1* +/+ (**A, C**) and a mutant embryo, *aqp1a.1* -/- (**A', C'**) at 48 hpf. Blue dotted lines outline the endocardium. Scale bar, 50 µm. (**A-A'**) Aqp1a +/+ embryos come from the incross of the *aqp1a* +/- tank and the mutants from the incross of the *aqp1a.1* -/- tank. (**C-C'**) Both *aqp1a.1* +/+ and *aqp1a.1* -/- come from the incross of the *aqp1a.1* +/- tank, and were sequenced after imaging. (**B**) Quantification of nucleus volume in atrium, AVC, and ventricle in controls (*aqp1a.1* +/+*)* and mutant embryos (*aqp1a.1* -/-) based on the data presented on A and A'. (N=3 embryos, *aqp1a.1* +/+ and N=5 embryos, *aqp1a.1* -/-). Unpaired two-tailed t-test.

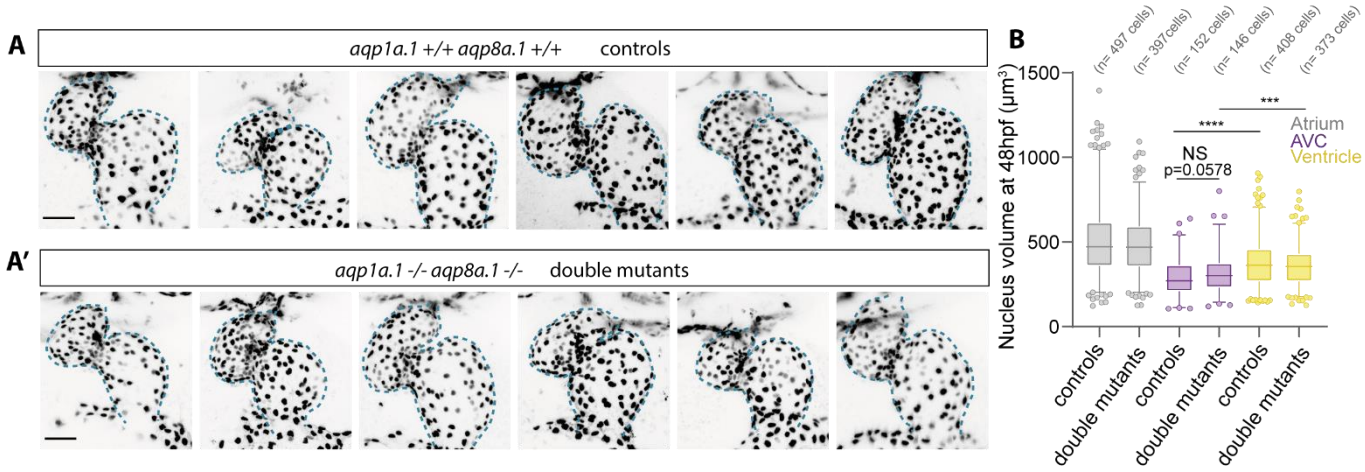

<u>Figure 5: Phenotype of the *aqp1a.1 aqp8a.1* double CRISPR mutants.</u> (**A-A'**) Maximal projection of *kdrl:nls-mCherry* embryos in controls, *aqp1a.1* +/+ *aqp8a.1* +/+ (**A**) and in *aqp1a.1 -/- aqp8a.1 -/-* double mutant embryos (**A'**). Blue dotted lines outline the endocardium. Scale bar, 50 µm. (**B**) Quantification of nucleus volume in atrium, AVC, and ventricle in controls (*aqp1a.1* +/+ *aqp8a.1* +/+) and double mutant embryos (*aqp1a.1 -/- aqp8a.1 -/-*). (N=6 embryos, *aqp1a.1* +/+ *aqp8a.1* +/+ and N=6 embryos, *aqp1a.1 -/- aqp8a.1 -/-*). Unpaired two-tailed t-test.

No such drastic phenotype of heart looping and AVC development defects were observed in the double mutants compared to the first results obtained with the *aqp1a.1-/-* single mutants (Figure 5.A, Figure 4.A'). Moreover, in a few control embryos (*aqp1a.1*+/+ *aqp8a.1*+/+), the heart did not seem to develop properly (Figure 5.A). When comparing the nuclei volume in the three regions of the heart (atrium, AVC, ventricle), the cell volume at the AVC was noticed to be smaller compared to the nuclei in the two chambers, in both controls and double mutants (Figure 5.B). Therefore, these data suggest that the aquaporin channels do not regulate the cell volume at the AVC by enabling the water efflux. However, we cannot rule out any compensation effect in the double mutant embryos, by a another aquaporin channel such as the *aqp3*, which has also been reported to be expressed in the heart at 48hpf, based on RNA-sequencing data (Burkhard & Bakkers, 2018). However, we did not check the spatio-temporal expression of this specific aquaporin.

B. Pharmacological treatments to inhibit the aquaporin channels

To test the possible involvement of additional aquaporins in cell size regulation, we turned to pharmacological treatments in order to abolish aquaporin's activity (Abir-Awan et al., 2019). Experiments were performed by using the putative aquaporin inhibitor called Phloretin already reported in zebrafish studies (Kwong et al., 2013) and Copper Sulfate ($CuSO_4$), a well-known AQP inhibitor that has been recently used in intestinal organoids (Yang et al., 2020). As it was done for the hyaluronidase treatment, both drugs were injected directly within the blood circulation at 30hpf, near the inflow region of the heart (Mat & Med, Figure 5.B of the article's manuscript).

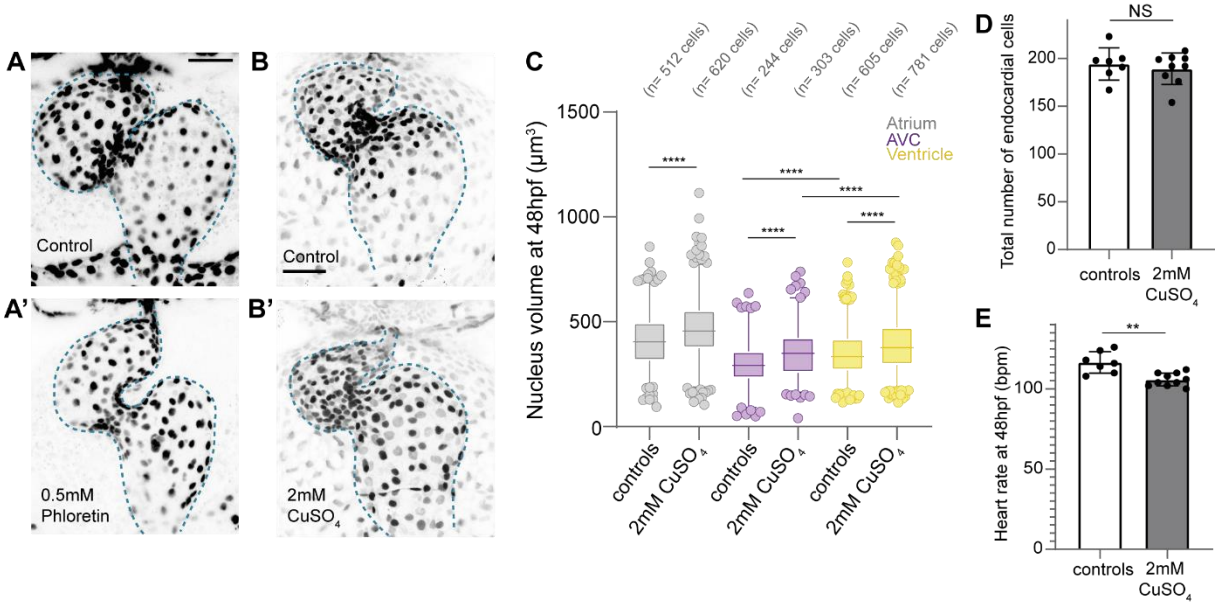

<u>Figure 6. Treatments with aquaporin inhibitors affect the endocardial cell size.</u> (**AA'-BB'**) Maximal projection of *fli:nEGFP* embryos showing a DMSO-injected control (**A**) or a water-injected control (**B**) and an embryo injected with 2.3nL of 0.5mM of Phloretin (**A'**) or 2mM of Copper Sulfate (**B'**) at 48 hpf. Blue dotted lines outline the endocardium. Scale bar, 50 µm. (**C**) Quantification of nucleus volume in atrium, AVC, and ventricle in controls and embryos injected with 2mM $CuSO_4$. (N=7 controls and N=9 embryos injected with Copper Sulfate). Unpaired two-tailed t-test. (**D**) Quantification of the total number of endocardial cells at 48hpf, in the same embryos analyzed in (C). Two-tailed Mann-Whitney test (**E**) Heart rate at 48hpf, measured at room temperature. Two-tailed Mann-Whitney test.

In both cases, Phloretin and Copper Sulfate treatments affected the cellular density at the AVC (Figure 6.A-B'). For the injection of Phloretin, the experiment needs to be repeated, and data analyzed in details but the preliminary

results are promising (Figure 6.A-A'). The nuclei volume were quantified in Copper Sulfate-injected embryos, and showed that AVC cells were bigger than controls (Figure 6.C, mean nucleus volume of 351.0±6.9 μm^3 in Copper Sulfate-injected embryos compared to 298.3±6.8 μm^3 in controls, ratio of 1.18). This clearly demonstrates that the treatment impairs the cell volume decrease at the AVC. However, the cells in the atrium and in the ventricle were also found to be bigger (atrium: 466.3±5.8 μm^3 compared to 411.6±5.9 μm^3 for the controls, ratio of 1.13; ventricle: 389.0±4.7 μm^3 compared to 347.1±4.5 μm^3 for the controls, ratio of 1.12) as it was already the case in the *aqp1a.1* single mutant (Figure 6.C, Figure 4.B). The fact that cells in each compartment of the heart are bigger is similar to the result obtained when proliferation was inhibited (Figure 3 of the paper's manuscript). Therefore, this result could be explained by the fact that fewer cells are present within the heart but the overall size of the heart is not changed, so that cells end up being larger. To test this hypothesis, the total number of endocardial cells was counted (Figure 6.D) but was not different between controls and Copper Sulfate-injected embryos, indicating that the overall increase in cell volume is not due to impaired cell proliferation (Figure 6.D). Moreover, Copper Sulfate-injected embryos had a very slight decrease of the heart rate at 48hpf compared to controls but this cannot account for the observed phenotype (Figure 6.E).

On top of assessing the function of the aquaporin channels, we also tried to identify ion channels and pumps that could generate an osmotic gradient and drive the water efflux that could mediate the cell volume decrease.

II. Altering the osmotic gradient by targeting the ion channels with pharmacological treatments

To study the importance of the ion channels in driving the water efflux from the AVC cells, we analyzed the effects of inhibiting:

- the K+ channels by tetraethylammonium chloride (TEA) (Saias et al., 2015),
- the Chloride channels with Cystic Fibrosis Transmembrane Conductance Regulator inhibitor 172 (CFTRinh-172),
- the Na^+-K^+-ATPase with Ouabain (Dasgupta et al., 2018).

For each drugs, several concentrations were tested, to test if these channels play a role in the decrease of cell volume. The experiments were performed by directly diluting the drug within the fish water at 30hpf and not by injecting the drugs inside the blood circulation, as it was done previously (Hyaluronidase, Phloretin, Copper). No defects were observed when embryos were treated with the TEA drug (data not shown).

By using the CFTRinh-172, defects in the AVC development were noticed especially for high concentrations of the drug (50μM, 100μM) (Figure 7.A-A''''). However, the drug also decreased the heart rate at 48hpf in a dose-dependent manner (Figure 7.B). It is therefore complicated to decipher if the phenotype is due to the lack of chloride ions transport establishing an osmotic gradient across the membrane, or if it is due to mechanotransduction defects caused by a lack or decreased mechanical forces experienced by the endocardial cells.

Inhibition of the Na^+-K^+-ATPase with the drug Ouabain was also found to dramatically alter the conduction system established within the myocardium as embryos were found to have the heart stopped or non-periodically beating (data not shown). When the heart was stopped at 48hpf, it had a phenotype that resembled to the one obtained with the *silent heart* mutant, with a low density of cells at the AVC (Figure 7.C-C'', C'': heart stopped at 48hpf). This result was expected as both Na^+ and K^+ transmembrane gradients are key for the myocardial cell electrophysiology in order to propagate the action potential through the heart (Klabunde, 2017). As observed with the CFTR-inh172, inhibiting the ion channels also alters the way the heart is beating, rendering impossible to identify the cause of the defects in at the AVC.

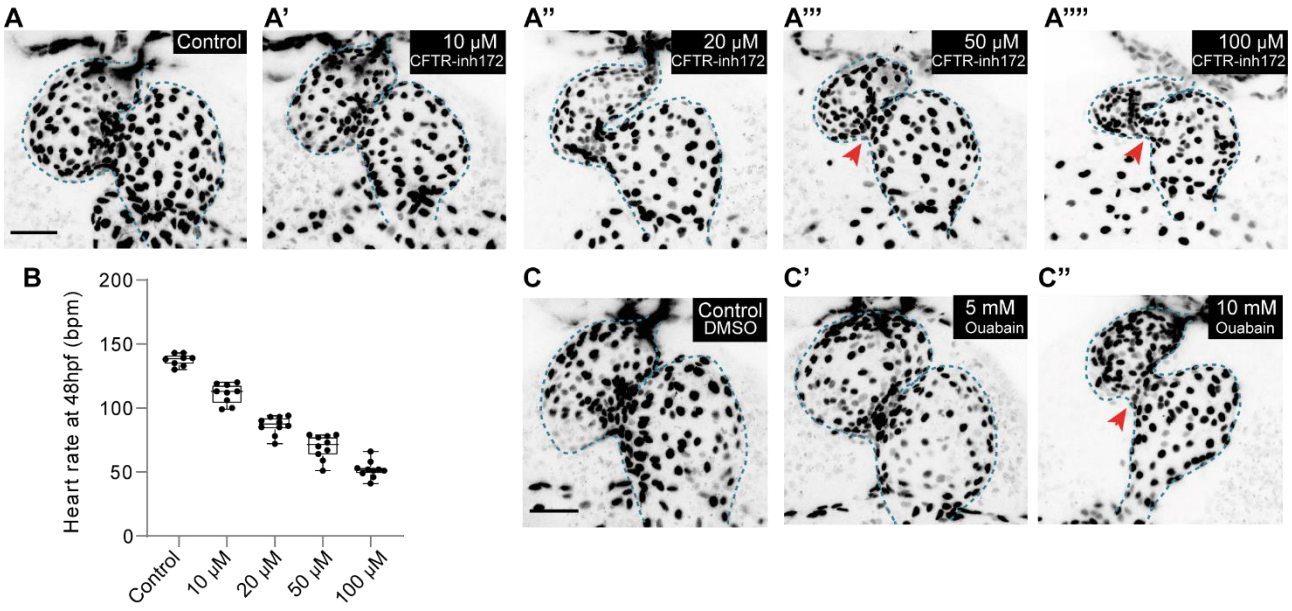

Figure 7. CFTRinh-172 and Ouabain treatments from 30hpf to 48hpf affect both the heart rate and the AVC morphogenesis. (**A-A''''**) Maximal projection of *fli:nEGFP* embryos showing a control (DMSO) (**A**) and the phenotype of embryos treated with increasing concentrations of CFTRinh-172 (**A'-A''''**). Red arrowheads indicate defects of the cell clustering in the AVC region. Blue dotted lines outline the endocardium. Scale bar, 50 µm. (**B**) Quantification of the heart rate at 48hpf after incubation from 30hpf to 48hpf with different concentrations of CFTR-inh172. (**C-C''**) Maximal projection of *fli:nEGFP* embryos showing a control (DMSO) (**C**) and the phenotype of embryos treated with 5mM Ouabain (**C'**) and 10mM Ouabain (**C''**). The red arrowhead indicates defects of the cell clustering in the AVC region. Blue dotted lines outline the endocardium. Scale bar, 50 µm.

Discussion

In this part, we studied the function of the two aquaporin channels (aqp1a.1 and aqp8a.1) during AVC morphogenesis, based on the generation of two CRISPR mutant zebrafish lines and on pharmacological inhibition using two drugs ($CuSO_4$, Phloretin). Furthermore, we tested the potential establishment of an osmotic gradient at the AVC by inhibiting different ions channels (with CFTR-inh172 and Ouabain). The analysis of *aqp1a.1* mutants and *aqp1a.1 aqp8a.1* double mutants gave inconsistent results from which it was impossible to conclude on the role of the aquaporin in the process. In contrast, the preliminary data obtained with the drug treatments gave promising results that support the idea that aquaporins are important for water efflux in the AVC cells, as cells were bigger at the AVC after an injection of $CuSO_4$ in the bloodstream. In this discussion, I will first provide clues to explain the CRISPR phenotype and also prospects for experiments in order to validate or invalidate the role of the aquaporins in the process of cell volume decrease. Second, I will focus on the technical challenge of altering ion transport in the heart.

The phenotype that we obtained for the CRISPR mutants is particularly difficult to interpret. We could think of mainly two hypotheses that could explain i) the absence of phenotype, by the compensation of the mutated aquaporins by other aquaporins, and ii) defects in control embryos, by the presence of off-target cleavage sites by the sgRNAs, repaired by NHEJ.

The aquaporin family is composed of numerous members (thirteen members in mammals) and even more in the zebrafish genome that code for several paralogs (due to the duplication of the genome). In total, eighteen sequences correspond to aquaporin genes in the zebrafish genome (Tingaud-Sequeira et al., 2010), therefore the absence of phenotype could be linked to **compensation** by other aquaporins that may be overexpressed in a given mutant conditions (El-Brolosy et al., 2019; El-Brolosy & Stainier, 2017). Exploring this possibity would require to perform qPCR on isolated hearts, with different aquaporin primers to unravel if some are overexpressed within the *aqp8a.1*, *aqp1a.1* mutants compared to controls.

Although the designed gRNAs were selected on the basis of bioinformatics algorithms for a high efficiency score and a low risk of targeting error which is never

null (Zhang et al., 2015), we cannot exclude that the successful mutation within the targeted genes could be associated with **off-target** mutation(s) elsewhere. Identifying these off-targets should be possible by genome-wide sequencing but this would require heavy bioinformatics analyses. An alternative would have been to create several mutant lines for each genes using different sgRNAs, supposedly avoiding identical off-target effects. Also, it has been recommended to use truncated gRNAs of 17-18bp rather than 20bp, reducing the binding energy and therefore promoting only perfect target matches (Fu et al., 2014).

Moreover, we could think of alternative ways to investigate the function of the aquaporin channels in the process of cell size regulation. The injection of the **morpholinos** for aqp1a.1 and aqp8a.1 would give us indications of the possible phenotype that could be obtained in absence of those aquaporins. Alternatively, the **crispant** method, leading biallelic knockouts in F0, would be interesting to perform as the experimental time required is faster than the establishment of CRISPR mutant lines (Kroll et al., 2021).

Moreover, the structure of the aquaporin gene is well described and presents in particular two highly conserved motifs located inside the narrow pore of the channel (Hub & De Groot, 2008):

- The **NPA** (Asn-Pro-Ala) motif, which is important for the specificity towards water as well as the targeting of the aquaporin towards the plasma membrane (Guan et al., 2010).
- The selectivity filter, which consists of a constricted region with aromatic and arginine residues that also plays a role for the channel selectivity (Hub & De Groot, 2008).

These two structural elements establish the water flow through the aquaporin channel, which prevents the flow of other molecules and protons via electrostatic and steric factors (Hub & De Groot, 2008). Therefore, mutating these specific residues by expressing an endothelium-specific **dominant negative form of the aquaporin channel** would allow us to investigate the aquaporin's function. This approach would

be interesting as it would not affect other tissues within the embryo and it would not lead to compensation.

Nevertheless, this approach might (also) lead to the absence of phenotype during AVC development. How could we interpret that?

As aquaporins are **passive transmembrane channels,** the observed phenotype could result from passive water diffusion through the plasma membrane that does not necessarily require the presence of aquaporins. Indeed, the plasma membrane is permeable to water, but aquaporins increase the diffusion rate by enhancing the membrane permeability (Ibata et al., 2011; Mola et al., 2016). This suggests that the steady-state reached at the end of the process (the final AVC cell volume) will be the same but the **kinetics** to reach this value will be different. Assessing this point would be possible by measuring the cell volume decrease with time in the mutants. Indeed, so far, I have only observed and quantified the data at 48hpf, when the steady state may have had sufficient time to be reached.

Another issue addressed in these results was the effect of altered ions transports across the plasma membrane. This proved to be particularly challenging in the context of the study of heart morphogenesis. Indeed, this also impaired the contraction forces generated by the myocardium and therefore the forces experienced by the endocardial cells that are essential for proper development of the tissue. Therefore, it is impossible to determine whether the defects in cell clustering at the AVC are the result of these deficient mechanical forces or the absence of an osmotic gradient. To go further in this direction and conclude about the influence of heart rate decrease on AVC development, we would need to find a condition in which the heartbeat would be altered independently of ion channel inactivation. Moreover, we will also try to inject those compounds directly into the bloodstream as it was performed for the hyaluronidase, Copper and Phloretin treatements. Like this, this could affect ion transports within the endocardium and perhaps less in the myocardium.

In the article manuscript, we propose that the localization of HA inside the cardiac jelly is causing the osmotic gradient across the plasma membrane of the AVC endocardial cells. Interestingly, it has been reported that the CFTR channel is also involved in HA export in epithelial cells (Schulz et al., 2010). Therefore, we could imagine that the phenotype observed for high doses of CFTRinh-172 could be linked

to a deficit of HA in the cardiac jelly, resulting in lower osmotic pressure exerted on the endocardial cells. To check that hypothesis, an immunofluorescence with the hyaluronan-binding protein (HA-BP) could be performed to unravel if the signal intensity would be decreased in the embryos treated with CFTR-inh172 compared to controls.

METHODS

The gRNAs were generated following the protocol of Gagnon et al., 2014:

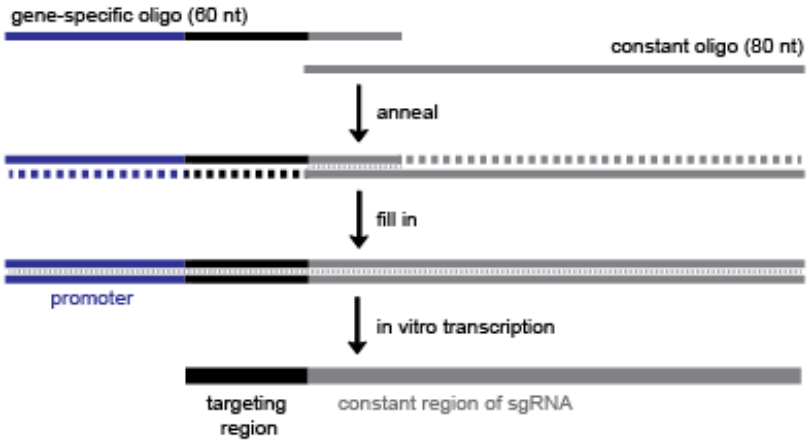

Figure 8: Explanation of the way the sgRNA is generated in vitro. For each sgRNA two primers are needed: one primer with the promoter necessary for the transcription, the targeting region onto the genome and the overlapping region with the constant region of the sgRNA.; the other primer consists of the constant region of the sgRNA. The first step consists in the annealing of the primers and then the fill in with the T4 DNA polymerase. Then, the PCR product is cleaned up and the size is verified on an agarose gel before doing the transcription step with the SP6 enzyme. DNA is then removed with the TURBO DNase before the cleaning step of the transcribed sgRNA. The RNA concentration at the end should be around 200ng/µl and ratio (260/280) closed to 2 (considered as pure RNA), and not close to 1.8 (considered as pure DNA). The final stock should be around 300ng/µL, aliquoted and conserved at -80°C [Picture of the process from (Gagnon et al., 2014)]

Primers used for the generation of the gRNAs:

The part in blue corresponds to the SP6 promoter sequence that is used for the *in vitro* transcription.
The part in bold and black represents the 20 bases specific to the targeted region of the *aqp8a.1* or *aqp1a.1* gene. The specific targeted region was designed by using the combined results obtained by the CHOPCHOP and Benchling websites. The PAM sequence (**NGG**) which is essential for proper binding of the Cas9 to the target region should not be included onto the primer sequence but should be present on the genome.

The part in gray is the overlapping sequence to the constant region of the sgRNA that was ordered as an independent primer of 80 nucleotides (constant oligonucleotide primer).

sgRNA1 - aqp8a.1:

5'ATTTAGGTGACACTATAG**GATTTCTGCCCGGAGCTTCA**GTTTTAGAGCTAGAAATAGCAAG 3'

sgRNA2 - aqp8a.1:

5'ATTTAGGTGACACTATAG**TGAGTAAGAACTACAGCACG**GTTTTAGAGCTAGAAATAGCAAG 3'

sgRNA - aqp1a.1:

5' ATTTAGGTGACACTATAG**CAGAGCCTGGGACACATCAG**GTTTTAGAGCTAGAAATAGCAAG

Constant oligonucleotide primer:

5'AAAAGCACCGACTCGGTGCCACTTTTTCAAGTTGATAACGGACTAGCCTTATTTTAACTTGCTATTTCTAGCTCTAAAAC3'

The incubation step with the SP6 enzyme was performed during 2.5 hours, using the MEGAscript SP6 kit from Ambion.

Injection of the sgRNA inside the first cell of the egg:

The injection that I followed was the following (in case 1nL is injected):

Cas 9 protein at 1000ng/µL	**1µL**
sgRNA at 300ng/µL	should be around 1**µL**
Phenol Red	15% of the Volume (Cas9+sgRNA); should be around **0.3 µL**

The Cas9 protein was ordered from the PNA Bio (reference: CP01-20). As the injector available in the lab could not inject less than 2.3nL, this mix was diluted with pure RNAase-free water 2.3 times.
The morning of the injection: the mix Cas9+sgRNA was first incubated at RT for 5 minutes to allow the complex to form. Then, the water and the Phenol Red was added. The mix was then let on ice and injected inside the first cell.

T7 endonuclease I assay to verify that the injection was successful (Trompouki's lab protocol):

When the region around the targeted region will get amplified in that step then, at the annealing step if non-homogous end-joining happened leading to random insertion or deletion, this will lead to mistmatches. Those DNA mistmitaches will be recognize by the T7 endonuclease I than will cut at the site of mismatches, indicating that the CRISPR-mutant generation worked.

For this step, specific primers need to be design (with the same annealing temperature) in order to amplify a fragment of approximately 500bp around the targeted region. And, the important thing is that they have to be positioned asymmetrically around the PAM sequence (such as for instance 100 nucleotides and 400 nucleotides).

Primers used for the gRNA-*aqp1a.1* (Annealing temperature of 62.9°C):

T7_gRNA_*aqp1a.1*_RP: CGAGCTGCTGGGAATGAC (fragment size: 150 nucleotides)

T7_gRNA_*aqp1a.1*_LP: CTGTAGGACAGATGCGGTATG (fragment size: 383 nucleotides)

For the *aqp8a.1*, as the deletion was really big, two different PCRs were performed instead of performing a T7 endonuclease assay. The first PCR “Big deletion” corresponds to a set of primers located outside the deleted region leading to a fragment of 1585 bp in mutated embryos and to the absence or a very large fragment wild-type embryos. The second PCR “Outside-Inside” corresponds to a set primers with one inside the deleted region (right after the exon1) and one outside (before the exon1). Like this, this fragment of 619bp will be amplified only if the wild-type sequence is present.

PCR "Big deletion"	RP: 5'-GCCTACCTTGCTGCCATCTTCCT-3'	LP : 5'-CCGCCCCGGGAACCCTG-3'	Tm: 69,6°C
PCR "Outside-Inside"	RP_inside: 5'GACTTGTAAAGTGGAATCATGATG-3'	LP_outside: 5'-GAGTTGCATAACAGACGAGC-3'	Tm: 60,9°C

Genotyping of the embryos after imaging:

The genotyping of the embryos was done with the two PCR programs exposed ahead for the *aqp8a.1* mutant embryos followed by a 1.5% Agarose gel.

The region containing the mutation for the *aqp1a.1* was amplified with the following primers: RP 5’- GAACGAGCTGAAGAGCAAG-3’ and LP 5’- CTGTGCTGTAAATGTAAATACTG-3’, Tm of 58.7°C. The amplified fragment was then sequenced with 5’- CGAGCTGCTGGGAATGAC-3’.

Pharmacological treatments:

Compound	Manufacturer	Reference
Phloretin	Sigma-Aldrich	P7912
Copper Sulfate solution	Sigma-Aldrich	C2284
CFTR inhibitor-172	AdooQ Bioscience	A12897
Ouabain	Sigma-Aldrich	PHR1945
Tetraethylammonium Chloride	Sigma-Aldrich	T2265

Imaging: See the Material and Methods of the article's manuscript

Box plots were generated with the Prism software where horizontal lines show the median. The whiskers extend to the 2.5th and 97.5th percentiles. Data points outside whiskers are shown as individual circles.

GENERAL DISCUSSSION AND PERSPECTIVES

GENERAL DISCUSSION AND PERSPECTIVES

In my thesis research project, I focused on the early developmental stages of heart morphogenesis, when valves are starting to morph between the atrium and the ventricle. I studied the cellular behaviors underlying the tissue convergence towards the AVC region. I found out that a cell volume decrease occurs at the AVC from 36hpf to 48hpf, concomitantly with the expression of aquaporins (*aqp8a.1* & *aqp1a.1*) in these cells. Altering the mechanical forces produced by the heart led to defects in endocardial cell size regulation. I observed that the cell volume decrease is dependent upon myocardial-generated contractions and resulting blood flow as well as mechanosensitivity/mechanotransduction through the TRP channels (TRPP2/TRPV4). In addition, I uncovered that the presence of hyaluronic acid within the cardiac jelly is essential for the cell volume decrease.

Here, I would like to discuss some of the methods we used as well as the results we obtained.

- Nucleus volume, used as a tool to observe cell volume changes within the tissue

During my PhD, I had the chance to develop a collaboration with the Jug lab (MPI-CBG, Dresden) to establish a deep-learning based segmentation method to extract the nuclei of all the endocardial cells of the heart from raw confocal images. This approach was essential as we first tried classical nuclei detection segmentation softwares (such as Ilastik and Labkit under FiJi) that could not give us satisfactory results, especially in the crowded AVC region.

Thanks to deep-learning, with the ground-truth that I did manually on Labkit and the work of our collaborators to train the classifier, I was able to show that the extracti

of the nucleus volume can give us a good approximation of the cell volume as a strong correlation between them was established. This validation was important because even if the nuclear-cytoplasmic ratio is often considered as constant for a given cell type and conserved among several organisms (from yeast to multicellular organisms) (Cantwell & Nurse, 2019; Huber & Gerace, 2007), a recent study pointed out that this is not necessarily the case during early embryogenesis (Mukherjee et al., 2020): in early blastomeres of sea urchin embryos, the cell size and the nuclear size can be uncoupled (Mukherjee et al., 2020). Therefore, it was essential for us to assess whether the nucleus volume can be used as a reliable tool in our developmental context to study cell volume changes under conditions other than those of wild-type embryos (heart contraction-altered conditions, TRP mutants, hyaluronidase-injected embryos). This approach proved to be highly beneficial as it was less time-consuming than manually segmenting cell and nucleus surfaces as well as cell heights to obtain a cell volume approximation, based on geometric calculations. I truly believe that this tool, available on GitHub, could shed light on unrelated morphogenetic processes in which cell volume changes might play an important role. Indeed, among all the different cell behaviors underlying tissue remodeling during embryogenesis, cell volume changes remain understudied. This is certainly due to the fact that it is a complex parameter to quantify as it has to be performed with precision and in a three-dimensional environment. Among the numerous morphogenetic processes involving cell shape changes, it would be of particular interest to investigate whether or not this is accompanied by changes in cell volume, as it has been recently explored during *Drosophila* dorsal closure (Saias et al., 2015).

By using this tool (on top of cell volume approximation), I was able to show that the clustering event taking place in the AVC region at the onset of valvulogenesis is associated with a significant cell volume decrease of these cells. Based on the cell volume approximation from geometric calculations, it seems that AVC cells would lose approximately 70% of volume compared to atrial cells, and 56% compared to ventricular cells. This result is certainly overestimated by errors due to the measurements performed with Imaris on raw confocal images, and the following geometric calculations that do not correspond to exact quantifications. Indeed, those values do not match with values obtained in *in vitro* experiments as in most cases,

even cells exposed to drastic osmotic shocks lose at most approximately 40% of their initial volume, otherwise they would become completely devoid of water and would die (E. H. Zhou et al., 2009). In order to get more accurate measurements of cell volume, we could envision to mosaically label endocardial cells (via injection of DNA or mRNA at the one cell stage) (Yu et al., 2015) with a construct enabling us to visualize the cell cytoplasm or, by using the *Zebrabow* transgenic line to get neighboring cells labeled with distinct colors (Albert Pan et al., 2013; Dasgupta, Jacob, et al., 2018). To get a clear quantification of single cell volume decrease, labeled cells could be imaged at different timepoints during endocardial tissue convergence.

Despite the fact that our actual measurements are certainly overestimated, we could conclude about the presence of a cell volume loss at the AVC. However, the different approaches suggested before, would make us more confident regarding our conclusions and would enable a quantification of the single cell volume.

- Cell volume changes: why? Water efflux or loss of dry mass? Implications on cell physiology?

This cell volume decrease could result from a **water efflux** or a **decrease of the cellular dry mass**. The presence of the aquaporin channels that are specific for water exchanges, as well as gazes for aqp1a.1 (NO, CO_2) (Herrera et al., 2006; Horng et al., 2015) and possibly urea for aqp8a.1(Holm et al., 2005), favors the hypothesis that it is mostly water that is moving into the extracellular space leading to subsequent cell shrinkage. However, at this point, we cannot rule out that **autophagy** could participate in cell size regulation by decreasing cellular dry mass. In fact, autophagy processes correspond to an accumulation of cellular components into a vacuole called autophagosome which is then degraded through a fusion with lysosomes that help to maintain cellular homeostasis (Offei et al., 2018). This process will be particularly exciting to investigate in our context as it has been recently reported that fluid flow forces could induce autophagy and subsequent cell volume decrease in kidney epithelial cells both *in vitro* and *in vivo* (Orhon et al., 2016).

To investigate the presence of autophagy within the AVC cells, a well-establish method is to look at the Lc3 ((microtubule-associated protein 1A/1B-light chain 3) protein. During autophagy, this protein which is normally cytoplasmic relocates to the autophagosome, and can be visualized as “puncta” within the cells (Kabeya et al., 2000; Mathai et al., 2017). In our case, we could use the transgenic zebrafish line GFP-Lc3, under the control of a *fli1a* endothelial specific promoter, which would enable to visualize *in vivo* the LC3 protein (Mathai et al., 2017).

Cell volume represents a highly regulated parameter that has to be kept constant for each differentiated cell. This is critical to sustain the cell’s physiological needs and to maintain its homeostasis (Hoffmann et al., 2009). Cells can be challenged by their external environment leading to changes of their volume, such as differences between the internal and external osmotic pressure, mechanical forces or mechanical properties of the ECM (Wang et al., 2020). However, as it is one of the parameters that the cell needs to maintain for its normal function (biochemical reactions, metabolism) and survival, numerous regulatory mechanisms exist that will adjust the osmolarity in order to come back to the steady-state cell volume. Those mechanisms will activate different ion pumps to move osmolytes (mainly Na+, K+, Cl-) to readjust the osmolarity by Regulatory Volume Decrease (RVD) if the cell had swollen, or for Regulatory Volume Increase (RVI) if the cell had shrinked (Jentsch, 2016; Mongin & Orlov, 2009). For instance, budding yeast can produce osmotically active compounds such as glycogen to restore the initial osmotic pressure and therefore recover its initial cell size (Hoffmann et al., 2009).

In our work, we did observe the cell volume decrease from 36hpf but we did not see that cells returned afterwards to their original volume. Therefore, AVC cells seem to establish a new steady-state volume that may result from a new equilibrium between the forces applied on them. This volume decrease might be seen as an **adaptive response** of the cells towards the new constraints exerted on them (shear stress, osmotic pressure), thereby favoring survival in this changing environment. Indeed, the loss of volume could help to release cellular tension and therefore bring the tension back to homeostatic values that would prevent the cell from bursting.

But, what would be the consequence of this loss of cell volume on the cell’s physiology? Cell volume shrinkage has an impact on the intracellular concentration of molecules leading to increased molecular crowding (Minton, 2001; Neurohr & Amon,

2020). Recently, cell volume decrease following different mechanical cues experienced by the cell during spreading, or faced to an increased stiffness of the substrate or an external osmotic pressure, has been shown to change the differentiation paths of mesenchymal stem cells (Guo et al., 2017). Therefore, it is tempting to speculate that the decreased cell volume observed locally at the AVC could participate in the **differentiation** of these endocardial cells that express specific genetic markers in comparison to their neighboring cells into the ventricle and atrium. Through the inhibition of the aquaporin channels (*aqp8a.1*, *aqp1a.1*), I was hoping to alter exclusively the cell volume change and therefore, assessing whether in absence of cell volume change the cell differentiation would have been affected or not. However, no defects in cell size regulation were found in our generated CRISPR mutants (see Results-PartII and associated discussion).

If we take the example of the Klf2a expression profile which corresponds to one of the genetic markers of AVC cell identity, our laboratory already demonstrated that its expression is reduced in both the *trpv4* and *trpp2* single mutants concomitantly with a decrease in calcium signaling in these cells (Heckel et al., 2015). Here, no defect in AVC cell volume has been observed in each single mutants. Therefore, we hypothesize that the TRP-dependent increased intracellular Ca2+ signaling could specifically influence *klf2a* expression, rather than cell volume decrease *per se*.

- TRP channels: osmo-sensor? Shear-stress sensor?

What are the roles of the TRP channels in the process of cell size regulation, and how do they get activated?

In the context of heart valve development, it has been shown that TRP channels are activated by the oscillatory flow present in the lumen at the AVC region (Heckel et al., 2015). However, a huge literature regarding Trpv4 channels has revealed that they can be activated by stimuli of different nature such as heat (Todaka et al., 2004; Watanabe et al., 2002), mechanical forces like stretching (Thodetti et al., 2009), shear stresses (Heckel et al., 2015) or osmotic challenges, particularly hypotonic stresses (Liedtke et al., 2000; Strotmann et al., 2000).The latter stimulus was the first one described for the Trpv4 channel and has earned it the name of osmosis-activated

vanilloid receptor-related channel (VR-OAC) (Liedtke et al., 2000). In the presented data, we showed that altering the osmotic pressure applied on the endocardial cells through the removing of HA (that attracts both cations and water, thus changing osmotic pressure) led to the absence of cell volume decrease at the AVC. Moreover, the inhibition of both the TRPV4 and the TRPP2 channels also led to impaired cell volume decrease at the AVC, indicating that these channels could play a role for the osmo-sensation.

However, even if we identified several actors (HA, TRPs, AQPs) involved in the AVC cell size regulation, the interactions between them remain largely unknown in our context [Figure 1]. We can get some clues about their possible interactions from mostly *in vitro* studies. Benfenati and colleagues reported via co-immunoprecipitation and immunofluorescent assays that the TRPV4 channel and AQP4 are colocalized in astrocytes and form a functional complex (Benfenati et al., 2011). In retinal Müller glia, the same TRPV4-AQP4 interactions were shown to be essential for cell swelling (Jo et al., 2015) and in salivary gland cells, a functional coupling was reported between TRPV4 and AQP5 (X. Liu et al., 2006). More recently, a study performed in *Xenopus laevis* oocytes in which TRPV4 and AQP1 were co-expressed unveiled that TRPV4 can also interact with AQP1 (same results obtained with AQP4), suggesting that TRP4 does not show specificity towards an AQP channel in particular (Toft-Bertelsen et al., 2017). The same authors showed that the presence of AQPs increased the water permeability of cell membranes by approximately 20-fold, thereby mediating accelerated cell volume change, as already reported in Mola et al., 2016. Interestingly, they revealed that this rapid cell volume change is critical and needed for proper TRPV4 channel activation. Therefore, as exposed previously, we could think that the Aqp8a.1 and Aqp1a.1 present in our context could be important for the rate of the cell volume decrease and subsequent activation of the TRP channels. However, if TRP channels activation rely on cell volume changes, this does not explain why an absence of cell volume decrease was reported in the TRP double mutants. Another study performed on HEK 293 cells, showed that the rising intracellular Ca2+ concentration following the TRPC1 activation is crucial for the translocation of the AQP1 channel at the plasma membrane (Conner et al., 2012). We could easily check this last point by exploring the cellular localization by immunofluorescence of the aquaporins when the TRP channels are inhibited. It would be important to further investigate a functional link

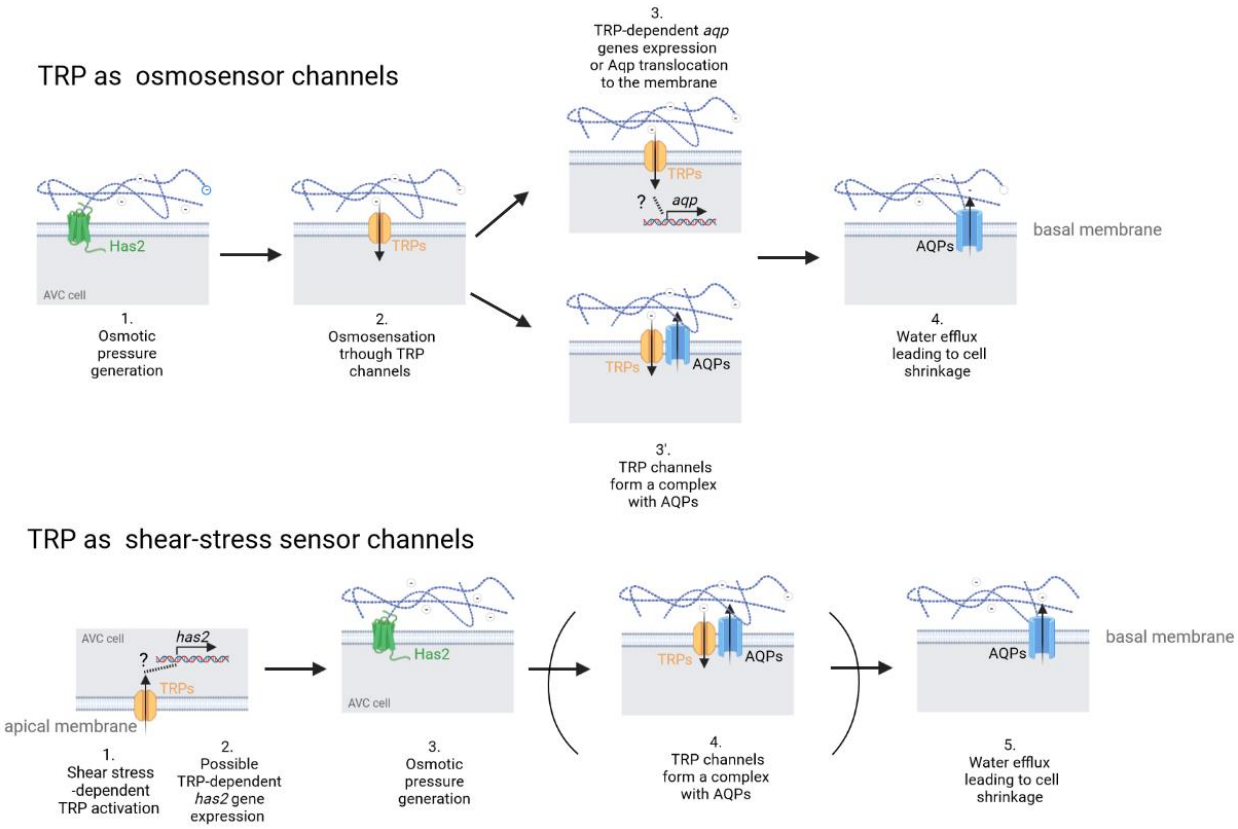

Figure 1. Possible interactions between the different actors of the AVC cell size regulation process

between these two actors in our *in vivo* context. To decipher if the aquaporins are downstream to TRP channels [Figure 1- top panel], we are currently testing if the aquaporins expression rely on the presence of the TRP channels by performing in situ hybridization experiments with the *aqp8a.1* and *aqp1a.1* probes in the *trpv4 -/- trpp2 -/-* embryos, with the help of Christina (first year PhD student in our laboratory).

One fundamental question that is quite challenging to address is how the TRP channels could be gated by the osmotic pressure driven by the presence of HA inside the cardiac jelly. I think that we should envision the osmo-sentation as resulting from a membrane stretching induced by the applied osmotic pressure on the AVC cells (Jiao et al., 2017). This might lead to TRP channel opening concomitantly to a water efflux via the AQP channels. Actors that we did not investigate in that direction correspond to integrins that play a critical role in transducing signals between the extracellular and the intracellular environments (Jiao et al., 2017). We could think of inhibiting α5 and β1 Integrins expressed in the endocardial cells at these developmental stages (Gunawan et al., 2019) and see whether this affects the final AVC cell volume. This would suggest a role of integrins in the transduction of the mechanical forces and the activation of the TRP channels.

Importantly, such an interplay between the cytoskeleton remodeling and the TRP channels activity could be envisioned as TRPV4 channels have been shown to directly interact via their C-terminal part with the cytoskeleton (F-actin and microtubules), by co-immunoprecipitation (Goswami et al., 2010).

We will therefore now discuss the remodeling of the cytoskeletal network specifically within the cells that lost volume.

- Cortex remodeling: higher tension?

One important point that we did not discuss so much in the paper's manuscript is the remodeling of the F-actin network and the increased phospho-myosin light chain expression in the same cells that decrease their volume. This observation led us to suspect that these cells might certainly contract and would exhibit a higher cortical tension in comparison to the other endocardial cells present in the atrial and ventricular chambers. I tried to measure the tension *in vivo* by performing laser cuts on stopped

hearts (with the BDM drug) within the different regions of the heart (atrium, AVC, ventricle). However, this proved to be challenging as the laser light can be scattered by passing through the pericardial cavity, the myocardium, the cardiac jelly before entering in contact with the endocardial cells. As a result, I ended up having no cut at all or a big hole within the tissue when I increased the laser power. Alternatively, to quantify the tension in the endocardial tissue, it would be possible to use the FRET-based-Ve-cadherin tension sensor line (Lagendijk et al., 2017), but I did not have time to implement that during my thesis. Despite the lack of experimental quantifications/ validation, our observations (strong F-actin signal, and enriched phospho-myosin antibody at the AVC) strongly suggest that these cells will certainly be more tensed and have a higher cell stiffness. This observation is consistent with several studies which highlighted an increase of cell stiffness concomitantly to a cell volume shrinkage (Guo et al., 2017; E. H. Zhou et al., 2009).

However, the driving force that leads to this remodeling of the acto-myosin network remains unclear in our context. Several scenarios could explain this observation, first it might be that it is the cell volume decrease itself that has increased the cell stiffness as shown in Guo et al., 2017. Furthermore, we could imagine that the increased external hydrostatic pressure due to the highly hydrated HA polymers within the ECM could exert a compressive force onto the endocardial cell surface, therefore increasing the cellular tension through a remodeling of the cytoskeleton. This mechanism is proposed in the recent paper of Munjal and colleagues, who showed that in zebrafish inner ear, the presence of HA applies an isotropic pressure at sites where the semicircular canals develop, and the epithelium resists to this force by an accumulation of F-actin and myosin II in structures called cellular tethers (Munjal et al., 2020). Interestingly, in the heart, we reported that the inhibition of HA by the hyaluronidase disrupted the accumulation of F-actin within the AVC cells, which support this hypothesis. Finally, a last alternative could be that the activation of the TRP channels through the process, and the subsequent entry of Ca^{2+} ions could induce signaling pathways that will mediate the remodeling of the cytoskeleton.

Moreover, this increase of the cellular tension could participate in driving water efflux from the AVC cells. To assess the possible involvement of cellular contractility for cell volume decrease, we could try to inhibit it. This point can be addressed *in vivo* by inhibiting the actin polymerization (through Latrunculin or Cytochalasin D) or the

myosin activity (through Blebbistatin) and exploring the effects of the cell size regulation. However, in the context of the heart morphogenesis, this would have an impact on the activity of the myocardial cells and therefore on the way the heart will beat. This would require to target only the endocardial cells. We could manipulate the contractility of single endocardial cells by expressing dominant-negative forms of myosin light chains for instance. However, as it has to be done from the first cell stage, prior morphogenetic processes may be affected during development and may also lead to the extrusion of the defective cells from the endocardial tissue. Another way would be to implement optogenetic methods allowing to specifically target the cells we are interested in and at a particular moment during embryonic development.

- Hyaluronic acid: restricted to the AVC? Roles of other ECM components?

The presence of HA in the heart from 28hpf to 48hpf was examined by an immunofluorescence assay with the HA- Binding Protein (BP). As the *has2* gene, which is responsible for the assembly and exportation of HA, is expressed locally within the AVC cells, we were expected to visualize a gradient of the HA protein within the cardiac jelly at the vicinity of AVC cells. However, we detected it almost homogeneously distributed inside the ECM with our assay. This result was particularly intriguing, and I would like to comment on it, as we expected a local accumulation of HA. First, it might be that this method did not allow us to distinguish between regions with high *vs* low density of HA. Indeed, we could imagine that in the AVC region where the ECM components are crowded, the HA-BP does not manage to reach all the binding sites to HA. For that, it would be pertinent to perform scanning electron microscopy in order to see the density of HA molecules inside the cardiac jelly.

Moreover, our experiment was performed on deyolked embryos in which the cardiac jelly is directly accessible to binding proteins. It might be possible that the concentration of HA-BP was too high and that nonspecific bindings were still present after the washes, therefore giving us a strong signal everywhere within the cardiac jelly. However, the fact that no signal was found in the hyaluronidase-injected embryos kind of rule out this hypothesis.

In our work, we only focused on HA as it is the best described among the other glycosaminoglycans (GAGs) present inside the cardiac jelly. However, the GAG chondroitin sulfate, which is also negatively charged and has the same tendency to attract water, also shows defects in the AVC development when inhibited (Peal et al., 2009). On top of that, the authors could show that this particular GAG is found exclusively in the AVC region using a specific antibody. Therefore, we would also like to study the effect of removing the chondroitin sulfate on the process of AVC cell size regulation (via the biosynthesis inhibitor: cis/trans-decahydro-2-napthol-β-D-xyloside (DX) (Peal et al., 2009). It might be that the presence of both GAG molecules (HA and chondroitin sulfate) is needed in order to produce an osmotic pressure sufficient to alter the cell volume of the AVC cells.

- A pulling or a pushing force towards the AVC?

For the last point addressed in this discussion, I would like to come back to the last aim of my project, which consisted in determining the driving force behind the tissue convergence. We hypothesized that the tissue movement could result from a pushing force towards the AVC mediated by cell proliferation or cell migration or, on the opposite by a pulling force generated by cell volume decrease at the AVC. By completely abolishing the cell proliferation between 30hpf and 48hpf, we could show that it was not the driver of the movement as both AVC cluster formation and the orientations of nucleus-to-Golgi axes were normal. However, the fact that both ventricular and atrial endocardial have their nucleus-to-Golgi axes pointing towards the AVC does not help us to decipher between hypotheses of the cell migration *vs* cell volume decrease. To go further, additional experiments should be performed. Cell migration could be accompanied by a cell shape change via the formation of protrusions. To test this, endocardial cells could be mosaically labeled in order to assess single cell protrusive activity to test if they actively migrate towards the AVC. However, the amplitude of the tissue movement assessed by photoconversion experiments seemed quite low (Boselli et al., 2017), which does not support the hypothesis of an active migration. Rather, we therefore propose that the cell volume decrease at the AVC might be sufficient to drive the tissue movement, as reported in the Drosophila dorsal closure (Saias et al., 2015). To test this hypothesis, we could

turn to *in vitro* experiments, where endothelial cells would be labeled for both Golgi and nucleus, and a hyperosmotic shock would be performed in some cells in the middle of the plate. This experiment would enable us to decipher if a local cell volume decrease can drive an orientation change over multiple cells and a concomitant cell movement. This would be essential in order to demonstrate that the driving force of the endocardial movement could be due to a pulling force from the decrease in AVC cell volume applied to the surrounding cells.

To conclude this discussion section, I would like to remind you that morphogenetic processes have often been described as autonomous processes involving mainly forces generated by the cell cytoskeleton (Heisenberg & Bellaïche, 2013; Munjal & Lecuit, 2014). However, a fascinating question in the field of developmental biology, is to understand how the external forces can influence morphogenesis of the tissue, by changing the individual cell behaviors. In my thesis, I demonstrated the particular importance of these forces in the context of the early AVC morphogenesis. I hope that more and more studies will shed light on the role that the external cell microenvironment plays in dictating cell behaviors. Beyond being relevant for basic research, they might also increase our knowledge and identify novel targets to treat diseases such as cancer, in which a complex environment is built up around tumor cells (Baghban et al., 2020).

RESULTATS (EN FRANÇAIS)

INTRODUCTION

La plupart des organes doivent acquérir une forme définie pour une fonction optimale. L'organogenèse est contrôlée à la fois dans l'espace et dans le temps grâce à l'interaction entre des facteurs génétiques et mécaniques (Mammoto & Ingber, 2010 ; Sivakumar & Kurpios, 2018). Les signaux mécaniques peuvent provenir de divers contextes : l'environnement de la cellule, par exemple la matrice extracellulaire (MEC) environnante, les cellules voisines ou les tissus voisins (Charras & Sahai, 2014 ; Hannezo & Heisenberg, 2019 ; Martino et al., 2018 ; Petridou et al., 2017 ; Villedieu et al., 2020). En outre, les forces mécaniques peuvent provenir du tissu lui-même (Boselli et al., 2015 ; Xiong et al., 2020). Les cellules constituent l'unité fonctionnelle de chaque tissu et peuvent détecter et réagir à ces différentes forces qui entraînent des comportements cellulaires coordonnés (changements de forme, intercalation, apoptose, etc.) qui sont essentiels au remodelage des tissus (Heisenberg & Bellaïche, 2013 ; Lecuit et al., 2011). Pourtant, la manière dont les forces mécaniques affectent les comportements cellulaires et la forme des tissus à l'échelle cellulaire reste mal connue.

Parmi les différents mécanismes cellulaires qui contrôlent les processus morphogénétiques (Heisenberg & Bellaïche, 2013 ; Lecuit et al., 2011 ; Mao & Baum, 2015), les changements de volume cellulaire sont récemment apparus comme un modulateur essentiel de la forme des tissus. Chez *Drosophila Melanogaster*, la diminution du volume cellulaire entraîne le mouvement du tissu pendant la fermeture

dorsale (Saias et al., 2015). De plus, les changements de volume cellulaire sont également essentiels pour réguler le volume de la lumière des organoïdes intestinaux (Yang et al., 2020) et la morphogenèse des vésicules de Küpffer chez le poisson zèbre (Dasgupta et al., 2018). In vitro, des signaux mécaniques externes peuvent déclencher des changements de volume cellulaire (Guo et al., 2017 ; Wang et al., 2020 ; Xie et al., 2018). Le volume cellulaire est contrôlé par la régulation osmotique, la contractilité du cytosquelette cellulaire ainsi que la croissance et la division cellulaire (Cadart et al., 2019). Cependant, la façon dont les changements de volume cellulaire peuvent conduire à un remodelage tissulaire dans des contextes morphogénétiques plus larges, tels que le système cardiovasculaire, reste peu claire.

Le cœur acquiert sa fonction tôt au cours du développement embryonnaire afin de pomper le sang dans tout le corps. Les défauts de formation du cœur, et en particulier les anomalies des valves cardiaques, peuvent conduire à des cardiopathies congénitales qui amènent à des implications médicales majeures (Lincoln & Yutzey, 2011). La contrainte de cisaillement des fluides et les forces d'étirement générées par les battements cardiaques sont considérées comme essentielles afin d'obtenir un développement correct des valves (Auman et al., 2007 ; Bartman et al., 2004 ; Hove et al., 2003 ; Kalogirou et al., 2014 ; Vermot et al., 2009). La couche tissulaire interne du cœur correspond à l'endocarde, constitué de cellules endothéliales spécialisées appelées cellules endocardiques (EdC). Comme les cellules endothéliales, les EdC sont de puissants mécanosenseurs et mécanotransducteurs des forces mécaniques (Campinho et al., 2020). Les canaux membranaires sensibles à l'étirement Piezo1, TRPP2 et TRPV4 sont importants pour la détection des forces mécaniques pendant le développement des valves cardiaques (Duchemin et al., 2019 ; Faucherre et al., 2020 ; Heckel et al., 2015). En outre, les EdC interagissent également avec leur MEC (c'est-

à-dire la gelée cardiaque), produite par les cellules myocardiques et endocardiques, et qui joue des rôles clés au cours de la morphogenèse cardiaque (Steed et al., 2016 ; Derrick et al., 2019 ; Derrick & Noël, 2021 ; Grassini et al., 2018).

L'un des principaux composants de la gelée cardiaque est l'acide hyaluronique (AH), qui est un glycosaminoglycane (GAG) chargé négativement. L'AH a la propriété de générer une pression osmotique et attire donc l'eau, ce qui entraîne un gonflement local de la gelée cardiaque au niveau de l'AVC (Camenisch et al., 2000 ; Cowman et al., 2015 ; Lockhart et al., 2011 ; Schroeder et al., 2003 ; Tong et al., 2014). Cependant, les rôles des forces générées par les battements cardiaques ainsi que l'impact des propriétés biophysiques de la MEC sur la modulation de la forme de l'EdC pendant la formation du tube cardiaque primitif ne sont actuellement pas bien compris.

Chez le poisson zèbre, la formation d'un cluster cellulaire local au sein de la monocouche de l'endocarde au niveau de l'AVC marque le début de la formation de la valve cardiaque (Pestel et al., 2016 ; Steed et al., 2016). Au niveau tissulaire, cet événement est précédé d'une rupture de symétrie favorisée par une convergence tissulaire vers l'AVC (Boselli et al., 2017). Ici, nous avons utilisé ce modèle morphogénétique pour étudier les caractéristiques cellulaires précoces impliquées dans la convergence des tissus endocardiques, à partir de 28hpf, lorsque le cœur du poisson zèbre a une structure tubulaire, jusqu'à 48hpf, lorsque les deux chambres (oreillette, ventricule) sont formées. Nous avons constaté que la convergence des tissus est associée à un changement d'orientation global de l'EdC dirigé vers l'AVC et à un événement de regroupement cellulaire qui est associé à une diminution locale du volume des cellules composant l'AVC. Il est intéressant de noter que ni la formation d'amas cellulaires ni les changements de volume cellulaire ne sont liés à la prolifération cellulaire. Au niveau moléculaire, nous avons découvert que la diminution du volume

cellulaire dépend des canaux TRP mécanosensibles (TRPP2 et TRPV4) et l'acide hyaluronique présent au sein de la MEC. Nous proposons un modèle dans lequel la mécanotransduction et la pression osmotique générée par l'accumulation d'AH dans la gelée cardiaque dictent les changements de volume des cellules locales dans l'endocarde. Il pourrait s'agir d'une caractéristique générale par laquelle les forces mécaniques façonnent le système cardiovasculaire, comme le cœur ou les vaisseaux sanguins et lymphatiques du système vasculaire.

RESULTATS

L'orientation des cellules de l'endocarde pendant le développement de l'AVC

En utilisant le poisson zèbre pour une imagerie live de haute précision, nous avons analysé les modèles morphogénétiques de l'endocarde à une résolution cellulaire. La polarité cellulaire axiale est un indicateur bien établi de l'orientation et de la coordination des mouvements cellulaires dans les tissus endothéliaux (Franco et al., 2015 ; Kwon et al., 2016 ; Pouthas et al., 2008). Profitant de ce fait, nous avons étudié la dynamique de l'orientation des cellules endocardiques pendant le développement de l'AVC *in vivo* afin de caractériser les caractéristiques générales de la morphogénèse l'AVC. Nous avons utilisé une lignée transgénique de poisson zèbre qui marque l'appareil de Golgi et le noyau spécifiquement dans les cellules endothéliales Tg(fli1:nEGFP) ; Tg(fli1a:B4GALT1-mCherry) (Kwon et al., 2016), fournissant ainsi des données sur la configuration globale du tissu à l'échelle cellulaire. L'orientation de l'axe Nucleus-to-Golgi a été analysée toutes les deux heures de 28hpf à 36hpf et à 48hpf afin de suivre les changements d'orientation de l'EdC (Figure 1.A,

Figure S1.A, Vidéo S1). Nous avons classé les cellules en trois catégories : 1) axe noyau-Golgi vers la sortie du coeur, 2) axe noyau-Golgi vers l'entrée du coeur et 3) aucune orientation claire de l'axe noyau-Golgi (Figure 1.B ; Figure S1.B). Pour l'analyse statistique, nous avons quantifié les changements de l'axe noyau-Golgi dans le ventricule (Figure 1.C) et dans l'oreillette au fil du temps (Figure 1.C'). Avant le battement du cœur (22hpf), 48,6±5,7% des cellules présentaient un axe noyau-Golgi vers la sortie (n=130 cellules, N=3 embryons) (Figure S1.C). Après le déclenchement du flux sanguin, nous avons constaté que la majorité des cellules (66,5±2,0 %, n=271 cellules, N=5 embryons pour l'oreillette et 70,2±4,6 %, n=198 cellules, N=5 embryons pour le ventricule) présentaient un axe noyau-Golgi vers la sortie à 28 hpf dans les deux chambres (Figure 1 C-C'). Alors que l'orientation de l'axe noyau-Golgi est restée inchangée de 28hpf à 48hpf dans l'oreillette (Figure 1.C'), les cellules ventriculaires ont progressivement inversé leur axe noyau-Golgi entre 28 et 48hpf (48,2±2,0%, n=578 cellules, N=7 embryons) pour pointer vers l'AVC (Figure 1.C). Ces résultats indiquent que la convergence des tissus s'accompagne d'une orientation globale de l'axe noyau-Golgi vers l'AVC à partir de 30 hpf, soulignant les mouvements collectifs des cellules endocardiques nécessaires pour initier la formation des valves cardiaques (Figure 1.F).

Le volume des cellules de l'endocarde au cours du développement de l'AVC

Compte tenu du changement global de l'orientation de l'EdC au début de la morphogenèse de l'AVC, nous avons pensé que les cellules situées dans la zone de convergence devaient changer spécifiquement de forme au sein de l'AVC. Nous avons donc émis l'hypothèse qu'un changement local de la taille des cellules au niveau de

l’AVC pourrait contribuer au processus de morphogenèse de l’AVC. Pour répondre à cette hypothèse, nous avons analysé les changements de volume de l'EdC pendant la morphogenèse de l’AVC. Nous avons d'abord quantifié séparément la surface et la hauteur des cellules (direction apicobasale) afin de comparer la taille des cellules entre les trois régions (atrium, AVC, ventricule) pour calculer le volume moyen des cellules. Pour mesurer l'aire de la surface cellulaire apicale, nous avons utilisé une lignée de poisson zèbre transgénique (TgBAC(ve-cad:ve-cad-TS)) marquant la cadhérine endothéliale vasculaire (VE) (Lagendijk et al., 2017) (Figure 2.A). Nous avons estimé la taille des cellules en multipliant la surface cellulaire apicale par l'épaisseur de la cellule (figure 2.B). D'après ces calculs, la taille des cellules de l'AVC est de 412,2±21,6 µm3 (n= 41 cellules), tandis que celle des cellules situées dans l'oreillette et le ventricule est de 1348±67,9 µm3 (n= 48 cellules) et 933,1±47,8 µm3 (n= 34 cellules), respectivement (Figure 2.C). Nous avons conclu que la taille des cellules varie en fonction des différentes régions du cœur, les cellules étant plus petites dans l’AVC.

Pour surmonter les difficultés associées à la segmentation manuelle 3D, nous avons développé une routine robuste et quantitative basée sur le Deep Learning pour obtenir une évaluation fiable du volume cellulaire à partir de la segmentation des noyaux. En effet, il a été rapporté que le volume nucléaire est proportionel au volume cellulaire dans différents contextes (Cantwell & Nurse, 2019 ; Greiner et al., 2015 ; Huber & Gerace, 2007). Nous nous sommes donc concentrés sur l'extraction du volume des noyaux qui est plus facile à segmenter que les cellules lorsqu'elles sont en 3D. Pour confirmer la validité de l'approche, nous avons montré que le volume des noyaux est corrélé au volume des cellules dans notre système (figure 2.D). Pour démontrer plus clairement cette corrélation, nous avons analysé les cellules individuelles à la fois pour

leur surface cellulaire et leur volume de noyau et avons trouvé une forte corrélation entre ces deux paramètres (Figure 2.E).

Nous avons ensuite évalué la variation temporelle du volume cellulaire au cours de la progression de la convergence tissulaire. A 28hpf, les cellules de l'AVC n'étaient pas différentes en taille par rapport aux cellules situées dans le ventricule (426.7±32.8 µm3 à 28hpf dans l'AVC), alors qu'elles ont commencé à être plus petites de 36hpf à 48hpf (390.6±12.9 µm3 à 36hpf, et de 284.9±6.1 µm3 à 48hpf) (Figure 2F). Nous avons confirmé ces résultats en quantifiant la distance moyenne entre chaque noyau et ses trois plus proches voisins (Figure S2.A). De plus, nous avons constaté que le changement de volume cellulaire est corrélé à l'enrichissement en filaments d'actine (F-actine) et en chaîne légère de phospho-myosine (p-MLC) spécifiquement dans les cellules qui formeront l'AVC, ce qui suggère que les cellules présentent une contractilité active dans l'AVC (Figure 1.D-E, Vidéo S2). Cette observation indique que les propriétés mécaniques et les comportements des cellules de l'AVC pourraient être différents de ceux des cellules endocardiques situées dans les deux chambres. Dans l'ensemble, ces résultats montrent que les EdC de l'AVC subissent une forte diminution du volume cellulaire ainsi qu'un remodelage du cortex d'actine. Cela indique que la contractilité des EdC et la diminution du volume cellulaire sont impliquées dans le remodelage du tissu endocardique.

La diminution du volume cellulaire est indépendante de la prolifération cellulaire dans l'AVC

Des taux de prolifération cellulaire différentiels ou une progression différentielle à travers le cycle cellulaire entre les trois régions du tube cardiaque primitif (oreillette, AVC, ventricule) pourraient entraîner la formation du cluster de cellules au sein de

l’AVC. Nous avons donc évalué si la prolifération cellulaire est associée à des changements de volume cellulaire spécifiques aux chambres cardiaques. Pour ce faire, nous avons aboli la division cellulaire en utilisant une combinaison de 30mM Hydroxyurea et 150µM Aphidicolin, deux médicaments qui induisent l'arrêt du cycle cellulaire en phase S (Figure 3.A). Les embryons ont été traités de 30hpf à 48hpf sans défauts phénotypiques majeurs (Figure S1A-A'). L'immunomarquage anti-phospho-Histone 3 a confirmé que l'inhibition de la prolifération cellulaire était effective en présence des médicaments (Figure S3.B-B'). Pendant le traitement, le nombre d'EdCs a doublé alors que le nombre de cellules est resté similaire entre 30hpf et 48hpf lorsque la prolifération était inhibée (Figure 3.A). Le tissu endocardique et la forme du cœur global sont restés qualitativement inchangés : le cœur a « loopé » et le volume global du cœur n'était pas significativement différent entre les embryons témoins et traités (Figure 3.B, Figure S3.C-C'). Lorsque le volume des noyaux a été quantifié, nous n'avons pas pu détecter de différence dans le rapport de taille des cellules entre les trois régions du cœur (oreillette, VCA, ventricule) chez les embryons témoins et traités (rapport de 1,48, 1,48 et 1,53 respectivement dans l'oreillette, le VCA et le ventricule), ce qui suggère un effet d'échelle global reliant le nombre et la taille des cellules (Figure 3.C). De même, nous n'avons pas pu détecter de différence dans la distance moyenne noyau-noyau (rapport de 1,26, 1,27 et 1,15 respectivement dans l'oreillette, l'AVC et le ventricule) entre les embryons témoins et traités (Figure S3.D). Il est important de noter que les cellules étaient significativement plus petites dans l'AVC des embryons traités en l'absence de prolifération comparable aux cellules situées dans le ventricule (Figure 3.C). Ces résultats montrent que la diminution du volume des cellules présentes dans la région de l'AVC est indépendante de la prolifération cellulaire. De plus, l’orientation de l'axe noyau-Golgi à 48hpf était similaire chez les embryons traités

et les embryons témoins, tant dans le ventricule (Figure 3.D) que dans l'atrium (Figure 3.D'). Cela suggère également que la convergence des tissus se produit normalement indépendamment de la prolifération cellulaire.

Les forces mécaniques sont des régulateurs importants de la diminution du volume cellulaire

Comme il a été démontré que les forces mécaniques sont impliquées dans le remodelage des tissus endocardiques (Steed et al., 2016, Heckel et al., 2015, Dietrich et al., 2014), nous avons ensuite étudié l'impact de la modification de la contraction cardiaque et du flux sanguin sur la taille des cellules de l'endocarde. Pour ce faire, nous avons d'abord analysé les changements de volume cellulaire basés sur le marquage des noyaux dans des mutants *silent heart* (sih-/-), qui portent une mutation dans le gène de la troponine T2a (tnnt2a) et sont donc dépourvus de contraction cardiaque et du flux sanguin qui en résulte (Sehnert et al., 2002) (Figure 4.A-A'). Le volume cellulaire n'a pas montré de différences significatives entre les trois régions du cœur (oreillette, AVC, ventricule) et les cellules situées dans le l'AVC n'ont pas montré un volume plus petit par rapport aux embryons témoins (volume du noyau de 481,7±25,5 µm3 chez les *sih-/-,* n=68 cellules, N=12 embryons, volume du noyau de 273,2±7,6 µm3 chez les *sih*+/+ *sih*+/-, n=197 cellules, N=8 embryons) (Figure 4.B). Moins de cellules étaient présentes dans l'AVC par rapport aux témoins (Figure 4.D) et la distance noyau-noyau était significativement augmentée au niveau de l'AVC chez les embryons *sih-/-* (Figure S4.B). Il est intéressant de noter que le remodelage de la F-actine était absent dans les cellules de l'AVC des embryons *sih-/-* par rapport aux témoins (Figure S4.A). En outre, à 48hpf, les cellules situées dans l'atrium présentaient

une distribution aléatoire des axes noyau-Golgi (Figure 4.F') (vers la sortie du cœur: 35,3±2,9% ; vers l'entrée du cœur: L'inversion de l'axe noyau-Golgi ventriculaire ne s'est pas produite chez les embryons *sih-/-* et les cellules ont plutôt eu tendance à présenter un axe noyau-Golgi vers l'écoulement du cœur (vers l'écoulement du cœur : 46,0±2,6 %, vers l'entrée du cœur : 27,3±4,4 %, n=314 cellules, N=6 embryons) par rapport aux témoins (vers l'entrée du cœur: 53,5±2,5 %, n=217 cellules, N=3 embryons) (Figure 4.F). Ces données sont cohérentes avec l'observation selon laquelle la convergence des tissus ne se produit pas en l'absence de forces mécaniques générées par le battement du cœur (Boselli et al., 2017). Pour confirmer ces résultats, nous avons partiellement inhibé l'activité cardiaque en injectant une faible concentration du morpholino *tnnt2a* (Vidéo S3) (Figure A''). Comme prévu, la vitesse du flux sanguin était plus faible (176,7±30,0 µm/s, N=12 embryons), par rapport aux témoins (1222,6±128,0 µm/s, N= 3 embryons) (Figure 4.E). Il est intéressant de noter que la diminution du volume cellulaire au niveau de l'AVC a été affectée volume du noyau de 360,9±11,7 µm3, n=153 cellules, N=12 embryons chez les morphants tnnt2a, volume du noyau de 324,9±10,5 µm3, n=114 cellules, N=3 embryons) (Figure 4.C) suggérant que même une diminution subtile des forces générées par le cœur modifie le volume cellulaire. Globalement, ces résultats indiquent que les forces mécaniques sont des régulateurs importants de la diminution du volume cellulaire.

Les canaux sensibles à l'étirement TRPP2 et TRPV4 sont des modulateurs clés de la diminution du volume cellulaire

Les canaux sensibles à l'étirement Transient Receptor Potential Polycystin 2 (TRPP2) et Transient Receptor Potential Vanilloid 4 (TRPV4) sont des régulateurs importants du développement des valves cardiaques (Heckel et al., 2015). De plus, TRPV4 est également un contributeur bien connu de la régulation du volume cellulaire dans les

astrocytes où il agit comme un canal osmosensible (Benfenati et al., 2011). Nous avons donc émis l'hypothèse que les canaux TRP pourraient moduler le volume cellulaire pendant la morphogenèse de l'AVC. Nous avons étudié des mutants pour les canaux *trpv4* et *trpp2*. L'ARNm *trpp2* est distribué de manière ubiquitaire dans l'embryon mais est enrichi dans la couche endocardique du cœur alors que *trpv4* est principalement exprimé dans l'endocarde et spécifiquement enrichi dans la région de l'AVC (Figure 4.H). En examinant les embryons mutants simples *trpv4 -/- et trpp2 -/-,* nous avons constaté que le volume du noyau EdC au niveau de l'AVC était inchangé par rapport aux témoins (Figure S4.D). La compensation génétique étant une caractéristique répandue chez le poisson zèbre (El-Brolosy & Stainier, 2017), nous avons analysé les mutants doubles *trpv4 -/-;trpp2 -/-* (Figure 4.G-G'). La diminution du volume cellulaire n'a pas été observée dans l'AVC des *trpv4 -/-;trpp2 -/-* par rapport aux témoins (volume du noyau de 351,9±7,9 µm3, n=333 cellules, N=15 embryons chez les *trpv4 -/-;trpp2 -/-,* volume du noyau de 282. 4±9,8 µm3, n=129 cellules, N=6 chez *trpv4 +/+;trpp2 +/+)* (Figure 4.I), et la distance noyau-noyau était significativement augmentée au sein de l'endocarde des doubles mutants (Figure S4.E).De plus, la fréquence cardiaque n'était pas significativement différente entre les mutants, ce qui suggère que la fonction cardiaque et les forces d'écoulement sont normales (figure S4.F). Ces données montrent que les canaux mécanosensibles Trpp2 et Trpv4 sont des régulateurs importants de la diminution du volume cellulaire. En outre, le pourcentage de cellules de l'endocarde dont l'axe noyau-Golgi est orienté vers l'écoulement du cœur dans le ventricule 36,9±1,7 % (n= 309 cellules, N=4 embryons) est réduit par rapport aux témoins (49,0±3,8 % (n= 223 cellules, N=3 embryons) (Figure 4.J) et la distribution des axes noyau-Golgi est inchangée dans l'oreillette

(Figure 4.J'). Ceci suggère que la convergence tissulaire est affectée en l'absence des canaux TRP.

Dans le contexte d'une augmentation du volume cellulaire d'origine osmotique (c'est-à-dire le gonflement des cellules), TRPV4 interagit avec les canaux aquaporines pour moduler le volume cellulaire (Benfenati et al., 2011 ; Conner et al., 2012 ; Iuso & Križaj, 2016). Les aquaporines sont des canaux transmembranaires passifs qui peuvent augmenter la perméabilité de la membrane (Ibata et al., 2011 ; Mola et al., 2016). Nous avons étudié l'expression spatio-temporelle des aquaporines et nous nous sommes concentrés sur deux canaux aquaporines présents dans le système cardiovasculaire en développement : *aqp8a.1* et *aqp1a.1* (Figure S2.B-S2.D). L'ARNm d'*aqp8a.1* et d'*aqp1a.1* est exprimé dans le cœur (Figure S2.B), avec une expression commençant à partir de 30hpf spécifiquement dans les cellules de l'AVC (9/32 embryons (*aqp8a.1*), 4/20 embryons (*aqp1a.1*)). A ce stade, l'*aqp1a.1* est également exprimé dans les globules rouges, comme précédemment rapporté (16/20 embryons) (Chen et al., 2010) (Figure S2.B). A 36hpf, les ARNm *aqp8a.1* et *aqp1a.1* sont exprimés dans les cellules de l'AVC et de l'OFT (24/27 embryons (aqp8a.1), 19/19 embryons (*aqp1a.1*). A 48 hpf, *aqp8a.1* est indétectable (36/36) alors que l'expression de l'ARNm *aqp1a.1* est hautement spécifique dans les régions de l'AVC et de l'OFT (31/31). En utilisant des sondes fluorescentes, nous confirmons que ces canaux sont exprimés spécifiquement dans les régions de l'AVC et de l'OFT et nous montrons également que leur expression est limitée à l'endocarde (Figure S2.C). De manière intéressante, l'expression d'*aqp8a.*1 et d'*aqp1a.1* était absente dans les embryons *sih -/-,* ce qui suggère que leur expression dépend des forces mécaniques (Figure S4.C). Ces données indiquent que les cellules spécifiquement situées dans l'AVC sont équipées de pores à eau dont l'expression dépend de la fonction cardiaque.

L'acide hyaluronique module les changements de volume des cellules endocardiques de l'AVC

L'un des composants les plus abondants de la gelée cardiaque est le glycosaminoglycane (GAG) acide hyaluronique (AH). L'accumulation de GAG est connue pour appliquer une pression osmotique et attirer l'eau (Cowman et al., 2015 ; Lockhart et al., 2011). *In vitro*, les GAG entraînent un rétrécissement des cellules HEK (Joerges et al., 2012). L'AH est assemblé par les gènes hyaluronan synthase et est ensuite sécrété dans la MEC. En particulier, *has2* est spécifiquement exprimé par les cellules de l'encodarde présentes au sein de l'AVC (Patra et al., 2011 ; Tong et al., 2014). Comme prévu, l'expression de *has2* dans le cœur commence à 30hpf et est limitée à l'AVC de 30hpf à 48hpf (Figure S5.A). Nous avons utilisé la protéine de liaison à l'AH (HA-BP) pour étudier la localisation de la protéine (Figure 5.A). L'AH s'est avérée être présente exclusivement dans la gelée cardiaque (Figure 5.A, Figure S5.B) et semble uniformément distribuée dans toute la gelée cardiaque du cœur. Nous avons ensuite évalué son rôle potentiel dans la régulation du volume cellulaire à l'échelle de la cellule en injectant de la hyaluronidase (HAase), qui décompose les chaînes d'AH (Figure 5.B). Les embryons injectés avec de la HAase présentaient un œdème péricardique après 18 heures de traitement (Figure S5.C) mais ne présentaient pas de défauts de fréquence cardiaque à 48hpf (Figure S5.E). Dans ces conditions, l'AH n'a pas été détectée à l'intérieur de la gelée cardiaque des embryons injectés à la HAase, ce qui confirme que la dégradation de l'HA a été efficace (Figure 5.C). Il est intéressant de noter que le remodelage de la F-actine dans les EdC et la diminution du volume cellulaire n'ont pas eu lieu dans les embryons traités (Figure S5.D) (N=7/7 embryons injectés à l'HAase, N=7/7 contrôles). La diminution du volume cellulaire n'a pas été

observée dans l'AVC des embryons ayant reçu une injection de HAase par rapport aux témoins (volume du noyau de 422±10,0 µm3, n=177 cellules, N=12 embryons dans les embryons ayant reçu une injection de HAase, volume du noyau de 290,6±7,0 µm3, n=266 cellules, N=8 dans les témoins) (Figure 5.E). De même, la distance entre les noyaux des AVC était accrue chez les embryons ayant reçu une injection de HAase (Figure S5.F). En outre, le nombre de cellules ventriculaires dont l'axe noyau-Golgi est orienté vers l'influx 30,1±2,2 % (n=523 cellules, N=7 embryons) est réduit par rapport aux témoins 53,4±3,3 % (n=425 cellules, N=5 embryons) (Figure 5.F) et la distribution des axes noyau-golgi était inchangée dans l'atrium (Figure 5.F'). Ce résultat indique que la convergence des tissus est réduite en l'absence d'AH à l'intérieur de la gelée cardiaque. Nous concluons que la mécanosensibilité et l'AH sont tous deux des modulateurs essentiels de la diminution du volume cellulaire dans l'AVC (Figure 5.G).

DISCUSSION

En utilisant l'imagerie *in vivo*, nous montrons que la diminution du volume des cellules endocardiques est essentielle à la convergence des tissus et à la formation de l'AVC, ce qui prépare le terrain pour la formation ultérieure de la valve (Pestel et al., 2016 ; Steed et al., 2016). Nous avons observé que la diminution du volume cellulaire est concomitante avec l'inversion de l'axe noyau-Golgi ainsi au sein du ventricule ainsi qu'avec le remodelage de la F-actine dans l'AVC. De plus, nous montrons que le changement de volume cellulaire est indépendant de la prolifération cellulaire et est régulé par les forces mécaniques causées par la fonction cardiaque, les canaux TRP et l'AH situé au sein de la gelée cardiaque. Ensemble, nos résultats montrent que la

diminution du volume cellulaire est une caractéristique cellulaire importante impliquée dans la morphogenèse cardiovasculaire en réponse à la mécanotransduction activée par les canaux TRP. Nous proposons que la modification du volume cellulaire puisse être une caractéristique cellulaire générale activée par les forces mécaniques pour contrôler la forme des tissus.

Les canaux TRP sont des acteurs clés dans la voie de mécanotransduction menant à la formation des valves cardiaques (Duchemin et al., 2019 ; Heckel et al., 2015). Le modèle actuel suggère que ces canaux détectent le flux sanguin oscillant au niveau de l'AVC, qui est ensuite transposé en informations électrochimiques, conduisant à l'expression de gènes mécanosensibles (Steed, Boselli, et al., 2016, Heckel et al., 2015). Nos résultats suggèrent que des signaux supplémentaires, en plus du flux sanguin oscillant, pourraient affecter l'activité des canaux TRP par la génération d'une pression osmotique générée dans la gelée cardiaque. Les composants de la gelée cardiaque sont importants pour la formation correcte de l'AVC (Derrick & Noël, 2021 ; Grassini et al., 2018 ; Hernandez et al., 2019). Par exemple, la modulation de l'expression du gène *ugdh* codant pour les blocs de construction des GAG ou l'altération du dépôt d'AH dans la gelée cardiaque conduit à des défauts dans le développement de l'AVC (Segert et al., 2018 ; Walsh & Stainier, 2001). Ici, nous montrons que l'AH régule la taille des EdC dans l'AVC, révélée par l'absence de diminution du volume cellulaire chez les embryons traités à la hyaluronidase. De manière intéressante, il est connu que les GAG peuvent établir une pression osmotique (Cowman et al., 2015) et les canaux TRPV4 sont connus pour être des canaux osmosensibles (Hoffmann et al., 2009) qui interagissent physiquement avec l'aquaporine pour moduler le volume cellulaire en réponse aux stress osmotiques (Benfenati et al., 2011). Il est intéressant de noter que les cellules qui perdent du

volume se sont également révélées être équipées de canaux d'aquaporine (aqp8a.1, aqp1a.1). Considérant que l'aquaporine améliore la perméabilité à l'eau (Ibata et al., 2011 ; Mola et al., 2016), le complexe TRPV4-Aquaporine pourrait augmenter le taux d'efflux d'eau suite à l'établissement d'un gradient osmotique. De plus, l'entrée intracellulaire d'ions calcium suite à l'ouverture des canaux TRP pourrait conduire à la translocation des canaux aquaporines vers la membrane plasmique (Conner et al., 2012). Dans ce contexte, nous proposons un modèle dans lequel l'accumulation d'AH crée une pression osmotique entre les EdC et la gelée cardiaque pour favoriser la diminution du volume cellulaire observée dans l'AVC (Figure 5.G). Dans ce modèle, les canaux TRP seraient impliqués à la fois dans la détection osmotique et dans la détection de la contrainte de cisaillement.

Quelle est la force motrice de la convergence tissulaire ? Au niveau des tissus, nous avons observé un changement de l'axe noyau-Golgi qui est concomitant aux changements de volume cellulaire et qui dépend à la fois du flux sanguin et de la présence de canaux TRP et d'AH. Par conséquent, la diminution locale du volume cellulaire des cellules de l'AVC pourrait avoir une influence sur les cellules environnantes et entraîner la convergence des tissus ainsi que le regroupement des cellules. De plus, nous ne pouvons pas exclure que la convergence des tissus soit en partie due à une migration active des EdCs vers la région de l'AVC. En effet, la présence d'AH au sein de la MEC a été rapportée comme étant essentielle dans le contexte de la migration cellulaire dans plusieurs études (Derrick & Noël, 2021) et la MEC est clé pour réguler le renouvellement des signaux angiogéniques (De Angelis et al., 2017). Deux scénarios principaux peuvent donc expliquer nos résultats : une migration active vers l'AVC a lieu et est ensuite suivie d'un rétrécissement adaptatif du volume cellulaire et/ou le rétrécissement du volume cellulaire au niveau de l'AVC tire

sur les cellules environnantes et conduit à la convergence tissulaire. Compte tenu de la faible amplitude des mouvements tissulaires, nous privilégions le second scénario dans lequel la diminution du volume cellulaire est suffisante pour entraîner le mouvement des tissus, comme décrit chez d'autres espèces (Saias et al., 2015).

En résumé, nous avons observé que la perte des canaux TRP mécanosensibles/osmosensibles en présence d'un flux sanguin normal affecte la capacité des EdCs de l'AVC à diminuer leur volume cellulaire et la morphogenèse ultérieure de la valve cardiaque. Ces résultats indiquent que les cellules de l'endocarde traitent les signaux mécaniques locaux pour réguler leur taille par le biais de canaux ioniques. Les interactions coordonnées entre les processus extracellulaires et intracellulaires impliqués dans la régulation du volume cellulaire sont essentielles pour expliquer les mécanismes conduisant au remodelage des tissus. Dans l'ensemble, une meilleure compréhension de ces mécanismes pourrait avoir des implications pour le traitement de certaines pathologies.

ANNEX 1

ANNEX 1

eLIFE elifesciences.org

RESEARCH ARTICLE

Mechanically activated piezo channels modulate outflow tract valve development through the Yap1 and Klf2-Notch signaling axis

Anne-Laure Duchemin[1,2,3,4], Hélène Vignes[1,2,3,4], Julien Vermot[1,2,3,4]*

[1]Institut de Génétique et de Biologie Moléculaire et Cellulaire, Illkirch, France; [2]Centre National de la Recherche Scientifique, Illkirch, France; [3]Institut National de la Santé et de la Recherche Médicale, Illkirch, France; [4]Université de Strasbourg, Illkirch, France

Abstract Mechanical forces are well known for modulating heart valve developmental programs. Yet, it is still unclear how genetic programs and mechanosensation interact during heart valve development. Here, we assessed the mechanosensitive pathways involved during zebrafish outflow tract (OFT) valve development in vivo. Our results show that the hippo effector Yap1, Klf2, and the Notch signaling pathway are all essential for OFT valve morphogenesis in response to mechanical forces, albeit active in different cell layers. Furthermore, we show that Piezo and TRP mechanosensitive channels are important factors modulating these pathways. In addition, live reporters reveal that Piezo controls Klf2 and Notch activity in the endothelium and Yap1 localization in the smooth muscle progenitors to coordinate OFT valve morphogenesis. Together, this work identifies a unique morphogenetic program during OFT valve formation and places Piezo as a central modulator of the cell response to forces in this process.
DOI: https://doi.org/10.7554/eLife.44706.001

***For correspondence:** julien@igbmc.fr

Competing interests: The authors declare that no competing interests exist.

Funding: See page 22

Received: 24 December 2018
Accepted: 14 September 2019
Published: 16 September 2019

Reviewing editor: Holger Gerhardt, Max Delbrück Center for Molecular Medicine, Germany

Introduction

Heart pumping and shaping take place concomitantly during embryonic development. These two processes require a tight and dynamic coordination between mechanical forces and tissue morphogenesis. Heart valve development is a great model for studying these interactions when considering that heart valve defects are common congenital cardiac malformation in human (***Hoffman and Kaplan, 2002***; ***Øyen et al., 2009***). The four-chambered heart contains two different sets of valves (***Lin et al., 2012***):

- Tricuspide valves including the two semilunar (SL) valves, the aortic valve and the pulmonary valve, as well as the tricuspide valve located between the right atrium and the right ventricle.

- A bicuspide valve called the mitral valve separating the left atrium from the left ventricle. Abnormalities of the arterial valve leaflets are the most-common congenital malformations, in particular bicuspid aortic valve (***Hoffman and Kaplan, 2002***). Aortic valves mainly derive from endocardial cushion progenitors with a potential contribution from other cellular sources (epicardial cells and neural crest) (***Wu et al., 2017***). Generally, valve formation depends on two main events: cell proliferation, which is mainly mediated by the *vegf-nfat1* pathway, matrix deposition and an endothelial-to-mesenchymal transformation (endMT) under the control of Gata transcription factors (***Laforest et al., 2011***; ***Stefanovic et al., 2014***), Notch signaling (***Luxán et al., 2016***), *Smad/tgf-beta/Bmp*, and *Wnt-beta catenin* signals (***Combs and Yutzey, 2009***). Nevertheless, recent evidence

suggests that arterial valves develop differently from atrioventricular valves by differentiating directly from progenitors in the outflow wall independently from endMT in mouse (**Eley et al., 2018**).

Congenital valve defects may originate from developmental origins and/or abnormal haemodynamic forces between these two sets of valves, and it remains unclear how general these developmental programs are. Aortic valves are located in areas of high flow velocity and mechanical forces have a great impact on valve morphogenesis (**Butcher et al., 2008**). Abnormal blood circulation is widely recognized as a cardiovascular risk factor and abnormal mechanotransduction has been associated with valvulopathies (**Bäck et al., 2013**). Congenital heart valve malformations are usually associated with genetic mutations in genes essential for heart valve development, such as signaling factors (Notch1, TGFβ) for the aortic valves (**Bäck et al., 2013**), and actin-binding proteins (FilaminA) for the mitral valves (**Sauls et al., 2012**). The reoccurring discovery of genetic mutations linking valve defects with genes involved in controlling developmental programs (e.g., in NOTCH1, TBX5, GATA4, TBX20, LMCD1, TNS1, and DCHS1) (**PROMESA investigators et al., 2015**; **Durst et al., 2015**; **Garg et al., 2005**; **Richards and Garg, 2010**), has spurred interest in valve morphogenesis. A key issue is to further define the genetic or environmental causes of valve malformation.

The zebrafish constitutes a powerful model to study cardiac valve development and the role of mechanical forces at the cellular scale. Zebrafish heart is two chambered and contains three sets of valves (the outflow tract (OFT), atrioventricular (AVC) and the inflow tract (IFT) valve [**Figure 1A**]) that are all bicuspid (**Beis et al., 2005**; **Hsu et al., 2019**; **Tessadori et al., 2012**). While the developmental programs driving mitral valve development in response to mechanical forces start to be well established in zebrafish, less is known about OFT and IFT valves (**Paolini and Abdelilah-Seyfried, 2018**; **Steed et al., 2016a**). The cellular processes leading to valve formation are dynamic and are particularly challenging to address in vivo. Zebrafish heart valves originate from progenitors located in the ventricle and atrium that generate the valve leaflets through a coordinated set of endocardial tissue movements (**Boselli et al., 2017**; **Pestel et al., 2016**; **Steed et al., 2016a**; **Steed et al., 2016b**; **Vermot et al., 2009**). The sequence of cellular events leading to AVC valve formation in zebrafish embryonic hearts is initiated through cell shape changes that lead to EC convergence towards the AVC (**Boselli et al., 2017**) and cellular rearrangements that will form a multilayered tissue (**Beis et al., 2005**; **Pestel et al., 2016**; **Scherz et al., 2008**; **Steed et al., 2016b**). In the zebrafish AVC, blood flow and Klf2a control *notch1b* and *bmp4* expression, both of which are necessary for valve formation (**Vermot et al., 2009**). Klf2a regulates the deposition of matrix protein (in particular Fibronectin1) in the valve forming area (**Steed et al., 2016b**), as well as Wnt signaling by controlling *wnt9b* expression (**Goddard et al., 2017**). The latter is consistent with the fact that canonical Wnt signals arise specifically in sub-endocardial, abluminal cells and that these Wnt signals are dependent upon hemodynamic forces in zebrafish (**Pestel et al., 2016**). In addition, Notch signaling is essential for aortic valve formation (**Garg, 2016**) and OFT development (**MacGrogan et al., 2016**; **Wang et al., 2017**). The role of mechanical forces during OFT valve development at the cellular and molecular scale, however, is largely unknown.

Fluid shear stress is an important environmental cue that governs vascular physiology and pathology (**Baeyens et al., 2016**), but the molecular mechanisms that mediate endocardial responses to flow are only partially understood. In zebrafish, the mechanosensitive channels Trpv4 and Trpp2 modulate endocardial calcium signaling and *klf2a* expression is necessary for valve morphogenesis and downstream pathway activation (**Heckel et al., 2015**; **Steed et al., 2016b**). Notch signaling is tightly involved in cellular mechanosensitive responses in human aortic valves (**Godby et al., 2014**) and Notch1 is a potent mechanosensor in adult arteries (**Mack et al., 2017**). More recently, it has been shown that stretch-sensitive channels from the Piezo family (**Murthy et al., 2017**) are important for vascular development (**Li et al., 2014**; **Ranade et al., 2014**) and lymphatic valve formation (**Nonomura et al., 2018**). In the embryo, Piezo channels exert essential roles during cell differentiation (**He et al., 2018**) and can affect lineage choice by modulating the nuclear localization of the mechanoreactive transcription coactivator Yap (**Pathak et al., 2014**). Nevertheless, the role of Piezo-mediated mechanotransduction during cardiac development and its potential targets remain unclear.

In the developing cardiovascular system, biomechanics is key for modulating flow propagation (**Anton et al., 2013**). In the teleost heart, the OFT constitutes a specialized organ comprising the conus arteriosus (CA) and the bulbus arteriosus (BA) (**Figure 1A**). The BA dampens the pressure wave down the arterial tree (**Braun et al., 2003b**). To perform its function, the BA expresses elastic

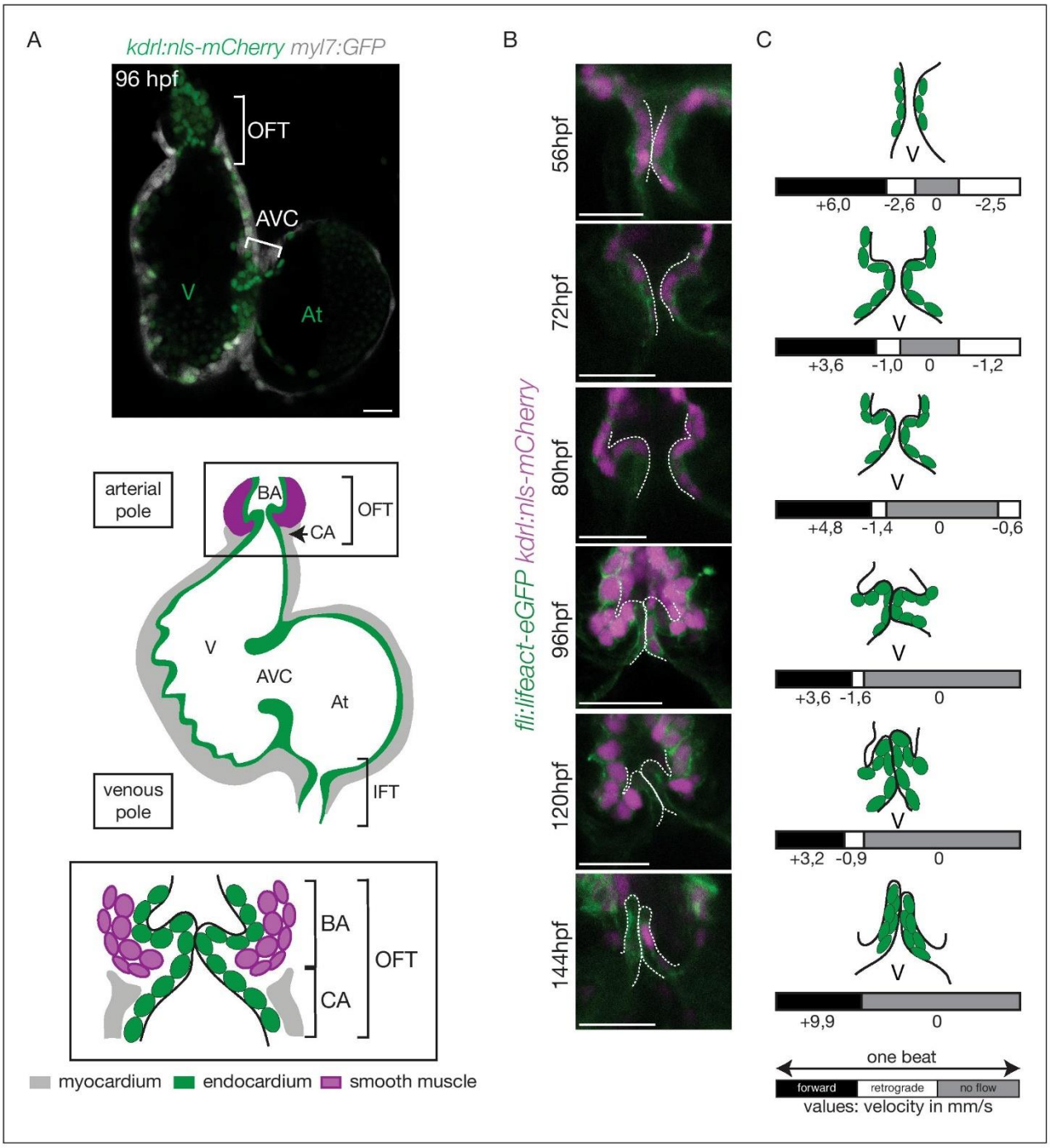

Figure 1. The OFT develops from 56 hpf to form functional valves at 144 hpf. (**A**) Top: Z-section of the double transgenic line *Tg(kdrl:nls-mCherry; myl7:GFP)* showing the overall structure of the heart. Bottom: Scheme of the zebrafish heart with the endocardium, myocardium and smooth muscles and zoom on the OFT structure. The OFT includes the CA and the BA. The CA is the zone of the myocardial connection of the ventricle to the BA. The BA is after the ventricle and is surrounded by smooth muscles. Scheme adapted from ***Felker et al. (2018)***. OFT: outflow tract, IFT: inflow tract, AVC: atrioventricular canal, At: atrium, V: ventricle, BA: bulbus arteriosus, CA: conus arteriosus. Scale bar: 20 µm. (**B**) Z-sections of the double transgenic line

Figure 1 continued on next page

Figure 1 continued

Tg(fli:lifeact-EGFP; kdrl:nls-mCherry) at different time-points showing the endocardial OFT structure. Scale bar: 25 μm. (**C**) Schematic representation summarizing the formation of the valve leaflets over time and flow profile in the OFT during development (from 56 hpf to 144 hpf) showing the forward flow (black), retrograde flow (white) and no flow (grey) fractions with the velocity of the red blood cells (in mm/s) using the double transgenic line *Tg (gata1:ds-red; kdrl:EGFP)*. V: ventricle.

DOI: https://doi.org/10.7554/eLife.44706.002

fiber genes that are thought to provide the mechanical properties necessary for its physiological function (***Braun et al., 2003a***; ***Braun et al., 2003b***; ***Keith et al., 1977***). The BA is separated from the ventricle by the OFT valve and is composed of smooth muscle. The extracellular matrix (ECM) gene, *elastin b*, contributes to the development of the BA by regulating cell fate determination of cardiac precursor cells into smooth muscle via a process that involves the mechanotransducer Yap1 (***Moriyama et al., 2016***). How these factors contribute to OFT valve development and interact with other mechanosensitive pathways remains unclear.

In this study, we investigated the signaling events taking place during OFT valve formation and addressed their regulation by the mechanosensitive channels Piezo and transient potential channels (Trp) as well as the flow-responsive transcription factor Klf2a. We show that OFT valve formation proceeds via an initial stage of endothelial cell folding, which is associated with the generation of a cluster of smooth muscle cell progenitors surrounding the endothelial layer. Subsequent global tissue remodeling events result in the appearance of functional leaflets, which defines a unique process of valvulogenesis. Using live reporters to highlight the signaling changes accompanying these temporally coordinated cell-movement events and genetics, we identified Notch and Klf2 as key flow-dependent factors as well as Yap1 as necessary factors for the correct coordination of OFT valvulogenesis. We show that Piezo and Trp channels are key regulators of *klf2* activity in the endothelium and that piezo modulates Yap1 localization in the smooth muscle cells, providing a molecular link between mechanosensitivity and cell signaling in the multilayered valve structure. These data describe the cell responses that are coordinated by the mechanical environment and mechanotransduction via mechanosensitive channels in the endothelium.

Results

Outflow tract valve morphogenesis is unique

In order to better understand the roles played by blood flow during outflow tract (OFT) valve development, we have developed imaging techniques to capture cardiac motion and analyze blood flow in the OFT. Live imaging of the double transgenic line *Tg(gata1:ds-red; kdrl:EGFP)* to follow red blood cells and endothelial cell wall movements reveal dramatic changes in intracardiac blood flow patterns during OFT valve development: as the heart matures, blood flow in the OFT is bidirectional until functional valve leaflets emerge in the OFT at 144 hpf (***Figure 1A–C***). Throughout development, the periods within the cardiac cycle in which reversing flow can be observed decrease in length until 144 hpf, the stage at which we could not observe reversing flow anymore (***Figure 1C***). Using the *Tg(fli:lifeact-EGFP; kdrl:nls-mCherry)* line, which labels endothelial cells, we found that these flow profile modifications are linked to changes in OFT tissue geometry and the state of OFT maturation (***Figure 1B***). At 56 hpf, the endothelium resembles a tube (***Figure 1B,C***), maturing into cushions by 72 hpf, into premature leaflets by 96 hpf and finally into elongated, thin leaflets by 144 hpf (***Figure 1B,C***).

To better characterize how the endothelium changes shape over time and how cells reorganize to form OFT valves, we performed photoconversion experiments using the *Tg (fli:gal4FF;UAS:kaede)* (***Figure 2A***). We photoconverted Kaede from green to red in the cells located in the anterior, middle or posterior part of the valve at 72 hpf and assessed their position at 96 hpf and 120 hpf (***Figure 2A, B***). The results suggest that the endothelium folds to form the valve without multilayering (***Figure 2B,C*** and ***Figure 2—figure supplement 1A***). Indeed, we could observe that the photoconverted cells remain attached to each other and do not show signs of delamination as observed in the AVC (***Figure 2B,C*** and ***Figure 2—figure supplement 1B***).

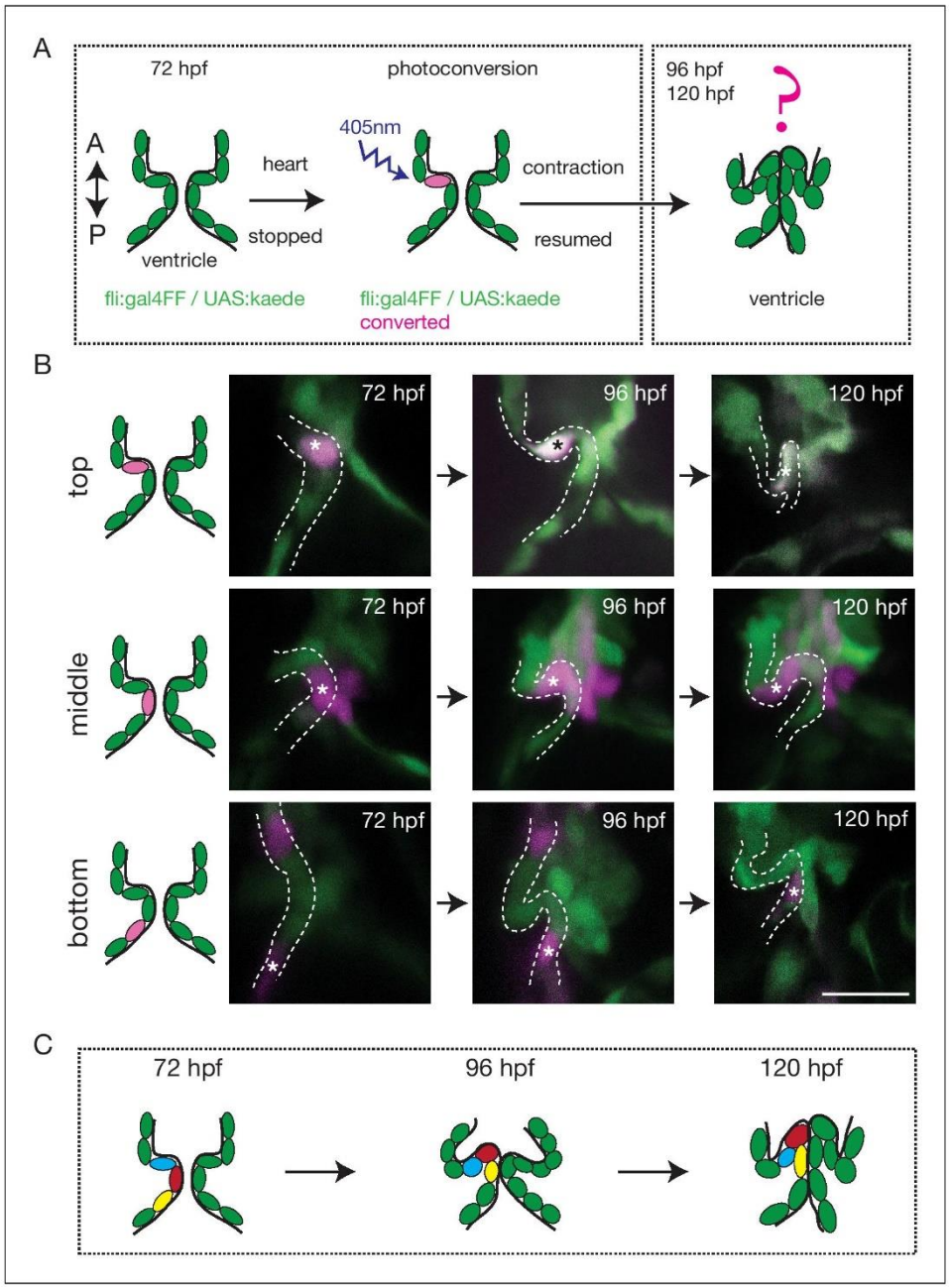

Figure 2. The endothelium contribution to emerging OFT valve leaflets. (**A**) Experimental set-up for the photoconversion studies. Heart was stopped at 72 hpf, the region of interest exposed to 405 nm light to convert kaede from green to red (shown in magenta) fluorescent form and heart contraction was resumed until 120 hpf. Beating hearts were imaged at 96 hpf and 120 hpf by spinning disk microscopy. A. Anterior, P. Posterior. (**B**) Z-sections of the *Tg(fli:gal4FF; UAS:Kaede)* line just after photoconversion (72 hpf), and at 96 hpf and 120 hpf. The star highlights the photoconverted cell in the top (n = 6), middle (n = 5) and bottom (n = 4) part of the OFT valve. The other photoconverted cell anteriorly goes out of the frame. Scale bar: 20 μm. Results obtained from three independent experiments. (**C**) Schematic representation of the results of the photoconversion studies showing the folding of the endothelium in the OFT.

Figure 2 continued on next page

Figure 2 continued

DOI: https://doi.org/10.7554/eLife.44706.003

The following figure supplement is available for figure 2:

Figure supplement 1. The endothelium contribution to emerging OFT versus AVC valves.

DOI: https://doi.org/10.7554/eLife.44706.004

Together, these results suggest that OFT valves form by a folding process that might involve the adjacent tissue.

The cellular contribution of the OFT valve led us to the hypothesis that the surrounding tissue could contribute to valve morphogenesis. We analyzed Fibronectin1 (Fn1) expression in the OFT by counterstaining the *Tg(kdrl:EGFP)* with the Fn1 antibody (***Figure 3A–D***). We found that Fn1 deposition in the OFT is different from that in the AVC (***Steed et al., 2016a***). At 72 hpf, cushions appear and Fn1 is observed in the cells around the endothelial cells, that are themselves surrounded at their base by myocardium in the posterior part (***Figure 3A,B,C,D,E***). Fn1 expression level increases at 96 hpf and delineates a group of cells surrounding the OFT as well as in the basal side of a few endothelial cells that form the cushions (***Figure 3C***, arrows, E). In the developed leaflets at 120 hpf, Fn1 expression is maintained within the leaflets (***Figure 3D,E***). We found that most of the cells surrounding the endothelium expressing Fn1 also express Elastin b (Elnb, Eln2 or Tropoelastin), a marker of smooth muscle cells (***Grimes et al., 2006***; ***Miao et al., 2007***; ***Paffett-Lugassy et al., 2017***) (***Figure 3B', C', D'***). We could confirm that the cells surrounding the Fn1 cells are not myocardial cells as the myocardium stops just before the BA region (***Figure 3A,E***). To better characterize the smooth muscle identity and their activity, we performed a DAF-FMDA assay and counterstained with Fn1 at 72 hpf, 96 hpf and 120 hpf (***Figure 3—figure supplement 1A***). These results suggest that all cells expressing Fn1 are also DAF-FMDA-positive (***Figure 3—figure supplement 1A***). Some of these cells also express *Tg(wt1a:GFP)* (asterisks in ***Figure 3—figure supplement 1B***) a marker of epicardial cells (***Peralta et al., 2013***). One hypothesis could therefore be that they might have originated from epicardial precursors. Together, these results suggest a developmental sequence of OFT morphogenesis in vivo where endothelial cell reorganization is associated with changes in gene expression in the surrounding smooth muscle cell progenitors. This indicates that the OFT morphogenesis involves remodeling of not just the endothelium, but also of a group of smooth muscle cells that express Fn1 and Elnb, and are functionally active.

We conclude that the tissue remodeling occurring during OFT valve development is significantly different from AVC valve development where the endocardium is the main remodeling tissue (***Beis et al., 2005***; ***Pestel et al., 2016***; ***Steed et al., 2016b***).

Klf2, Notch signaling, and Hippo pathways are active in the OFT in different cell layers and are all necessary for proper OFT valve development

To elucidate how these early events are regulated, we sought to determine the mechanosensitive signaling pathways activated at these early stages of OFT valve formation. We first assessed the activity of a Klf2a reporter line (*Tg(klf2a:H2B-GFP)*) (***Figure 4A***), which is a well described flow responsive reporter (***Heckel et al., 2015***; ***Steed et al., 2016b***) and the Notch reporter *Tg(tp1:dGFP)* (***Figure 4B***) which is well active in the progenitors of the AVC cardiac valves (***Pestel et al., 2016***). We could observe a specific activation of the Klf2a reporter in the OFT endothelium (***Figure 4A,C*** and ***Figure 4—figure supplement 1***), in particular in the ventricular part of the valve (posterior) from 72 hpf to 120 hpf (***Figure 4C,D*** and ***Figure 4—figure supplement 1***). Similarly, the Notch reporter *Tg(tp1:dGFP)* is specifically expressed in the OFT endothelium (***Figure 4B,C***), in the ventricular part of the valve from 72 hpf to 120 hpf (***Figure 4C,D***). Interestingly, the spatial activation of the reporter varies within the valve forming area - the transgene activation is stronger in the posterior part of the valve than the anterior part of the valve throughout the process of valve maturation (***Figure 4C,D***). We made similar observations for the Notch reporter (***Figure 4C,D***). These results suggest that Klf2a and Notch signaling are activated specifically in the part of the valve corresponding to where the OFT has the smallest diameter and where shear stress is expected to be the highest, consistent with the hypothesis that Klf2a and Notch signaling are flow-responsive.

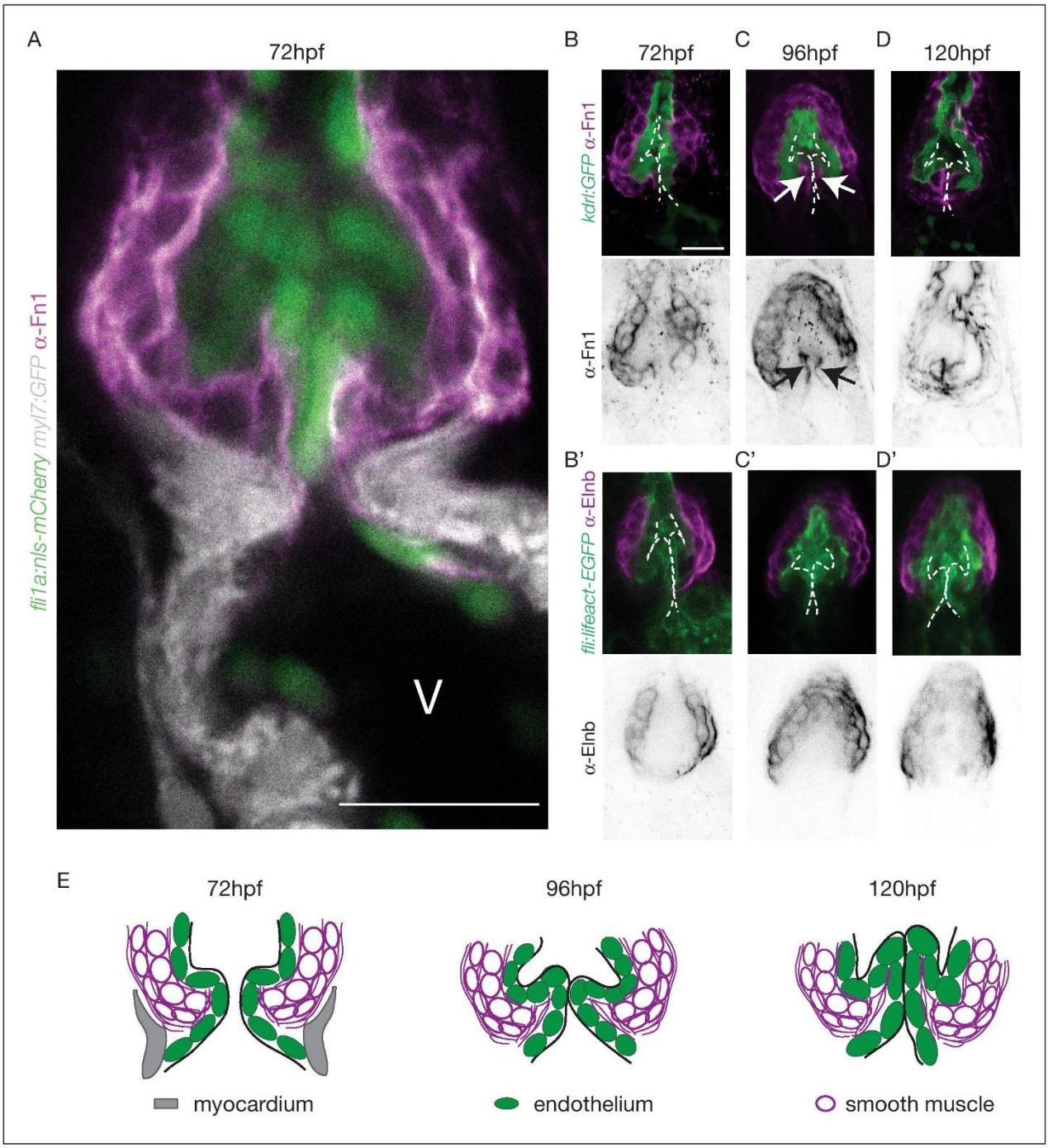

Figure 3. The OFT endothelium is surrounded by smooth muscle cell progenitors expressing fibronectin and elastin. (**A**) Staining of Fibronectin1 (magenta) on *Tg(myl7:GFP; fli1a:nls-mCherry)*, highlighting the myocardium (white) and the endothelium (green) at 72 hpf. Scale bar: 20 μm. V: ventricle. Fibronectin1 (anti-Fn1, magenta) counterstaining on *Tg(kdrl:GFP)* and Elastinb (anti-Elnb, magenta) counterstaining on *Tg(fli:lifeact-EGFP)* showing their expressions in the OFT at 72 hpf (**B**), (**B'**) respectively) at 96 hpf (**C**), (**C'**) respectively) and at 120 hpf (D, D' respectively). Scale bar: 20 μm. Arrows show

Figure 3 continued on next page

Figure 3 continued

the Fn1 localisation within the valve leaflets. Results obtained from three independent experiments. (**E**) Scheme of the three layers shown in **A'**, **B**, **C** and **D** (magenta, smooth muscles; green, endothelium; grey, myocardium; Fibronectin1, magenta lines) at 72hpf, 96hpf and 120hpf.

DOI: https://doi.org/10.7554/eLife.44706.005

The following figure supplement is available for figure 3:

Figure supplement 1. Smooth muscle identity is revealed by NO.

DOI: https://doi.org/10.7554/eLife.44706.006

We next investigated the expression of the Hippo effector Yap1 and a reporter of the Hippo pathway in vivo. We found that Yap1 is localized in the heart at 72 hpf, in particular in the OFT smooth muscle cells (***Figure 5—figure supplement 1A,B***). To better characterize its tissue-specific expression, we used the double transgenic line *Tg(fli:lifeact-EGFP; kdrl:nls-mCherry)* and could show that the smooth muscle cells surrounding the OFT, but also some OFT endothelial cells express Yap1 (asterisks in ***Figure 5—figure supplement 1B***). To assess the activity of the Hippo pathway in the heart at 72 hpf, we made use of the *Tg(4xGTIIC:d2GFP)* and could see that the Yap/Wwtr1-Tead reporter was activated in the OFT endothelial cells (labelled using the *kdrl:membrane-mCherry* line) as well as the smooth muscle cells surrounding the OFT (labelled by the Elnb staining) (***Figure 5A***). To assess the implication of Yap1 during OFT valve development, we followed the same embryos over time and looked at the valve phenotype in *yap1* mutant embryos, *yap* embryos and *yap1* control embryos (***Agarwala et al., 2015***) (***Figure 5B***). When analyzed from 72 hpf until 120 hpf, a significant fraction of *yap1-/-* embryos displayed abnormal valves (17% at 72 hpf, 8% at 96 hpf, 17% at 120 hpf, n = 12) and an increasing fraction of *yap1* embryos did not have recognizable OFT valves (58% at 120hpf, n = 12). Thus, these results suggest that *yap1* is involved during OFT valve morphogenesis (***Figure 5B***) and that smooth muscle cell progenitors are likely to play a role in the process.

Together, these results show that Klf2a, Notch signaling, and Hippo pathways are active in the OFT during valve morphogenesis.

Klf2a and notch reporter activity is flow-dependent in the OFT

As blood flow is an important regulator of *klf2a* expression and cardiac valve formation, we next wanted to assess whether changes in flow properties impact Klf2a and the Notch reporter activity in the OFT.

We analyzed the reporters activity following injection of a morpholino specific for *troponin T2a* (*tnnt2a*), which is necessary for heart contraction and reliably mimics the *sih* mutants (***Sehnert et al., 2002***), to determine whether these signaling pathways were impacted when heart contraction is abnormal and/or are activated upon shear stress forces. As the absence of heart contraction can impact heart morphogenesis, we injected highly diluted *tnnt2a* morpholino (hypomorphic condition) into these two reporter lines (***Figure 6A,B***). Such treatment allows us to decrease heart function and flow without dramatically altering heart shape (***Figure 6A,B***, ***Videos 1*** and ***2***). Depending on the knockdown efficiency in single embryos, this treatment leads to the generation of two groups of embryos: group1 where the heart beats 'normally' (normal heart rate at 2–3 Hz and function) and group2 where the heartbeat is slower. In the group of 'beating heart' embryos (group1, ***Video 1***), we still observe stronger GFP expression in the posterior part of the valve for both reporters at every stage analyzed (***Figure 6A***). In the group of embryos where the heart is still beating but at an abnormal slow rate (less than 2 Hz, group2, ***Video 2***), we observe no difference between the anterior and posterior part of the valve (p=0.99) for the Klf2a reporter at 72 hpf (***Figure 6B***). For the Notch reporter, we observed no difference in fluorescence intensity at 72 hpf (p=0.1) (***Figure 6B***). In addition, we analyzed the localization of Fn1, Elnb and Yap1 by immunostaining in both 'beating heart' (n = 4, n = 7 and n = 7, respectively) and 'slow beating heart' (n = 6, n = 7 and n = 7 respectively) groups and could observe that Fn1, Elnb, and Yap1 are down-regulated in the smooth muscle cells of the 'slow beating heart' embryos (***Figure 6D,F***). Moreover, we assessed the BA diameter and the activity of the smooth muscle using the DAF-FMDA assay (***Figure 6E***). The results suggest that the 'slow beating heart' group has a smaller BA (p<0,001) and the smooth muscle are much less active (p=0,05) (***Figure 6E,F***). We next assessed valve morphology in which blood flow is altered due to slow heart contraction and selected the fish with almost no contraction (group2). All the *tnnt2a*MO-

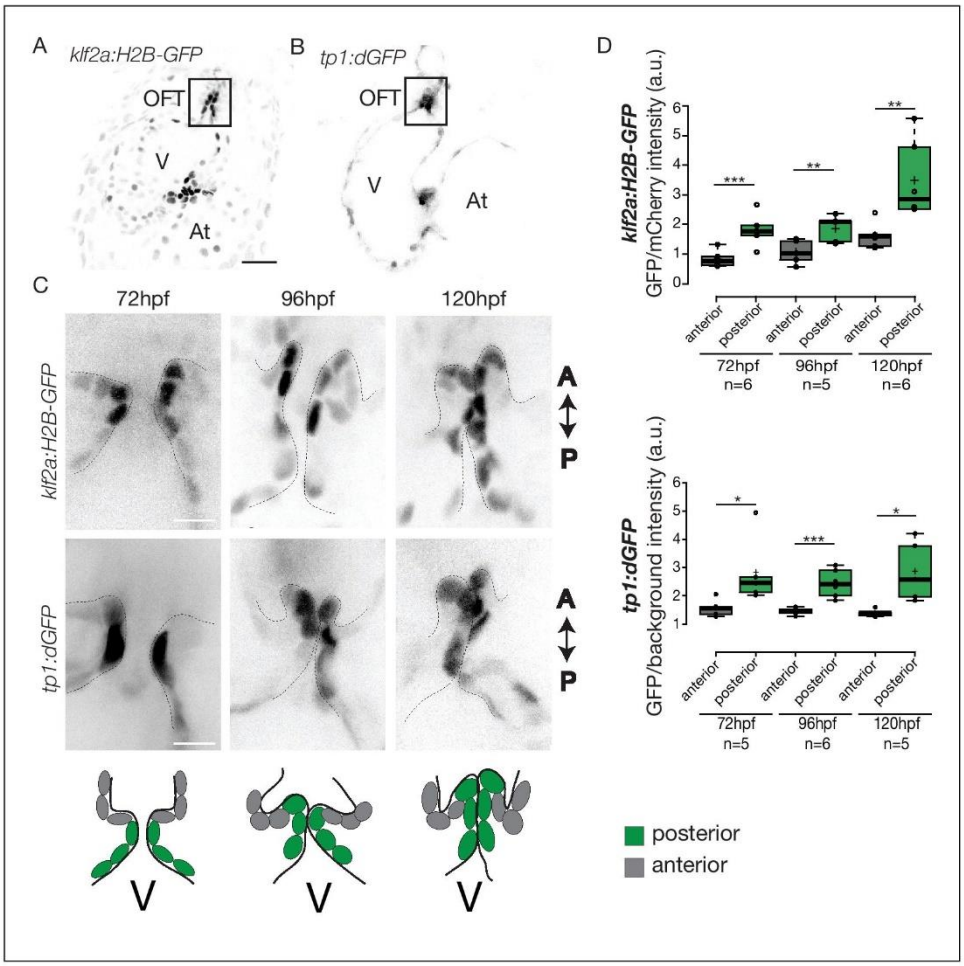

Figure 4. Klf2a and Notch reporters are activated in the OFT endothelium Confocal z-section of the *Tg(klf2a:H2B-GFP; fli:nls-mCherry).* (**A**) and *Tg(tp1:dGFP)* (**B**) at 72hpf. OFT: outflow tract, At: atrium, V: ventricle. Scale bar: 20 µm. (**C**) Confocal z-section of OFT valves expressing the Klf2a reporter and Notch reporter at 72 hpf, 96 hpf, and 120 hpf. Schemes explaining the considered anterior (grey) and posterior (green) parts of the valve at 72 hpf, 96 hpf, and 120 hpf. A: anterior, P: posterior. V: ventricle. Scale bar: 10 µm. (**D**) Quantification of the fluorescent intensity of the Klf2a (GFP over mCherry) and Notch (GFP over background) reporters in the anterior versus posterior part of the valves at 72 hpf (n = 6 embryos, p=0001 and n = 5 embryos, p=0,02 respectively), 96 hpf (n = 5 embryos, p=0005 and n = 6 embryos, p=0,0007 respectively) and 120 hpf (n = 6 embryos, p=0,01 and n = 5 embryos, p=0,01) in wild-type embryos using the student's t-test. Boxplots: Center lines show the medians; box limits indicate the 25th and 75th percentiles as determined by R software; whiskers extend 1.5 times the interquartile range from the 25th and 75th percentiles, outliers are represented by dots. Results obtained from three independent experiments.

DOI: https://doi.org/10.7554/eLife.44706.007

The following source data and figure supplement are available for figure 4:

Source data 1. Fluorescence intensity measurements.

DOI: https://doi.org/10.7554/eLife.44706.009

Figure supplement 1. Expression of the *klf2a* reporter Z-section of the *Tg(klf2a:H2B-EGFP; kdrl:nls-mCherry)* at 72 hpf, 96 hpf and 120 hpf used to quantify the reporter expression.

DOI: https://doi.org/10.7554/eLife.44706.008

injected embryos have no valve (n = 9/9, $p<10^{-6}$) (***Figure 6C***). To confirm the role of flow in the process, we analyzed the effect of altered blood viscosity and shear stress by lowering red blood cell content in the *gata1* mutants (*Vlad Tepes*) as previously described (***Steed et al., 2016b***;

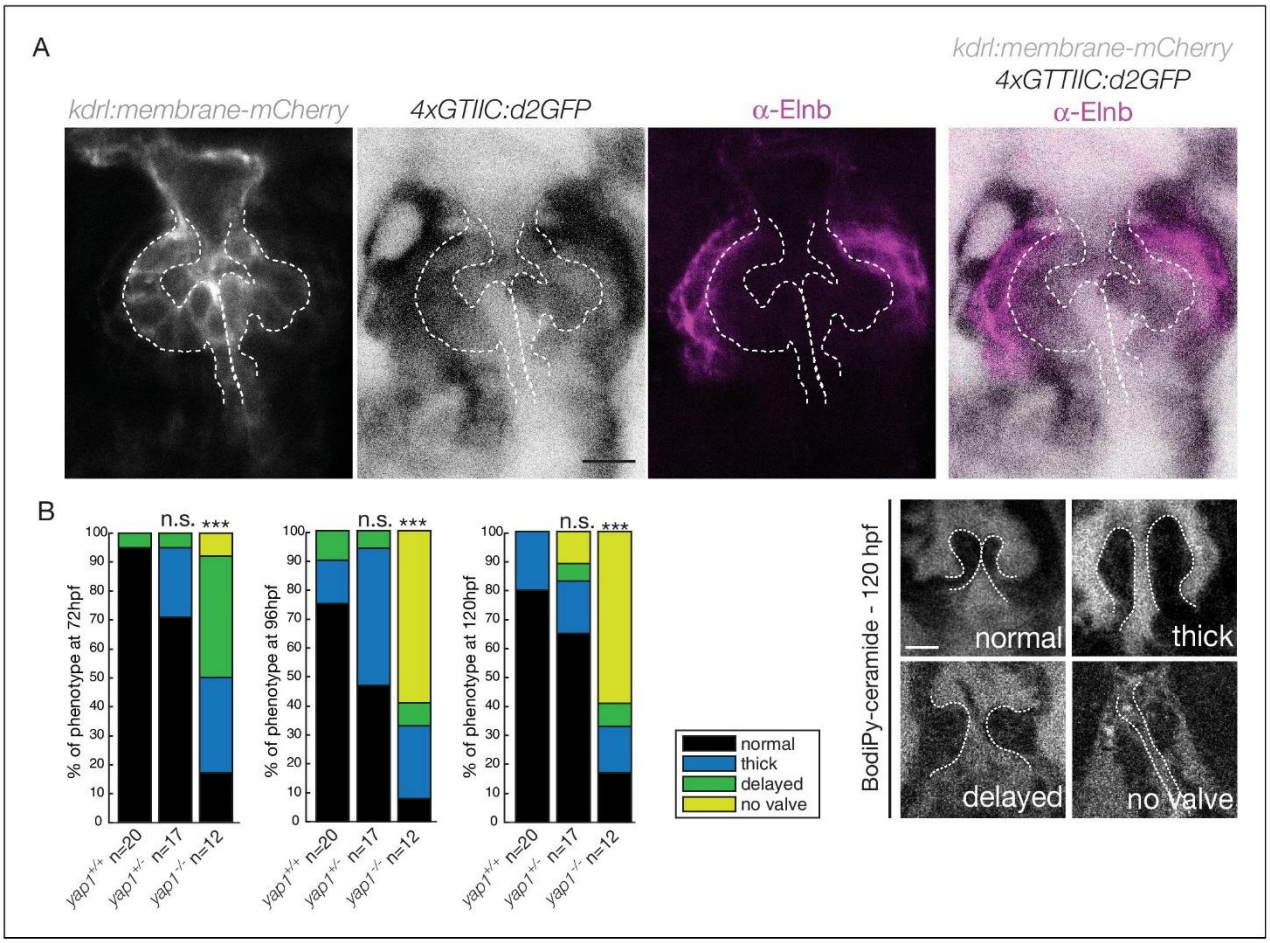

Figure 5. Hippo pathway effector Yap1 is active and Yap1 is essential for valve formation in the OFT. (**A**) Confocal z-sections of the double transgenic line *4xGTIIC:d2GFP; kdrl:membrane-mCherry* counterstained with the Elnb antibody and focused on the OFT. Scale bar: 20 µm. (**B**) Example of the valve phenotypes (normal, thick, delayed and no valve) and quantification of the phenotypes in the *yap1*$^{+/+}$ controls embryos, *yap1*$^{+/-}$ and in *yap1*$^{-/-}$ mutant embryos. Chi-square test. n.s.: non significant, ***: $p<10^{-3}$. Scale bar: 10 µm. Results obtained from two independent experiments.

DOI: https://doi.org/10.7554/eLife.44706.010

The following source data and figure supplement are available for figure 5:

Source data 1. Phenotypic quantifications.

DOI: https://doi.org/10.7554/eLife.44706.012

Figure supplement 1. Yap1 is expressed in the OFT Yap1 antibody staining on *Tg(fli:lifeact-EGFP; kdrl:nls-mCherry)* (**A**) and zoom on the OFT (**B**) at 72 hpf.

DOI: https://doi.org/10.7554/eLife.44706.011

Vermot et al., 2009). In *vlad tepes* mutant embryos (n = 21, $p<10^{-2}$), more than 80% of the mutants displayed abnormal OFT valves (***Figure 6C***).

Together, these results suggest that the expression of both Klf2a and Notch reporters is flow-dependent and that mechanical forces associated with heart activity are necessary for valve development and smooth muscle cell identity in the OFT.

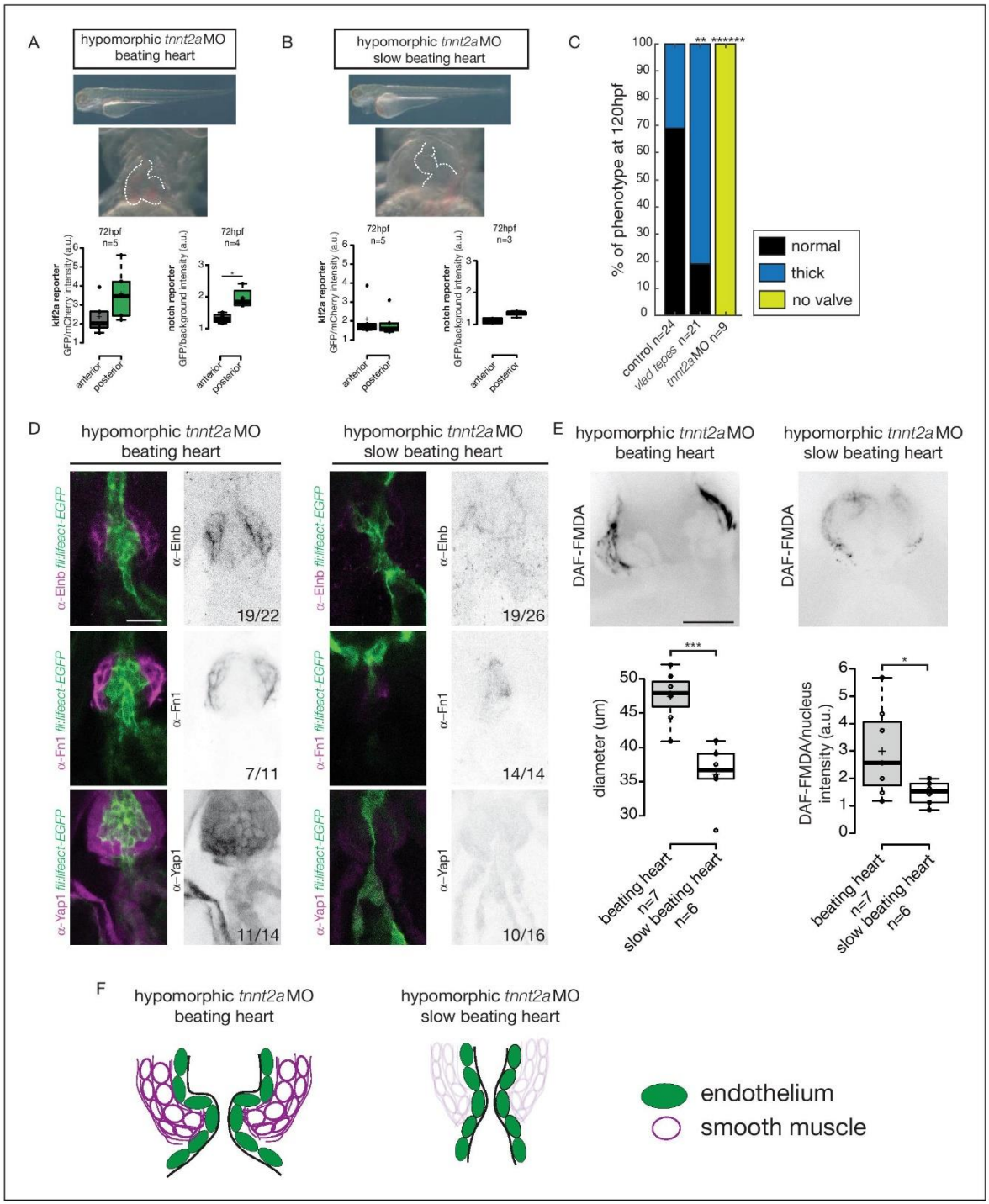

Figure 6. Klf2a and notch response, as well as the smooth muscle cell identity, are flow-dependent. Quantification of the Klf2a and Notch reporter expressions in *tnnt2a*-morpholino injected embryos showing a 'beating heart' (p=0,27 and p=0,01 respectively). (**A**) and a 'slow beating heart' (p=0,7 and p=0,1 respectively) (**B**) at 72 hpf. N = 2 independent experiments. (**C**) Quantification of the phenotypes in the control (n = 24), vlad tepes mutant (n = 21 embryos from two independent experiments), *tnnt2a*MO-injected embryos (n = 9 embryos from two independent experiments). Chi-square test.

Figure 6 continued on next page

Figure 6 continued

: $p<10^{-2}$, ******: $p<10^{-6}$. (D**) Z-sections of the *Tg(fli:lifeact-eGFP)* counterstained with either Fibronectin1 (Fn1), elastin (Elnb) or Yap1 in *tnnt2a*-morpholino injected embryos (slow beating and beating heart). Scale bar: 20 μm. N = 2 independent experiments. (**E**) Z-section and quantification of the BA diameter and DAF-FMDA intensity in tnnt2a-morpholino injected embryos (p=0,0005 and p=0,05 respectively). Student's t-test. Boxplots: Center lines show the medians; box limits indicate the 25th and 75th percentiles as determined by R software; whiskers extend 1.5 times the interquartile range from the 25th and 75th percentiles, outliers are represented by dots. (**F**) Scheme summarizing the down-regulation of the smooth muscle markers in 'slow beating heart' embryos compared to 'beating heart"embryos.

DOI: https://doi.org/10.7554/eLife.44706.013

The following source data is available for figure 6:

Source data 1. Phenotypic and fluorescence reporters quantifications.

DOI: https://doi.org/10.7554/eLife.44706.014

Klf2a regulates OFT valve morphogenesis via notch signaling activation and is necessary for the smooth muscle cells differentiation

As *notch1b* and *klf2a* are expressed in the OFT endothelium in response to flow forces, we hypothesized that they have a role during OFT valve morphogenesis. Therefore, we imaged the *Tg(fli:gal4/UAS:kaede)* and *Tg(flli:lifeact-EGFP; kdrl:nls-mCherry)* transgenic lines (***Figure 7A,B***). We looked at the phenotype of OFT valve endothelium in the *klf2a*$^{-/-}$ and *notch1b*$^{-/-}$ embryos at 72 hpf, 96 hpf and 120 hpf (***Figure 7A,B***). We found that most of the *klf2a*$^{-/-}$ embryos display proper valves at 72 hpf (n = 7/12), 96 hpf (n = 6/12) and 120 hpf (n = 6/12). However, 33% of the *klf2a*$^{-/-}$ embryos have abnormal 'delayed phenotype' at 72 hpf (n = 4/12), at 96 hpf (n = 4/12) and 120 hpf (n = 4/12) (***Figure 7A***). In this case, the OFT valves are larger, leading to big cushions instead of thin valve leaflets (***Figure 7A***). In addition, *notch1b* is also necessary for proper valve formation since 30% (n = 6/20) of the *notch1b*$^{-/-}$ embryos have a 'delayed phenotype' at 72 hpf, 35% (n = 7/20) at 96 hpf and 45% (n = 9/20) at 120 hpf (***Figure 7B***) while almost all control embryos have proper valves at 72 hpf (n = 6/7), 96 hpf (n = 7/7) and 120 hpf (n = 7/7) (***Figure 7B***). Next, we wondered whether a cross-regulation between *notch1b* and *klf2a* exists since they are both necessary for proper valve formation. First, we compared *notch1b* expression between *klf2a*$^{-/-}$ embryos and *klf2a*$^{+/+}$ control embryos (***Figure 7—figure supplement 1A***). In controls, 85% and 91% of the embryos have *notch1b* expression in the OFT at 48 hpf and 72 hpf, respectively (***Figure 7—figure supplement 1A–C***). However, in *klf2a*$^{-/-}$ embryos, *notch1b* expression is altered with no clear expression defining the OFT region at 48 hpf (64%) and at 72 hpf (78%) (***Figure 7—figure supplement 1A,B***). However, in the reverse experiment, most of the embryos show proper *klf2a* expression in *notch1b* -/- embryos (61% at 48 hpf and 51% at 72 hpf) (***Figure 7—figure supplement 1C***).

In order to assess the regulation of the Notch pathway activity by Klf2a in the endothelium, we analyzed the Notch reporter activity in the posterior and anterior parts of the valve in *klf2a*$^{+/+}$ (n = 5) versus *klf2a*$^{-/-}$ (n = 4) embryos. As for Notch reporter expression in wild-type (***Figure 4C,D***), the Notch reporter is significantly more expressed in the posterior part compared to the anterior part of the valves at 72 hpf ($p<10^{-2}$), 96 hpf ($p<10^{-2}$) and 120 hpf ($p<10^{-1}$) (***Figure 7C,C'***) in the *klf2a*$^{+/+}$ embryos. Interestingly, the stronger posterior expression is lost in the *klf2a*$^{-/-}$ embryos and the fluorescent intensity in the posterior part of the valve is significantly reduced in the *klf2a*$^{-/-}$ compared to *klf2a*$^{+/+}$ at 72 hpf (p<10–1), 96 hpf ($p<10^{-1}$) and 120 hpf ($p<10^{-1}$) (***Figure 7C,C'***). In comparison, the expression in the posterior part of the valve in the *notch1b*$^{-/-}$ embryos compared to the *notch1b*$^{+/+}$ control embryos is not significantly different at any time point analyzed (***Figure 7—figure supplement 1D***). To further assess whether Klf2 has an effect on the OFT formation, we performed Fn1, Elnb and Yap1 stainings on *klf2a*$^{-/-}$ and controls at 72

Video 1. Bright field videomicroscopy of the typical heart function of a *tnnt2a* MO group1 embryo where the heart is still beating normally.

DOI: https://doi.org/10.7554/eLife.44706.015

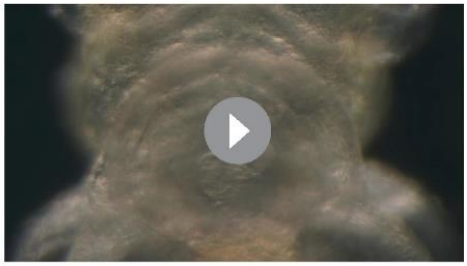

Video 2. Bright field videomicroscopy of the typical heart function of a *tnnt2a* MO group2 embryo where the heart is still beating but at an abnormal slow rate (less than 2 Hz).
DOI: https://doi.org/10.7554/eLife.44706.016

hpf. We could observe that Fn1, Elnb, and Yap1 are properly localized in controls (n = 13/13, n = 7/7 and n = 4/4, respectively), *klf2a*$^{-/-}$ (n = 5/6, n = 3/4, and n = 3/3) (***Figure 7—figure supplement 1E***).

These results suggest that *klf2a* and *notch1b* are involved for proper valve morphogenesis and that Klf2a modulates *notch* expression in the process. Moreover, *klf2a* does not seem necessary for the smooth muscle cell differentiation surrounding the endothelium.

Piezo channels regulate both the endothelial and smooth muscle cell markers expression

In order to decipher whether flow and mechanosensitive channels could be involved in the regulation the OFT valve formation, we proceeded to analyze the phenotype of different potent mechanosensitive channel mutants. We focused on the non-selective ion channels Trpp2, Trpv4, Piezo1 and Piezo2a (***Figure 8—figure supplement 1A,B,C***) that are known for their mechanosensitive properties (***Coste et al., 2010***; ***Köttgen et al., 2008***; ***Li et al., 2014***; ***Sharif-Naeini et al., 2009***; ***Thodeti et al., 2009***). First, we evaluated the relative fractional shortening (RFS) at 72hpf in the atrium and in the ventricle of each mutant and their corresponding controls (***Figure 8—figure supplement 1A***). We did not observe any significant difference in the RFS between mutants and their respective controls neither in the atrium nor in the ventricle, suggesting that heart function in these mutants is normal. As another readout of flow forces and heart function, we quantified the retrograde flow fraction (RFF) at 72hpf and 120hpf in these mutants and the time windows for forward, reverse or no flow. We found that they are equivalent in all mutants when compared to their respective controls (***Figure 8—figure supplement 1B***), confirming that heart function is not different in these mutants. We looked at valve morphology at 120 hpf when leaflets are normally fully formed. In control embryos, the valves are extending into the lumen (***Figure 8—figure supplement 1C***). We found that 33% of the *trpv4* mutant embryos (n = 7) have normal valves and mainly display thick valves (67%). In the *trpp2* mutant embryos (n = 20), a stronger phenotype is observed with only 10% of normal valves. We observed that some embryos are delayed with respect to valve phenotype, meaning that the valve forming area still displays cushions at 120 hpf instead of having leaflets (35%). The *trpv4*$^{-/-}$*; trpp2*$^{+/-}$ (n = 8) has an intermediate phenotype with 25% of the embryos having normal valves. Finally, the *trpp2*$^{-/-}$*; trpv4*$^{-/-}$ embryos (n = 11) have a stronger phenotype, with none of the embryos showing proper OFT valve development and displaying mainly a delayed valve phenotype (45%). Interestingly, the *piezo1* mutant embryos (n = 14) show mainly a delayed valve formation (50%), similarly to the *trpv4*$^{-/-}$*; trpp2*$^{-/-}$ embryos. The *piezo2a*$^{-/-}$ (n = 9) has a less stringent phenotype with mainly normal valves (44%) but nevertheless 11% of *piezo2a*$^{-/-}$ fish do not have valves at all. This phenotype is even more prevalent in *piezo1*$^{-/-}$*; piezo2a*$^{-/-}$ embryos (n = 11), where none of the fish display proper valve development and most of them do not form any valves (36%).

To better characterize the valve phenotype in *trpp2*$^{-/-}$ and *piezo1*$^{-/-}$ embryos, we made use of the *Tg(fli:lifeact-EGFP; kdrl:nls-mCherry)* transgenic line and assessed the shape of the endothelium at 72 hpf (***Figure 8A*** and ***Figure 8—figure supplement 2A***), 96 hpf (***Figure 8B*** and ***Figure 8—figure supplement 2A***) and 120 hpf (***Figure 8C*** and ***Figure 8—figure supplement 2A***). *trpp2*$^{-/-}$ embryos display mainly thick valves at all time points (n = 4/8 at 72 hpf, n = 8/13 at 96 hpf and n = 5/11 at 120 hpf) (***Figure 8A–C*** and ***Figure 8—figure supplement 2A***). Indeed, the endothelial layer is not a single cell layer anymore (***Figure 8B***) which leads to a thicker leaflet at 120 hpf (***Figure 8C***). Although *piezo1*$^{-/-}$ embryos have mainly normal valves at 72 hpf (***Figure 8A*** and ***Figure 8—figure supplement 2A***) (n = 6/10), they display a delayed phenotype (still cushions) at 96 hpf (***Figure 8B*** and ***Figure 8—figure supplement 2***) (n = 4/10) and thick or delayed phenotype at 120 hpf (***Figure 8C*** and ***Figure 8—figure supplement 2A***) (n = 3/10 and n = 3/10 respectively). To assess the redundancy between *trpp2* and *piezo1*, we performed the same experiment in *piezo1*$^{-/-}$*; trpp2*-morpholino injected embryos at 72 hpf (***Figure 8A***), 96hpf (***Figure 8B***) and 120 hpf (***Figure 8C***). Although the

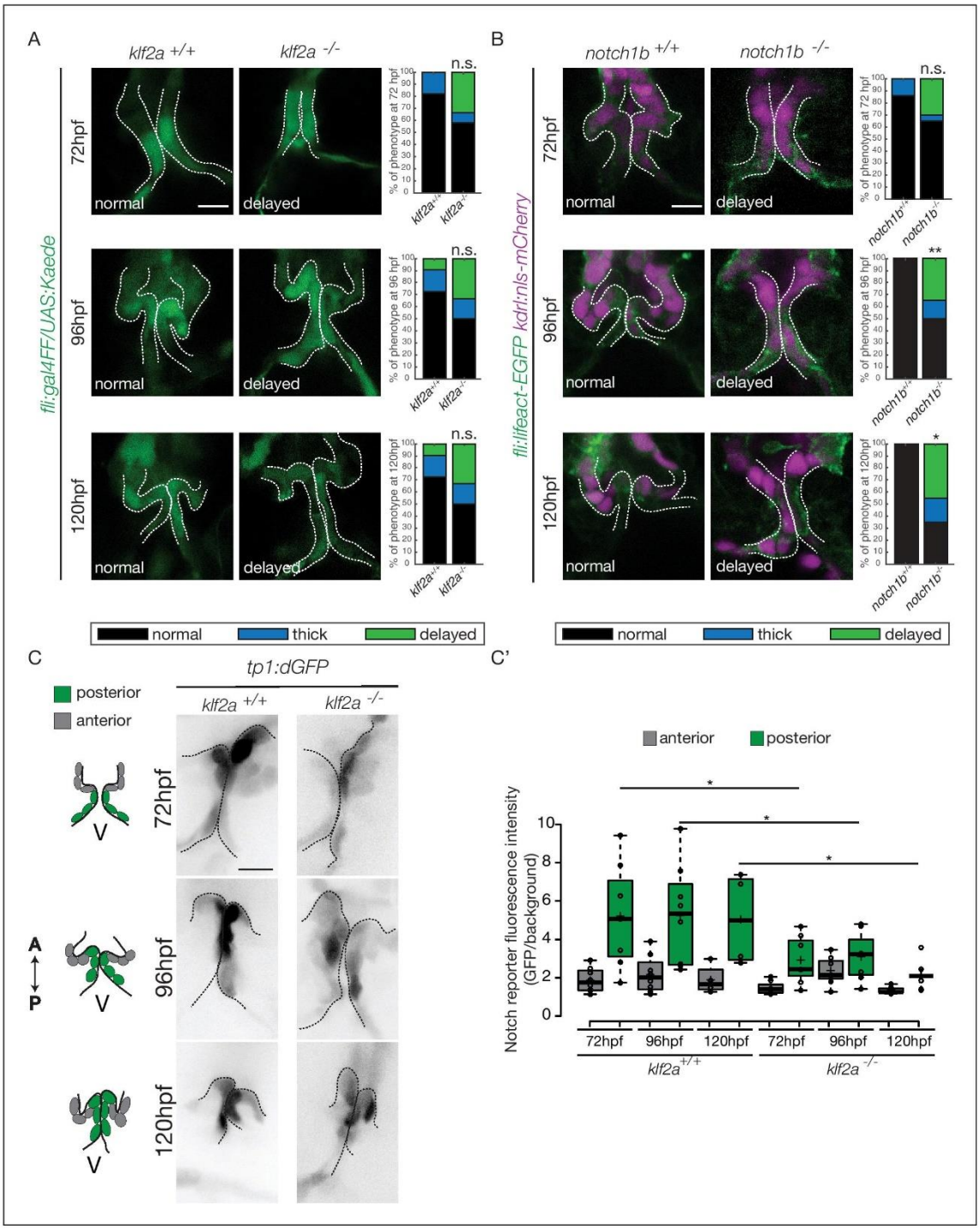

Figure 7. Klf2a and notch are necessary for valve formation. Quantification of the valve phenotypes at 72 hpf, 96 hpf and 120 hpf (normal, thick, delayed) in *klf2a*$^{+/+}$(n = 11), and *klf2a*$^{-/-}$ (n = 12) using the *Tg(fli:gal4FF/UAS:Kaede)*. (**A**) and *notch1b*$^{+/+}$ (n = 7) and *notch1b*$^{-/-}$ (n = 20) using *Tg(fli:lifeact-EGFP; kdrl:nls-mCherry)* embryos. (**B**) Scale bar: 10 μm. N = 3 independent experiments. (**C**) Confocal z-sections of the *Tg(tp1:dGFP)* in *klf2a*$^{+/+}$ and *klf2a*$^{-/-}$ embryos at 72 hpf, 96 hpf and 120 hpf. V: ventricle. Scale bar: 10 μm. (**C'**) Quantification of the fluorescent intensity of the Notch reporter

Figure 7 continued on next page

Figure 7 continued

(GFP over background) in the anterior versus posterior parts of the valves in in *klf2a*$^{+/+}$ (n = 5) and *klf2a*$^{-/-}$ (n = 4) embryos. Statistical test were performed to compare the posterior intensities in *klf2a*$^{+/+}$versus *klf2a*$^{-/-}$ at 72 hpf (p=0,05), 96 hpf (p=0,03) and 120 hpf (p=0,04). Student's t-test. Boxplot: Center lines show the medians; box limits indicate the 25th and 75th percentiles as determined by R software; whiskers extend 1.5 times the interquartile range from the 25th and 75th percentiles, outliers are represented by dots. Results obtained from three independent experiments.

DOI: https://doi.org/10.7554/eLife.44706.017

The following source data and figure supplement are available for figure 7:

Source data 1. Fluorescent intensity quantifications.

DOI: https://doi.org/10.7554/eLife.44706.019

Figure supplement 1. Klf2a regulates *notch1b* expression but Notch1b does not regulate *klf2a* expression.

DOI: https://doi.org/10.7554/eLife.44706.018

trpp2-MOrpholino injected embryos do not show a phenotype as strong as the *trpp2*$^{-/-}$ mutant embryos at 96 hpf and 120 hpf (possibly due to less effective morpholinos at these stages), the double *piezo1*$^{-/-}$*; trpp2*-MO do not clearly show a stronger phenotype than the single *trpp2*$^{-/-}$ or *piezo1*$^{-/-}$ embryos (normal valves in n = 6/7, n = 2/7 n = 4/7 and at 72 hpf, 96 hpf and 120 hpf respectively). These results suggest that Trp and Piezo channels are necessary for the proper folding of the endothelium from 72 hpf to 120 hpf.

To better characterize the cell layer affected by *piezo1* loss of function, we performed immunohistochemistry against Yap1 and two smooth muscle identity markers (Fn1 and Elnb) as well as their active functionality in *piezo1*$^{+/+}$ controls and *piezo1*$^{-/-}$ mutants at 72 hpf (***Figure 8D*** and ***Figure 8—figure supplement 2B***). A bit more than two thirds of *piezo1*$^{-/-}$ embryos (n = 7/10) display reduced Yap1 expression as well as a down-regulation of Elnb (n = 9/12) and Fn1 (n = 3/4) (***Figure 8E***). However, the BA diameter as well as the DAF-FMDA fluorescence intensity are not affected in the *piezo1*$^{-/-}$ compared to *piezo1*$^{+/+}$ (***Figure 8D*** and ***Figure 8—figure supplement 2B***) demonstrating that smooth muscle cells are still present in the piezo mutants. These results suggest a selective role of *piezo1* in the regulation of the smooth muscle cell maturation and proper Yap1 localization in the OFT. We next assessed Klf2a reporter expression in *piezo1*$^{-/-}$ and *trpp2*$^{-/-}$. We found that Klf2a expression was misregulated in *piezo1*$^{-/-}$ mutant embryos with stronger Klf2a reporter activation in the anterior and posterior part of the valve endothelium when compared to controls ($p<10^{-3}$ for the anterior part and $p<10^{-2}$ for the posterior part of the valves) (***Figure 8F,F'***). By contrast, we found that the posterior part of the valve has a decreased expression of GFP ($p<10^{-2}$), highlighting a down-regulation of *klf2a* in the *trpp2*$^{-/-}$ embryos (***Figure 8G,G'***). These results suggest that Piezo1 inhibits *klf2a* overall the valve endothelium (***Figure 8F,F'***) while Trpp2 is required for *klf2a* activation in the posterior part of the OFT valve endothelium (***Figure 8G,G'***). To assess if the localization of *piezo1* and *trpp2* mRNA could explain the differential function of these channels, we performed RNAscope assay at 72hpf (***Figure 8—figure supplement 3A***). We found that *trpp2* is ubiquitously expressed in the embryo, including in the different layers composing the OFT. Similarly, we found that *piezo1* is expressed in both endothelium and smooth muscles, albeit at a lower level than *trpp2* (***Figure 8—figure supplement 3A***). To confirm these results, we generated a transgenic reporter line with 3 kb of the *piezo1* promoter upstream of the start codon (*piezo1:nls-Venus*). We observed the expression of the reporter line mostly in smooth muscles at 72hpf (***Figure 8—figure supplement 3B***) and cells of the endothelium of the OFT valve. Trpp2 immunohistochemistry showed that Trpp2 is expressed in the endothelium and the smooth muscles confirming that *trpp2* is ubiquitously expressed in the OFT (arrow in ***Figure 8—figure supplement 3B***). We conclude that Piezo1 plays a dual role in the OFT: it modulates *klf2a* expression in the endothelium and it is necessary for proper smooth muscle cell maturation around the OFT endothelium.

Discussion

Using cardiac live imaging and functional studies combined with in vivo reporter analysis, we uncover key mechanosensitive signaling pathways involved in OFT valve morphogenesis (***Figure 9***). We identify two tissue layers sensitive to mechanical forces in the OFT: (1) The endothelial cells where *klf2a* expression is modulated both by Piezo and Trp channels (2) The smooth muscles surrounding the endothelium, where Piezo channels regulate Yap1 localization and smooth muscle cell specific

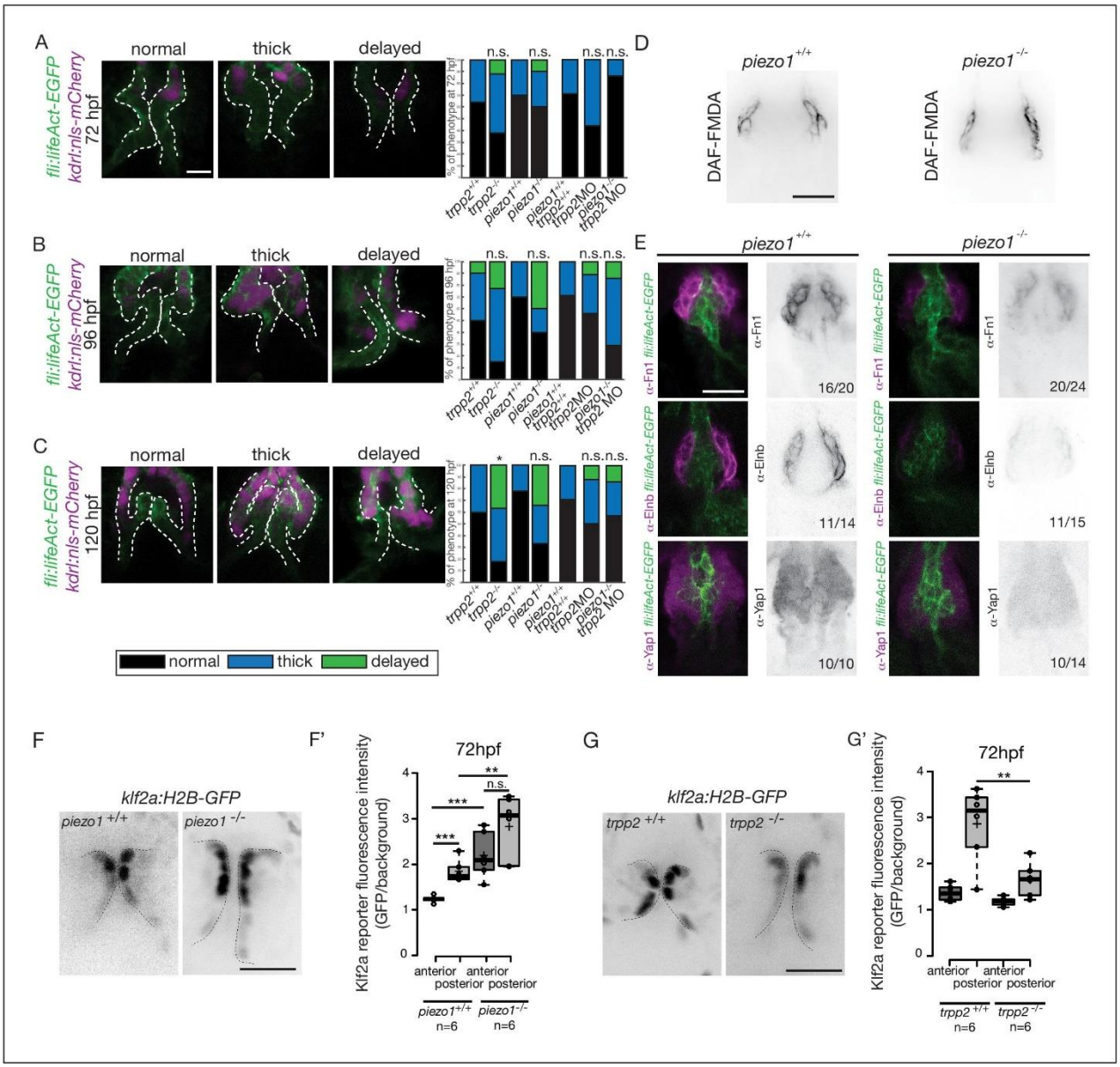

Figure 8. Flow and mechanosensitive channels are necessary for proper OFT valve formation. (**A**) Z-sections and quantifications of the valves phenotypes (normal, thick, delayed) of the *Tg(fli:lifeaAct-EGFP; kdrl:nls-mCherry)* at 72 hpf (**B**), 96 hpf (**C**) and 120 hpf (**D**) in *trpp2*$^{+/+}$(n = 11, n = 10, n = 10), *trpp2*$^{-/-}$ (n = 8, n = 13, n = 13 from three independent experiments), *piezo1*$^{+/+}$ (n = 10, n = 10, n = 9), *piezo1*$^{-/-}$(n = 10, n = 10, n = 9 from two independent experiments), *piezo1*$^{+/+}$; *trpp2*$^{+/+}$ (n = 7), trpp2-morpholino injected embryos (n = 9) and *piezo1*$^{-/-}$; *trpp2*-morpholino injected embryos (n = 7). Scale bar: 10 µm. (**D**) Z-section of the OFT stained with DAF-FMDA in *piezo1*$^{+/+}$ and *piezo1*$^{-/-}$. Scale bar: 20 µm. (**E**) Fibronectin1 (Fn1), elastin (Elnb) and Yap1 staining on *Tg(fli:lifeact-eGFP)* in *piezo1*$^{+/+}$ (n = 12, n = 4 and n = 10 respectively) and *piezo1*$^{-/-}$ (n = 12, n = 4 and n = 10 respectively from three independent experiments). Scale bar: 20 µm. Z-sections (**F**) and quantification (**F'**) of the klf2a reporter (GFP over background) in the anterior and posterior parts of the valves in *piezo1*$^{+/+}$ (n = 6) and *piezo1*$^{-/-}$ (n = 6) obtained from two independent experiments). Scale bar: 20 µm. Z-sections (**G**) and quantification (**G'**) of the *klf2a* reporter (GFP over background) in the anterior and posterior parts of the valves in *trpp2*$^{+/+}$ (n = 6) and *trpp2*$^{-/-}$ (n = 6) (obtained from two independent experiments). Scale bar: 20 µm. Student's t-test. Boxplot: Center lines show the medians; box limits indicate the 25th and 75th percentiles as determined by R software; whiskers extend 1.5 times the interquartile range from the 25th and 75th percentiles, outliers are represented by dots.

Figure 8 continued on next page

Figure 8 continued

DOI: https://doi.org/10.7554/eLife.44706.020

The following source data and figure supplements are available for figure 8:

Source data 1. Phenotypic and fluorescence reporters quantifications.

DOI: https://doi.org/10.7554/eLife.44706.024

Figure supplement 1. Embryo phenotypes in controls and mutants.

DOI: https://doi.org/10.7554/eLife.44706.021

Figure supplement 2. Valve phenotypes in trpp2$^{-/-}$ and in piezo1$^{-/-}$.

DOI: https://doi.org/10.7554/eLife.44706.022

Figure supplement 3. Trpp2 and Piezo1 expression in the OFT.

DOI: https://doi.org/10.7554/eLife.44706.023

marker expression (***Figure 9***). These observations enable us to confirm the universal role of mechanical forces in cardiac valve morphogenesis and suggest a specific mechanism for OFT valve morphogenesis in which the origins of the valve progenitors, the implication of particular groups of cells, the mechanosensors involved and the impact of the mechanotransduction cascade are identified.

Klf2a modulates notch signaling specifically in the OFT endothelium

Valve morphogenesis occurs in complex mechanical environments. In the AVC, endocardial cells experience both shearing forces and mechanical deformation due to the contraction of the heart and its associated blood flow. The situation is slightly different in the OFT because endothelial valvular progenitors are not surrounded by contractile cardiomyocytes but passive smooth muscle cells

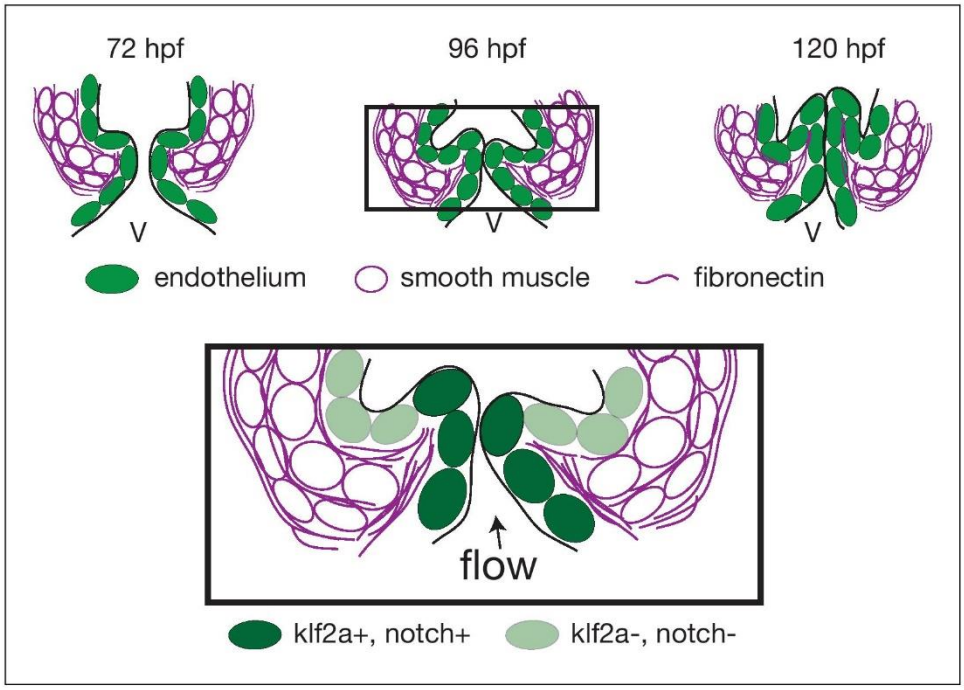

Figure 9. Working model summarizing OFT valve morphogenesis in response to mechanical forces. Two cell layers forming the OFT respond to piezo1 activity: the endothelium (green) and smooth muscle cells (magenta). Endothelial *klf2a* expression is repressed by Piezo1. In the smooth muscle cells, the expression of elastin (Elnb), fibronectin (Fn1) and Yap1 is modulated by Piezo1. Fibronectin is localized in the smooth muscle cell layer and within the forming valve (magenta lines). Future work will help to decipher how the two cell layers interact with each other to modulate OFT valve formation. V, ventricle.

DOI: https://doi.org/10.7554/eLife.44706.025

that can provide a counter force to flow and pressure. Here, we show that the main mechanosensitive pathways involved in AVC valve development are required for OFT valve development, even though the mechanical stimuli vary greatly between these two sets of valves. Previous studies have proposed that *klf2a* and *notch1b* are important during the formation of functional cardiac valve leaflets in zebrafish. Both are specifically expressed in the AVC (**Beis et al., 2005**; **Pestel et al., 2016**; **Steed et al., 2016b**; **Vermot et al., 2009**) and are transcriptionally misregulated in models of Cerebral cavernous malformation (CCM) where cardiac valve development is altered (**Donat et al., 2018**). Here, we show that both Notch signaling and *klf2a* are active in the endothelial cells of the OFT between 48 hpf and 120 hpf. During the process in which zebrafish cardiac AVC cushion remodel into valve leaflets, endocardial Klf2a expression and Notch activity are high on the luminal side of the developing valve leaflet, which is exposed to blood-flow, whereas their expression is lower on the abluminal side of the leaflet (**Pestel et al., 2016**; **Steed et al., 2016b**). In the OFT, Klf2a expression and Notch activation follow a different pattern because we could not clearly identify abluminal cells in the OFT. This might reflect a complete lack of endothelial to mesenchymal transition in the OFT by comparison to the AVC. Nevertheless, the impact of both pathways on valve morphogenesis remains the same as we found that *klf2a*$^{-/-}$ and *notch1b*$^{-/-}$ embryos show similar valve phenotypes and Notch signaling pathway is significantly decreased in *klf2a*$^{-/-}$ mutants. Even though the downstream players of the notch pathway remain to be established in the OFT, these results validate previous observations, suggesting that *klf2a* acts upstream of *Notch* signaling in the endocardium (**Donat et al., 2018**; **Samsa et al., 2015**; **Vermot et al., 2009**). Considering that Notch has been proposed to be mechanosensitive in blood vessels (**Mack et al., 2017**), an attractive hypothesis is that the Klf2-Notch axis could be a general mechanosensitive cascade in endothelial cells. In that case, it would be interesting to address *notch* activity in a flow related context, similarly to what is currently being done with Nf-kb, Klf2a, and other flow responsive pathways (**Feaver et al., 2013**). This assumption is particularly interesting in the context of sprouting angiogenesis and other aspects of angiogenesis where Notch is broadly required (**Choi et al., 2017**; **Hasan et al., 2017**; **Pitulescu et al., 2017**; **Tammela et al., 2011**). We further show that the expression of Fibronectin1 and Elastinb in the smooth muscle cells surrounding the OFT is not altered in the *klf2a*$^{-/-}$embryos. Considering that Piezo is emerging as an important contributor to human diseases related to blood cells (**Ma et al., 2018**; **Zarychanski et al., 2012**) and lymphatic diseases in humans (**Lukacs et al., 2015**), our work should motivate the search of potential involvement of Piezo in cardiac pathologies such as valvulopathies.

Piezo is necessary for proper OFT smooth muscle cell identity and endothelial *klf2a* expression in the OFT

Cardiac valve development is highly dependent on endothelial/endocardial cell mechanosentivity. Previous work identified the membrane-bound mechanosensitive channels (Trpp2 and Trpv4) and a calcium-activated intracellular signaling cascade leading to Klf2a expression and valve morphogenesis as key elements of the endocardial mechanodetection-signaling pathway (**Heckel et al., 2015**) Consistently, we found that these Trp channels are also required for endothelial Klf2a expression and OFT valve formation. In addition, we identify another type of mechanosensitive channel belonging to the Piezo family. Piezo channel mutants show valve dysgenesis phenotype, suggesting their requirement during OFT valve morphogenesis. Interestingly, Piezo channels are important both for modulating Klf2a expression in the endothelium and for smooth muscle cell-specific expression of Elnb and Fn1. Piezo function in these two cell layers is consistent with the fact that Piezo1 is expressed in smooth muscle cells and is important for tissue remodeling in mouse arteries (**Retailleau et al., 2015**) as well as in endothelial cells in mouse vasculature (**Li et al., 2014**; **Ranade et al., 2014**) and lymphatic valves (**Nonomura et al., 2018**). These studies along with our results suggest that Piezo1 might be necessary for both layers to regulate distinguishable functions: activation of signaling cascade upon shear stress in the OFT endothelium and proper cell identity acquisition in smooth muscles. Both tissue layers might be sensing different stimuli: shear plus strain for the endothelial cells and strain for the smooth muscle cells. This hypothesis is consistent with the fact that Piezo is sensitive to stretch (**Ranade et al., 2015**), compression (**Lee et al., 2014**; **Qi et al., 2015**), and rhythmic mechanical stimuli (**Lewis et al., 2017**). Importantly, Piezo-dependent mechanisms can transduce forces at the cell-cell or cell-matrix interface (**Eisenhoffer et al., 2012**; **Poole et al., 2014**). Thus, Piezo can have different mechanosensitive roles both in smooth muscle

cells and endothelium to coordinate the expression of Klf2 and ECM proteins. An interesting hypothesis is that the smooth muscle cell layer participates in the shaping up of the OFT valve and that both tissue layers establish paracrine interactions to fine tune the morphogenetic process. Further work will be needed to identify if this is the case and how it affects OFT valve morphogenesis at the cellular scale.

Yap1 and hippo pathways are regulators of the OFT valve formation in the endothelium and smooth muscles

Our work shows that Yap1 is specifically localized in the OFT in both endothelial cells and smooth muscle cells and is required for valvulogenesis. Accordingly, the Hippo pathway is active in smooth muscles and in the endothelium. Our work suggests that Piezo constitutes a plausible regulator of Yap1 localization as Piezo1 seems important for its localization in smooth muscle cells. Interestingly, Yap1 has been shown to translocate less in the nucleus in Piezo1 mutant mice neural stem cells (**Pathak et al., 2014**) and to induce proliferation in smooth muscles during cardiovascular development in mouse (Wang et al., 2014). Even though we were not able to assess Yap1 subcellular localization in vivo, the regulation of Yap1 activity and ECM assembly might be a general feature of Piezo function. The connection between Piezo and Yap1 is particularly interesting in the context of OFT development and function. In teleost, the OFT has an important biomechanical role for the control of flow propagation within the vascular networks by contributing to the dampening of the pressure wave down the arterial tree (**Braun et al., 2003b**). In zebrafish, Yap1 is involved in the determination of cardiac precursor cells into smooth muscle cell fate via a process that involves the regulation of Elastinb expression (**Moriyama et al., 2016**). Besides the control of cell identity, ECM contributes to biomechanical properties of tissues (**Dzamba and DeSimone, 2018**). It is thus possible that Piezo acts as a regulator of tissue mechanical properties by regulating Yap1 expression both in the OFT and in the vascular system where Yap1 expression is flow inducible (**Nakajima et al., 2017**).

In summary, this study reveals a novel function for mechanosensitive Piezo and Trp channels in modulating OFT valve development as well OFT smooth muscle cell maturation. It will be important to further investigate endothelial-smooth muscle cells interactions during OFT cardiac wall maturation.

Materials and methods

Zebrafish strains, husbandry, embryo treatments, and morpholinos

Animal experiments were approved by the Animal Experimentation Committee of the Institutional Review Board of the IGBMC (reference numbers MIN APAFIS#4669–2016032411093030 v4 and MIN 4669–2016032411093030 v4-detail of entry 1). Zebrafish lines used in this study were *Tg(fli1a:lifeact-EGFP)* (**Phng et al., 2013**), *Tg(kdrl:nls-mCherry)* (**Nicenboim et al., 2015**), *Tg(kdrl:EGFP)* (**Jin et al., 2005**), *Tg(fli1a:nls-mCherry)* (**Heckel et al., 2015**), *Tg(myl7:egfp)* (**Huang et al., 2003**), Tg(−*26.5Hsa.WT1-gata2:eGFP)*^{cn12} (**Sánchez-Iranzo et al., 2018**), *Tg(klf2a(6 kb):H2B-eGFP)* (**Heckel et al., 2015**), *Tg(tp1:dGFP)* (**Ninov et al., 2012**), *Tg(4xGTIIC:d2GFP)* (**Miesfeld and Link, 2014**), *vlad tepes*^{m651} (**Lyons et al., 2002**), *cup*^{tc321} (**Schottenfeld et al., 2007**), *piezo1*^{sa12608} (EZRC), *piezo2a*^{sa12414} (ZIRC), *trpv4*^{sa1671} (ZIRC), *notch1b*^{sa11236} (ZIRC), *klf2a*^{ig4} (**Steed et al., 2016b**), *yap1*^{fu48} (**Agarwala et al., 2015**) and wild-type AB. Cup mutant embryos were phenotyped based on the curled tail phenotype. The *Tg(piezo1:nls-Venus)* was generated by injection of the *piezo1:nls-Venus* plasmid and the mRNA of the Tol2 transposase. The plasmid was generated by cloning of 3 kb of the zebrafish *piezo1* promoter upstream of the ATG start site and 3xnls-Venus into a pTol2-GAGGS vector. All animals were incubated at 28.5˚C for 5 hr before treatment with 1-phenyl- 2-thiourea (PTU) (Sigma Aldrich) to prevent pigment formation. Morpholino specific for *tnnt2a* (**Sehnert et al., 2002**) (5'-CATGTTTGCTCTGATCTGACACGCA-3') were obtained from GeneTools. It was injected into the yolk at the one-cell stage at a concentration of 5,8 ng to stop the heart. It was diluted 40 times in order to get fish with either a decreased heartbeat ('slow beating heart' group in this study) or close to the non-injected fish heartbeat ('beating heart' group in this study).

Immunofluorescence

Embryos were fixed at the desired stage in 4% paraformaldehyde overnight at 4˚C. After washing in 1X PBST (PBS-0.1% Tween-20), embryos were permeabilized in 1X PBST containing 1% Triton-X 100 for 30 min at room temperature or overnight at 4˚C. For Fibronectin1 staining, the pericardial cavity was then carefully pierced with the tip of a needle to facilitate antibody penetration before blocking in permeabilization buffer supplemented with 5% BSA. Embryos were incubated in blocking solution containing 5% BSA and 15% NGS (α-Fn1), 1% BSA, 2% NGS (anti-Elnb) and 2% BSA, 2% MgCl2 (1M), 5% NGS supplemented by 1,5% Tween-20 (anti-Yap1) for 2 hr at room temperature or overnight at 4˚C. Primary antibodies were added to the relevant blocking solution and incubated 2 overnights at 4˚C. Secondary antibodies were added in blocking solution after thorough washing in PBST and incubated for 2 days at 4˚C. Embryos were thoroughly washed in PBST and mounted for imaging on a Leica SP8 confocal. Antibodies were used as follows: rabbit α-Fn1 (F3648, Sigma) 1:100, rabbit anti-Elnb (**Miao et al., 2007**; kind gift from Burns lab; **Paffett-Lugassy et al., 2017**) 1:1000, rabbit anti-Yap1 (generated by the Lecaudey lab; **Agarwala et al., 2015**) 1:300, rabbit anti-Trpp2 (kind gift from Drummond lab) 1:100 and Alexa Fluor 647 goat anti-rabbit IgG secondary antibody (A21245, Life Technologies) were used at 1:500.

In situ hybridization

In situ hybridization was performed as in **Thisse and Thisse (2008)**. Anti-sense probes for *notch1b* and *klf2a* were generated from a plasmid containing the cDNA of zebrafish *notch1b* in pCR-script SK+ (provided by the Bakkers lab, The Netherlands) and zebrafish *klf2a* in IRBOp991B0734D (provided by RPDZ, Berlin; **Vermot et al., 2009**) and subsequently transcribed using the T3 polymerase and T7 polymerase, respectively. After ISH, embryos were incubated subsequently in 45% and 90% D-fructose (Sigma F0127) containing 0.5% of 1-Thioglycerol (Sigma M6145) for 20 min. Imaging of ISH was done using a Leica M165 macroscope with a TrueChrome Metrics (Tucsen) with a Leica 1.0X objective (10450028).

RNAscope

72 hpf wildtype zebrafish embryos were fixed in 4% PFA overnight at 4˚C. The fixed embryos were dehydrated to 100% ethanol gradually. Embryos were stained using the RNAscope Fluorescent Multiplex kit (Advanced Cell Diagnostics).

Confocal imaging

For live imaging, zebrafish embryos were staged, anaesthetized with 0.02% tricaine solution or 50 mM BDM, to stop the heart when necessary, and mounted in 0.7% low melting-point agarose (Sigma Aldrich). Confocal imaging was performed either on a Leica SP8 confocal microscope (experiments with BODIPY-ceramide or fixed samples) or a Leica spinning disk (valve structure, flow profile, reporter experiments). Fast confocal imaging to image valve leaflets from 72 hpf to 120 hpf stained with BODIPY-ceramide was performed using the resonant scanner mode of the Sp8 microscope. Images were acquired with a low-magnification water immersion objective (Leica HCX IRAPO L, 25X, N.A. 0.95). The optical plane was moved 2 µm between the z-sections until the whole OFT was acquired. 2-colored fast confocal imaging was used to image valve structure, red blood cells, and reporter activities from 56 hpf to 144 hpf was performed using a Leica DMi8 combined with a CSU-X1 (Yokogawa) spinning at 10 000 rpm, two simultaneous cameras (TuCam Flash4.0, Hamamatsu) and a water immersion objective (Leica 20X, N.A. 0.75 or Leica 40X, N.A. 1.1). 1 ms exposure was used for red blood cells imaging and 20 ms exposure for valve structure and reporter activity experiments. 50% of 488 laser power and 40% of 561 laser power were used for reporter activity experiments.

BODIPY-ceramide imaging

Embryos were incubated with 4 mM BODIPY-ceramide (Molecular Probes) overnight and then processed as in **Heckel et al. (2015)** and **Vermot et al. (2009)** to visualize the valve shape.

DAF-FMDA labelling

To reveal the presence of NO, embryos were incubated in zebrafish medium containing 5 µM DAF-FM DA (Life Technologies, D23842) for 30 min in the dark at 28˚C. Fluorescence intensities of the smooth muscles were measured using ImageJ software.

Photoconversion

Photoconversion was performed using the FRAP module on a SP8 confocal microscope and a Leica HCX IRAPO L, 25X, NA0.95 water immersion objective. *Tg(fli1a:Gal4FF; UAS:Kaede)* embryos were mounted in 0.7% low melting-point agarose supplemented with 50 mM BDM to inhibit heart contraction for the duration of the procedure. A region of interest corresponding to the anterior, middle or posterior part of the valve was selected and exposed to 405 nm light (25% laser power). One pre-bleach frame was acquired, followed by 3–6 bleach pulses (3–5 ms each) without acquisition to achieve conversion of the kaede protein to its red form. A z-stack of the photoconverted heart was then acquired in the standard confocal mode to record the starting point of each experiment. Embryos were then carefully dissected from the agarose, placed in fish water for 5–10 min until heart contraction resumed and then put at 28.5˚C to develop individually under standard conditions until the next time point of interest.

Fractional shortening

Imaging was performed on a Leica DMIRBE inverted microscope using a Photron SA3 high-speed CMOS camera (Photron, San Diego, CA) and water immersion objective (Leica 20X, NA 0.7). Image sequences were acquired at a frame rate of 1000 frames per second. FS% = (Dm diastole- Dm systole)/ (Dm diastole) and where Dm is the diameter of the chamber of interest (atrium or ventricle).

Flow analysis

Red blood cells were manually tracked through the OFT and their velocity calculated from image sequences of the *Tg(gata1:ds-red; kdrl:EGFP)* beating heart, acquired at 1000 frames per second as described previously. Red blood cells transiting through the OFT were tracked manually on Imaris and their velocity calculated. The tracks of multiple cells in at least four embryos per stage were assembled to obtain an estimate of the flow velocity over multiple cardiac cycles (typically 3). Velocities estimated at the same time point by tracking different cells were averaged.

Image analysis

For fluorescence intensity analysis of the Klf2a reporter, the *Tg(klf2a:H2B-EGFP)* reporter line was crossed with the *Tg(fli1a:nls-mCherry)* line and the mCherry signal was used for normalization. The maximum intensity of each channel on a single Z-section through the valves was quantified and the *E*GFP over mCherry ratio generated. For fluorescence intensity analysis of the Notch reporter, the ratio of the maximum intensity of the GFP signal from the *Tg(tp1:dGFP)* reporter line on a single Z-section through the valves over the maximum intensity of the background was generated.

These ratios were then averaged for three cells in the anterior part and three cells in the posterior part of both valves in the OFT of individual embryos. Finally, the averages of the anterior and posterior parts were compared.

Statistical analyses

We did not compute or predict the number of samples necessary for statistical differences because the standard deviation of our study's population was not known before starting our analysis. Biological replicate corresponds to the analysis of different embryos of the same stage. Technical replicate corresponds to the analysis of the same embryo imaged the same way. The sample size (biological replicate and number) to use was as defined by our ability to generate our datasets. For analyses between two groups of embryos, differences were considered statistically significant when the p-value<0.05, as determined using a two-tailed and paired Student's t-test (*klf2a* and *notch* reporter expression). For boxplots, center lines show the medians, crosses show the means, box limits indicate the 25th and 75th percentiles as determined by R software; whiskers extend 1.5 times the interquartile range from the 25th and 75th percentiles, data points are represented as circles.

Acknowledgements

We thank the Vermot laboratory for discussion and H Fukui and R Chow for thoughtful comments on the manuscript. We thank C Burns, V Lecaudey and I Drummond for providing antibodies, mutants and protocols for immunohistochemistry. We thank J-M Garnier for the cloning of the *piezo1:nls-Venus* construct. We thank the IGBMC fish facility (S Pajot and C Moebs) and the IGBMC imaging center, in particular B Gurchenkov, D Hentsch, E Guiot and E Grandgirard. This project has received funding from the European Research Council (ERC) under the European Union's Horizon 2020 research and innovation programme: GA N°682939, the Fondation pour la Recherche Médicale: DEQ29553, Agence Nationale de la Recherche: ANR-15-CE13-0015-01, ANR-10-IDEX-0002–02, ANR-12-ISV2-0001-01 and ANR-10-LABX-0030-INRT and the European Molecular Biology Organization Young Investigator Program. HV was supported by the IGBMC International PhD program: ANR-10-LABX-0030-INRT. ALD was supported by a post doctoral fellowship from the Lefoulon-Delalande Foundation.

Additional information

Funding

Funder	Grant reference number	Author
H2020 European Research Council	682938 - EVALVE	Julien Vermot
Fondation pour la Recherche Médicale	DEQ29553	Julien Vermot
Agence Nationale de la Recherche	ANR-15-CE13-0015-01	Anne-Laure Duchemin Hélène Vignes Julien Vermot
European Molecular Biology Organization	Young Investigator Program	Julien Vermot
Fondation Lefoulon Delalande		Anne-Laure Duchemin
Agence Nationale de la Recherche	ANR-10-IDEX-0002-02	Anne-Laure Duchemin Hélène Vignes Julien Vermot
Agence Nationale de la Recherche	ANR-12-ISV2-0001-01	Anne-Laure Duchemin Hélène Vignes Julien Vermot
Agence Nationale de la Recherche	ANR-10-LABX-0030-INRT	Anne-Laure Duchemin Hélène Vignes Julien Vermot

The funders had no role in study design, data collection and interpretation, or the decision to submit the work for publication.

Author contributions

Anne-Laure Duchemin, Conceptualization, Data curation, Formal analysis, Methodology, Writing—original draft; Hélène Vignes, Data curation; Julien Vermot, Conceptualization, Supervision, Funding acquisition, Writing—original draft, Project administration

Author ORCIDs

Julien Vermot https://orcid.org/0000-0002-8924-732X

Ethics

Animal experimentation: Animal experiments were approved by the Animal Experimentation Committee of the Institutional Review Board of the IGBMC.(reference numbers MIN APAFIS#4669-2016032411093030 v4 and MIN 4669-2016032411093030 v4-detail of entry 1).

Decision letter and Author response
Decision letter https://doi.org/10.7554/eLife.44706.028
Author response https://doi.org/10.7554/eLife.44706.029

Additional files

Supplementary files

- Transparent reporting form

DOI: https://doi.org/10.7554/eLife.44706.026

Data availability

Source data for the figures has been uploaded.

References

Agarwala S, Duquesne S, Liu K, Boehm A, Grimm L, Link S, König S, Eimer S, Ronneberger O, Lecaudey V. 2015. Amotl2a interacts with the hippo effector Yap1 and the wnt/β-catenin effector Lef1 to control tissue size in zebrafish. *eLife* **4**:e08201. DOI: https://doi.org/10.7554/eLife.08201, PMID: 26335201

Anton H, Harlepp S, Ramspacher C, Wu D, Monduc F, Bhat S, Liebling M, Paoletti C, Charvin G, Freund JB, Vermot J. 2013. Pulse propagation by a capacitive mechanism drives embryonic blood flow. *Development* **140**: 4426–4434. DOI: https://doi.org/10.1242/dev.096768

Bäck M, Gasser TC, Michel JB, Caligiuri G. 2013. Biomechanical factors in the biology of aortic wall and aortic valve diseases. *Cardiovascular Research* **99**:232–241. DOI: https://doi.org/10.1093/cvr/cvt040, PMID: 23459103

Baeyens N, Bandyopadhyay C, Coon BG, Yun S, Schwartz MA. 2016. Endothelial fluid shear stress sensing in vascular health and disease. *Journal of Clinical Investigation* **126**:821–828. DOI: https://doi.org/10.1172/JCI83083, PMID: 26928035

Beis D, Bartman T, Jin SW, Scott IC, D'Amico LA, Ober EA, Verkade H, Frantsve J, Field HA, Wehman A, Baier H, Tallafuss A, Bally-Cuif L, Chen JN, Stainier DY, Jungblut B. 2005. Genetic and cellular analyses of zebrafish atrioventricular cushion and valve development. *Development* **132**:4193–4204. DOI: https://doi.org/10.1242/dev.01970, PMID: 16107477

Boselli F, Steed E, Freund JB, Vermot J. 2017. Anisotropic shear stress patterns predict the orientation of convergent tissue movements in the embryonic heart. *Development* **144**:4322–4327. DOI: https://doi.org/10.1242/dev.152124, PMID: 29183943

Braun MH, Brill RW, Gosline JM, Jones DR. 2003a. Form and function of the bulbus arteriosus in yellowfin tuna (Thunnus albacares), bigeye tuna (Thunnus obesus) and blue marlin (Makaira nigricans): static properties. *Journal of Experimental Biology* **206**:3311–3326. DOI: https://doi.org/10.1242/jeb.00575, PMID: 12939364

Braun MH, Brill RW, Gosline JM, Jones DR. 2003b. Form and function of the bulbus arteriosus in yellowfin tuna (Thunnus albacares): dynamic properties. *Journal of Experimental Biology* **206**:3327–3335. DOI: https://doi.org/10.1242/jeb.00576, PMID: 12939365

Butcher JT, Simmons CA, Warnock JN. 2008. Mechanobiology of the aortic heart valve. *The Journal of Heart Valve Disease* **17**:62–73. PMID: 18365571

Choi D, Park E, Jung E, Seong YJ, Yoo J, Lee E, Hong M, Lee S, Ishida H, Burford J, Peti-Peterdi J, Adams RH, Srikanth S, Gwack Y, Chen CS, Vogel HJ, Koh CJ, Wong AK, Hong YK. 2017. Laminar flow downregulates notch activity to promote lymphatic sprouting. *Journal of Clinical Investigation* **127**:1225–1240. DOI: https://doi.org/10.1172/JCI87442, PMID: 28263185

Combs MD, Yutzey KE. 2009. Heart valve development. *Circulation Research* **105**:408–421. DOI: https://doi.org/10.1161/CIRCRESAHA.109.201566

Coste B, Mathur J, Schmidt M, Earley TJ, Ranade S, Petrus MJ, Dubin AE, Patapoutian A. 2010. Piezo1 and Piezo2 are essential components of distinct mechanically activated cation channels. *Science* **330**:55–60. DOI: https://doi.org/10.1126/science.1193270, PMID: 20813920

Donat S, Lourenço M, Paolini A, Otten C, Renz M, Abdelilah-Seyfried S. 2018. Heg1 and Ccm1/2 proteins control endocardial mechanosensitivity during zebrafish valvulogenesis. *eLife* **7**:e28939. DOI: https://doi.org/10.7554/eLife.28939, PMID: 29364115

Durst R, Sauls K, Peal DS, deVlaming A, Toomer K, Leyne M, Salani M, Talkowski ME, Brand H, Perrocheau M, Simpson C, Jett C, Stone MR, Charles F, Chiang C, Lynch SN, Bouatia-Naji N, Delling FN, Freed LA, Tribouilloy C, et al. 2015. Mutations in DCHS1 cause mitral valve prolapse. *Nature* **525**:109–113. DOI: https://doi.org/10.1038/nature14670, PMID: 26258302

Dzamba BJ, DeSimone DW. 2018. Extracellular matrix (ECM) and the sculpting of embryonic tissues. *Current Topics in Developmental Biology* **130**:245–274. DOI: https://doi.org/10.1016/bs.ctdb.2018.03.006, PMID: 29853179

Eisenhoffer GT, Loftus PD, Yoshigi M, Otsuna H, Chien CB, Morcos PA, Rosenblatt J. 2012. Crowding induces live cell extrusion to maintain homeostatic cell numbers in epithelia. *Nature* **484**:546–549. DOI: https://doi.org/10.1038/nature10999, PMID: 22504183

Eley L, Alqahtani AM, MacGrogan D, Richardson RV, Murphy L, Salguero-Jimenez A, Sintes Rodriguez San Pedro M, Tiurma S, McCutcheon L, Gilmore A, de La Pompa JL, Chaudhry B, Henderson DJ. 2018. A novel source of arterial valve cells linked to bicuspid aortic valve without raphe in mice. *eLife* **7**:e34110. DOI: https://doi.org/10.7554/eLife.34110, PMID: 29956664

Feaver RE, Gelfand BD, Blackman BR. 2013. Human haemodynamic frequency harmonics regulate the inflammatory phenotype of vascular endothelial cells. *Nature Communications* **4**:1525. DOI: https://doi.org/10.1038/ncomms2530, PMID: 23443553

Felker A, Prummel KD, Merks AM, Mickoleit M, Brombacher EC, Huisken J, Panáková D, Mosimann C. 2018. Continuous addition of progenitors forms the cardiac ventricle in zebrafish. *Nature Communications* **9**:2001. DOI: https://doi.org/10.1038/s41467-018-04402-6, PMID: 29784942

Garg V, Muth AN, Ransom JF, Schluterman MK, Barnes R, King IN, Grossfeld PD, Srivastava D. 2005. Mutations in NOTCH1 cause aortic valve disease. *Nature* **437**:270–274. DOI: https://doi.org/10.1038/nature03940

Garg V. 2016. Notch Signaling in Aortic Valve Development and Disease. In: Nakanishi T, Markwald R. R, Baldwin H. S, Keller B. B, Srivastava D, Yamagishi H (Eds). *Etiology and Morphogenesis of Congenital Heart Disease: From Gene Function and Cellular Interaction to Morphology*. Springer. p. 371–376.

Godby R, Munjal C, Opoka A, Smith J, Yutzey K, Narmoneva D, Hinton R. 2014. Cross talk between NOTCH signaling and biomechanics in human aortic valve disease pathogenesis. *Journal of Cardiovascular Development and Disease* **1**:237–256. DOI: https://doi.org/10.3390/jcdd1030237

Goddard LM, Duchemin AL, Ramalingan H, Wu B, Chen M, Bamezai S, Yang J, Li L, Morley MP, Wang T, Scherrer-Crosbie M, Frank DB, Engleka KA, Jameson SC, Morrisey EE, Carroll TJ, Zhou B, Vermot J, Kahn ML. 2017. Hemodynamic forces sculpt developing heart valves through a KLF2-WNT9B paracrine signaling Axis. *Developmental Cell* **43**:274–289. DOI: https://doi.org/10.1016/j.devcel.2017.09.023, PMID: 29056552

Grimes AC, Stadt HA, Shepherd IT, Kirby ML. 2006. Solving an enigma: arterial pole development in the zebrafish heart. *Developmental Biology* **290**:265–276. DOI: https://doi.org/10.1016/j.ydbio.2005.11.042, PMID: 16405941

Hasan SS, Tsaryk R, Lange M, Wisniewski L, Moore JC, Lawson ND, Wojciechowska K, Schnittler H, Siekmann AF. 2017. Endothelial notch signalling limits angiogenesis via control of artery formation. *Nature Cell Biology* **19**:928–940. DOI: https://doi.org/10.1038/ncb3574, PMID: 28714969

He L, Si G, Huang J, Samuel ADT, Perrimon N. 2018. Mechanical regulation of stem-cell differentiation by the stretch-activated piezo channel. *Nature* **555**:103–106. DOI: https://doi.org/10.1038/nature25744, PMID: 29414942

Heckel E, Boselli F, Roth S, Krudewig A, Belting HG, Charvin G, Vermot J. 2015. Oscillatory flow modulates mechanosensitive klf2a expression through trpv4 and trpp2 during heart valve development. *Current Biology* **25**:1354–1361. DOI: https://doi.org/10.1016/j.cub.2015.03.038, PMID: 25959969

Hoffman JI, Kaplan S. 2002. The incidence of congenital heart disease. *Journal of the American College of Cardiology* **39**:1890–1900. DOI: https://doi.org/10.1016/S0735-1097(02)01886-7, PMID: 12084585

Hsu JJ, Vedula V, Baek KI, Chen C, Chen J, Chou MI, Lam J, Subhedar S, Wang J, Ding Y, Chang C-C, Lee J, Demer LL, Tintut Y, Marsden AL, Hsiai TK. 2019. Contractile and hemodynamic forces coordinate Notch1b-mediated outflow tract valve formation. *JCI Insight* **4**:124460. DOI: https://doi.org/10.1172/jci.insight.124460

Huang CJ, Tu CT, Hsiao CD, Hsieh FJ, Tsai HJ. 2003. Germ-line transmission of a myocardium-specific GFP transgene reveals critical regulatory elements in the cardiac myosin light chain 2 promoter of zebrafish. *Developmental Dynamics* **228**:30–40. DOI: https://doi.org/10.1002/dvdy.10356, PMID: 12950077

Jin SW, Beis D, Mitchell T, Chen JN, Stainier DY. 2005. Cellular and molecular analyses of vascular tube and lumen formation in zebrafish. *Development* **132**:5199–5209. DOI: https://doi.org/10.1242/dev.02087, PMID: 16251212

Keith DA, Paz A, Gallop PM, Glimcher MJ. 1977. Histologic and biochemical identification and characterization of an elastin in cartilage. *Journal of Histochemistry & Cytochemistry* **25**:1154–1162. DOI: https://doi.org/10.1177/25.10.72098

Köttgen M, Buchholz B, Garcia-Gonzalez MA, Kotsis F, Fu X, Doerken M, Boehlke C, Steffl D, Tauber R, Wegierski T, Nitschke R, Suzuki M, Kramer-Zucker A, Germino GG, Watnick T, Prenen J, Nilius B, Kuehn EW, Walz G. 2008. TRPP2 and TRPV4 form a polymodal sensory channel complex. *The Journal of Cell Biology* **182**:437–447. DOI: https://doi.org/10.1083/jcb.200805124, PMID: 18695040

Laforest B, Andelfinger G, Nemer M. 2011. Loss of Gata5 in mice leads to bicuspid aortic valve. *Journal of Clinical Investigation* **121**:2876–2887. DOI: https://doi.org/10.1172/JCI44555, PMID: 21633169

Lee W, Leddy HA, Chen Y, Lee SH, Zelenski NA, McNulty AL, Wu J, Beicker KN, Coles J, Zauscher S, Grandl J, Sachs F, Guilak F, Liedtke WB. 2014. Synergy between Piezo1 and Piezo2 channels confers high-strain mechanosensitivity to articular cartilage. *PNAS* **111**:E5114–E5122. DOI: https://doi.org/10.1073/pnas.1414298111, PMID: 25385580

Lewis AH, Cui AF, McDonald MF, Grandl J. 2017. Transduction of repetitive mechanical stimuli by Piezo1 and Piezo2 ion channels. *Cell Reports* **19**:2572–2585. DOI: https://doi.org/10.1016/j.celrep.2017.05.079, PMID: 28636944

Li J, Hou B, Tumova S, Muraki K, Bruns A, Ludlow MJ, Sedo A, Hyman AJ, McKeown L, Young RS, Yuldasheva NY, Majeed Y, Wilson LA, Rode B, Bailey MA, Kim HR, Fu Z, Carter DA, Bilton J, Imrie H, et al. 2014. Piezo1 integration of vascular architecture with physiological force. *Nature* **515**:279–282. DOI: https://doi.org/10.1038/nature13701, PMID: 25119035

Lin C-J, Lin C-Y, Chen C-H, Zhou B, Chang C-P. 2012. Partitioning the heart: mechanisms of cardiac septation and valve development. *Development* **139**:3277–3299. DOI: https://doi.org/10.1242/dev.063495

Lukacs V, Mathur J, Mao R, Bayrak-Toydemir P, Procter M, Cahalan SM, Kim HJ, Bandell M, Longo N, Day RW, Stevenson DA, Patapoutian A, Krock BL. 2015. Impaired PIEZO1 function in patients with a novel autosomal recessive congenital lymphatic dysplasia. *Nature Communications* **6**:8329. DOI: https://doi.org/10.1038/ncomms9329, PMID: 26387913

Luxán G, D'Amato G, MacGrogan D, de la Pompa JL. 2016. Endocardial notch signaling in cardiac development and disease. *Circulation Research* **118**:e1–e18. DOI: https://doi.org/10.1161/CIRCRESAHA.115.305350, PMID: 26635389

Lyons SE, Lawson ND, Lei L, Bennett PE, Weinstein BM, Liu PP. 2002. A nonsense mutation in zebrafish gata1 causes the bloodless phenotype in vlad tepes. *PNAS* **99**:5454–5459. DOI: https://doi.org/10.1073/pnas.082695299, PMID: 11960002

Ma S, Cahalan S, LaMonte G, Grubaugh ND, Zeng W, Murthy SE, Paytas E, Gamini R, Lukacs V, Whitwam T, Loud M, Lohia R, Berry L, Khan SM, Janse CJ, Bandell M, Schmedt C, Wengelnik K, Su AI, Honore E, et al. 2018. Common PIEZO1 allele in african populations causes RBC dehydration and attenuates plasmodium infection. *Cell* **173**:443–455. DOI: https://doi.org/10.1016/j.cell.2018.02.047, PMID: 29576450

MacGrogan D, D'Amato G, Travisano S, Martinez-Poveda B, Luxán G, Del Monte-Nieto G, Papoutsi T, Sbroggio M, Bou V, Gomez-Del Arco P, Gómez MJ, Zhou B, Redondo JM, Jiménez-Borreguero LJ, de la Pompa JL. 2016. Sequential Ligand-Dependent notch signaling activation regulates valve primordium formation and morphogenesis. *Circulation Research* **118**:1480–1497. DOI: https://doi.org/10.1161/CIRCRESAHA.115.308077, PMID: 27056911

Mack JJ, Mosqueiro TS, Archer BJ, Jones WM, Sunshine H, Faas GC, Briot A, Aragón RL, Su T, Romay MC, McDonald AI, Kuo CH, Lizama CO, Lane TF, Zovein AC, Fang Y, Tarling EJ, de Aguiar Vallim TQ, Navab M, Fogelman AM, et al. 2017. NOTCH1 is a mechanosensor in adult arteries. *Nature Communications* **8**:1620. DOI: https://doi.org/10.1038/s41467-017-01741-8, PMID: 29158473

Miao M, Bruce AE, Bhanji T, Davis EC, Keeley FW. 2007. Differential expression of two tropoelastin genes in zebrafish. *Matrix Biology* **26**:115–124. DOI: https://doi.org/10.1016/j.matbio.2006.09.011, PMID: 17112714

Miesfeld JB, Link BA. 2014. Establishment of transgenic lines to monitor and manipulate Yap/Taz-Tead activity in zebrafish reveals both evolutionarily conserved and divergent functions of the Hippo pathway. *Mechanisms of Development* **133**:177–188. DOI: https://doi.org/10.1016/j.mod.2014.02.003

Moriyama Y, Ito F, Takeda H, Yano T, Okabe M, Kuraku S, Keeley FW, Koshiba-Takeuchi K. 2016. Evolution of the fish heart by sub/neofunctionalization of an elastin gene. *Nature Communications* **7**:10397. DOI: https://doi.org/10.1038/ncomms10397

Murthy SE, Dubin AE, Patapoutian A. 2017. Piezos thrive under pressure: mechanically activated ion channels in health and disease. *Nature Reviews Molecular Cell Biology* **18**:771–783. DOI: https://doi.org/10.1038/nrm.2017.92

Nakajima H, Yamamoto K, Agarwala S, Terai K, Fukui H, Fukuhara S, Ando K, Miyazaki T, Yokota Y, Schmelzer E, Belting H-G, Affolter M, Lecaudey V, Mochizuki N. 2017. Flow-Dependent endothelial YAP regulation contributes to vessel maintenance. *Developmental Cell* **40**:523–536. DOI: https://doi.org/10.1016/j.devcel.2017.02.019

Nicenboim J, Malkinson G, Lupo T, Asaf L, Sela Y, Mayseless O, Gibbs-Bar L, Senderovich N, Hashimshony T, Shin M, Jerafi-Vider A, Avraham-Davidi I, Krupalnik V, Hofi R, Almog G, Astin JW, Golani O, Ben-Dor S, Crosier PS, Herzog W, et al. 2015. Lymphatic vessels arise from specialized angioblasts within a venous niche. *Nature* **522**:56–61. DOI: https://doi.org/10.1038/nature14425, PMID: 25992545

Ninov N, Borius M, Stainier DY. 2012. Different levels of notch signaling regulate quiescence, renewal and differentiation in pancreatic endocrine progenitors. *Development* **139**:1557–1567. DOI: https://doi.org/10.1242/dev.076000, PMID: 22492351

Nonomura K, Lukacs V, Sweet DT, Goddard LM, Kanie A, Whitwam T, Ranade SS, Fujimori T, Kahn ML, Patapoutian A. 2018. Mechanically activated ion channel PIEZO1 is required for lymphatic valve formation. *PNAS* **115**:12817–12822. DOI: https://doi.org/10.1073/pnas.1817070115, PMID: 30482854

Øyen N, Poulsen G, Boyd HA, Wohlfahrt J, Jensen PK, Melbye M. 2009. Recurrence of congenital heart defects in families. *Circulation* **120**:295–301. DOI: https://doi.org/10.1161/CIRCULATIONAHA.109.857987, PMID: 19597048

Paffett-Lugassy N, Novikov N, Jeffrey S, Abrial M, Guner-Ataman B, Sakthivel S, Burns CE, Burns CG. 2017. Unique developmental trajectories and genetic regulation of ventricular and outflow tract progenitors in the zebrafish second heart field. *Development* **144**:4616–4624. DOI: https://doi.org/10.1242/dev.153411

Paolini A, Abdelilah-Seyfried S. 2018. The mechanobiology of zebrafish cardiac valve leaflet formation. *Current Opinion in Cell Biology* **55**:52–58. DOI: https://doi.org/10.1016/j.ceb.2018.05.007

Pathak MM, Nourse JL, Tran T, Hwe J, Arulmoli J, Le DT, Bernardis E, Flanagan LA, Tombola F. 2014. Stretch-activated ion channel Piezo1 directs lineage choice in human neural stem cells. *PNAS* **111**:16148–16153. DOI: https://doi.org/10.1073/pnas.1409802111, PMID: 25349416

Peralta M, Steed E, Harlepp S, González-Rosa JM, Monduc F, Ariza-Cosano A, Cortés A, Rayón T, Gómez-Skarmeta JL, Zapata A, Vermot J, Mercader N. 2013. Heartbeat-driven pericardiac fluid forces contribute to epicardium morphogenesis. *Current Biology* **23**:1726–1735. DOI: https://doi.org/10.1016/j.cub.2013.07.005, PMID: 23954432

Pestel J, Ramadass R, Gauvrit S, Helker C, Herzog W, Stainier DY. 2016. Real-time 3D visualization of cellular rearrangements during cardiac valve formation. *Development* **143**:2217–2227. DOI: https://doi.org/10.1242/dev.133272, PMID: 27302398

Phng LK, Stanchi F, Gerhardt H. 2013. Filopodia are dispensable for endothelial tip cell guidance. *Development* **140**:4031–4040. DOI: https://doi.org/10.1242/dev.097352, PMID: 24046319

Pitulescu ME, Schmidt I, Giaimo BD, Antoine T, Berkenfeld F, Ferrante F, Park H, Ehling M, Biljes D, Rocha SF, Langen UH, Stehling M, Nagasawa T, Ferrara N, Borggrefe T, Adams RH. 2017. Dll4 and Notch signalling couples sprouting angiogenesis and artery formation. *Nature Cell Biology* **19**:915–927. DOI: https://doi.org/10.1038/ncb3555, PMID: 28714968

Poole K, Herget R, Lapatsina L, Ngo HD, Lewin GR. 2014. Tuning piezo ion channels to detect molecular-scale movements relevant for fine touch. *Nature Communications* **5**:3520. DOI: https://doi.org/10.1038/ncomms4520, PMID: 24662763

PROMESA investigators, MVP-France, Leducq Transatlantic MITRAL Network,Dina C, Bouatia-Naji N, Tucker N, Delling FN, Toomer K, Durst R, Perrocheau M, Fernandez-Friera L, Solis J, Le Tourneau T, Chen MH, Probst V, Bosse Y, Pibarot P, Zelenika D, Lathrop M, Hercberg S, Roussel R, Benjamin EJ, Bonnet F, et al. 2015. Genetic association analyses highlight biological pathways underlying mitral valve prolapse. *Nature Genetics* **47**:1206–1211. DOI: https://doi.org/10.1038/ng.3383, PMID: 26301497

Qi Y, Andolfi L, Frattini F, Mayer F, Lazzarino M, Hu J. 2015. Membrane stiffening by STOML3 facilitates mechanosensation in sensory neurons. *Nature Communications* **6**:8512. DOI: https://doi.org/10.1038/ncomms9512

Ranade SS, Qiu Z, Woo SH, Hur SS, Murthy SE, Cahalan SM, Xu J, Mathur J, Bandell M, Coste B, Li YS, Chien S, Patapoutian A. 2014. Piezo1, a mechanically activated ion channel, is required for vascular development in mice. *PNAS* **111**:10347–10352. DOI: https://doi.org/10.1073/pnas.1409233111, PMID: 24958852

Ranade SS, Syeda R, Patapoutian A. 2015. Mechanically Activated Ion Channels. *Neuron* **87**:1162–1179. DOI: https://doi.org/10.1016/j.neuron.2015.08.032

Retailleau K, Duprat F, Arhatte M, Ranade SS, Peyronnet R, Martins JR, Jodar M, Moro C, Offermanns S, Feng Y, Demolombe S, Patel A, Honoré E. 2015. Piezo1 in smooth muscle cells is involved in Hypertension-Dependent arterial remodeling. *Cell Reports* **13**:1161–1171. DOI: https://doi.org/10.1016/j.celrep.2015.09.072, PMID: 26526998

Richards AA, Garg V. 2010. Genetics of congenital heart disease. *Current Cardiology Reviews* **6**:91–97. DOI: https://doi.org/10.2174/157340310791162703, PMID: 21532774

Samsa LA, Givens C, Tzima E, Stainier DY, Qian L, Liu J. 2015. Cardiac contraction activates endocardial notch signaling to modulate chamber maturation in zebrafish. *Development* **142**:4080–4091. DOI: https://doi.org/10.1242/dev.125724, PMID: 26628092

Sánchez-Iranzo H, Galardi-Castilla M, Minguillón C, Sanz-Morejón A, González-Rosa JM, Felker A, Ernst A, Guzmán-Martínez G, Mosimann C, Mercader N. 2018. Tbx5a lineage tracing shows cardiomyocyte plasticity during zebrafish heart regeneration. *Nature Communications* **9**:428. DOI: https://doi.org/10.1038/s41467-017-02650-6, PMID: 29382818

Sauls K, de Vlaming A, Harris BS, Williams K, Wessels A, Levine RA, Slaugenhaupt SA, Goodwin RL, Pavone LM, Merot J, Schott J-J, Le Tourneau T, Dix T, Jesinkey S, Feng Y, Walsh C, Zhou B, Baldwin S, Markwald RR, Norris RA. 2012. Developmental basis for filamin-A-associated myxomatous mitral valve disease. *Cardiovascular Research* **96**:109–119. DOI: https://doi.org/10.1093/cvr/cvs238

Scherz PJ, Huisken J, Sahai-Hernandez P, Stainier DY. 2008. High-speed imaging of developing heart valves reveals interplay of morphogenesis and function. *Development* **135**:1179–1187. DOI: https://doi.org/10.1242/dev.010694, PMID: 18272595

Schottenfeld J, Sullivan-Brown J, Burdine RD. 2007. Zebrafish curly up encodes a Pkd2 ortholog that restricts left-side-specific expression of southpaw. *Development* **134**:1605–1615. DOI: https://doi.org/10.1242/dev.02827

Sehnert AJ, Huq A, Weinstein BM, Walker C, Fishman M, Stainier DY. 2002. Cardiac troponin T is essential in sarcomere assembly and cardiac contractility. *Nature Genetics* **31**:106–110. DOI: https://doi.org/10.1038/ng875, PMID: 11967535

Sharif-Naeini R, Folgering JHA, Bichet D, Duprat F, Lauritzen I, Arhatte M, Jodar M, Dedman A, Chatelain FC, Schulte U, Retailleau K, Loufrani L, Patel A, Sachs F, Delmas P, Peters DJ, Honoré E. 2009. Polycystin-1 and -2 dosage regulates pressure sensing. *Cell* **139**:587–596. DOI: https://doi.org/10.1016/j.cell.2009.08.045, PMID: 19879844

Steed E, Boselli F, Vermot J. 2016a. Hemodynamics driven cardiac valve morphogenesis. *Biochimica et Biophysica Acta (BBA) - Molecular Cell Research* **1863**:1760–1766. DOI: https://doi.org/10.1016/j.bbamcr.2015.11.014

Steed E, Faggianelli N, Roth S, Ramspacher C, Concordet JP, Vermot J. 2016b. klf2a couples mechanotransduction and zebrafish valve morphogenesis through fibronectin synthesis. *Nature Communications* **7**:11646. DOI: https://doi.org/10.1038/ncomms11646, PMID: 27221222

Stefanovic S, Barnett P, van Duijvenboden K, Weber D, Gessler M, Christoffels VM. 2014. GATA-dependent regulatory switches establish atrioventricular canal specificity during heart development. *Nature Communications* **5**:3680. DOI: https://doi.org/10.1038/ncomms4680

Tammela T, Zarkada G, Nurmi H, Jakobsson L, Heinolainen K, Tvorogov D, Zheng W, Franco CA, Murtomäki A, Aranda E, Miura N, Ylä-Herttuala S, Fruttiger M, Mäkinen T, Eichmann A, Pollard JW, Gerhardt H, Alitalo K. 2011. VEGFR-3 controls tip to stalk conversion at vessel fusion sites by reinforcing notch signalling. *Nature Cell Biology* **13**:1202–1213. DOI: https://doi.org/10.1038/ncb2331, PMID: 21909098

Tessadori F, van Weerd JH, Burkhard SB, Verkerk AO, de Pater E, Boukens BJ, Vink A, Christoffels VM, Bakkers J. 2012. Identification and functional characterization of cardiac pacemaker cells in zebrafish. *PLOS ONE* **7**: e47644. DOI: https://doi.org/10.1371/journal.pone.0047644, PMID: 23077655

Thisse C, Thisse B. 2008. High-resolution in situ hybridization to whole-mount zebrafish embryos. *Nature Protocols* **3**:59–69. DOI: https://doi.org/10.1038/nprot.2007.514, PMID: 18193022

Thodeti CK, Matthews B, Ravi A, Mammoto A, Ghosh K, Bracha AL, Ingber DE. 2009. TRPV4 channels mediate cyclic strain-induced endothelial cell reorientation through integrin-to-integrin signaling. *Circulation Research* **104**:1123–1130. DOI: https://doi.org/10.1161/CIRCRESAHA.108.192930, PMID: 19359599

Vermot J, Forouhar AS, Liebling M, Wu D, Plummer D, Gharib M, Fraser SE. 2009. Reversing blood flows act through klf2a to ensure normal valvulogenesis in the developing heart. *PLOS Biology* **7**:e1000246. DOI: https://doi.org/10.1371/journal.pbio.1000246, PMID: 19924233

Wang Y, Wu B, Farrar E, Lui W, Lu P, Zhang D, Alfieri CM, Mao K, Chu M, Yang D, Xu D, Rauchman M, Taylor V, Conway SJ, Yutzey KE, Butcher JT, Zhou B. 2017. Notch-Tnf signalling is required for development and homeostasis of arterial valves. *European Heart Journal* **38**:675–686. DOI: https://doi.org/10.1093/eurheartj/ehv520, PMID: 26491108

Wu B, Wang Y, Xiao F, Butcher JT, Yutzey KE, Zhou B. 2017. Developmental mechanisms of aortic valve malformation and disease. *Annual Review of Physiology* **79**:21–41. DOI: https://doi.org/10.1146/annurev-physiol-022516-034001, PMID: 27959615

Zarychanski R, Schulz VP, Houston BL, Maksimova Y, Houston DS, Smith B, Rinehart J, Gallagher PG. 2012. Mutations in the mechanotransduction protein PIEZO1 are associated with hereditary xerocytosis. *Blood* **120**: 1908–1915. DOI: https://doi.org/10.1182/blood-2012-04-422253, PMID: 22529292

ANNEX 2

ANNEX 2

Available online at www.sciencedirect.com

ScienceDirect

Current Opinion in Genetics & Development

Mechanotransduction in cardiovascular morphogenesis and tissue engineering

Anne-Laure Duchemin[1,2,3,4,5], Helene Vignes[1,2,3,4,5], Julien Vermot[1,2,3,4] and Renee Chow[1,2,3,4,5]

Cardiovascular morphogenesis involves cell behavior and cell identity changes that are activated by mechanical forces associated with heart function. Recently, advances in *in vivo* imaging, methods to alter blood flow, and computational modelling have greatly advanced our understanding of how forces produced by heart contraction and blood flow impact different morphogenetic processes. Meanwhile, traditional genetic approaches have helped to elucidate how endothelial cells respond to forces at the cellular and molecular level. Here we discuss the principles of endothelial mechanosensitity and their interplay with cellular processes during cardiovascular morphogenesis. We then discuss their implications in the field of cardiovascular tissue engineering.

Addresses
[1] Institut de Génétique et de Biologie Moléculaire et Cellulaire, 67404 Illkirch, France
[2] Centre National de la Recherche Scientifique, UMR7104, 67404 Illkirch, France
[3] Institut National de la Santé et de la Recherche Médicale, U964, 67404 Illkirch, France
[4] Université de Strasbourg, 67404 Illkirch, France

Corresponding author: Vermot, Julien (julien@igbmc.fr)
[5] These authors contributed equally.

Current Opinion in Genetics & Development 2019, **57**:106–116

This review comes from a themed issue on **Developmental mechanisms, patterning and evolution**

Edited by **Gáspár Jékely** and **Maria Ina Arnone**

For a complete overview see the Issue and the Editorial

Available online 3rd October 2019

https://doi.org/10.1016/j.gde.2019.08.002

Introduction

The development of the vertebrate cardiovascular system involves the morphogenesis of the heart from a simple tubular structure to its final complex form as well as the building of a vast network of blood vessels either through vasculogenesis or angiogenesis. Mechanical forces generated by heart contraction and blood flow play key roles in both of these developmental processes.

Various animal models have been used to improve our understanding of the role of mechanical forces caused by heartbeat and blood flow in cardiovascular morphogenesis, including mouse, chicken, and zebrafish. Signaling pathways and genes involved in cardiovascular development are best studied in the mouse and several transgenic lines that alter cardiac contractility or blood flow are available [1,2]. However, since mice develop within the mother, quantification, modelling and perturbation of mechanical forces and live imaging studies in mouse have been limited. Chicken embryos develop outside the mother and are therefore accessible to surgical interventions that alter blood flow. Chicken embryos have been particularly useful for studying early cardiovascular development when the embryos are optically accessible. However, there are few genetic tools available for this model. More recently, zebrafish has been a valuable addition to mouse and chicken models of cardiovascular development. Although, unlike humans, the zebrafish heart is two-chambered instead of four-chambered and its vasculature is specialized for aquatic environments [3], the optically clear zebrafish develop externally and facilitate the imaging of complex cardiovascular cell behaviors. Like mice, there is a vast and growing number of transgenic and mutant lines available. Additionally, zebrafish can survive without heartbeat throughout early stages of development [4], which enables experimental manipulations to impair heart contractility or blood flow not possible in mice or chicken.

Here, we review the role of mechanical forces caused by cardiac function on cardiovascular morphogenesis and its implications for cardiovascular tissue engineering. We first discuss recent advances on the impact of different mechanical forces and associated force parameters on cardiovascular morphogenesis. We then explore how endothelial and endocardial cells (ECs and EdCs respectively) convert mechanical signals into electrochemical activity, leading to changes in gene expression, cell behavior, and cell identity. In both sections, we focus our attention on *in vivo* studies. Finally, we extend our discussion to cardiovascular tissue engineering and examine the ways, in which our understanding of the interplays between mechanical forces, mechanical environment, and cell behaviors can improve technologies required for engineering efficient tissues.

Recent advances in the understanding of the mechanical forces regulating cardiovascular morphogenesis

Forces associated with cardiac function include wall shear stress (WSS), pressure, and circumferential stress due to

stretch. The response of cardiovascular cells to mechanical force is complex and often depends on the dynamics of the force amplitude and direction, as well as on the biological and mechanical environment. Uncovering the contribution of different forces and force parameters to developmental processes *in vivo* has proven challenging, but recent advances in computational modelling and imaging have successfully chipped away at the mystery surrounding how complex force patterns regulate key cardiovascular morphogenetic events.

Blood vessel lumen formation

The role of mechanical forces during blood vessel morphogenesis is one of the oldest and best-studied fields in mechanobiology [5–7]. Until recently, however, the role of mechanical forces in lumen formation during angiogenesis has not been appreciated. While lumen formation of early vessels occurs before the onset of circulation [8], strong evidence now suggests that blood flow can drive lumen formation during sprouting angiogenesis. Using the development of zebrafish intersegmental vessels as a model, it was found that blood flow drives lumen expansion by inducing spherical deformations of the apical membrane in endothelial tip cells (Figure 1a). These membrane intrusions are dynamic and cause the local and transient recruitment and contraction of actomyosin within the angiogenic sprout [9••]. The similarity of these membrane intrusions to blebs, whose growth is driven by intracellular pressure generated in the cytoplasm when the actin cortex undergoes actomyosin contractions [10], suggests that the formation of these membrane intrusions is driven by blood pressure. It would be interesting to assess if actomyosin is mechanosensitive during lumen formation as shown in other systems [11]. The role of blood plasma pressure have been addressed during the process of lumen spreading in the cranial vasculature of the zebrafish embryo between two endothelial tip cells that just meet and fuse [12••]. When endothelial tip cells meet, their filopodial activity is dramatically reduced (Figure 1b). In this minimal setting, the luminal pocket of each cells is simply deliminated by apical membrane insertion. As lumen growth under pressure, the apical membranes that connect the tip cells to their corresponding stalk cells are invaginating rapidly, and eventually connect to the *de novo* generated luminal pocket. Here, plasma blood pressure promotes these initial steps allowing the generation of a transcellular lumen (Figure 1b).

Pharyngeal arch artery network growth and remodeling

During the growth and remodeling of the bilaterally paired embryonic aortic arches into extracardiac great vessels, WSS is known to be correlated with developmental genes [13,14]. However, previous work in chicken that combines computational fluid dynamics simulations with a novel femtosecond laser-based method to obstruct blood flow in individual arch arteries showed that WSS alone cannot account for all hemodynamic adaptations of the vessel network [15]. A recent study describes a new imaging and image analysis pipeline that allows researchers to analyse the range and variability of pharyngeal arch

Figure 1

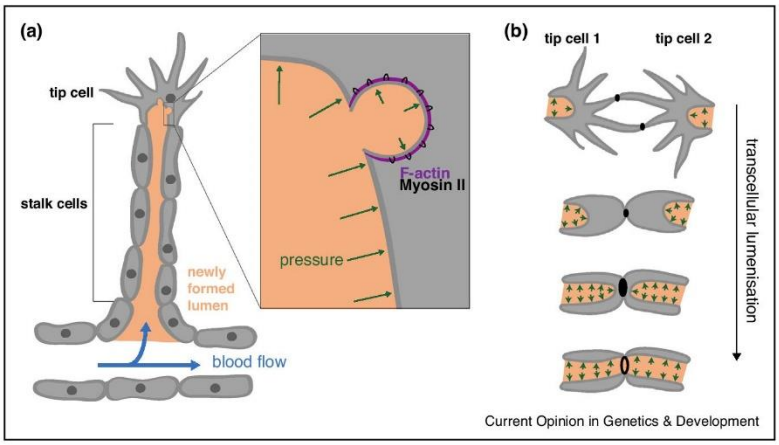

The importance of hemodynamics forces during lumen formation. **(a)** Schematic of flow-dependent lumen formation by inverse membrane blebbing, during sprouting angiogenesis. Blood flow drives lumen expansion by generating pressure differences between the luminal and the cytoplasmic sides of the apical membrane leading to inverse membrane blebbing at the tip position. Inverse membrane blebbing involves F-actin polymerization and myosin II recruitment in areas where membranes get deformed in response to pressure variations driven by heartbeat. Actomyosin contractility allows to modulate bleb formation and help guiding unidirectional lumen expansion. Adapted from Ref. [9••]. **(b)** Palatocerebral Artery Forms through Fusion of Two Lumenized Angiogenic Sprouts. Pressure is thought to allows growth of cell membrane invagination defining the newly formed lumen. When two cells meet (tip cell 1 and 2), pressure helps the transcellular lumen to go through contact sites (black rings) of both cells. Without pressure, unicellular tubes cannot form. Adapted from Ref. [12••].

artery network morphologies at different developmental stages and to computationally model hemodynamic forces acting on the network. This population-based study allowed the authors to provide a comprehensive atlas of chick pharyngeal arch artery network development and showed that although WSS acts as the primary driver of pharyngeal arch artery growth, a combination of pressure and WSS maps is necessary to predict many of the developmental changes [16••] (Figure 2).

Valve formation

Since the landmark study by Hove *et al.* in 2003 [17], numerous studies have highlighted the essential role of mechanical forces in valve formation [18••,19•,20–29]. Through the use of computational modelling and live imaging, it is known that the oscillatory component of WSS is able to predict both the expression levels of the mechanosensitive gene *klf2a* and the intracellular calcium levels of EdCs during early valvulogenesis [23] (Figure 3b). More recently, a similar approach has been used to determine the role of hemodynamic frequency harmonics during the convergent movement of tissues toward the atrioventricular canal (Figure 3a) [18••]. This latest study refines the *in silico* models to account for the non-homogeneity of blood and the WSS caused by red blood cell dynamics [18••]. In doing so, the authors found that the spatial patterns of the periodic components of WSS are similar in the heart tubes of both wild-type embryos and in mutant embryos lacking red blood cells, and that these periodic components are a good predictor of where the endocardial tissue will converge.

Trabeculation

Previous studies have shown that perturbing blood flow or heartbeat causes trabeculation defects [30–33], but our understanding of how spatial and temporal changes in mechanical forces regulate trabeculation remains limited. In zebrafish, the onset of trabeculation is marked by the delamination of cardiomyocytes to seed the trabecular layer [34]. This process involves the apical constriction of the delaminating myocardial cell, followed by the depolarization of the myocardial cell [35] (Figure 3c). Recently, a method combining selective plane illumination microscopy with computational fluid dynamics in zebrafish has enabled the quantification of 4D WSS in the moving ventricle [36]. These models revealed that endothelia experience high pulsatile WSS along trabecular ridges and high oscillatory WSS in trabecular grooves (Figure 3d) [37]. It has been postulated that cells of the ventricle are able to distinguish pulsatile versus

Figure 2

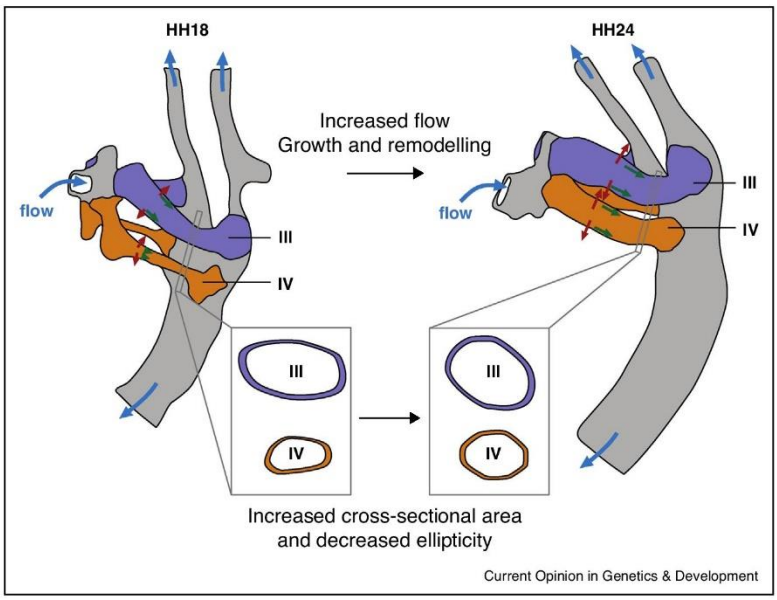

Recent high-resolution maps of vessel morphology and haemodynamic parameters suggest that the combination of wall shear stress and pulsatility (transmural pressure at peak flow minus the transmural pressure at the minimum flow) drives pharyngeal arch artery network remodeling in chick embryos. For example, between embryonic stages HH18 and HH24, changes in peak wall shear stress correlate with the increase in the cross-sectional area of the left IV arch, as well as changes in the minimum diameter of the left III arch and right IV arch. Changes in pulsatility are positively and negatively correlated to changes in the maximum and minimum diameter of the left III arch, respectively. (Wall shear stress: green arrows; pressure: red arrows; flow: blue arrows.) Adapted from Ref. [16••].

Figure 3

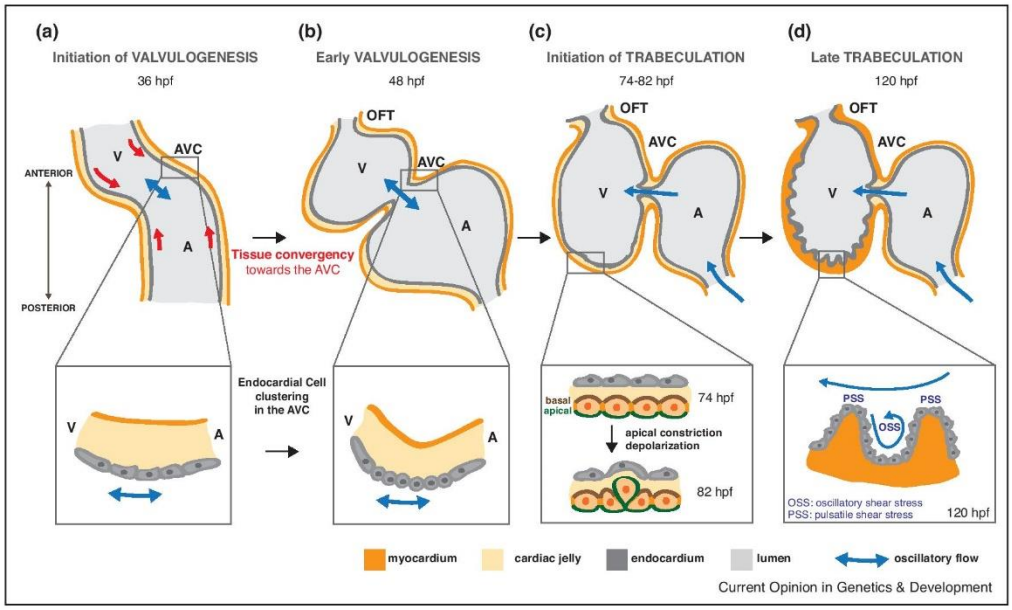

The importance of hemodynamics forces during early cardiac morphogenesis, valvulogenesis and trabeculation in zebrafish. **(a)** Schematic of the primary heart tube at 36hpf. The periodic components of shear stress are thought to drive the convergence of the EdCs toward the AVC (red arrows). **(b)** Oscillatory shear stress leads to cell clustering, locally at the AVC, at 48hpf. Adapted from Refs. [18••,27]. **(c)** Blood flow drives changes in cardiomyocyte apicobasal polarity and delamination leading to cardiac trabeculation. Adapted from Ref. [35]. **(d)** Pulsatile WSS along the trabecular ridges and oscillatory WSS in the trabecular grooves. Adapted from Ref. [37].

oscillatory WSS and respond differently to produce the ridges and grooves of trabeculae [37]. Testing this hypothesis will require further studies that combine 4D modelling with simultaneous imaging of the heart at cellular resolution to see if the grooves and ridges observed in the models correlates to areas where trabeculation is initiated. Given the sensitivity of blood flow patterns to changes in morphology and blood rheology [38], it will be interesting to measure WSS and morphological variation across individuals and species to see whether WSS can predict intra-species and inter-species differences in trabeculae location and morphology.

Mechanotransduction pathways mediating the cell response to forces during cardiovascular morphogenesis

Cardiovascular cells have diverse behavioral responses to heartbeat and blood flow, and studies over the years have established the existence of multiple force sensors as well as mechanosensitive signaling pathways and gene sets (Table 1). Although various cell types in the cardiovascular system are responsive to mechanical forces caused by heartbeat and blood flow, we choose to only discuss mechanotransduction pathways found in ECs and EdCs, where the field is most mature and where a number of exciting discoveries have recently been made.

Direct force transducers and sensory organelles

Perhaps the best established mechanosensitive machinery in ECs is the junctional complex, which comprises PECAM1, VE-cadherin, VEGFR2 [39••], and VEGFR3 [40] (Figure 4). Pulling on this complex using magnetic tweezers in cultured cells demonstrated direct mechanotransduction by PECAM1, which leads to downstream VEGFR signalling [39••,41]. This complex is well known to modulate EC alignment in response to WSS *in vivo* [39••] and modulate blood vessel compliance by altering extra cellular matrix assembly [42]. More recently, the transmembrane heparin sulfate proteoglycan receptor syndecan-4 [43] emerged as another regulator of WSS-induced EC alignment [44]. In addition to flow, Syndecan-4 is a central mediator of cell adhesion, migration, proliferation, endocytosis, and mechanotransduction *in vivo* [45] and has the ability to respond to directly applied mechanical tension in cultured EC [46]. In endothelial cells, Syndecan-4 plays a critical role in sensing flow direction to promote cell alignment and inhibit atherosclerosis [44]. Interestingly, both PECAM and Syndecan-4, are important to modulate lymphatic vasculature development, which is known to depend on WSS [47] (Figure 4).

Table 1

Mechanotransduction pathways and cell responses involved in cardiovascular morphogenesis

Tissue	Mechanosensor	Gene or pathway activated	Mechanical stimulus (shear dyn/cm^2 flow velocity μm/sec)	Cell response (tissue, animal model)	Reference
Blood vessel	VE-cadherin PECAM-1 VEGFR2/VEGFR3	 Src PI(3)K leading to integrin activation	Stretch/flow: 12 dyn/cm^{2a}	Vascular remodeling, angiogenic sprouting (intersegmental vessel, ZF)	[39**,48]
	Primary cilia Trpp2	$Ca2^+$	Blood flow Hertbeat: 2.63 ± 0.17 Hz Blood flow velocities (peak; mean): 883 ± 118 μm/s; 192 ± 13 μm/s (AA) 1159 ± 187 μm/s; 170 ± 15 μm/s (LDA)	Vascular remodeling (vascular plexus, ZF)	[55]
	Primary cilia	BMP signaling (Bmp9)	Shear stress: 2 dyn/cm^2 (HUVECs)	Vessel connection stabilization in the retina (endothelium of the retina, mouse)	[76]
	Not assessed	Endoglin	Not assessed	Vessel diameter control (endothelium, ZF)	[75]
	Not assessed	Yap Taz	Shear stress: 15 dyn/cm^2 (HPAECs)	Blood vessel maintenance (endothelium, ZF)	[71**]
	Apelin receptor	Klf2	Shear stress: 12 dyn/cm^2 (HUVECs)	Cell polarity changes: against the direction of the flow in vessels (endothelium, ZF)	[82**]
Lymphatic valve	Piezo channels (Piezo1)	Foxc2, Gata2, Cx37	Oscillatory lymphatic flow	Valve morphogenesis (lymphatic vessels, mouse)	[53,97]
Heart valve (atrioventricular canal)	TRP channels (Trpp2, Trpv4)	$Ca2^+$ *klf2a* *wnt9b* *fibronectin1b*	 Blood velocity V_{max} ~5 mm/s 61 dyn/cm^2	 AVC valve morphogenesis: regulation of synthesis (endocardium, ZF)	[21,23,27]
Heart valve (outflow tract)	Piezo1, Trpp2	Yap1, *klf2a*, *notch1b*	Blood flow from 56 hpf: forward flow: +3.6 mm/s retrograde flow: −1.2 mm/s 120hpf: forward flow: +9.9 mm/s no retrograde flow	OFT valve development (endocardium, ZF)	[19*]
Heart trabeculation	Not assessed	*klf2a* fgf signaling	Not assessed	Trabeculation, maintenance of myocardial wall integrity (ventricular myocardium, ZF)	[67]
	Not assessed	*notch1b*	Oscillatory shear stress: 0 ± 3 dyn cm^{-2} with 0 net flow	Trabeculation (ventricle, ZF)	[37]

ZF = Zebrafish, AA = Aortic Arches, LDA = Lateral Dorsal Arteries, HUVECs = Human Umbilical Vein Endothelial Cells, HPAECs = Human Pulmonary Artery Endothelial Cells.
[a] Measurements performed using magnetic beads (max force on a 4.5 μm diameter bead of ~130 pN, ~10% of the grad force exerted by shear stress on a 30 μm × 30 μm endothelial cells).

Figure 4

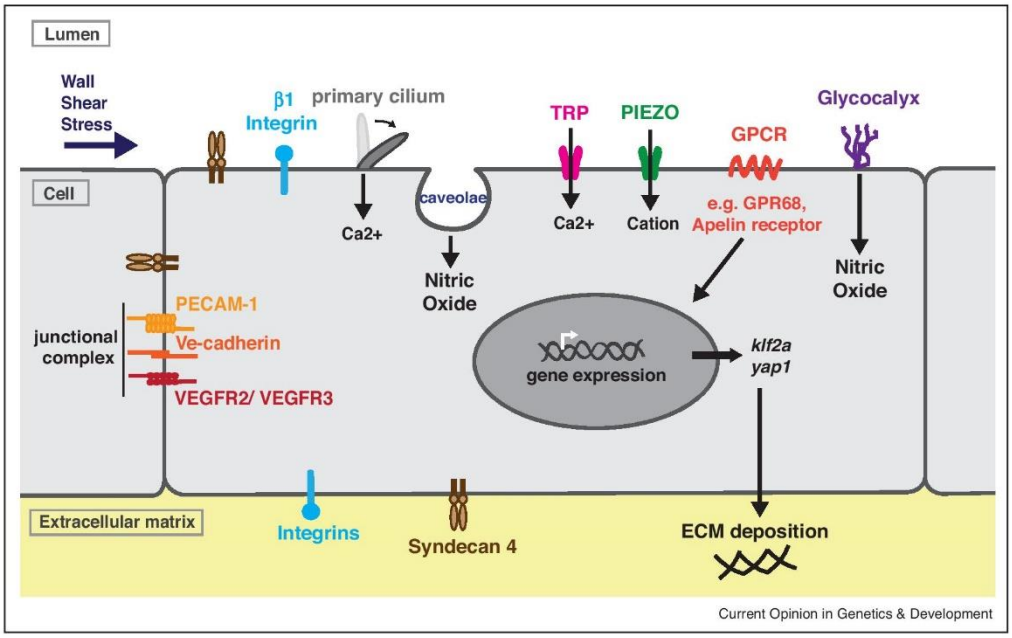

Mechanosensors and mechanotransduction pathways involved in cardiovascular development (*in vivo* and *in vitro*): transduction of hemodynamic forces toward cell responses. On the cell surface, junctional complexes (PECAM-1, Ve-cadherin, VEGFR2–VEGFR3), the stretch-activated ion channels TRP, PIEZO, as well as β1 Integrin, Syndecan4, GPCR, caveolae, glycocalyx and primary cilium act as mechanosensors. Downstream of the mechanosensitive channels, different signaling pathways and gene expression are activated.

VE-cadherin is required during vascular development [12••,48] although whether VE-cadherin is involved in sensing mechanical forces associated with cardiac function during development is unclear. Acute termination of blood flow during zebrafish dorsal aorta maturation does not cause detectable changes in VE-cadherin tension as measured using a FRET (Förster resonance energy transfer) sensor, suggesting blood flow plays little role in the maintenance of tension through VE-cadherin in developing arteries [49••]. Stretch-activated ion channels have been shown to serve as additional mechanosensors whose rapid activation and inactivation rates may account for the capacity of ECs to decode subsecond-frequency characteristics [50,51]. In particular, Piezo1 ion channels have been shown to be important for heart valve formation and vascular development in vertebrates [19•,20,52–54]. The potent mechanosensitive channels from the transient receptor potential family, Trpp2 and Trpv4, have been shown to be expressed in EdCs and are necessary for both heart valve and vascular development [23,52,55] (Figure 4). Stretch activated ion channels are often considered as the initial mechanosensitive trigger leading to cell response. However, the precise mechanism of action of these channels, including whether or not they act as direct mechanosensors, remains to be systematically established [23,52]. Nevertheless, it was recently established that β1-integrins can sense specifically unidirectional flow *in vitro*, leading to intracellular calcium signalling through Piezo1 and Trpv4 and trigger the alignment of the ECs [56••] (Figure 4). Beyond junctional complexes and ion channels, G Protein-Coupled Receptors, long suspected to be direct mechanosensors, have recently been shown to function as shear sensors in ECs of small-diameter arteries *in vivo* [57••]. The thin layer of biopolymers such as glycolipids, glycoproteins, and proteoglycans located on the surface of ECs called glycocalyx is also regularly discussed as an important mechanosensitive system. In ECs, the glycocalyx is a significant mediator of NO production and is known to modulate vascular development [58]. Recent *in cellulo* study provided direct evidences of the mechanosensitivity of glycocalyx by using atomic force microscopy to apply force selectively on the glycocalyx for regulating the production of endothelial nitric oxide in response to fluid shear stress [59]. In addition, it was recently demonstrated in isolated cells that the biopolymer density in glycocalyx can define cell membrane curvature and, ultimately, its shape [60••]. These observations certainly promotes a different view on how glycocalyx can impact ECs mechanosensitivity and morphogenetic processes involving cell shape changes in the cardiovascular system.

Mechanosensitive organelles such as primary cilia and caveolae constitute intriguing elements potentially involved in providing cell sensitivity to WSS. Cilia have been shown to play a role during early stages of vessel development in regions of lower shear where they bend in response to flow [55] (Figure 4) as well as in arteries where endothelial cilia are required for the activation of Notch signalling and vascular mural cell recruitment [61]. Caveolae are specialized type of lipid raft composing the plasma cell membrane. Endothelial cells express high levels of Cav-1, which is involved in endothelial inflammation, adhesion, and phagocytosis [62]. Endothelial Cav-1 regulates endothelial NO production, microvascular permeability and vascular remodelling in response to mechanical signals [63]. In addition, caveolae have been proposed to help buffering membrane tension surges in response to mechanical stress [64]. Considering the diversity of mechanical stresses are generated in the developing vascular and cardiac system [18••,55,65,66], it will be interesting to address if any of these stresses can impact endothelial caveolae and their function during cardiovascular morphogenesis.

Signalling pathways and gene expression

Downstream of the mechanosensitive channels, one of the most studied flow-responsive genes in cardiovascular development is the zinc-finger transcription factor Krüppel-like factor 2 [21,27,29,67,68]. Klf2 is expressed upon mechanical forces and is vital for mammalian cardiovascular development [21,69]. Various studies in zebrafish have complemented studies in mouse and provided additional insights into the role of klf2 in cardiovascular development. It was first shown that *klf2a* was highly expressed in the endocardium of the developing zebrafish atrioventricular valve leaflet and is essential for proper valve formation [27]. It was then shown that *klf2a* expression levels depend on the oscillatory flow amplitude in the atrioventricular canal and the presence of Trp channels [23]. Furthermore, *klf2a* regulates the deposition of extracellular matrix proteins, such as *fibronectin1b* [27]. In an atherosclerosis pathological context, Syndecan-4 depleted mice show poor EC alignment in the flow direction and complementary *in vitro* experiments showed that Syndecan-4 depleted HUVECs increase pro-inflammatory NF-kB pathway and decrease anti-inflammatory KLF2 and KLF4 induction [44] (Figure 4). Moreover, *klf2* has been known to play a role during trabeculation by maintaining myocardial wall integrity by modulating Fgf signalling [67] and during valve formation by regulating canonical Wnt signalling in the neighboring mesenchymal cells, leading to cushion remodelling and valve morphogenesis [21]. Interestingly, non-canonical Wnt signalling is also important to raise the threshold of WSS above which EdCs change their properties [70]. This work highlights the complex feedback loop operating to modulate the response to flow.

Blood flow is also a potent regulator of Yap1 localization in ECs [71] and is thought to modulate vessel development by lowering BMP signalling [72]. In particular, Yap1 is translocated into the nucleus of zebrafish ECs and cultured cells in response to blood flow [71]. In zebrafish, Yap1 expression is modulated by Piezo1 and Trpp2 during OFT valve development [19•] (Figure 4). In addition, it has been shown that YAP and its paralog WWTR1 (TAZ) respond to disturbed flow in lymphatic ECs *in vitro* [73••]. Thus, Yap1 is certainly an important player of the mechanosensitive response activated during cardiovascular development.

In addition to these flow-responsive pathways acting in ECs, the BMP–ALK1/End–SMAD pathway also recently emerged as an important player in both endothelial flow responses and vessel stability [70,74–77]. Indeed, blood flow promotes the association of the Endoglin and Alk1 tyrosine kinase that triggers the activity and phosphorylation of Smad1/5/8 at low concentrations of Bmp9, leading to the recruitment of mural cells and therefore vessel quiescence [70,74,76]. Mechanosensitivity may take place through mechanosensitive primary cilia in regions of low shear levels as it has been shown that primary cilia modulate BMP activity [76].

Cell behavior

ECs and EdCs respond and adapt to stress by altering their cytoskeleton, shape, patterns of gene activity and internal organization. Flow triggers association of PECAM with vimentin, which transmits myosin-generated forces to PECAM and therefore vascular remodeling [78]. At the cellular level, the regulation of contractility via the actomyosin network controls cell rearrangements and migration during vessel growth [79•]. In addition, blood flow causes ECs to elongate and align following the flow direction [75]. EdCs of the heart ventricle also change shape in response to heart function by elongating and getting smaller as cell number increases [80]. Finally, ECs orient against the direction of flow in developing blood vessels at low shear levels [70]. This polarity change can be accompanied by cell migration to remodel the blood vessel network into arteries and vein remodeling in response to Notch signaling [81,98]. Polarization and cell migration within maturing blood vessels are dependent on the Apelin receptor [82••], a potential mechanosensitive g-protein acting through beta-arrestin. Here, it seems that klf2 expression activated by the Apelin receptor is required to set cell polarity, establishing an exciting link between cell response to force and morphogenesis.

The use of mechanical forces in cardiovascular tissue engineering

Deciphering how hemodynamic forces control cell behaviors during cardiovascular morphogenesis have strong implications in cardiac tissue engineering, which aims to restore the function of a damaged tissue by replacing it

with a biomimetic construct [83]. The understanding of how ECs and EdCs sense and respond to mechanical forces helps to design adequate approaches for engineering cardiovascular tissue. Moreover, knowing the hemodynamic forces in place within the developing heart and blood vessels should help to develop and improve approaches aiming at engineering heart valves and blood vessels *de novo*. Interestingly, tissue engineering requires a deep understanding of the mechanical and biochemical environment the cells experience.

Tissue Engineered Blood Vessels (TEBV)

TEBV requires smooth muscle cells and EdCs that are incorporated into a tubular scaffold in order to mimic a native blood vessel [84]. Angiogenesis is a crucial step as it is required in nearly all types of tissue engineering and is largely dependent upon mechanical forces. *In vitro*, it has been shown that the differentiation of pluripotent stem cells (PSCs) into EdCs can be robustly promoted by exposing them to fluid shear stress within embryoid bodies [85]. This approach could be applied to promote pre-vascularization of tissue-engineered vessels derived from PSCs [85]. During vessel formation in 3D Gelfoam scaffolds cocultured with EdCs and fibroblasts, static stretch induces parallel vessel orientation whereas the orientation becomes diagonal under cyclic stretching [86]. Like in the embryo and in regenerative processes, the host environment surrounding the transplanted engineered tissue adds another layer of complexity. For example, the implantation of a vascular network whose orientation has been controlled *in vitro* to match that of the host tissue improves graft integration [86]. Moreover, in an *in vivo* rat bone wound healing model, it has been demonstrated that mechanical conditions of the surrounding environment modulate neovascular growth and remodeling [87]. They showed that an early mechanical loading impaired regeneration as it disrupted the formation of new vessels. However, delayed mechanical loading stimulated the neovascular remodeling and therefore regeneration [87]. Thus, it is essential to integrate mechanical forces for creating relevant and successful TEBV.

Tissue Engineered Heart Valves (TEHV)

The replacement of defective heart valves with mechanical heart valves or bi-leaflet valves have often been associated with the production of non-physiological flow patterns that could lead to thromboembolism [88,89]. Bioprosthetic valves produce more physiological flow patterns but are often degraded after a few years [90]. TEHV is therefore needed, especially for young patients, where full integration and remodeling of the implanted valve is essential [91]. The latest progress in this field is the development of personalized 3D-printed cardiovascular prostheses leading to the proper design of TEHVs that will reproduce physiological forces [92]. Yet, the complexity of the valve leaflet is only starting to be better understood, and different cell types within the valve can influence key aspects of valve pathology [93]. Shear stress can also be used to activate endothelial-to-mesenchymal transition of adult endothelial cells *in vitro* [94]. This suggests that the developmental program can be reactivated in adult, differentiated tissues and illustrate how cardiogenesis and cardiac tissue engineering are complementary.

Conclusions and outlook

Heart mechanics and blood flow have diverse roles in cardiovascular development. This diversity could in part be explained by the sensitivity of ECs and EdCs to subtle differences in force profiles and their potential to activate discrete signaling pathways that, in turn, will modulate different cell behaviors. In the embryo, force profiles experienced by EdCs are constantly changing as heart function and the geometry of the heart and vascular network changes. Despite this diversity, the basic principles associated with cardiovascular morphogenesis are conserved and certainly are key to improving cardiovascular tissue engineering. Advances in our understanding of these basic principles will help achieve the production of truly functional engineered tissues that generate the same hemodynamic forces as native ones. More work needs to be done in order to understand how EdCs integrate environmental information so that the heart and blood vessels develop harmoniously. In addition, understanding heart valve cell lineage *in vivo* will be essential for mimicking valve maturation *in vitro* [99]. Lastly, the recent advances in live imaging applied to mouse models will be key to moving the field forward [95••,96••].

Conflict of interest statement

Nothing declared.

Acknowledgements

This project has received funding from the European Research Council (ERC) under the European Union's Horizon 2020 research and innovation programme: GA N°682939 and an ANR (liveheart-ANR-15-CE13-0015). AL Duchemin and R. Chow are supported by a post-doctoral fellowship from the Lefoullon-Delalande fondation.

References and recommended reading

Papers of particular interest, published within the period of review, have been highlighted as:

- • of special interest
- •• of outstanding interest

1. Hwa JJ, Beckouche N, Huang L, Kram Y, Lindskog H, Wang RA: **Abnormal arterial-venous fusions and fate specification in mouse embryos lacking blood flow**. *Sci Rep* 2017, **7**:11965.
2. Lucitti JL, Jones EA, Huang C, Chen J, Fraser SE, Dickinson ME: **Vascular remodeling of the mouse yolk sac requires hemodynamic force**. *Development* 2007, **134**:3317-3326.
3. Hogan BM, Schulte-Merker S: **How to plumb a pisces: understanding vascular development and disease using zebrafish embryos**. *Dev Cell* 2017, **42**:567-583.
4. Sehnert AJ, Huq A, Weinstein BM, Walker C, Fishman M, Stainier DY: **Cardiac troponin T is essential in sarcomere assembly and cardiac contractility**. *Nat Genet* 2002, **31**:106-110.

5. Freund JB, Goetz JG, Hill KL, Vermot J: **Fluid flows and forces in development: functions, features and biophysical principles**. *Development* 2012, **139**:1229-1245.

6. Hoefer IE, den Adel B, Daemen MJ: **Biomechanical factors as triggers of vascular growth**. *Cardiovasc Res* 2013, **99**:276-283.

7. Roman BL, Pekkan K: **Mechanotransduction in embryonic vascular development**. *Biomech Model Mechanobiol* 2012, **11**:1149-1168.

8. Isogai S, Lawson ND, Torrealday S, Horiguchi M, Weinstein BM: **Angiogenic network formation in the developing vertebrate trunk**. *Development* 2003, **130**:5281-5290.

9. •• Gebala V, Collins R, Geudens I, Phng LK, Gerhardt H: **Blood flow drives lumen formation by inverse membrane blebbing during angiogenesis in vivo**. *Nat Cell Biol* 2016, **18**:443-450.
This imaging-based study provides another look at blood vessel lumen formation by focusing on the local membrane curvature generated at time of lumenization. The authors document an unexpected actomyosin accumulation in areas when cell membrane deformation does not follow the axis of lumen elongation. Through its contracting activity, actomyosin counteract pressure driven membrane deformation and promotes unidirectional lumen formation.

10. Paluch EK, Raz E: **The role and regulation of blebs in cell migration**. *Curr Opin Cell Biol* 2013, **25**:582-590.

11. Sumi A, Hayes P, D'Angelo A, Colombelli J, Salbreux G, Dierkes K, Solon J: **Adherens junction length during tissue contraction is controlled by the mechanosensitive activity of actomyosin and junctional recycling**. *Dev Cell* 2018, **47**:453-463 e453.

12. •• Lenard A, Ellertsdottir E, Herwig L, Krudewig A, Sauteur L, Belting HG, Affolter M: **In vivo analysis reveals a highly stereotypic morphogenetic pathway of vascular anastomosis**. *Dev Cell* 2013, **25**:492-506.
Using high resolution live imaging, the authors assess the progression of lumen formation that occurs during blood vessel morphogenesis in the cranial vasculature of the zebrafish embryo. They could describe for the first time the early steps of the membrane fusion process leading to lumen formation between two meeting cells and the requirement of blood plasma pressure in the process.

13. Karakaya C, Goktas S, Celik M, Kowalski WJ, Keller BB, Pekkan K: **Asymmetry in mechanosensitive gene expression during aortic arch morphogenesis**. *Sci Rep* 2018, **8**:16948.

14. Goktas S, Uslu FE, Kowalski WJ, Ermek E, Keller BB, Pekkan K: **Time-series interactions of gene expression, vascular growth and hemodynamics during early embryonic arterial development**. *PLoS One* 2016, **11**:e0161611.

15. Lindsey SE, Menon PG, Kowalski WJ, Shekhar A, Yalcin HC, Nishimura N, Schaffer CB, Butcher JT, Pekkan K: **Growth and hemodynamics after early embryonic aortic arch occlusion**. *Biomech Model Mechanobiol* 2015, **14**:735-751.

16. •• Lindsey SE, Butcher JT, Vignon-Clementel IE: **Cohort-based multiscale analysis of hemodynamic-driven growth and remodeling of the embryonic pharyngeal arch arteries**. *Development* 2018, **145**.
This population-based study provides a comprehensive atlas of chick pharyngeal arch artery network development that provides quantitative information about morphological variability. It also calculates the correlation between various force parameters and morphological changes, thereby showing that WSS acts as the primary driver of pharyngeal arch artery growth, while pressure acts as a secondary driver.

17. Hove JR, Koster RW, Forouhar AS, Acevedo-Bolton G, Fraser SE, Gharib M: **Intracardiac fluid forces are an essential epigenetic factor for embryonic cardiogenesis**. *Nature* 2003, **421**:172-177.

18. •• Boselli F, Steed E, Freund JB, Vermot J: **Anisotropic shear stress patterns predict the orientation of convergent tissue movements in the embryonic heart**. *Development* 2017, **144**:4322-4327.
This study showed that tissue convergence during zebrafish atrioventricular canal development is associated with the direction of mean wall shear stress and the gradient of harmonic phase-averaged shear stresses, rather than the time-averaged direction of flow which is what usually seen in developing blood vessels. This suggests that the shear stress patterns rather than flow directionality are potential determinants of the flow dependent morphogenetic events in the cardiovascular system.

19. • Duchemin AL, Vignes H, Vermot J: **Mechanically activated Piezo channels control outflow tract valve development through Yap1 and Klf 2-Notch signaling axis**. *Elife* 2019:8.
This work demonstrates that Piezo is a central modulator of the cell response to mechanical forces during the morphogenetic processes associated with heart valve formation (see also 20) and provides identify yap1, klf2a and Notch as downstream effectors activated in response to forces.

20. Faucherre A, Moha ou Maati H, Nasr N, Pinard H, Theron A, Odelin G, Desvignes JP, Salgado D, Collod Beroud G, Avierinos JF, et al.: **Piezo1 is required for outflow tract and aortic valve development**. https://doi.org/10.1101/528588.

21. Goddard LM, Duchemin AL, Ramalingan H, Wu B, Chen M, Bamezai S, Yang J, Li L, Morley MP, Wang T *et al.*: **Hemodynamic forces sculpt developing heart valves through a KLF2-WNT9B paracrine signaling axis**. *Dev Cell* 2017, **43**:274-289 e275.

22. Gould RA, Yalcin HC, MacKay JL, Sauls K, Norris R, Kumar S, Butcher JT: **Cyclic mechanical loading is essential for Rac1-mediated elongation and remodeling of the embryonic mitral valve**. *Curr Biol* 2016, **26**:27-37.

23. Heckel E, Boselli F, Roth S, Krudewig A, Belting HG, Charvin G, Vermot J: **Oscillatory flow modulates mechanosensitive klf2a expression through trpv4 and trpp2 during heart valve development**. *Curr Biol* 2015, **25**:1354-1361.

24. Menon V, Eberth JF, Goodwin RL, Potts JD: **Altered hemodynamics in the embryonic heart affects outflow valve development**. *J Cardiovasc Dev Dis* 2015, **2**:108-124.

25. Pestel J, Ramadass R, Gauvrit S, Helker C, Herzog W, Stainier DY: **Real-time 3D visualization of cellular rearrangements during cardiac valve formation**. *Development* 2016, **143**:2217-2227.

26. Slough J, Cooney L, Brueckner M: **Monocilia in the embryonic mouse heart suggest a direct role for cilia in cardiac morphogenesis**. *Dev Dyn* 2008, **237**:2304-2314.

27. Steed E, Faggianelli N, Roth S, Ramspacher C, Concordet JP, Vermot J: **klf2a couples mechanotransduction and zebrafish valve morphogenesis through fibronectin synthesis**. *Nat Commun* 2016, **7**:11646.

28. Tan H, Biechler S, Junor L, Yost MJ, Dean D, Li J, Potts JD, Goodwin RL: **Fluid flow forces and rhoA regulate fibrous development of the atrioventricular valves**. *Dev Biol* 2013, **374**:345-356.

29. Vermot J, Forouhar AS, Liebling M, Wu D, Plummer D, Gharib M, Fraser SE: **Reversing blood flows act through klf2a to ensure normal valvulogenesis in the developing heart**. *PLoS Biol* 2009, **7**:e1000246.

30. Peshkovsky C, Totong R, Yelon D: **Dependence of cardiac trabeculation on neuregulin signaling and blood flow in zebrafish**. *Dev Dyn* 2011, **240**:446-456.

31. Cherian AV, Fukuda R, Augustine SM, Maischein HM, Stainier DY: **N-cadherin relocalization during cardiac trabeculation**. *Proc Natl Acad Sci U S A* 2016, **113**:7569-7574.

32. Samsa LA, Givens C, Tzima E, Stainier DY, Qian L, Liu J: **Cardiac contraction activates endocardial Notch signaling to modulate chamber maturation in zebrafish**. *Development* 2015, **142**:4080-4091.

33. Lee J, Fei P, Packard RR, Kang H, Xu H, Baek KI, Jen N, Chen J, Yen H, Kuo CC *et al.*: **4-Dimensional light-sheet microscopy to elucidate shear stress modulation of cardiac trabeculation**. *J Clin Invest* 2016, **126**:1679-1690.

34. Staudt DW, Liu J, Thorn KS, Stuurman N, Liebling M, Stainier DY: **High-resolution imaging of cardiomyocyte behavior reveals two distinct steps in ventricular trabeculation**. *Development* 2014, **141**:585-593.

35. Jimenez-Amilburu V, Rasouli SJ, Staudt DW, Nakajima H, Chiba A, Mochizuki N, Stainier DYR: **In vivo visualization of cardiomyocyte apicobasal polarity reveals epithelial to mesenchymal-like transition during cardiac trabeculation**. *Cell Rep* 2016, **17**:2687-2699.

36. Vedula V, Lee J, Xu H, Kuo CJ, Hsiai TK, Marsden AL: **A method to quantify mechanobiologic forces during zebrafish cardiac development using 4-D light sheet imaging and computational modeling**. *PLoS Comput Biol* 2017, **13**:e1005828.

37. Lee J, Vedula V, Baek KI, Chen J, Hsu JJ, Ding Y, Chang CC, Kang H, Small A, Fei P *et al.*: **Spatial and temporal variations in hemodynamic forces initiate cardiac trabeculation**. *JCI Insight* 2018, **3**.

38. Battista NA, Douglas DR, Lane AN, Samsa LA, Liu J, Miller LA: **Vortex dynamics in trabeculated embryonic ventricles**. *J Cardiovasc Dev Dis* 2019, **6**.

39. •• Tzima E, Irani-Tehrani M, Kiosses WB, Dejana E, Schultz DA, Engelhardt B, Cao G, DeLisser H, Schwartz MA: **A mechanosensory complex that mediates the endothelial cell response to fluid shear stress**. *Nature* 2005, **437**:426-431.
This landmark study establishes the first comprehensive description of a mechanosensory complex active in endothelial cells.

40. Coon BG, Baeyens N, Han J, Budatha M, Ross TD, Fang JS, Yun S, Thomas JL, Schwartz MA: **Intramembrane binding of VE-cadherin to VEGFR2 and VEGFR3 assembles the endothelial mechanosensory complex**. *J Cell Biol* 2015, **208**:975-986.

41. Collins C, Guilluy C, Welch C, O'Brien ET, Hahn K, Superfine R, Burridge K, Tzima E: **Localized tensional forces on PECAM-1 elicit a global mechanotransduction response via the integrin-RhoA pathway**. *Curr Biol* 2012, **22**:2087-2094.

42. Collins C, Osborne LD, Guilluy C, Chen Z, O'Brien ET 3rd, Reader JS, Burridge K, Superfine R, Tzima E: **Haemodynamic and extracellular matrix cues regulate the mechanical phenotype and stiffness of aortic endothelial cells**. *Nat Commun* 2014, **5**:3984.

43. Elfenbein A, Lanahan A, Zhou TX, Yamasaki A, Tkachenko E, Matsuda M, Simons M: **Syndecan 4 regulates FGFR1 signaling in endothelial cells by directing macropinocytosis**. *Sci Signal* 2012, **5** ra36.

44. Baeyens N, Mulligan-Kehoe MJ, Corti F, Simon DD, Ross TD, Rhodes JM, Wang TZ, Mejean CO, Simons M, Humphrey J *et al.*: **Syndecan 4 is required for endothelial alignment in flow and atheroprotective signaling**. *Proc Natl Acad Sci U S A* 2014, **111**:17308-17313.

45. Elfenbein A, Simons M: **Syndecan-4 signaling at a glance**. *J Cell Sci* 2013, **126**:3799-3804.

46. Bellin RM, Kubicek JD, Frigault MJ, Kamien AJ, Steward RL Jr, Barnes HM, Digiacomo MB, Duncan LJ, Edgerly CK, Morse EM *et al.*: **Defining the role of syndecan-4 in mechanotransduction using surface-modification approaches**. *Proc Natl Acad Sci U S A* 2009, **106**:22102-22107.

47. Wang Y, Baeyens N, Corti F, Tanaka K, Fang JS, Zhang J, Jin Y, Coon B, Hirschi KK, Schwartz MA *et al.*: **Syndecan 4 controls lymphatic vasculature remodeling during mouse embryonic development**. *Development* 2016, **143**:4441-4451.

48. Sauteur L, Krudewig A, Herwig L, Ehrenfeuchter N, Lenard A, Affolter M, Belting HG: **Cdh5/VE-cadherin promotes endothelial cell interface elongation via cortical actin polymerization during angiogenic sprouting**. *Cell Rep* 2014, **9**:504-513.

49. •• Lagendijk AK, Gomez GA, Baek S, Hesselson D, Hughes WE, Paterson S, Conway DE, Belting HG, Affolter M, Smith KA *et al.*: **Live imaging molecular changes in junctional tension upon VE-cadherin in zebrafish**. *Nat Commun* 2017, **8**:1402.
This study used a FRET-based VE-cadherin tension sensor to study zebrafish dorsal aorta development. The authors found that tension across VE-cadherin is associated with actomyosin contractility within endothelial cells, and that acute termination of blood flow does not noticeably affect VE-cadherin tension levels.

50. Lewis AH, Cui AF, McDonald MF, Grandl J: **Transduction of repetitive mechanical stimuli by Piezo1 and Piezo2 ion channels**. *Cell Rep* 2017, **19**:2572-2585.

51. Coste B, Xiao B, Santos JS, Syeda R, Grandl J, Spencer KS, Kim SE, Schmidt M, Mathur J, Dubin AE *et al.*: **Piezo proteins are pore-forming subunits of mechanically activated channels**. *Nature* 2012, **483**:176-181.

52. Li J, Hou B, Tumova S, Muraki K, Bruns A, Ludlow MJ, Sedo A, Hyman AJ, McKeown L, Young RS *et al.*: **Piezo1 integration of vascular architecture with physiological force**. *Nature* 2014, **515**:279-282.

53. Nonomura K, Lukacs V, Sweet DT, Goddard LM, Kanie A, Whitwam T, Ranade SS, Fujimori T, Kahn ML, Patapoutian A: **Mechanically activated ion channel PIEZO1 is required for lymphatic valve formation**. *Proc Natl Acad Sci U S A* 2018, **115**:12817-12822.

54. Ranade SS, Qiu Z, Woo SH, Hur SS, Murthy SE, Cahalan SM, Xu J, Mathur J, Bandell M, Coste B *et al.*: **Piezo1, a mechanically activated ion channel, is required for vascular development in mice**. *Proc Natl Acad Sci U S A* 2014, **111**:10347-10352.

55. Goetz JG, Steed E, Ferreira RR, Roth S, Ramspacher C, Boselli F, Charvin G, Liebling M, Wyart C, Schwab Y *et al.*: **Endothelial cilia mediate low flow sensing during zebrafish vascular development**. *Cell Rep* 2014, **6**:799-808.

56. •• Xanthis I, Souilhol C, Serbanovic-Canic J, Roddie H, Kalli AC, Fragiadaki M, Wong R, Shah DR, Askari JA, Canham L *et al.*: **beta1 integrin is a sensor of blood flow direction**. *J Cell Sci* 2019, **132**.
The authors use a nice combination of flow systems and magnetic tweezers to show that β1 integrin is a key sensor of force direction in endothelial cells. They show that β1 integrin is activated at sites of unidirectional flow and at sites of bidirectional flow. This suggests the interesting possibility that β1 integrin sensing of unidirectional force is important for decoding blood flow mechanics *in vivo*.

57. •• Xu J, Mathur J, Vessieres E, Hammack S, Nonomura K, Favre J, Grimaud L, Petrus M, Francisco A, Li J *et al.*: **GPR68 senses flow and is essential for vascular physiology**. *Cell* 2018, **173**:762-775 e716.
This study describes the isolation and identification of a novel endothelial flow sensor in endothelial cells. GPR68 is necessary and sufficient for mechanosenzation in cells. The study is remarkable for two reasons: it implicate g protein-coupled receptor in mechanosenzation is a gpcr and it shows it function in in small diameter blood vessel. The latter suggest that mechanosensitive proteins are optimized for specific type of stimuli and that there are numerous other mechanosensors to discover.

58. Henderson-Toth CE, Jahnsen ED, Jamarani R, Al-Roubaie S, Jones EA: **The glycocalyx is present as soon as blood flow is initiated and is required for normal vascular development**. *Dev Biol* 2012, **369**:330-339.

59. Bartosch AMW, Mathews R, Tarbell JM: **Endothelial glycocalyx-mediated nitric oxide production in response to selective AFM pulling**. *Biophys J* 2017, **113**:101-108.

60. •• Shurer CR, Kuo JC, Roberts LM, Gandhi JG, Colville MJ, Enoki TA, Pan H, Su J, Noble JM, Hollander MJ *et al.*: **Physical principles of membrane shape regulation by the glycocalyx**. *Cell* 2019, **177**:1757-1770 e1721.
This paper describes new principle of cell shape regulation dictated by the plasma membrane content in cell surface glycoproteins. These new interpretations of glycoprotein function are likely to change our understanding of endothelial glycocalyx role in the cardiovascular system.

61. Chen X, Gays D, Milia C, Santoro MM: **Cilia control vascular mural cell recruitment in vertebrates**. *Cell Rep* 2017, **18**:1033-1047.

62. Shihata WA, Michell DL, Andrews KL, Chin-Dusting JP: **Caveolae: a role in endothelial inflammation and mechanotransduction?** *Front Physiol* 2016, **7**:628.

63. Yu J, Bergaya S, Murata T, Alp IF, Bauer MP, Lin MI, Drab M, Kurzchalia TV, Stan RV, Sessa WC: **Direct evidence for the role of caveolin-1 and caveolae in mechanotransduction and remodeling of blood vessels**. *J Clin Invest* 2006, **116**:1284-1291.

64. Sinha B, Koster D, Ruez R, Gonnord P, Bastiani M, Abankwa D, Stan RV, Butler-Browne G, Vedie B, Johannes L *et al.*: **Cells respond to mechanical stress by rapid disassembly of caveolae**. *Cell* 2011, **144**:402-413.

65. Anton H, Harlepp S, Ramspacher C, Wu D, Monduc F, Bhat S, Liebling M, Paoletti C, Charvin G, Freund JB *et al.*: **Pulse propagation by a capacitive mechanism drives embryonic blood flow**. *Development* 2013, **140**:4426-4434.

66. Bernabeu MO, Jones ML, Nash RW, Pezzarossa A, Coveney PV, Gerhardt H, Franco CA: **PolNet: a tool to quantify network-level cell polarity and blood flow in vascular remodeling**. *Biophys J* 2018, **114**:2052-2058.

67. Rasouli SJ, El-Brolosy M, Tsedeke AT, Bensimon-Brito A, Ghanbari P, Maischein HM, Kuenne C, Stainier DY: **The flow responsive transcription factor Klf2 is required for myocardial wall integrity by modulating Fgf signaling**. *eLife* 2018, **7**.

68. Donat S, Lourenco M, Paolini A, Otten C, Renz M, Abdelilah-Seyfried S: **Heg1 and Ccm1/2 proteins control endocardial mechanosensitivity during zebrafish valvulogenesis**. *eLife* 2018, **7**.

69. Lee JS, Yu Q, Shin JT, Sebzda E, Bertozzi C, Chen M, Mericko P, Stadtfeld M, Zhou D, Cheng L *et al.*: **Klf2 is an essential regulator of vascular hemodynamic forces in vivo**. *Dev Cell* 2006, **11**:845-857.

70. Franco CA, Jones ML, Bernabeu MO, Vion AC, Barbacena P, Fan J, Mathivet T, Fonseca CG, Ragab A, Yamaguchi TP *et al.*: **Non-canonical Wnt signalling modulates the endothelial shear stress flow sensor in vascular remodelling**. *eLife* 2016, **5**:e07727.

71. •• Nakajima H, Yamamoto K, Agarwala S, Terai K, Fukui H, Fukuhara S, Ando K, Miyazaki T, Yokota Y, Schmelzer E *et al.*: **Flow-dependent endothelial YAP regulation contributes to vessel maintenance**. *Dev Cell* 2017, **40**:523-536 e526.
Through live imaging and genetical manipulation, the authors demonstrate that yap activity is regulated by blood flow during blood vessel development. this establishes a key signaling pathway acting downstream of blood flow in enthelial cells.

72. Neto F, Klaus-Bergmann A, Ong YT, Alt S, Vion AC, Szymborska A, Carvalho JR, Hollfinger I, Bartels-Klein E, Franco CA *et al.*: **YAP and TAZ regulate adherens junction dynamics and endothelial cell distribution during vascular development**. *eLife* 2018, **7**.

73. •• Sabine A, Bovay E, Demir CS, Kimura W, Jaquet M, Agalarov Y, Zangger N, Scallan JP, Graber W, Gulpinar E *et al.*: **FOXC2 and fluid shear stress stabilize postnatal lymphatic vasculature**. *J Clin Invest* 2015, **125**:3861-3877.
This study nicely describes the molecular mechanism activated by flow forces in the process of lymphatic vasculature stabilisation.

74. Baeyens N, Larrivee B, Ola R, Hayward-Piatkowskyi B, Dubrac A, Huang B, Ross TD, Coon BG, Min E, Tsarfati M *et al.*: **Defective fluid shear stress mechanotransduction mediates hereditary hemorrhagic telangiectasia**. *J Cell Biol* 2016, **214**:807-816.

75. Sugden WW, Meissner R, Aegerter-Wilmsen T, Tsaryk R, Leonard EV, Bussmann J, Hamm MJ, Herzog W, Jin Y, Jakobsson L *et al.*: **Endoglin controls blood vessel diameter through endothelial cell shape changes in response to haemodynamic cues**. *Nat Cell Biol* 2017, **19**:653-665.

76. Vion AC, Alt S, Klaus-Bergmann A, Szymborska A, Zheng T, Perovic T, Hammoutene A, Oliveira MB, Bartels-Klein E, Hollfinger I *et al.*: **Primary cilia sensitize endothelial cells to BMP and prevent excessive vascular regression**. *J Cell Biol* 2018, **217**:1651-1665.

77. Jin Y, Muhl L, Burmakin M, Wang Y, Duchez AC, Betsholtz C, Arthur HM, Jakobsson L: **Endoglin prevents vascular malformation by regulating flow-induced cell migration and specification through VEGFR2 signalling**. *Nat Cell Biol* 2017, **19**:639-652.

78. Conway DE, Breckenridge MT, Hinde E, Gratton E, Chen CS, Schwartz MA: **Fluid shear stress on endothelial cells modulates mechanical tension across VE-cadherin and PECAM-1**. *Curr Biol* 2013, **23**:1024-1030.

79. • Angulo-Urarte A, Casado P, Castillo SD, Kobialka P, Kotini MP, Figueiredo AM, Castel P, Rajeeve V, Mila-Guasch M, Millan J *et al.*: **Endothelial cell rearrangements during vascular patterning require PI3-kinase-mediated inhibition of actomyosin contractility**. *Nat Commun* 2018, **9**:4826.

80. Dietrich AC, Lombardo VA, Veerkamp J, Priller F, Abdelilah-Seyfried S: **Blood flow and Bmp signaling control endocardial chamber morphogenesis**. *Dev Cell* 2014, **30**:367-377.

81. Weijts B, Gutierrez E, Saikin SK, Ablooglu AJ, Traver D, Groisman A, Tkachenko E: **Blood flow-induced Notch activation and endothelial migration enable vascular remodeling in zebrafish embryos**. *Nat Commun* 2018, **9**:5314.

82. •• Kwon HB, Wang S, Helker CS, Rasouli SJ, Maischein HM, Offermanns S, Herzog W, Stainier DY: **In vivo modulation of endothelial polarization by apelin receptor signalling**. *Nat Commun* 2016, **7**:11805.
This paper describes a robust tool to study the changes in endothelial cells polarity *in vivo*.

83. Truskey GA: **Advancing cardiovascular tissue engineering**. *F1000Res* 2016, **5**.

84. Nemeno-Guanzon JG, Lee S, Berg JR, Jo YH, Yeo JE, Nam BM, Koh YG, Lee JI: **Trends in tissue engineering for blood vessels**. *J Biomed Biotechnol* 2012, **2012**:956345.

85. Nsiah BA, Ahsan T, Griffiths S, Cooke M, Nerem RM, McDevitt TC: **Fluid shear stress pre-conditioning promotes endothelial morphogenesis of embryonic stem cells within embryoid bodies**. *Tissue Eng Part A* 2014, **20**:954-965.

86. Rosenfeld D, Landau S, Shandalov Y, Raindel N, Freiman A, Shor E, Blinder Y, Vandenburgh HH, Mooney DJ, Levenberg S: **Morphogenesis of 3D vascular networks is regulated by tensile forces**. *Proc Natl Acad Sci U S A* 2016, **113**:3215-3220.

87. Boerckel JD, Uhrig BA, Willett NJ, Huebsch N, Guldberg RE: **Mechanical regulation of vascular growth and tissue regeneration in vivo**. *Proc Natl Acad Sci U S A* 2011, **108**:E674-680.

88. Sotiropoulos F, Le TB, Gilmanov A: **Fluid mechanics of heart valves and their replacements**. *Ann Rev Fluid Mech* 2016, **48**.

89. Vu V, Rossini L, Montes R, Campos J, Moon J, Martinez-Legazpi P, Bermejo J, Del Álamo JC, May-Newman K: **Mitral valve prosthesis design affects hemodynamic stasis and shear in the dilated left ventricle**. *Ann Biomed Eng* 2019:1-16.

90. Rodriguez-Gabella T, Voisine P, Puri R, Pibarot P, Rodes-Cabau J: **Aortic bioprosthetic valve durability: incidence, mechanisms, predictors, and management of surgical and transcatheter valve degeneration**. *J Am Coll Cardiol* 2017, **70**:1013-1028.

91. Motta SE, Lintas V, Fioretta ES, Hoerstrup SP, Emmert MY: **Off-the-shelf tissue engineered heart valves for in situ regeneration: current state, challenges and future directions**. *Expert Rev Med Devices* 2018, **15**:35-45.

92. Vashistha R, Kumar P, Dangi AK, Sharma N, Chhabra D, Shukla P: **Quest for cardiovascular interventions: precise modeling and 3D printing of heart valves**. *J Biol Eng* 2019, **13**:12.

93. Farrar EJ, Pramil V, Richards JM, Mosher CZ, Butcher JT: **Valve interstitial cell tensional homeostasis directs calcification and extracellular matrix remodeling processes via RhoA signaling**. *Biomaterials* 2016, **105**:25-37.

94. Mahler GJ, Frendl CM, Cao Q, Butcher JT: **Effects of shear stress pattern and magnitude on mesenchymal transformation and invasion of aortic valve endothelial cells**. *Biotechnol Bioeng* 2014, **111**:2326-2337.

95. •• Ivanovitch K, Temino S, Torres M: **Live imaging of heart tube development in mouse reveals alternating phases of cardiac differentiation and morphogenesis**. *eLife* 2017, **6**.
This impressive imaging study revealed the dynamics of early heart tube formation. One of their interesting findings is that cells from the first heart field start beating before heart tube is fully formed and that cells from the second heart field help close the early heart tube and start beating later.

96. •• McDole K, Guignard L, Amat F, Berger A, Malandain G, Royer LA, Turaga SC, Branson K, Keller PJ: **In toto imaging and reconstruction of post-implantation mouse development at the single-cell level**. *Cell* 2018, **175**:859-876 e833.
This study develops a novel adaptive light-sheet microscope that allows one to follow mouse development with single cell resolution. This allowed the authors to create high-resolution maps of cell fate and tissue morphogenesis against which future analyses can be benchmarked. Such technology will open up to numerous application in the cardiovascular research field.

97. Choi D, Park E, Jung E, Cha B, Lee S, Yu J, Kim PM, Lee S, Hong YJ, Koh CJ *et al.*: **Piezo1 incorporates mechanical force signals into the genetic program that governs lymphatic valve development and maintenance**. *JCI Insight* 2019, **4**.

98. Geudens I, Coxam B, Alt S, Gebala V, Vion AC, Meier K, Rosa A, Gerhardt H: **Artery-vein specification in the zebrafish trunk is pre-patterned by heterogeneous Notch activity and balanced by flow-mediated fine-tuning**. *Development* 2019, **146**.

99. Neri T, Hiriart E, van Vliet PP, Faure E, Norris RA, Farhat B, Jagla B, Lefrancois J, Sugi Y, Moore-Morris *et al.*: **Human pre-valvular endocardial cells derived from pluripotent stem cells recapitulate cardiac pathophysiological valvulogenesis**. *Nat Commun* 2019, **10**:1929.

REFERENCES

REFERENCES

Abir-Awan, M., Kitchen, P., Salman, M. M., Conner, M. T., Conner, A. C., & Bill, R. M. (2019). Inhibitors of mammalian aquaporin water channels. In *International Journal of Molecular Sciences* (Vol. 20, Issue 7). MDPI AG. https://doi.org/10.3390/ijms20071589

Alan Mathison Turing. (1952). The chemical basis of morphogenesis. *Philosophical Transactions of the Royal Society of London. Series B, Biological Sciences*, *237*(641), 37–72. https://doi.org/10.1098/rstb.1952.0012

Albert Pan, Y., Freundlich, T., Weissman, T. A., Schoppik, D., Cindy Wang, X., Zimmerman, S., Ciruna, B., Sanes, J. R., Lichtman, J. W., & Schier, A. F. (2013). Zebrabow: Multispectral cell labeling for cell tracing and lineage analysis in zebrafish. *Development (Cambridge)*, *140*(13), 2835–2846. https://doi.org/10.1242/dev.094631

Alexander, J., Stainier, D. Y. R., & Yelon, D. (1998). Screening mosaic F1 females for mutations affecting zebrafish heart induction and patterning. *Developmental Genetics*, *22*(3), 288–299. https://doi.org/10.1002/(SICI)1520-6408(1998)22:3<288::AID-DVG10>3.0.CO;2-2

Ambrosini, A., Gracia, M., Proag, A., Rayer, M., Monier, B., & Suzanne, M. (2017). Apoptotic forces in tissue morphogenesis. In *Mechanisms of Development* (Vol. 144, pp. 33–42). Elsevier Ireland Ltd. https://doi.org/10.1016/j.mod.2016.10.001

Andrés-Delgado, L., & Mercader, N. (2016). Interplay between cardiac function and heart development. *Biochimica et Biophysica Acta - Molecular Cell Research*, *1863*(7), 1707–1716. https://doi.org/10.1016/j.bbamcr.2016.03.004

Arniges, M., Vázquez, E., Fernández-Fernández, J. M., & Valverde, M. A. (2004). Swelling-activated Ca2+ entry via TRPV4 channel is defective in cystic fibrosis airway epithelia. *Journal of Biological Chemistry*, *279*(52), 54062–54068. https://doi.org/10.1074/jbc.M409708200

Auman, H. J., Coleman, H., Riley, H. E., Olale, F., Tsai, H.-J., & Yelon, D. (2007). Functional Modulation of Cardiac Form through Regionally Confined Cell Shape Changes. *PLoS Biology*, *5*(3), e53. https://doi.org/10.1371/journal.pbio.0050053

Aupperle, H., & Disatian, S. (2012). Pathology, protein expression and signaling in myxomatous mitral valve degeneration: Comparison of dogs and humans. *Journal of Veterinary Cardiology*. https://doi.org/10.1016/j.jvc.2012.01.005

Bäck, M., Gasser, T. C., Michel, J. B., & Caligiuri, G. (2013). Biomechanical factors in the biology of aortic wall and aortic valve diseases. *Cardiovascular Research* (Vol. 99, Issue 2, pp. 232–241). Cardiovasc Res. https://doi.org/10.1093/cvr/cvt040

Baghban, R., Roshangar, L., Jahanban-Esfahlan, R., Seidi, K., Ebrahimi-Kalan, A., Jaymand, M., Kolahian, S., Javaheri, T., & Zare, P. (2020). Tumor microenvironment complexity and therapeutic implications at a glance. In *Cell Communication and Signaling* (Vol. 18, Issue 1). BioMed Central Ltd. https://doi.org/10.1186/s12964-020-0530-4

Bajanca, F., Gouignard, N., Colle, C., Parsons, M., Mayor, R., & Theveneau, E. (2019). In vivo topology

converts competition for cell-matrix adhesion into directional migration. *Nature Communications*, *10*(1), 1–17. https://doi.org/10.1038/s41467-019-09548-5

Balaban, N. Q., Schwarz, U. S., Riveline, D., Goichberg, P., Tzur, G., Sabanay, I., Mahalu, D., Safran, S., Bershadsky, A., Addadi, L., & Geiger, B. (2001). Force and focal adhesion assembly: A close relationship studied using elastic micropatterned substrates. *Nature Cell Biology*, *3*(5), 466–472. https://doi.org/10.1038/35074532

Barriga, E. H., Franze, K., Charras, G., & Mayor, R. (2018). Tissue stiffening coordinates morphogenesis by triggering collective cell migration in vivo. *Nature*, *554*(7693), 523–527. https://doi.org/10.1038/nature25742

Bartman, T., Walsh, E. C., Wen, K.-K., McKane, M., Ren, J., Alexander, J., Rubenstein, P. A., & Stainier, D. Y. R. (2004). Early Myocardial Function Affects Endocardial Cushion Development in Zebrafish. *PLoS Biology*, *2*(5), e129. https://doi.org/10.1371/journal.pbio.0020129

Behrndt, M., Salbreux, G., Campinho, P., Hauschild, R., Oswald, F., Roensch, J., Grill, S. W., & Heisenberg, C. P. (2012). Forces driving epithelial spreading in zebrafish gastrulation. *Science*, *338*(6104), 257–260. https://doi.org/10.1126/science.1224143

Beis, D., Bartman, T., Jin, S. W., Scott, I. C., D'Amico, L. A., Ober, E. A., Verkade, H., Frantsve, J., Field, H. A., Wehman, A., Baier, H., Tallafuss, A., Bally-Cuif, L., Chen, J. N., Stainier, D. Y. R., & Jungblut, B. (2005). Genetic and cellular analyses of zebrafish atrioventricular cushion and valve development. *Development*, *132*(18), 4193–4204. https://doi.org/10.1242/dev.01970

Benfenati, V., Caprini, M., Dovizio, M., Mylonakou, M. N., Ferroni, S., Ottersen, O. P., & Amiry-Moghaddam, M. (2011). An aquaporin-4/transient receptor potential vanilloid 4 (AQP4/TRPV4) complex is essential for cell-volume control in astrocytes. *Proceedings of the National Academy of Sciences of the United States of America*, *108*(6), 2563–2568. https://doi.org/10.1073/pnas.1012867108

Berdougo, E., Coleman, H., Lee, D. H., Stainier, D. Y. R., & Yelon, D. (2003). Mutation of weak atrium/atrial myosin heavy chain disrupts atrial function and influences ventricular morphogenesis in zebrafish. *Development*, *130*(24), 6121–6129. https://doi.org/10.1242/dev.00838

Berleth, T., Burri, M., Thoma, G., Bopp, D., Richstein, S., Frigerio, G., Noll, M., & Nüsslein-Volhard, C. (1988). The role of localization of bicoid RNA in organizing the anterior pattern of the Drosophila embryo. *The EMBO Journal*, *7*(6), 1749–1756. https://doi.org/10.1002/j.1460-2075.1988.tb03004.x

Bertet, C., Sulak, L., & Lecuit, T. (2004). Myosin-dependent junction remodeling controls planar cell intercalation and axis elongation. *Nature*, *429*(6992), 667–671. https://doi.org/10.1038/nature02590

Bolender, D. L., & Markwald, R. R. (1979). Epithelial-mesenchymal transformation in chick atrioventricular cushion morphogenesis. *Scanning Electron Microscopy*, *VOL. 3*(3), 313–321. https://europepmc.org/article/med/524004

Borisy, G. G., & Svitkina, T. M. (2000). Actin machinery: Pushing the envelope. In *Current Opinion in Cell Biology* (Vol. 12, Issue 1, pp. 104–112). Current Biology Ltd. https://doi.org/10.1016/S0955-0674(99)00063-0

Bornhorst, D., Xia, P., Nakajima, H., Dingare, C., Herzog, W., Lecaudey, V., Mochizuki, N., Heisenberg, C. P., Yelon, D., & Abdelilah-Seyfried, S. (2019). Biomechanical signaling within the developing zebrafish heart attunes endocardial growth to myocardial chamber dimensions. *Nature Communications*, *10*(1). https://doi.org/10.1038/s41467-019-12068-x

Boselli, F., Freund, J. B., & Vermot, J. (2015). Blood flow mechanics in cardiovascular development. In *Cellular and Molecular Life Sciences* (Vol. 72, Issue 13, pp. 2545–2559). Birkhauser Verlag AG. https://doi.org/10.1007/s00018-015-1885-3

Boselli, F., Steed, E., Freund, J. B., & Vermot, J. (2017). Anisotropic shear stress patterns predict the orientation of convergent tissue movements in the embryonic heart. *Development (Cambridge)*, *144*(23), 4322–4327. https://doi.org/10.1242/dev.152124

Brown, D., Samsa, L., Qian, L., & Liu, J. (2016). Advances in the Study of Heart Development and Disease Using Zebrafish. *Journal of Cardiovascular Development and Disease*, *3*(2), 13. https://doi.org/10.3390/jcdd3020013

Burkhard, S. B., & Bakkers, J. (2018). Spatially resolved RNA-sequencing of the embryonic heart identifies a role for Wnt/β-catenin signaling in autonomic control of heart rate. *ELife*, *7*. https://doi.org/10.7554/eLife.31515

Caballero, D., Comelles, J., Piel, M., Voituriez, R., & Riveline, D. (2015). Ratchetaxis: Long-Range Directed Cell Migration by Local Cues. In *Trends in Cell Biology* (Vol. 25, Issue 12, pp. 815–827). Elsevier Ltd. https://doi.org/10.1016/j.tcb.2015.10.009

Cadart, C., Zlotek-Zlotkiewicz, E., Venkova, L., Thouvenin, O., Racine, V., Le Berre, M., Monnier, S., & Piel, M. (2017). Fluorescence eXclusion Measurement of volume in live cells. *Methods in Cell Biology*, *139*, 103–120. https://doi.org/10.1016/bs.mcb.2016.11.009

Cadart, Clotilde, Venkova, L., Recho, P., Lagomarsino, M. C., & Piel, M. (2019). The physics of cell-size regulation across timescales. In *Nature Physics* (Vol. 15, Issue 10, pp. 993–1004). Nature Publishing Group. https://doi.org/10.1038/s41567-019-0629-y

Camenisch, T. D., & McDonald, J. A. (2000). Hyaluronan is bigger better? In *American Journal of Respiratory Cell and Molecular Biology* (Vol. 23, Issue 4, pp. 431–433). American Lung Association. https://doi.org/10.1165/ajrcmb.23.4.f201

Camenisch, Todd D., Spicer, A. P., Brehm-Gibson, T., Biesterfeldt, J., Augustine, M. Lou, Calabro, A., Kubalak, S., Klewer, S. E., & McDonald, J. A. (2000). Disruption of hyaluronan synthase-2 abrogates normal cardiac morphogenesis and hyaluronan-mediated transformation of epithelium to mesenchyme. *Journal of Clinical Investigation*, *106*(3), 349–360. https://doi.org/10.1172/JCI10272

Campinho, P., Behrndt, M., Ranft, J., Risler, T., Minc, N., & Heisenberg, C. P. (2013). Tension-oriented cell divisions limit anisotropic tissue tension in epithelial spreading during zebrafish epiboly. *Nature Cell Biology*, *15*(12), 1405–1414. https://doi.org/10.1038/ncb2869

Campinho, P., Lamperti, P., Boselli, F., Vilfan, A., & Vermot, J. (2020). Blood Flow Limits Endothelial Cell Extrusion in the Zebrafish Dorsal Aorta. *Cell Reports*, *31*(2). https://doi.org/10.1016/j.celrep.2020.03.069

Cantwell, H., & Nurse, P. (2019). Unravelling nuclear size control. In *Current Genetics* (Vol. 65, Issue 6,

pp. 1281–1285). Springer Verlag. https://doi.org/10.1007/s00294-019-00999-3

Carl J. Neumann and Stephen M. Cohen. (1997). Long-range action of Wingless organizes the dorsal-ventral axis of the Drosophila wing. *Development*, 871–880. moz-extension://d6522e6a-202a-46a2-aa53-a17881dccce6/enhanced-reader.html?openApp&pdf=https%3A%2F%2Fdev.biologists.org%2Fcontent%2Fdevelop%2F124%2F4%2F871.full.pdf

Carmona-Fontaine, C., Matthews, H. K., Kuriyama, S., Moreno, M., Dunn, G. A., Parsons, M., Stern, C. D., & Mayor, R. (2008). Contact inhibition of locomotion in vivo controls neural crest directional migration. *Nature*, *456*(7224), 957–961. https://doi.org/10.1038/nature07441

Caussinus, E., Colombelli, J., & Affolter, M. (2008). Tip-Cell Migration Controls Stalk-Cell Intercalation during Drosophila Tracheal Tube Elongation. *Current Biology*, *18*(22), 1727–1734. https://doi.org/10.1016/j.cub.2008.10.062

Chen, J. N., Haffter, P., Odenthal, J., Vogelsang, E., Brand, M., van Eeden, F. J., Furutani-Seiki, M., Granato, M., Hammerschmidt, M., Heisenberg, C. P., Jiang, Y. J., Kane, D. A., Kelsh, R. N., Mullins, M. C., & Nusslein-Volhard, C. (1996). Mutations affecting the cardiovascular system and other internal organs in zebrafish. *Development*, *123*(1), 293–302. https://doi.org/10.1242/dev.123.1.293

Chen, J. N., van Eeden, F. J., Warren, K. S., Chin, A., Nusslein-Volhard, C., Haffter, P., & Fishman, M. C. (1997). Left-right pattern of cardiac BMP4 may drive asymmetry of the heart in zebrafish. *Development*, *124*(21), 4373–4382. https://doi.org/10.1242/dev.124.21.4373

Chi, N. C., Shaw, R. M., Jungblut, B., Huisken, J., Ferrer, T., Arnaout, R., Scott, I., Beis, D., Xiao, T., Baier, H., Jan, L. Y., Tristani-Firouzi, M., & Stainier, D. Y. R. (2008). Genetic and Physiologic Dissection of the Vertebrate Cardiac Conduction System. *PLoS Biology*, *6*(5), e109. https://doi.org/10.1371/journal.pbio.0060109

Chin, A. J., Tsang, M., & Weinberg, E. S. (2000). *Heart and Gut Chiralities Are Controlled Independently from Initial Heart Position in the Developing Zebrafish*. https://doi.org/10.1006/dbio.2000.9924

Chu, Y. S., Thomas, W. A., Eder, O., Pincet, F., Perez, E., Thiery, J. P., & Dufour, S. (2004). Force measurements in E-cadherin-mediated cell doublets reveal rapid adhesion strengthened by actin cytoskeleton remodeling through Rac and Cdc42. *Journal of Cell Biology*, *167*(6), 1183–1194. https://doi.org/10.1083/jcb.200403043

Comper, W. D., & Laurent, T. C. (1978). Physiological function of connective tissue polysaccharides. *Physiological Reviews*, *58*(1), 255–315. https://doi.org/10.1152/physrev.1978.58.1.255

Conner, M. T., Conner, A. C., Bland, C. E., Taylor, L. H. J., Brown, J. E. P., Parri, H. R., & Bill, R. M. (2012). Rapid aquaporin translocation regulates cellular water flow: mechanism of hypotonicity-induced subcellular localization of aquaporin 1 water channel. *The Journal of Biological Chemistry*, *287*(14), 11516–11525. https://doi.org/10.1074/jbc.M111.329219

Dasgupta, A., Jacob, A., & Amack, J. (2018). Mosaic Labeling and 3-Dimensional Morphological Analysis of Single Cells in the Zebrafish Left-right Organizer. *BIO-PROTOCOL*, *8*(22). https://doi.org/10.21769/bioprotoc.3090

Dasgupta, A., Merkel, M., Clark, M. J., Jacob, A. E., Dawson, J. E., Manning, M. L., & Amack, J. D.

(2018). Cell volume changes contribute to epithelial morphogenesis in zebrafish Kupffer's vesicle. *ELife*, *7*. https://doi.org/10.7554/eLife.30963

de Pater, E., Clijsters, L., Marques, S. R., Lin, Y. F., Garavito-Aguilar, Z. V., Yelon, D., & Bakkers, J. (2009). Distinct phases of cardiomyocyte differentiation regulate growth of the zebrafish heart. *Development*, *136*(10), 1633–1641. https://doi.org/10.1242/dev.030924

Derrick, C. J., & Noël, E. S. (2021). The ECM as a driver of heart development and repair. In *Development (Cambridge, England)* (Vol. 148, Issue 5). NLM (Medline). https://doi.org/10.1242/dev.191320

Desgrange, A., Garrec, J. F. Le, & Meilhac, S. M. (2018). Left-right asymmetry in heart development and disease: Forming the right loop. *Development (Cambridge)* (Vol. 145, Issue 22). Company of Biologists Ltd. https://doi.org/10.1242/dev.162776

Dietrich, A. C., Lombardo, V. A., & Abdelilah-Seyfried, S. (2014). Blood Flow and Bmp Signaling Control Endocardial Chamber Morphogenesis. *Developmental Cell*, *30*(4), 367–377. https://doi.org/10.1016/j.devcel.2014.06.020

Discher, D. E., Janmey, P., & Wang, Y. L. (2005). Tissue cells feel and respond to the stiffness of their substrate. In *Science* (Vol. 310, Issue 5751, pp. 1139–1143). American Association for the Advancement of Science. https://doi.org/10.1126/science.1116995

Driever, W., Solnica-Krezel, L., Schier, A. F., Neuhauss, S. C. F., Malicki, J., Stemple, D. L., Stainier, D. Y. R., Zwartkruis, F., Abdelilah, S., Rangini, Z., Belak, J., & Boggs, C. (1996). A genetic screen for mutations affecting embryogenesis in zebrafish. *Development*, *123*, 37–46. https://doi.org/10.5167/uzh-215

Driever, Wolfgang, & Nü Sslein-Volhard, C. (1988). The bicoid Protein Determines Position in the Drosophila Embryo in a Concentration-Dependent Manner. In *Cell* (Vol. 54).

Duchemin, A. L., Vignes, H., & Vermot, J. (2019). Mechanically activated Piezo channels modulate outflow tract valve development through the yap1 and KLF2-notch signaling axis. *ELife*, *8*. https://doi.org/10.7554/eLife.44706

Duda, M., Kirkland, N. J., Khalilgharibi, N., Tozluoglu, M., Yuen, A. C., Carpi, N., Bove, A., Piel, M., Charras, G., Baum, B., & Mao, Y. (2019). Polarization of Myosin II Refines Tissue Material Properties to Buffer Mechanical Stress. *Developmental Cell*, *48*(2), 245-260.e7. https://doi.org/10.1016/j.devcel.2018.12.020

El-Brolosy, M. A., Kontarakis, Z., Rossi, A., Kuenne, C., Günther, S., Fukuda, N., Kikhi, K., Boezio, G. L. M., Takacs, C., Lai, S.-L., Fukuda, R., Gerri, C., Giraldez, A. J., & Stainier, Y. R. (2019). Genetic compensation triggered by mutant mRNA degradation Europe PMC Funders Group. *Nature*, *568*(7751), 193–197. https://doi.org/10.1038/s41586-019-1064-z

El-Brolosy, M. A., & Stainier, D. Y. R. (2017). Genetic compensation: A phenomenon in search of mechanisms. In *PLoS Genetics* (Vol. 13, Issue 7). Public Library of Science. https://doi.org/10.1371/journal.pgen.1006780

Engler, A. J., Sen, S., Sweeney, H. L., & Discher, D. E. (2006). Matrix Elasticity Directs Stem Cell Lineage Specification. *Cell*, *126*(4), 677–689. https://doi.org/10.1016/j.cell.2006.06.044

Eritano, A. S., Bromley, C. L., Bolea Albero, A., Schütz, L., Wen, F. L., Takeda, M., Fukaya, T., Sami,

M. M., Shibata, T., Lemke, S., & Wang, Y. C. (2020). Tissue-Scale Mechanical Coupling Reduces Morphogenetic Noise to Ensure Precision during Epithelial Folding. *Developmental Cell*, *53*(2), 212-228.e12. https://doi.org/10.1016/j.devcel.2020.02.012

Forouhar, A. S., Liebling, M., Hickerson, A., Nasiraei-Moghaddam, A., Tsai, H. J., Hove, J. R., Fraser, S. E., Dickinson, M. E., & Gharib, M. (2006). The embryonic vertebrate heart tube is a dynamic suction pump. *Science*, *312*(5774), 751–753. https://doi.org/10.1126/science.1123775

Franco, C. A., Jones, M. L., Bernabeu, M. O., Geudens, I., Mathivet, T., Rosa, A., Lopes, F. M., Lima, A. P., Ragab, A., Collins, R. T., Phng, L.-K., Coveney, P. V., & Gerhardt, H. (2015). Dynamic Endothelial Cell Rearrangements Drive Developmental Vessel Regression. *PLOS Biology*, *13*(4), e1002125. https://doi.org/10.1371/journal.pbio.1002125

Freund, J. B., Goetz, J. G., Hill, K. L., & Vermot, J. (2012). Fluid flows and forces in development: Functions, features and biophysical principles. *Development*, *139*(7), 1229–1245. https://doi.org/10.1242/dev.073593

Friedl, P., & Gilmour, D. (2009). Collective cell migration in morphogenesis, regeneration and cancer. *Nature Reviews Molecular Cell Biology* (Vol. 10, Issue 7, pp. 445–457). Nature Publishing Group. https://doi.org/10.1038/nrm2720

Frigerio, G., Burri, M., Bopp, D., Baumgartner, S., & Noll, M. (1986). Structure of the segmentation gene paired and the Drosophila PRD gene set as part of a gene network. *Cell*, *47*(5), 735–746. https://doi.org/10.1016/0092-8674(86)90516-7

Frohnhöfer, H. G., & Nüsslein-Volhard, C. (1986). Organization of anterior pattern in the Drosophila embryo by the maternal gene bicoid. *Nature*, *324*(6093), 120–125. https://doi.org/10.1038/324120a0

Fu, Y., Sander, J. D., Reyon, D., Cascio, V. M., & Joung, J. K. (2014). Improving CRISPR-Cas nuclease specificity using truncated guide RNAs. *Nature Biotechnology*, *32*(3), 279–284. https://doi.org/10.1038/nbt.2808

Gagnon, J. A., Valen, E., Thyme, S. B., Huang, P., Ahkmetova, L., Pauli, A., Montague, T. G., Zimmerman, S., Richter, C., & Schier, A. F. (2014). Efficient Mutagenesis by Cas9 Protein-Mediated Oligonucleotide Insertion and Large-Scale Assessment of Single-Guide RNAs. *PLoS ONE*, *9*(5), e98186. https://doi.org/10.1371/journal.pone.0098186

Gierer, A., & Meinhardt, H. (1972). A Theory of Biological Pattern Formation. In *Kybernetik* (Vol. 12). Springer-Verlag.

Gilbert, S. F. (2000). *Mathematical Modeling of Development*. https://www.ncbi.nlm.nih.gov/books/NBK10126/

Gong, Y., Mo, C., & Fraser, S. E. (2004). Planar cell polarity signalling controls cell division orientation during zebrafish gastrulation. *Nature*, *430*(7000), 689–693. https://doi.org/10.1038/nature02796

Goswami, C., Kuhn, J., Heppenstall, P. A., & Hucho, T. (2010). Importance of non-selective cation channel TRPV4 interaction with cytoskeleton and their reciprocal regulations in cultured cells. *PLoS ONE*, *5*(7). https://doi.org/10.1371/journal.pone.0011654

Guan, X. G., Su, W. H., Yi, F., Zhang, D., Hao, F., Zhang, H. G., Liu, Y. J., Feng, X. C., & Ma, T. H. (2010). NPA motifs play a key role in plasma membrane targeting of aquaporin-4. *IUBMB Life*,

62(3), 222–226. https://doi.org/10.1002/iub.311

Gumbiner, B. M. (1996). Cell adhesion: The molecular basis of tissue architecture and morphogenesis. In *Cell* (Vol. 84, Issue 3, pp. 345–357). Elsevier B.V. https://doi.org/10.1016/S0092-8674(00)81279-9

Gunawan, F., Gentile, A., Fukuda, R., Tsedeke, A. T., Jiménez-Amilburu, V., Ramadass, R., Iida, A., Sehara-Fujisawa, A., & Stainier, D. Y. R. (2019). Focal adhesions are essential to drive zebrafish heart valve morphogenesis. *Journal of Cell Biology*, *218*(3), 1039–1054. https://doi.org/10.1083/jcb.201807175

Guo, M., Pegoraro, A. F., Mao, A., Zhou, E. H., Arany, P. R., Han, Y., Burnette, D. T., Jensen, M. H., Kasza, K. E., Moore, J. R., Mackintosh, F. C., Fredberg, J. J., Mooney, D. J., Lippincott-Schwartz, J., & Weitz, D. A. (2017). Cell volume change through water efflux impacts cell stiffness and stem cell fate. *Proceedings of the National Academy of Sciences of the United States of America*, *114*(41), E8618–E8627. https://doi.org/10.1073/pnas.1705179114

Gutzman, J. H., Graeden, E., Brachmann, I., Yamazoe, S., Chen, J. K., & Sive, H. (2018). Basal constriction during midbrain–hindbrain boundary morphogenesis is mediated by Wnt5b and focal adhesion kinase. *Biology Open*, *7*(11). https://doi.org/10.1242/bio.034520

Haack, T., & Abdelilah-Seyfried, S. (2016). The force within: Endocardial development, mechanotransduction and signalling during cardiac morphogenesis. In *Development (Cambridge)* (Vol. 143, Issue 3, pp. 373–386). Company of Biologists Ltd. https://doi.org/10.1242/dev.131425

Haffter, P., Granato, M., Brand, M., Mullins, M. C., Hammerschmidt, M., Kane, D. A., Odenthal, J., van Eeden, F. J., Jiang, Y. J., Heisenberg, C. P., Kelsh, R. N., Furutani-Seiki, M., Vogelsang, E., Beuchle, D., Schach, U., Fabian, C., & Nusslein-Volhard, C. (1996). The identification of genes with unique and essential functions in the development of the zebrafish, Danio rerio. *Development*, *123*(1), 1–36. https://doi.org/10.1242/dev.123.1.1

Heisenberg, C. P., & Bellaïche, Y. (2013). XForces in tissue morphogenesis and patterning. *Cell* (Vol. 153, Issue 5, p. 948). Elsevier B.V. https://doi.org/10.1016/j.cell.2013.05.008

Hernandez, L., Ryckebüsch, L., Wang, C., Ling, R., & Yelon, D. (2019). Tmem2 restricts atrioventricular canal differentiation by regulating degradation of hyaluronic acid. *Developmental Dynamics*, *248*(12), 1195–1210. https://doi.org/10.1002/dvdy.106

Herrera, M., Hong, N. J., & Garvin, J. L. (2006). Aquaporin-1 transports NO across cell membranes. *Hypertension*, *48*(1), 157–164. https://doi.org/10.1161/01.HYP.0000223652.29338.77

Hinton, R. B., Lincoln, J., Deutsch, G. H., Osinska, H., Manning, P. B., Benson, D. W., & Yutzey, K. E. (2006). Extracellular matrix remodeling and organization in developing and diseased aortic valves. *Circulation Research*, *98*(11), 1431–1438. https://doi.org/10.1161/01.RES.0000224114.65109.4e

Hinton, R. B., & Yutzey, K. E. (2011). Heart valve structure and function in development and disease. *Annual Review of Physiology*, *73*, 29–46. https://doi.org/10.1146/annurev-physiol-012110-142145

Hoffmann, E. K., Lambert, I. H., & Pedersen, S. F. (2009). Physiology of cell volume regulation in vertebrates. In *Physiological Reviews* (Vol. 89, Issue 1, pp. 193–277). Physiol Rev. https://doi.org/10.1152/physrev.00037.2007

Holm, L. M., Jahn, T. P., Møller, A. L. B., Schjoerring, J. K., Ferri, D., Klaerke, D. A., & Zeuthen, T.

(2005). NH3 and NH4+ permeability in aquaporin-expressing Xenopus oocytes. *Pflugers Archiv European Journal of Physiology*, *450*(6), 415–428. https://doi.org/10.1007/s00424-005-1399-1

Horng, J. L., Chao, P. L., Chen, P. Y., Shih, T. H., & Lin, L. Y. (2015). Aquaporin 1 is involved in acid secretion by ionocytes of zebrafish embryos through facilitating CO2 transport. *PLoS ONE*, *10*(8). https://doi.org/10.1371/journal.pone.0136440

Hove, J. R., Köster, R. W., Forouhar, A. S., Acevedo-Bolton, G., Fraser, S. E., & Gharib, M. (2003). Intracardiac fluid forces are an essential epigenetic factor for embryonic cardiogenesis. *Nature*, *421*(6919), 172–177. https://doi.org/10.1038/nature01282

Howe, K., Clark, M. D., Torroja, C. F., Torrance, J., Berthelot, C., Muffato, M., Collins, J. E., Humphray, S., McLaren, K., Matthews, L., McLaren, S., Sealy, I., Caccamo, M., Churcher, C., Scott, C., Barrett, J. C., Koch, R., Rauch, G. J., White, S., … Stemple, D. L. (2013). The zebrafish reference genome sequence and its relationship to the human genome. *Nature*, *496*(7446), 498–503. https://doi.org/10.1038/nature12111

Hub, J. S., & De Groot, B. L. (2008). Mechanism of selectivity in aquaporins and aquaglyceroporins. *Proceedings of the National Academy of Sciences of the United States of America*, *105*(4), 1198–1203. https://doi.org/10.1073/pnas.0707662104

Huber, M. D., & Gerace, L. (2007). The size-wise nucleus: Nuclear volume control in eukaryotes. In *Journal of Cell Biology* (Vol. 179, Issue 4, pp. 583–584). J Cell Biol. https://doi.org/10.1083/jcb.200710156

Humphrey, J. D., Dufresne, E. R., & Schwartz, M. A. (2014). Mechanotransduction and extracellular matrix homeostasis. In *Nature Reviews Molecular Cell Biology* (Vol. 15, Issue 12, pp. 802–812). Nature Publishing Group. https://doi.org/10.1038/nrm3896

Ibata, K., Takimoto, S., Morisaku, T., Miyawaki, A., & Yasui, M. (2011). Analysis of aquaporin-mediated diffusional water permeability by coherent anti-Stokes Raman scattering microscopy. *Biophysical Journal*, *101*(9), 2277–2283. https://doi.org/10.1016/j.bpj.2011.08.045

Jentsch, T. J. (2016). VRACs and other ion channels and transporters in the regulation of cell volume and beyond. *Nature Reviews Molecular Cell Biology* (Vol. 17, Issue 5, pp. 293–307). https://doi.org/10.1038/nrm.2016.29

Jiao, R., Cui, D., Wang, S. C., Li, D., & Wang, Y. F. (2017). Interactions of the mechanosensitive channels with extracellular matrix, integrins, and cytoskeletal network in osmosensation. In *Frontiers in Molecular Neuroscience* (Vol. 10, p. 96). Frontiers Media S.A. https://doi.org/10.3389/FNMOL.2017.00096

Jinek, M., Chylinski, K., Fonfara, I., Hauer, M., Doudna, J. A., & Charpentier, E. (2012). A programmable dual-RNA-guided DNA endonuclease in adaptive bacterial immunity. *Science*, *337*(6096), 816–821. https://doi.org/10.1126/science.1225829

Jo, A. O., Ryskamp, D. A., Phuong, T. T. T., Verkman, A. S., Yarishkin, O., Macaulay, N., & Križaj, D. (2015). TRPV4 and AQP4 channels synergistically regulate cell volume and calcium homeostasis in retinal müller glia. *Journal of Neuroscience*, *35*(39), 13525–13537. https://doi.org/10.1523/JNEUROSCI.1987-15.2015

Jones, A. R., Band, L. R., & Murray, J. A. H. (2019). Double or Nothing? Cell Division and Cell Size

Control. In *Trends in Plant Science* (Vol. 24, Issue 12, pp. 1083–1093). Elsevier Ltd. https://doi.org/10.1016/j.tplants.2019.09.005

Kabeya, Y., Mizushima, N., Ueno, T., Yamamoto, A., Kirisako, T., Noda, T., Kominami, E., Ohsumi, Y., & Yoshimori, T. (2000). LC3, a mammalian homologue of yeast Apg8p, is localized in autophagosome membranes after processing. *EMBO Journal*, *19*(21), 5720–5728. https://doi.org/10.1093/emboj/19.21.5720

Kalogirou, S., Malissovas, N., Moro, E., Argenton, F., Stainier, D. Y. R., & Beis, D. (2014). Intracardiac flow dynamics regulate atrioventricular valve morphogenesis. *Cardiovascular Research*, *104*(1), 49–60. https://doi.org/10.1093/cvr/cvu186

Katrin Weigmann, S. M. C. and C. F. L. (1997). Cell cycle progression, growth and patterning in imaginal discs despite inhibition of cell division after inactivation of Drosophila Cdc2 kinase. *Development*, 3555–3563. moz-extension://d6522e6a-202a-46a2-aa53-a17881dccce6/enhanced-reader.html?openApp&pdf=https%3A%2F%2Fdev.biologists.org%2Fcontent%2Fdevelop%2F124%2F18%2F3555.full.pdf

Keegan, B. R., Meyer, D., & Yelon, D. (2004). Organization of cardiac chamber progenitors in the zebrafish blastula. *Development*, *131*(13), 3081–3091. https://doi.org/10.1242/dev.01185

Kennedy, A., Finlay, D. D., Guldenring, D., Bond, R., Moran, K., & McLaughlin, J. (2016). The Cardiac Conduction System: Generation and Conduction of the Cardiac Impulse. *Critical Care Nursing Clinics of North America* (Vol. 28, Issue 3, pp. 269–279). W.B. Saunders. https://doi.org/10.1016/j.cnc.2016.04.001

Kim, H. Y., Varner, V. D., & Nelson, C. M. (2013). Apical constriction initiates new bud formation during monopodial branching of the embryonic chicken lung. *Development (Cambridge)*, *140*(15), 3146–3155. https://doi.org/10.1242/dev.093682

Kissa, K., & Herbomel, P. (2010). Blood stem cells emerge from aortic endothelium by a novel type of cell transition. *Nature*, *464*(7285), 112–115. https://doi.org/10.1038/nature08761

Klabunde, R. E. (2017). Cardiac electrophysiology: Normal and ischemic ionic currents and the ECG. *Advances in Physiology Education*, *41*(1), 29–37. https://doi.org/10.1152/advan.00105.2016

Kok, F. O., Shin, M., Ni, C. W., Gupta, A., Grosse, A. S., vanImpel, A., Kirchmaier, B. C., Peterson-Maduro, J., Kourkoulis, G., Male, I., DeSantis, D. F., Sheppard-Tindell, S., Ebarasi, L., Betsholtz, C., Schulte-Merker, S., Wolfe, S. A., & Lawson, N. D. (2015). Reverse genetic screening reveals poor correlation between morpholino-induced and mutant phenotypes in zebrafish. *Developmental Cell*, *32*(1), 97–108. https://doi.org/10.1016/j.devcel.2014.11.018

Kondo, T., & Hayashi, S. (2013). Mitotic cell rounding accelerates epithelial invagination. *Nature*, *494*(7435), 125–129. https://doi.org/10.1038/nature11792

Kroll, F., Powell, G. T., Ghosh, M., Gestri, G., Antinucci, P., Hearn, T. J., Tunbak, H., Lim, S., Dennis, H. W., Fernandez, J. M., Whitmore, D., Dreosti, E., Wilson, S. W., Hoffman, E. J., & Rihel, J. (2021). A simple and effective f0 knockout method for rapid screening of behaviour and other complex phenotypes. *ELife*, *10*, 1–34. https://doi.org/10.7554/eLife.59683

Kwon, H. B., Wang, S., Helker, C. S. M., Rasouli, S. J., Maischein, H. M., Offermanns, S., Herzog, W., & Stainier, D. Y. R. (2016). In vivo modulation of endothelial polarization by Apelin receptor

signalling. *Nature Communications*, *7*(1), 1–12. https://doi.org/10.1038/ncomms11805

Kwong, R. W. M., Kumai, Y., & Perry, S. F. (2013). The Role of Aquaporin and Tight Junction Proteins in the Regulation of Water Movement in Larval Zebrafish (Danio rerio). *PLoS ONE*, *8*(8), e70764. https://doi.org/10.1371/journal.pone.0070764

Lagendijk, A. K., Gomez, G. A., Baek, S., Hesselson, D., Hughes, W. E., Paterson, S., Conway, D. E., Belting, H. G., Affolter, M., Smith, K. A., Schwartz, M. A., Yap, A. S., & Hogan, B. M. (2017). Live imaging molecular changes in junctional tension upon VE-cadherin in zebrafish. *Nature Communications*, *8*(1), 1–12. https://doi.org/10.1038/s41467-017-01325-6

Lagendijk, A. K., Goumans, M. J., Burkhard, S. B., & Bakkers, J. (2011). MicroRNA-23 restricts cardiac valve formation by inhibiting has2 and extracellular hyaluronic acid production. *Circulation Research*, *109*(6), 649–657. https://doi.org/10.1161/CIRCRESAHA.111.247635

LaHaye, S., Lincoln, J., & Garg, V. (2014). Genetics of valvular heart disease. In *Current Cardiology Reports* (Vol. 16, Issue 6, p. 487). Current Medicine Group LLC. https://doi.org/10.1007/s11886-014-0487-2

Lecuit, T. (n.d.). *Cellular Growth and Form Course 2: What sets cell volume?*

Lecuit, T., Brook, W. J., Ng, M., Calleja, M., Sun, H., & Cohen, S. M. (1996). Two distinct mechanisms for long-range patterning by Decapentaplegic in the Drosophila wing. *Nature*, *381*(6581), 387–393. https://doi.org/10.1038/381387a0

Lecuit, T., Lenne, P.-F., & Munro, E. (2011). Force Generation, Transmission, and Integration during Cell and Tissue Morphogenesis. *Annual Review of Cell and Developmental Biology*, *27*(1), 157–184. https://doi.org/10.1146/annurev-cellbio-100109-104027

Lecuit, T., & Mahadevan, L. (2017). Morphogenesis one century after on growth and form. In *Development (Cambridge)* (Vol. 144, Issue 23, pp. 4197–4198). Company of Biologists Ltd. https://doi.org/10.1242/dev.161125

LeGoff, L., Rouault, H., & Lecuit, T. (2013). A global pattern of mechanical stress polarizes cell divisions and cell shape in the growing Drosophila wing disc. *Development (Cambridge)*, *140*(19), 4051–4059. https://doi.org/10.1242/dev.090878

Levesque, M. J., & Nerem, R. M. (1985). The elongation and orientation of cultured endothelial cells in response to shear stress. *Journal of Biomechanical Engineering*, *107*(4), 341–347. https://doi.org/10.1115/1.3138567

Levine, R. A., Hagége, A. A., Judge, D. P., Padala, M., Dal-Bianco, J. P., Aikawa, E., Beaudoin, J., Bischoff, J., Bouatia-Naji, N., Bruneval, P., Butcher, J. T., Carpentier, A., Chaput, M., Chester, A. H., Clusel, C., Delling, F. N., Dietz, H. C., Dina, C., Durst, R., … Yacoub, M. H. (2015). Mitral valve disease-morphology and mechanisms. *Nature Reviews Cardiology* (Vol. 12, Issue 12, pp. 689–710). https://doi.org/10.1038/nrcardio.2015.161

Lewis Wolpert, Cheryll Tickle, & Alfonso Martinez Arias. (2015). *Principles of Development -Fifth edition* (Fifth). https://books.google.fr/books?hl=en&lr=&id=WbO6BwAAQBAJ&oi=fnd&pg=PP1&ots=9pGoduRTNT&sig=ooyS5SFr9aV9ZBkZzRH21M_U9JU&redir_esc=y#v=onepage&q&f=false

Li, J., Hou, B., Tumova, S., Muraki, K., Bruns, A., Ludlow, M. J., Sedo, A., Hyman, A. J., McKeown, L.,

Young, R. S., Yuldasheva, N. Y., Majeed, Y., Wilson, L. A., Rode, B., Bailey, M. A., Kim, H. R., Fu, Z., Carter, D. A. L., Bilton, J., … Beech, D. J. (2014). Piezo1 integration of vascular architecture with physiological force. *Nature*, *515*(7526), 279–282. https://doi.org/10.1038/nature13701

Liedtke, W., Choe, Y., Martí-Renom, M. A., Bell, A. M., Denis, C. S., AndrejŠali, Hudspeth, A. J., Friedman, J. M., & Heller, S. (2000). Vanilloid receptor-related osmotically activated channel (VR-OAC), a candidate vertebrate osmoreceptor. *Cell*, *103*(3), 525–535. https://doi.org/10.1016/S0092-8674(00)00143-4

Liu, J., Bressan, M., Hassel, D., Huisken, J., Staudt, D., Kikuchi, K., Poss, K. D., Mikawa, T., & Stainier, D. Y. R. (2010). A dual role for ErbB2 signaling in cardiac trabeculation. *Development*, *137*(22), 3867–3875. https://doi.org/10.1242/dev.053736

Liu, X., Bandyopadhyay, B., Nakamoto, T., Singh, B., Liedtke, W., Melvin, J. E., & Ambudkar, I. (2006). A role for AQP5 in activation of TRPV4 by hypotonicity: Concerted involvement of AQP5 and TRPV4 in regulation of cell volume recovery. *Journal of Biological Chemistry*, *281*(22), 15485–15495. https://doi.org/10.1074/jbc.M600549200

Lloyd, A. C. (2013). XThe regulation of cell size. In *Cell* (Vol. 154, Issue 6, p. 1194). Elsevier B.V. https://doi.org/10.1016/j.cell.2013.08.053

Lo Vecchio, S., Thiagarajan, R., Caballero, D., Vigon, V., Navoret, L., Voituriez, R., & Riveline, D. (2020). Collective Dynamics of Focal Adhesions Regulate Direction of Cell Motion. *Cell Systems*, *10*(6), 535-542.e4. https://doi.org/10.1016/j.cels.2020.05.005

Maître, Jean Léon, Berthoumieux, H., Krens, S. F. G., Salbreux, G., Jülicher, F., Paluch, E., & Heisenberg, C. P. (2012). Adhesion functions in cell sorting by mechanically coupling the cortices of adhering cells. *Science*, *338*(6104), 253–256. https://doi.org/10.1126/science.1225399

Maître, Jean Leon, Niwayama, R., Turlier, H., Nedelec, F., & Hiiragi, T. (2015). Pulsatile cell-autonomous contractility drives compaction in the mouse embryo. *Nature Cell Biology*, *17*(7), 849–855. https://doi.org/10.1038/ncb3185

Mao, Y., & Baum, B. (2015). Tug of war-The influence of opposing physical forces on epithelial cell morphology. In *Developmental Biology* (Vol. 401, Issue 1, pp. 92–102). Academic Press Inc. https://doi.org/10.1016/j.ydbio.2014.12.030

Mao, Y., Tournier, A. L., Hoppe, A., Kester, L., Thompson, B. J., & Tapon, N. (2013). Differential proliferation rates generate patterns of mechanical tension that orient tissue growth. *The EMBO Journal*, *32*(21), 2790–2803. https://doi.org/10.1038/emboj.2013.197

Martin, A. C., & Goldstein, B. (2014). Apical constriction: themes and variations on a cellular mechanism driving morphogenesis. *Development*, *141*(10), 1987–1998. https://doi.org/10.1242/dev.102228

Martin, E., Theis, S., Gay, G., Monier, B., & Suzanne, M. (2020). Mechanical control of morphogenesis robustness. In *bioRxiv* (p. 2020.01.06.896266). bioRxiv. https://doi.org/10.1101/2020.01.06.896266

Mathai, B., Meijer, A., & Simonsen, A. (2017). Studying Autophagy in Zebrafish. *Cells*, *6*(3), 21. https://doi.org/10.3390/cells6030021

Matsubayashi, Y., Sánchez-Sánchez, B. J., Marcotti, S., Serna-Morales, E., Dragu, A., Díaz-de-la-Loza, M. del C., Vizcay-Barrena, G., Fleck, R. A., & Stramer, B. M. (2020). Rapid Homeostatic Turnover

of Embryonic ECM during Tissue Morphogenesis. *Developmental Cell*, *54*(1), 33-42.e9. https://doi.org/10.1016/j.devcel.2020.06.005

McDowell, N., Zorn, A. ., Crease, D. ., & Gurdon, J. . (1997). Activin has direct long-range signalling activity and can form a concentration gradient by diffusion. *Current Biology*, *7*(9), 671–681. https://doi.org/10.1016/S0960-9822(06)00294-6

Meilhac, S. M., & Buckingham, M. E. (2018). The deployment of cell lineages that form the mammalian heart. In *Nature Reviews Cardiology* (Vol. 15, Issue 11, pp. 705–724). Nature Publishing Group. https://doi.org/10.1038/s41569-018-0086-9

Meinhardt, H. (2012). Turing's theory of morphogenesis of 1952 and the subsequent discovery of the crucial role of local self enhancement and long-range inhibition. In *Interface Focus* (Vol. 2, Issue 4, pp. 407–416). Royal Society. https://doi.org/10.1098/rsfs.2011.0097

Mendoza, S. A., Fang, J., Gutterman, D. D., Wilcox, D. A., Bubolz, A. H., Li, R., Suzuki, M., & Zhang, D. X. (2010). TRPV4-mediated endothelial Ca2+ influx and vasodilation in response to shear stress. *American Journal of Physiology - Heart and Circulatory Physiology*, *298*(2), 466–476. https://doi.org/10.1152/ajpheart.00854.2009

Meyer, H. V., Dawes, T. J. W., Serrani, M., Bai, W., Tokarczuk, P., Cai, J., de Marvao, A., Henry, A., Lumbers, R. T., Gierten, J., Thumberger, T., Wittbrodt, J., Ware, J. S., Rueckert, D., Matthews, P. M., Prasad, S. K., Costantino, M. L., Cook, S. A., Birney, E., & O'Regan, D. P. (2020). Genetic and functional insights into the fractal structure of the heart. *Nature*, *584*(7822), 589–594. https://doi.org/10.1038/s41586-020-2635-8

Minton, A. P. (2001). The Influence of Macromolecular Crowding and Macromolecular Confinement on Biochemical Reactions in Physiological Media. *Journal of Biological Chemistry* (Vol. 276, Issue 14, pp. 10577–10580). Elsevier. https://doi.org/10.1074/jbc.R100005200

Mittal, N., Yoon, S. H., Enomoto, H., Hiroshi, M., Shimizu, A., Kawakami, A., Fujita, M., Watanabe, H., Fukuda, K., & Makino, S. (2019). Versican is crucial for the initiation of cardiovascular lumen development in medaka (Oryzias latipes). *Scientific Reports*, *9*(1), 1–17. https://doi.org/10.1038/s41598-019-45851-3

Mjaatvedt, C. H., Yamamura, H., Capehart, A. A., Turner, D., & Markwald, R. R. (1998). The Cspg2 gene, disrupted in the hdf mutant, is required for right cardiac chamber and endocardial cushion formation. *Developmental Biology*, *202*(1), 56–66. https://doi.org/10.1006/dbio.1998.9001

Mola, M. G., Sparaneo, A., Gargano, C. D., Spray, D. C., Svelto, M., Frigeri, A., Scemes, E., & Nicchia, G. P. (2016). The speed of swelling kinetics modulates cell volume regulation and calcium signaling in astrocytes: A different point of view on the role of aquaporins. *GLIA*, *64*(1), 139–154. https://doi.org/10.1002/glia.22921

Mongin, A. A., & Orlov, S. N. (2009). *Physiology and Maintenance - Volume I: General Physiology - Google Livres*. https://books.google.fr/books?id=vNnUCwAAQBAJ&pg=PA130&lpg=PA130&dq=Mongin+%26+Orlov,+Physiology+and+Maintenance&source=bl&ots=NduVbnKx1M&sig=ACfU3U2ERbNeVxGgFXCCAyANol0XSXuNRw&hl=fr&sa=X&ved=2ahUKEwiPg5qiw9HwAhUPrhQKHfGkD6AQ6AEwBXoECAoQAw#v=onepage&q=Mongin %26 Orlov%2C Physiology and Maintenance&f=false

Monier, B., Gettings, M., Gay, G., Mangeat, T., Schott, S., Guarner, A., & Suzanne, M. (2015). Apico-basal forces exerted by apoptotic cells drive epithelium folding. *Nature*, *518*(7538), 245–248. https://doi.org/10.1038/nature14152

Mosimann, C., Panáková, D., Werdich, A. A., Musso, G., Burger, A., Lawson, K. L., Carr, L. A., Nevis, K. R., Sabeh, M. K., Zhou, Y., Davidson, A. J., Dibiase, A., Burns, C. E., Burns, C. G., Macrae, C. A., & Zon, L. I. (2015). Chamber identity programs drive early functional partitioning of the heart. *Nature Communications*, *6*(1), 1–10. https://doi.org/10.1038/ncomms9146

Mukherjee, R. N., Sallé, J., Dmitrieff, S., Nelson, K. M., Oakey, J., Minc, N., & Levy, D. L. (2020). The Perinuclear ER Scales Nuclear Size Independently of Cell Size in Early Embryos. *Developmental Cell*, *54*(3), 395-409.e7. https://doi.org/10.1016/j.devcel.2020.05.003

Müller, P., Rogers, K. W., Jordan, B. M., Lee, J. S., Robson, D., Ramanathan, S., & Schier, A. F. (2012). Differential diffusivity of nodal and lefty underlies a reaction-diffusion patterning system. *Science*, *336*(6082), 721–724. https://doi.org/10.1126/science.1221920

Munjal, A., Hannezo, E., Mitchison, T. J., & Megason, S. G. (2020). Extracellular hyaluronate pressure shaped by cellular tethers drives tissue morphogenesis. In *bioRxiv* (p. 2020.09.28.316042). bioRxiv. https://doi.org/10.1101/2020.09.28.316042

Munjal, A., & Lecuit, T. (2014). Actomyosin networks and tissue morphogenesis. *Development (Cambridge)*, *141*(9), 1789–1793. https://doi.org/10.1242/dev.091645

Navis, A., & Bagnat, M. (2015). Developing pressures: FLUID forces driving morphogenesis. In *Current Opinion in Genetics and Development* (Vol. 32, pp. 24–30). Elsevier Ltd. https://doi.org/10.1016/j.gde.2015.01.010

Nelson, P. (2003). *Biological Physics: Energy, Information, Life* (W.H.Freeman & Co Ltd (ed.)). https://www.abebooks.fr/9780716743729/Biological-Physics-Energy-Information-Life-0716743728/plp

Neufeld, T. P., De La Cruz, A. F. A., Johnston, L. A., & Edgar, B. A. (1998). Coordination of growth and cell division in the Drosophila wing. *Cell*, *93*(7), 1183–1193. https://doi.org/10.1016/S0092-8674(00)81462-2

Neurohr, G. E., & Amon, A. (2020). Relevance and Regulation of Cell Density. In *Trends in Cell Biology* (Vol. 30, Issue 3, pp. 213–225). Elsevier Ltd. https://doi.org/10.1016/j.tcb.2019.12.006

Nilius, B., & Owsianik, G. (2011). The transient receptor potential family of ion channels. In *Genome Biology* (Vol. 12, Issue 3). Genome Biol. https://doi.org/10.1186/gb-2011-12-3-218

Nonomura, K., Lukacs, V., Sweet, D. T., Goddard, L. M., Kanie, A., Whitwam, T., Ranade, S. S., Fujimori, T., Kahn, M. L., & Patapoutian, A. (2018). Mechanically activated ion channel PIEZO1 is required for lymphatic valve formation. *Proceedings of the National Academy of Sciences of the United States of America*, *115*(50), 12817–12822. https://doi.org/10.1073/pnas.1817070115

Noria, S., Cowan, D. B., Gotlieb, A. I., & Langille, B. L. (1999). Transient and steady-state effects of shear stress on endothelial cell adherens junctions. *Circulation Research*, *85*(6), 504–514. https://doi.org/10.1161/01.RES.85.6.504

Noria, S., Xu, F., McCue, S., Jones, M., Gotlieb, A. I., & Langille, B. L. (2004). Assembly and Reorientation of Stress Fibers Drives Morphological Changes to Endothelial Cells Exposed to

Shear Stress. *American Journal of Pathology*, *164*(4), 1211–1223. https://doi.org/10.1016/S0002-9440(10)63209-9

Nüsslein-volhard, C., & Wieschaus, E. (1980). Mutations affecting segment number and polarity in drosophila. *Nature*, *287*(5785), 795–801. https://doi.org/10.1038/287795a0

O'Donnell, A., & Yutz, K. E. (2020). Mechanisms of heart valve development and disease. *Development (Cambridge)* (Vol. 147, Issue 13). Company of Biologists Ltd. https://doi.org/10.1242/dev.183020

Offei, E. B., Yang, X., & Brand-Saberi, B. (2018). The role of autophagy in morphogenesis and stem cell maintenance. *Histochemistry and Cell Biology* (Vol. 150, Issue 6, pp. 721–732). Springer Verlag. https://doi.org/10.1007/s00418-018-1751-0

Orhon, I., Dupont, N., Zaidan, M., Boitez, V., Burtin, M., Schmitt, A., Capiod, T., Viau, A., Beau, I., Wolfgang Kuehn, E., Friedlander, G., Terzi, F., & Codogno, P. (2016). Primary-cilium-dependent autophagy controls epithelial cell volume in response to fluid flow. *Nature Cell Biology*, *18*(6), 657–667. https://doi.org/10.1038/ncb3360

Paluch, E. K., & Raz, E. (2013). The role and regulation of blebs in cell migration. In *Current Opinion in Cell Biology* (Vol. 25, Issue 5, pp. 582–590). Elsevier. https://doi.org/10.1016/j.ceb.2013.05.005

Peal, D. S., Burns, C. G., Macrae, C. A., & Milan, D. (2009). Chondroitin sulfate expression is required for cardiac atrioventricular canal formation. *Developmental Dynamics*, *238*(12), 3103–3110. https://doi.org/10.1002/dvdy.22154

Peralta, M., Steed, E., Harlepp, S., González-Rosa, J. M., Monduc, F., Ariza-Cosano, A., Cortés, A., Rayón, T., Gómez-Skarmeta, J. L., Zapata, A., Vermot, J., & Mercader, N. (2013). Heartbeat-driven pericardiac fluid forces contribute to epicardium morphogenesis. *Current Biology*, *23*(18), 1726–1735. https://doi.org/10.1016/j.cub.2013.07.005

Pestel, J., Ramadass, R., Gauvrit, S., Helker, C., Herzog, W., & Stainier, D. Y. R. (2016). Real-time 3D visualization of cellular rearrangements during cardiac valve formation. *Development*, *143*(12), 2217–2227. https://doi.org/10.1242/dev.133272

Petridou, N. I., Grigolon, S., Salbreux, G., Hannezo, E., & Heisenberg, C. P. (2019). Fluidization-mediated tissue spreading by mitotic cell rounding and non-canonical Wnt signalling. *Nature Cell Biology*, *21*(2), 169–178. https://doi.org/10.1038/s41556-018-0247-4

Petridou, N. I., & Heisenberg, C. (2019). Tissue rheology in embryonic organization. *The EMBO Journal*, *38*(20). https://doi.org/10.15252/embj.2019102497

Petridou, N. I., Spiró, Z., & Heisenberg, C. P. (2017). Multiscale force sensing in development. In *Nature Cell Biology* (Vol. 19, Issue 6, pp. 581–588). Nature Publishing Group. https://doi.org/10.1038/ncb3524

Quijada, P., Trembley, M. A., & Small, E. M. (2020). The Role of the Epicardium during Heart Development and Repair. In *Circulation Research* (Vol. 126, Issue 3, pp. 377–394). Lippincott Williams and Wilkins. https://doi.org/10.1161/CIRCRESAHA.119.315857

Quintin, S., Gally, C., & Labouesse, M. (2008). Epithelial morphogenesis in embryos: asymmetries, motors and brakes. In *Trends in Genetics* (Vol. 24, Issue 5, pp. 221–230). Trends Genet. https://doi.org/10.1016/j.tig.2008.02.005

Ranade, S. S., Qiu, Z., Woo, S. H., Hur, S. S., Murthy, S. E., Cahalan, S. M., Xu, J., Mathur, J., Bandell,

M., Coste, B., Li, Y. S. J., Chien, S., & Patapoutian, A. (2014). Piezo1, a mechanically activated ion channel, is required for vascular development in mice. *Proceedings of the National Academy of Sciences of the United States of America*, *111*(28), 10347–10352. https://doi.org/10.1073/pnas.1409233111

Ribeiro, C., Ebner, A., & Affolter, M. (2002). In vivo imaging reveals different cellular functions for FGF and Dpp signaling in tracheal branching morphogenesis. *Developmental Cell*, *2*(5), 677–683. https://doi.org/10.1016/S1534-5807(02)00171-5

Rogers, K. (2010). *Blood: Physiology and Circulation* (Rosen Education Ser…). Rosen Education Service. https://www.amazon.fr/Blood-Physiology-Circulation-Kara-Rogers/dp/1615301216

Röper, K. (2013). Supracellular actomyosin assemblies during development. *BioArchitecture*, *3*(2), 45–49. https://doi.org/10.4161/bioa.25339

Rotstein, B., & Paululat, A. (2016). On the Morphology of the Drosophila Heart. *Journal of Cardiovascular Development and Disease*, *3*(2), 15. https://doi.org/10.3390/jcdd3020015

Saias, L., Swoger, J., D'Angelo, A., Hayes, P., Colombelli, J., Sharpe, J., Salbreux, G., & Solon, J. (2015). Decrease in Cell Volume Generates Contractile Forces Driving Dorsal Closure. *Developmental Cell*, *33*(5), 611–621. https://doi.org/10.1016/j.devcel.2015.03.016

Salbreux, G., Charras, G., & Paluch, E. (2012). Actin cortex mechanics and cellular morphogenesis. In *Trends in Cell Biology* (Vol. 22, Issue 10, pp. 536–545). Trends Cell Biol. https://doi.org/10.1016/j.tcb.2012.07.001

Samakovlis, C., Hacohen, N., Manning, G., Sutherland, D. C., Guillemin, K., & Krasnow, M. A. (1996). Development of the Drosophila tracheal system occurs by a series of morphologically distinct but genetically coupled branching events. *Development*, *122*(5), 1395–1407. https://doi.org/10.1242/dev.122.5.1395

Samsa, L. A., Givens, C., Tzima, E., Stainier, D. Y. R., Qian, L., & Liu, J. (2015). Cardiac contraction activates endocardial notch signaling to modulate chamber maturation in zebrafish. *Development (Cambridge)*, *142*(23), 4080–4091. https://doi.org/10.1242/dev.125724

Sanchez-Corrales, Y. E., Blanchard, G. B., & Röper, K. (2018). Radially patterned cell behaviours during tube budding from an epithelium. *ELife*, *7*. https://doi.org/10.7554/eLife.35717

Sanghvi-Shah, R., & Weber, G. F. (2017). Intermediate filaments at the junction of mechanotransduction, migration, and development. In *Frontiers in Cell and Developmental Biology* (Vol. 5, Issue SEP, p. 81). Frontiers Media S.A. https://doi.org/10.3389/fcell.2017.00081

Sato, K., Hiraiwa, T., Maekawa, E., Isomura, A., Shibata, T., & Kuranaga, E. (2015). Left-right asymmetric cell intercalation drives directional collective cell movement in epithelial morphogenesis. *Nature Communications*, *6*(1), 1–11. https://doi.org/10.1038/ncomms10074

Sawyer, J. M., Harrell, J. R., Shemer, G., Sullivan-Brown, J., Roh-Johnson, M., & Goldstein, B. (2010). Apical constriction: A cell shape change that can drive morphogenesis. In *Developmental Biology* (Vol. 341, Issue 1, pp. 5–19). Academic Press Inc. https://doi.org/10.1016/j.ydbio.2009.09.009

Schulz, T., Schumacher, U., Prante, C., Sextro, W., & Prehm, P. (2010). Cystic Fibrosis Transmembrane Conductance Regulator Can Export Hyaluronan. *Pathobiology*, *77*, 200–209. https://doi.org/10.1159/000295859

Schwartz, M. A. (2008). The importance of stupidity in scientific research. In *Journal of Cell Science* (Vol. 121, Issue 11, p. 1771). The Company of Biologists. https://doi.org/10.1242/jcs.033340

Sedmera, D., & McQuinn, T. (2008). Embryogenesis of the Heart Muscle. In *Heart Failure Clinics* (Vol. 4, Issue 3, pp. 235–245). NIH Public Access. https://doi.org/10.1016/j.hfc.2008.02.007

Segert, J., Schneider, I., Berger, I. M., Rottbauer, W., & Just, S. (2018). Mediator complex subunit Med12 regulates cardiac jelly development and AV valve formation in zebrafish. *Progress in Biophysics and Molecular Biology*, *138*, 20–31. https://doi.org/10.1016/j.pbiomolbio.2018.07.010

Sehnert, A. J., Huq, A., Weinstein, B. M., Walker, C., Fishman, M., & Stainier, D. Y. R. (2002). Cardiac troponin T is essential in sarcomere assembly and cardiac contractility. *Nature Genetics*, *31*(1), 106–110. https://doi.org/10.1038/ng875

Shi, Q., Chien, Y. H., & Leckband, D. (2008). Biophysical properties of cadherin bonds do not predict cell sorting. *Journal of Biological Chemistry*, *283*(42), 28454–28463. https://doi.org/10.1074/jbc.M802563200

Shirai, M., Imanaka-Yoshida, K., Schneider, M. D., Schwartz, R. J., & Morisaki, T. (2009). T-box 2, a mediator of Bmp-Smad signaling, induced hyaluronan synthase 2 and Tgfβ2 expression and endocardial cushion formation. *Proceedings of the National Academy of Sciences of the United States of America*, *106*(44), 18604–18609. https://doi.org/10.1073/pnas.0900635106

Sick, S., Reinker, S., Timmer, J., & Schlake, T. (2006). WNT and DKK determine hair follicle spacing through a reaction-diffusion mechanism. *Science*, *314*(5804), 1447–1450. https://doi.org/10.1126/science.1130088

Sidhaye, J., & Norden, C. (2017). Concerted action of neuroepithelial basal shrinkage and active epithelial migration ensures efficient optic cup morphogenesis. *ELife*, *6*. https://doi.org/10.7554/eLife.22689

Singh, A., Saha, T., Begemann, I., Ricker, A., Nüsse, H., Thorn-Seshold, O., Klingauf, J., Galic, M., & Matis, M. (2018). Polarized microtubule dynamics directs cell mechanics and coordinates forces during epithelial morphogenesis. *Nature Cell Biology* (Vol. 20, Issue 10, pp. 1126–1133). https://doi.org/10.1038/s41556-018-0193-1

Smith, K. A., Lagendijk, A. K., Courtney, A. D., Chen, H., Paterson, S., Hogan, B. M., Wicking, C., & Bakkers, J. (2011). Transmembrane protein 2 (Tmem2) is required to regionally restrict atrioventricular canal boundary and endocardial cushion development. *Development*, *138*(19), 4193–4198. https://doi.org/10.1242/dev.065375

Solon, J., Kaya-Çopur, A., Colombelli, J., & Brunner, D. (2009). Pulsed Forces Timed by a Ratchet-like Mechanism Drive Directed Tissue Movement during Dorsal Closure. *Cell*, *137*(7), 1331–1342. https://doi.org/10.1016/j.cell.2009.03.050

Stainier, D. Y., Lee, R. K., & Fishman, M. C. (1993). Cardiovascular development in the zebrafish. I. Myocardial fate map and heart tube formation. *Development*, *119*(1), 31–40. https://doi.org/10.1242/dev.119.1.31

Stainier, D. Y. R. (2002). Contribution du poisson zèbre à l'étude moléculaire du développement du cœur des vertébrés. *Médecine/Sciences*, *18*(4), 448–456. https://doi.org/10.1051/medsci/2002184448

Stainier, D. Y. R., Fouquet, B., Chen, J. N., Warren, K. S., Weinstein, B. M., Meiler, S. E., Mohideen, M. A. P. K., Neuhauss, S. C. F., Solnica-Krezel, L., Schier, A. F., Zwartkruis, F., Stemple, D. L., Malicki, J., Driever, W., & Fishman, M. C. (1996). Mutations affecting the formation and function of the cardiovascular system in the zebrafish embryo. *Development*, *123*, 285–292. https://doi.org/10.5167/uzh-237

Stainier, D. Y. R., Raz, E., Lawson, N. D., Ekker, S. C., Burdine, R. D., Eisen, J. S., Ingham, P. W., Schulte-Merker, S., Yelon, D., Weinstein, B. M., Mullins, M. C., Wilson, S. W., Ramakrishnan, L., Amacher, S. L., Neuhauss, S. C. F., Meng, A., Mochizuki, N., Panula, P., & Moens, C. B. (2017). Guidelines for morpholino use in zebrafish. *PLOS Genetics*, *13*(10), e1007000. https://doi.org/10.1371/journal.pgen.1007000

Staudt, D., & Stainier, D. (2012). Uncovering the molecular and cellular mechanisms of heart development using the zebrafish. In *Annual Review of Genetics* (Vol. 46, pp. 397–418). Annu Rev Genet. https://doi.org/10.1146/annurev-genet-110711-155646

Steed, E, Faggianelli, N., Roth, S., Ramspacher, C., Concordet, J. P., & Vermot, J. (2016). Klf2a Couples Mechanotransduction and Zebrafish Valve Morphogenesis Through Fibronectin Synthesis. *Nat Commun*, *7*(May), 11646. https://doi.org/10.1038/ncomms11646

Steed, Emily, Boselli, F., & Vermot, J. (2016). Hemodynamics driven cardiac valve morphogenesis. *Biochimica et Biophysica Acta - Molecular Cell Research*, *1863*(7), 1760–1766. https://doi.org/10.1016/j.bbamcr.2015.11.014

Steinberg, M. S. (1963). Reconstruction of tissues by dissociated cells. *Science Science*, *141*(3579), 401–408. https://doi.org/10.1126/science.141.3579.401

Steinberg, M. S., & Takeichi, M. (1994). Experimental specification of cell sorting, tissue spreading, and specific spatial patterning by quantitative differences in cadherin expression. *Proceedings of the National Academy of Sciences of the United States of America*, *91*(1), 206–209. https://doi.org/10.1073/pnas.91.1.206

Strotmann, R., Harteneck, C., Nunnenmacher, K., Schultz, G., & Plant, T. D. (2000). OTRPC4, a nonselective cation channel that confers sensivity to extracellular osmolarity. *Nature Cell Biology*, *2*(10), 695–702. https://doi.org/10.1038/35036318

Su, T. T., & O'Farrell, P. H. (1998). Size control: Cell proliferation does not equal growth. *Current Biology*, *8*(19), 687–689. https://doi.org/10.1016/s0960-9822(98)70436-1

Sugimura, K., Lenne, P. F., & Graner, F. (2016). Measuring forces and stresses in situ in living tissues. *Development (Cambridge)*, *143*(2), 186–196. https://doi.org/10.1242/dev.119776

Sutherland, D., Samakovlis, C., & Krasnow, M. A. (1996). branchless encodes a Drosophila FGF homolog that controls tracheal cell migration and the pattern of branching. *Cell*, *87*(6), 1091–1101. https://doi.org/10.1016/S0092-8674(00)81803-6

Thodeti, C. K., Matthews, B., Ravi, A., Mammoto, A., Ghosh, K., Bracha, A. L., & Ingber, D. E. (2009). TRPV4 channels mediate cyclic strain-induced endothelial cell reorientation through integrin-to-integrin signaling. *Circulation Research*, *104*(9), 1123–1130. https://doi.org/10.1161/CIRCRESAHA.108.192930

Thompson, D. W. (1942). On growth and form. *On Growth and Form.*

Tingaud-Sequeira, A., Calusinska, M., Finn, R. N., Chauvigné, F., Lozano, J., & Cerdà, J. (2010). The zebrafish genome encodes the largest vertebrate repertoire of functional aquaporins with dual paralogy and substrate specificities similar to mammals. *BMC Evolutionary Biology*, *10*(1), 38. https://doi.org/10.1186/1471-2148-10-38

Todaka, H., Taniguchi, J., Satoh, J. I., Mizuno, A., & Suzuki, M. (2004). Warm temperature-sensitive transient receptor potential vanilloid 4 (TRPV4) plays an essential role in thermal hyperalgesia. *Journal of Biological Chemistry*, *279*(34), 35133–35138. https://doi.org/10.1074/jbc.M406260200

Toft-Bertelsen, T. L., Križaj, D., & MacAulay, N. (2017). When size matters: transient receptor potential vanilloid 4 channel as a volume-sensor rather than an osmo-sensor. *The Journal of Physiology*, *595*(11), 3287–3302. https://doi.org/10.1113/JP274135

Tong, X., Zu, Y., Li, Z., Li, W., Ying, L., Yang, J., Wang, X., He, S., Liu, D., Zhu, Z., Chen, J., Lin, S., & Zhang, B. (2014). Kctd10 regulates heart morphogenesis by repressing the transcriptional activity of Tbx5a in zebrafish. *Nature Communications*, *5*. https://doi.org/10.1038/ncomms4153

Totong, R., Schell, T., Lescroart, F., Ryckebüsch, L., Lin, Y. F., Zygmunt, T., Herwig, L., Krudewig, A., Gershoony, D., Belting, H. G., Affolter, M., Torres-Vázquez, J., & Yelon, D. (2011). The novel transmembrane protein tmem2 is essential for coordination of myocardial and endocardial morphogenesis. *Development*, *138*(19), 4199–4205. https://doi.org/10.1242/dev.064261

Toyama, Y., Peralta, X. G., Wells, A. R., Kiehart, D. P., & Edwards, G. S. (2008). Apoptotic Force and Tissue Dynamics During Drosophila Embryogenesis. *Science*, *321*(5896), 1683–1686. https://doi.org/10.1126/science.1157052

Vermot, J., Forouhar, A. S., Liebling, M., Wu, D., Plummer, D., & Fraser, S. E. (2009). *Reversing Blood Flows Act through klf2a to Ensure Normal Valvulogenesis in the Developing Heart*. *7*(11), 12–14. https://doi.org/10.1371/journal.pbio.1000246

Villedieu, A., Bosveld, F., & Bellaïche, Y. (2020). Mechanical induction and competence in epithelial morphogenesis. In *Current Opinion in Genetics and Development* (Vol. 63, pp. 36–44). Elsevier Ltd. https://doi.org/10.1016/j.gde.2020.03.003

Voets, T., Talavera, K., Owsianik, G., & Nilius, B. (2005). Sensing with TRP channels. *Nature Chemical Biology* (Vol. 1, Issue 2, pp. 85–92). Nat Chem Biol. https://doi.org/10.1038/nchembio0705-85

Waldenström, A., Martinussen, H. J., Gerdin, B., & Hällgren, R. (1991). Accumulation of hyaluronan and tissue edema in experimental myocardial infarction. *Journal of Clinical Investigation*, *88*(5), 1622–1628. https://doi.org/10.1172/JCI115475

Walsh, E. C., & Stainier, D. Y. R. (2001). UDP-glucose dehydrogenase required for cardiac valve formation in zebrafish. *Science*, *293*(5535), 1670–1673. https://doi.org/10.1126/science.293.5535.1670

Wang, M., Yang, Y., Han, L., Xu, F., & Li, F. (2020). Cell mechanical microenvironment for cell volume regulation. *Journal of Cellular Physiology*, *235*(5), 4070–4081. https://doi.org/10.1002/jcp.29341

Watanabe, H., Vriens, J., Suh, S. H., Benham, C. D., Droogmans, G., & Nilius, B. (2002). Heat-evoked activation of TRPV4 channels in a HEK293 cell expression system and in native mouse aorta endothelial cells. *Journal of Biological Chemistry*, *277*(49), 47044–47051. https://doi.org/10.1074/jbc.M208277200

Watson, J. D., & Crick, F. H. C. (1953). Molecular structure of nucleic acids: A structure for deoxyribose nucleic acid. *Nature*, *171*(4356), 737–738. https://doi.org/10.1038/171737a0

Wolpert, L. (1969). Positional information and the spatial pattern of cellular differentiation. *Journal of Theoretical Biology*, *25*(1), 1–47. https://doi.org/10.1016/S0022-5193(69)80016-0

Wright, J., & Schneider, B. L. (2014). Cell growth: When less means more. In *Current Biology* (Vol. 24, Issue 7, pp. R283–R285). Cell Press. https://doi.org/10.1016/j.cub.2014.02.044

Yang, Q., Xue, S.-L., Chan, C. J., Rempfler, M., Vischi, D., Gutierrez, F. M., Hiiragi, T., Hannezo, E., & Liberali, P. (2020). Cell fate coordinates mechano-osmotic forces in intestinal crypt morphogenesis. *BioRxiv*, 2020.05.13.094359. https://doi.org/10.1101/2020.05.13.094359

Yu, J. A., Castranova, D., Pham, V. N., & Weinstein, B. M. (2015). Single-cell analysis of endothelial morphogenesis in vivo. *Development (Cambridge)*, *142*(17), 2951–2961. https://doi.org/10.1242/dev.123174

Zegers, M. M., & Friedl, P. (2014). Rho GTPases in collective cell migration. *Small GTPases*, *5*(3). https://doi.org/10.4161/sgtp.28997

Zeng, G., Taylor, S. M., McColm, J. R., Kappas, N. C., Kearney, J. B., Williams, L. H., Hartnett, M. E., & Bautch, V. L. (2007). Orientation of endothelial cell division is regulated by VEGF signaling during blood vessel formation. *Blood*, *109*(4), 1345–1352. https://doi.org/10.1182/blood-2006-07-037952

Zhang, X. H., Tee, L. Y., Wang, X. G., Huang, Q. S., & Yang, S. H. (2015). Off-target effects in CRISPR/Cas9-mediated genome engineering. *Molecular Therapy - Nucleic Acids* (Vol. 4, Issue 11, p. e264). https://doi.org/10.1038/mtna.2015.37

Zhou, E. H., Trepat, X., Park, C. Y., Lenormand, G., Oliver, M. N., Mijailovich, S. M., Hardin, C., Weitz, D. A., Butler, J. P., & Fredberg, J. J. (2009). Universal behavior of the osmotically compressed cell and its analogy to the colloidal glass transition. *Proceedings of the National Academy of Sciences of the United States of America*, *106*(26), 10632–10637. https://doi.org/10.1073/pnas.0901462106

Zhou, Y., Cashman, T. J., Nevis, K. R., Obregon, P., Carney, S. A., Liu, Y., Gu, A., Mosimann, C., Sondalle, S., Peterson, R. E., Heideman, W., Burns, C. E., & Burns, C. G. (2011). Latent TGF-βbinding protein 3 identifies a second heart field in zebrafish. *Nature*, *474*(7353), 645–648. https://doi.org/10.1038/nature10094

Zlotek-Zlotkiewicz, E., Monnier, S., Cappello, G., Le Berre, M., & Piel, M. (2015). Optical volume and mass measurements show that mammalian cells swell during mitosis. *Journal of Cell Biology*, *211*(4), 765–774. https://doi.org/10.1083/jcb.201505056

Zonia, L., & Munnik, T. (2007). Life under pressure: hydrostatic pressure in cell growth and function. *Trends in Plant Science*, *12*(3), 90–97. https://doi.org/10.1016/j.tplants.2007.01.006

Université de Strasbourg

Hélène VIGNES

École Doctorale des Sciences de la Vie et de la Santé STRASBOURG

Mécanismes moléculaires et cellulaires impliqués dans le processus de morphogenèse du canal atrio-ventriculaire chez le poisson zèbre

Résumé

La morphogenèse des organes implique des changements dynamiques des propriétés des tissus à l'échelle cellulaire. De plus, les cellules doivent s'adapter à leur environnement mécanique par des voies mécanosensibles. Cependant, la manière dont les signaux mécaniques influencent le comportement des cellules pendant la morphogenèse reste mal comprise. Nous avons étudié ici l'influence des forces mécaniques pendant la formation du canal atrio-ventriculaire (AVC) où se développent les valves cardiaques. Nous montrons que chez le poisson zèbre, le canal atrio-ventriculaire se forme dans une zone de convergence tissulaire entre l'atrium et le ventricule qui est associée à une activation accrue du réseau d'actomyosine et à des changements d'orientation des cellules endocardiques. Nous démontrons que la convergence tissulaire se produit avec une réduction majeure du volume des cellules endocardiques déclenchée par des forces mécaniques et les canaux mécanosensibles TRPP2/TRPV4. De plus, nous montrons qu'un composant de la matrice extracellulaire, l'acide hyaluronique, contrôle les changements de volume cellulaire. Ensemble, nos données suggèrent que le changement de volume cellulaire est une caractéristique cellulaire clé activée par les forces mécaniques pendant la morphogenèse cardiovasculaire. Ces travaux permettent de mieux comprendre comment les forces mécaniques et la matrice extracellulaire peuvent influencer le remodelage des tissus dans les organes en développement.

Mots clés : poisson zèbre, endocarde, matrice extracellulaire, mécanobiologie

Résumé en anglais

Organ morphogenesis involves dynamic changes of tissue properties at the cellular scale. In addition, cells need to adapt to their mechanical environment through mechanosensitive pathways. How mechanical cues influence cell behaviors during morphogenesis, however, remains poorly understood. Here we studied the influence of mechanical forces during the formation of the atrioventricular canal (AVC) where cardiac valves develop. We show that in zebrafish the AVC forms within a zone of tissue convergence between the atrium and the ventricle which is associated with increased activation of the actomyosin meshwork and endocardial cell orientation changes. We demonstrate that tissue convergence occurs with a major reduction of endocardial cell volume triggered by mechanical forces and the mechanosensitive channels TRPP2/TRPV4. In addition, we show that the extracellular matrix component hyaluronic acid controls cell volume changes. Together, our data suggest that cell volume change is a key cellular feature activated by mechanical forces during cardiovascular morphogenesis. This work further unravels how mechanical forces and extracellular matrix can influence tissue remodeling in developing organs.

Keywords: zebrafish, endocardium, ECM, mechanobiology